

N°: _____



THÈSE DE DOCTORAT

Flame retardancy of polyamide 6 fibers

The use of sulfamate salts

Présentée et soutenue publiquement à

L'UNIVERSITE LILLE 1

Pour obtenir le grade de

Docteur

Spécialité: Molécules et matière condensée

par

Mathieu Coquelle

Thèse dirigée par

Prof. Sophie Duquesne et Dr. Mathilde Casetta

Soutenue le 17 Juillet 2014 devant la Commission d'Examen composée de :

Prof. Serge BOURBIGOT	Université Lille 1	Président du jury
Prof. Baljinder KANDOLA	University of Bolton	Rapporteur
Prof. Isabelle VROMAN	Université de Reims	Rapporteur
Dr. Xavier COUILLENS	Rhodia	Examineur
Prof. Sophie DUQUESNE	Université Lille 1	Directrice de thèse
Dr. Mathilde CASSETTA	Université Lille 1	Co-encadrante de thèse

ACKNOWLEDGMENTS

The work described in this thesis manuscript has been carried out in the laboratory UMET (CNRS UMR 8207), led by Pr. Alexandre Legris, and more precisely in the team ISP led by Dr. Jean-Marc Lefebvre. I would like to thank them for giving me the opportunity to join this laboratory and work on this project.

Obviously I want to thank my supervisors, Sophie, Mathilde and Serge (aka the real man). They gave me the great opportunity to work with them in the team, but more than this, they warmly welcomed me, and taught me many things during these three years in the lab. The time shared with them was greatly appreciated.

I had the chance to work with Prof. Shang Zheng and Jun Sun in the framework of this international project. I would like to thank them for welcoming me in their lab in BUCT, Beijing. I also have to acknowledge Xiaodong and Chen Chen for their help and kindness when I was lost in China!

I also thank Prof. Baljinder Kandola, Prof. Isabelle Vroman and Dr. Xavier Couillens, who accepted to spend their time to review this work and be part of the jury.

I have, of course, special thanks to address to my friend Marion; I have known her during her own Ph.D. when I was a “small” Master trainee. She is the one who told me about this Ph.D. position, without her, I would not have been in the lab I guess.

I am indebted to my co-workers and friends, Jeremie for teaching me how to properly clean the microextruder!! Bastien for all the thermal analysis and Carlos... Pauline and Carmen for their friendship and the good time we spent in the lab and elsewhere. Gwen and Renaud for our wonderful conversations about PA6 (but not only). B & B for their ~~bad~~ jokes. Pierre for being... Pierre! I am running out of space to right a word for each of you... So I want to thank everyone in the lab for being very nice people and making the lab the best place to work. My thanks go to Anil, Andrea, Brigitte, Fabienne, Gaëlle, Maude, Marianne, Michel, Nico & Nico, Séverine, and Trang.

I also have to thank everyone who bore with me outside of the lab, family, friends and especially Teddie for her patience and her love.

CONTENTS

Acknowledgments	5
Contents	7
List of Figures.....	13
List of Tables.....	19
Abbreviations	21
General Introduction.....	23
I State of the Art: Flame retardancy of PA6	27
I.1 Introduction.....	29
I.2 Polyamide 6	31
I.2.1 Polyamides	31
I.2.2 Polyamide 6 polymerization.....	31
I.2.2.1 High temperature, water-catalyzed melt polymerization _____	32
I.2.2.2 Anionic chain polymerization using base initiators _____	34
I.2.3 Processing and spinning	35
I.2.4 Structure.....	37
I.2.4.1 NMR _____	39
I.2.4.2 FT-IR _____	40
I.2.4.3 Differential scanning calorimetry _____	41
I.2.5 Properties of polyamide 6	41
I.2.6 Applications.....	42
I.2.7 Thermal decomposition and flammability	43
I.2.7.1 Thermal decomposition _____	44
I.2.7.2 Flammability _____	46
I.3 Textile fibers and flame retardancy.....	48
I.3.1 General overview	48
I.3.2 High performance fibers	49
I.3.3 Flame retardant finishings	50
I.3.4 Flame retarding fibers with additives	51

I.4	Polymers flame retardancy	52
I.4.1	Combustion and thermal decomposition processes	52
I.4.2	Flame retardants mode of action.....	54
I.4.2.1	Halogen-containing flame retardants _____	56
I.4.2.2	Phosphorus-containing flame retardants _____	58
I.4.2.3	Melamine and its derivatives _____	61
I.4.2.4	Sulfur containing fire retardants _____	64
I.4.2.5	Metal hydroxides _____	65
I.4.2.6	Boron containing compounds _____	66
I.4.2.7	Nanoparticles _____	68
I.4.2.7.1	1D nanoparticles	68
I.4.2.7.2	2D nanoparticles	72
I.4.2.7.3	3D nanoparticles	74
I.5	Fire-retardant additives for fibers	75
I.6	Conclusion	79
II	<i>Experimental Techniques</i>	81
II.1	Introduction.....	82
II.2	Material Preparation and processing	82
II.2.1	Materials.....	82
II.2.1.1	Polyamide 6 _____	82
II.2.1.2	Flame retardants and additives _____	82
II.2.2	Extrusion and fiber spinning.....	84
II.2.3	Samples processing	85
II.2.3.1	Powders _____	85
II.2.3.2	Barrels and plates _____	85
II.3	Materials characterization	86
II.3.1	Mechanical testing	86
II.3.2	Digital microscopy and image processing	86
II.3.3	Electron probe micro analysis	87
II.3.4	Solid-state NMR.....	88
II.3.5	Differential scanning calorimetry.....	88

II.4	Thermal degradation and fire testing	89
II.4.1	Thermal degradation.....	89
II.4.1.1	ThermoGravimetric Analysis	89
II.4.1.2	TGA coupled with FTIR	90
II.4.1.3	py-GC-MS	90
II.4.1.4	Thermal treatments	92
II.4.2	Fire testings	93
II.4.2.1	Pyrolysis Combustion Flow Calorimetry	93
II.4.2.2	Mass Loss Calorimeter	94
II.4.2.3	Limiting Oxygen Index	95
II.4.2.4	UL-94	96
II.5	Conclusion	97
III	<i>Flame Retardant Screening for Polyamide 6 Fibers</i>	99
III.1	Introduction.....	100
III.2	Flame retardant screening.....	101
III.2.1	Selection of flame retardants.....	101
III.2.1.1	Phosphorus based fire retardant	102
III.2.1.2	Sulfur based flame retardants	102
III.2.1.3	Nanoparticles as fire retardants	102
III.2.2	Fire retardant properties and thermal stabilities	103
III.2.2.1	Phosphorus based fire retardants	103
III.2.2.2	Sulfur based fire retardants	106
III.2.1	The use of nanoparticles	109
III.2.1.1	Selection of processing parameters	109
III.2.1.2	Conclusions on the processing parameters for nanoparticles	113
III.2.1.3	Nanoparticles screening	114
III.3	Conclusion	117
IV	<i>Sulfamate Salts as Flame Retardant for Polyamide 6 Fibers.....</i>	119
IV.1	Introduction.....	120
IV.2	The use of ammonium sulfamate	120

IV.2.1	Mechanical properties of the PA6/AS fibers.....	122
IV.2.2	Additive dispersion in the fiber	123
IV.2.3	Fire tests on PA6/ammonium sulfamate formulations.....	124
IV.2.3.1	Pyrolysis combustion flow calorimetry _____	124
IV.2.3.2	Mass-loss calorimetry_____	125
IV.2.4	Comprehension of the modes of action	127
IV.2.4.1	Thermal stability of PA6/AS _____	127
IV.2.4.1.1	Thermo-oxidative degradation	127
IV.2.4.1.2	Pyrolysis	129
IV.2.4.2	Gas phase analysis _____	131
IV.2.4.2.1	TGA-FTIR.....	131
IV.2.4.2.2	Pyrolysis-GC-MS	136
IV.2.4.2.3	Conclusion.....	138
IV.2.4.3	Solid phase analysis _____	138
IV.2.5	Conclusion	140
IV.3	The use of guanidine sulfamate	140
IV.3.1	Processing issues solved?.....	140
IV.3.2	Mechanical properties of the PA6/GAS fibers	142
IV.3.3	Fire tests on PA6/guanidine sulfamate formulations	143
IV.3.4	Additive dispersion.....	145
IV.3.5	Degradation mechanism	147
IV.3.5.1	Gas phase analysis _____	147
IV.3.5.1.1	TGA-FTIR.....	147
IV.3.5.1.2	py-GC-MS	149
IV.3.5.2	Solid phase analysis _____	150
IV.4	Conclusion	152
V	<i>Scale-up of the sulfamate salts systems</i>	155
V.1	Introduction.....	156
V.2	Potential synergy between sulfamate salts and melamine polyphosphate.....	157
V.2.1	AS/MPP.....	157
V.2.1.1	PCFC Results and spinnability_____	157

V.2.1.2	Thermogravimetry	158
V.2.2	GAS/MPP	160
V.2.2.1	PCFC Results and spinnability	160
V.2.2.2	Thermogravimetry	161
V.2.3	Conclusion	162
V.3	Scale-up with the PA6/GAS/MPP system	163
V.3.1	Materials characterizations	164
V.3.1.1	Spinnability and additives dispersion	164
V.3.1.2	Thermogravimetric analysis	166
V.3.1.3	Differential scanning calorimetry (DSC)	167
V.3.1.4	PCFC	169
V.3.2	Fire performance of large-scale PA6/GAS/MPP	170
V.3.2.1	Cone calorimetry	170
V.3.2.2	UL-94 and LOI	173
V.3.3	Analysis of the decomposition gases	175
V.3.3.1	TGA-FTIR	175
V.3.3.2	py-GC-MS	178
V.3.4	Analysis of the condensed phase	180
V.4	Conclusion	183
	General conclusion	185
	Outlooks	189
	References	191
	Appendix A	205
	Appendix B	206
	Appendix C	207
	Appendix D	209
	Procédé d'ignifugation des fibres de polyamide 6 – utilisation des sels de sulfamate	211
	Résumé	211
	Mots clés :	211

Flame retardancy of polyamide 6 fibers - The use of sulfamate salts.....211

Abstract.....211

Keywords:.....211

LIST OF FIGURES

Figure 1: World plastics production 1950-2012, adapted from [1]	23
Figure 2: Polyamide 6 synthesis from ϵ -caprolactam	32
Figure 3: Ring opening of caprolactam by water	33
Figure 4: Ring opening of caprolactam by the amino acid.....	34
Figure 5: Anionic polymerization	35
Figure 6: Relationship between moisture content and temperature for an unvented cylinder during injection molding [14].....	36
Figure 7: Structures of the α and γ forms of nylon 6 The left side shows the view of the hydrogen-bonding planes, and the right side shows the view down the chain axis [38].....	39
Figure 8: ^{13}C NMR (CP) spectra that discriminate in favor of the crystalline phase for samples that are high in γ crystallinity (A) and high in α crystallinity (B), ^{13}C NMR (BD-MAS) spectra that discriminate in favor of the amorphous phase for samples that were predominantly amorphous(C) [39].	40
Figure 9: Examples of PA6 applications [48]	43
Figure 10: Dominant PA-6 thermal degradation products in the absence of a nucleophile (A) and in the presence of a nucleophile, such as water (B) [51]	45
Figure 11: Intra- and intermolecular routes that generate ϵ -caprolactam [51]	46
Figure 12: Summary of finishing and coating techniques [61]	51
Figure 13: Combustion cycle	53
Figure 14: Schematic representation of the self-sustaining polymer combustion cycle; a-d represent potential modes of action of flame retardants [75].....	55
Figure 15: Quenching mode of effective halogen-based species	56
Figure 16: Dechlorane Plus.....	57
Figure 17: Quenching mode of radical phosphorus-based species [80].....	59
Figure 18: Oxygen index for the PA6 formulations as a function of the APP weight content [90]	60
Figure 19: High temperature condensation of melamine	62
Figure 20: Examples of melamine salts	63
Figure 21: structure of montmorillonite [110].....	69
Figure 22: Dispersion of a lamellar filler within a polymer matrix [112]	69

Figure 23: Generic structure of a LDH with A = compensating anion, O = oxygen, H = hydrogen and M = any divalent or trivalent cation [122]	72
Figure 24: Sketches of CNTs: (A) SWNT (B) MWCNT , showing typical dimensions of length [132]	73
Figure 25: POSS structure.....	74
Figure 26: RHR curves of PA6 and PA6/nano fabrics at an external heat flux of 35 kW/m ² ...	77
Figure 27: Heat release rate (HRR) curves of (A) nylon 6 and nylon 6/OMMT 8% nanocomposite (8 NC) fabric of low tightness factor (LTF) and (B) nylon 6 and nylon 6/OMMT 8% nanocomposite fabric of high tightness factor (HTF) [142]	78
Figure 28: Rate of heat release (RHR) curves of PP and PP/FQ-POSS knitted fabrics at 35 kW/m ² [143].....	78
Figure 29: HRR values versus time of PP and PP/MWCNT fabrics at 35 kW/m ² [144].....	79
Figure 30: DSM microextruder and spinning unit in series (a) Thermo Scientific extruder (b)85	
Figure 31: Image processing steps	87
Figure 32: Temperature/time ramp used for DSC experiments	89
Figure 33: Schematic representation of the pyrolyzer-GCMS	91
Figure 34: Stepwise method used for py-GC-MS characterization.....	92
Figure 35: Tubular furnace used for thermal treatments	92
Figure 36: schematic PCFC representation	93
Figure 37: Schematic representation of a mass loss calorimeter	94
Figure 38: Experimental set-up for LOI measurement [74]	95
Figure 39: Schematic representation of UL-94 test [154].....	97
Figure 40: TG and DTG curves of neat PA6 and PA6 containing commercial products PA6/OP1230 5% and PA6/OP950 5% (10 °C/min, air)	105
Figure 41: TG and DTG curves of neat PA6 and PA6 containing commercial products PA6/PCO900 5% and PA6/PCO960 5% (10 °C/min, air).....	106
Figure 42: TG and DTG curves of neat PA6 and PA6 containing sulfamate salts PA6/AS 5%, PA6/GAS 5% and PA6/GAS 10% (10 °C/min, air)	108
Figure 43: Standard and "nano" screws used with the microextruder, the red circle on the zoomed part shows the notch on the "nano" screws.....	111
Figure 44: SEM pictures of a cross section of PA6/MWCNT 1% f1 (left) and f12 (right) formulations.....	112

Figure 45: Digital microscope pictures of PA6/MWCNT 1% f1 (left) and f12 (right) formulations, dark dots correspond to MWCNT aggregates.....	112
Figure 46: Particle size distribution of f1 and f12 formulations	113
Figure 47: TGA and DTG curves of neat PA6 and PA6 containing carbon-based nanoparticles PA6/MWCNT 1% and PA6/nanoGO 1% (10 °C/min, air).....	115
Figure 48: TG and DTG curves of neat PA6 and PA6 containing silicate-based nanoparticles PA6/C30B 5% and PA6/HNT 5% (10 °C/min, air)	116
Figure 49: Molecular structure of ammonium sulfamate.....	121
Figure 50: Elongation-at-break (%) and tensile strength (MPa) of PA6, PA6/AS 3% and PA6/AS5 % formulations	122
Figure 51: Digital microscope photographs of PA6 (a) and PA6/AS 5% (b) fibers	123
Figure 52: BSE picture (a) and EPMA sulphur cartography (b) of the cross section of PA6/AS 5% fibers.....	124
Figure 53: Heat release rate curves versus temperature for PA6 and PA6/AS formulations obtained with PCFC	125
Figure 54: Heat release rate versus time for PA6 and PA6/AS 5%	126
Figure 55: TG and DTG curves of PA6, AS and PA6/AS 5% (10 °C/min, air).....	128
Figure 56: Calculated and experimental TG curves and difference weight loss curve of the PA6/AS 5% formulation.....	129
Figure 57: TG and DTG curves of PA6 and PA6/AS 5% (10 °C/min, nitrogen)	130
Figure 58: FTIR spectra of the gases evolved during the thermo-oxidative degradation of PA6 (—) and PA6/AS 5% (--) at characteristic temperatures of degradation (PA6: (a) 320 °C; (b) 449 °C; (c) 500 °C, PA6/AS 5%: (a) 260 °C; (b) 447°C; (c) 550 °C).....	132
Figure 59: FTIR spectra of the gases evolved during the pyrolytic degradation of PA6 (—) and PA6/AS 5% (--) at characteristic temperatures of degradation (PA6: (a) 350 °C; (b) 449 °C; (c) 500 °C, PA6/AS 5%: (a) 260 °C; (b) 450°C; (c) 500 °C)	134
Figure 60: Intensity of the caprolactam (2938 cm ⁻¹ , (a)), NH ₃ (965 cm ⁻¹ , (b)) and CO ₂ (2354 cm ⁻¹ , (c)) peaks versus time (— : PA6, --- : PA6/AS 5%)	135
Figure 61: Intensity of the NH ₃ (965 cm ⁻¹) peak versus time for AS alone	136
Figure 62: TIC corresponding to the pyrolysis of PA6 between 350 °C and 490 °C, and PA6/AS 5% between 323 °C and 490 °C.....	137

Figure 63: ^{13}C CP-DD-MAS NMR spectra of the PA6 (—) and PA6/AS 5% (--) formulations residues obtained after thermal treatment at 20, 265, 323, 410 and 500 °C (*: spinning sideband, **: frequency carrier)	139
Figure 64: Molecular structure of guanidine sulfamate	140
Figure 65: TG and DTG curves of AS and GAS	141
Figure 66: Intensity of the NH_3 peak (965 cm^{-1}) versus time for GAS and AS.....	142
Figure 67: Elongation-at-break (%) and tensile strength (MPa) of PA6, PA6/GAS 5% and PA6/GAS 10% formulations.....	143
Figure 68: HRR curves versus temperature obtained with PCFC for PA6 and PA6/GAS formulations.....	144
Figure 69: pHRR of AS and GAS containing formulations in function of their loading	145
Figure 70: BSE picture (a) and EPMA sulfur cartography (b) of the cross section of PA6/GAS 5% fibers (circled in yellow)	146
Figure 71: BSE picture (a) and EPMA sulfur cartography (b) of the cross section of PA6/GAS 10% fibers (circled in yellow)	146
Figure 72: Experimental and theoretical TG curves of PA6/GAS 5% and PA6/GAS 10%, and their TGA difference curves (10 °C/min, air).....	147
Figure 73: FTIR spectra of the gases evolved during the thermo-oxidative degradation of PA6/GAS 5% (—) and PA6/GAS 10% (--) at characteristic temperatures of degradation.	148
Figure 74: TIC curves corresponding to the pyrolysis of PA6 between 350 °C and 490 °C, and PA6/GAS 5% between 366 °C and 490 °C	149
Figure 75: ^{13}C CP-DD-MAS NMR spectra of the PA6/GAS 5% formulation residues obtained after thermal treatment at 20, 270, 320, 410 and 500 °C (*: spinning sideband).....	151
Figure 76: Zoom made between 150 and 200 ppm on the ^{13}C CP-DD-MAS NMR spectra of the PA6/GAS 5% formulation obtained at room temperature	152
Figure 77: HRR curves versus temperature obtained with PCFC of PA6, PA6/AS/MPP formulations and PA6/AS 5%	158
Figure 78: TG and DTG curves of PA6/AS/MPP formulations and PA6/AS 5% (10 °C/min, air)	159
Figure 79: HRR curves versus temperature obtained with PCFC of PA6 and PA6/GAS/MPP formulations.....	160

Figure 80: TG and DTG curves of PA6/GAS/MPP formulations and PA6/GAS 5% (10 °C/min, air)	162
Figure 81: BSE picture (a), EPMA phosphorus cartography (b), EPMA sulfur cartography (c) of the cross section of PA6/GAS 2.5%/MPP 2.5% fibers (circled in yellow), and optical micrograph of the fiber (d) from microextrusion	165
Figure 82: BSE picture (a), EPMA phosphorus cartography (b), EPMA sulfur cartography (c) of the cross section of PA6/GAS 2.5%/MPP 2.5% fibers (circled in yellow), and optical micrograph of the fiber (d) from upscale.....	166
Figure 83: TG and DTG curves of PA6/GAS 2.5%/MPP 2.5% extruded at micro scale and larger scale (scale-up) (10 °C/min, air)	167
Figure 84: DSC thermograms of PA6 and PA6/GAS 2.5%/MPP 2.5% extruded at both scales	168
Figure 85: HRR curves versus temperature obtained with PCFC of PA6 and PA6/GAS 2.5%/MPP 2.5% formulations done with microextruder (μ extruder) and large scale extruder (scale-up).....	169
Figure 86: Cone calorimetry curves of PA6 and PA6/GAS 2.5%/MPP 2.5% formulation extruded at large scale (35kW/m ² , 25mm).....	170
Figure 87: Cone calorimetry residues of PA6 viewed from above.....	171
Figure 88: Char formation during the cone calorimetry experiment on PA6/GAS 2.5%/MPP 2.5%.....	172
Figure 89: Cone calorimetry residues of PA6/GAS 2.5%/MPP 2.5% viewed from above (yellow line: cross-section) (a) and view of the char cut in the cross section (b).....	173
Figure 90: PA6 sample tested at OI below 28 vol.-% (a) PA6/GAS 2.5%/MPP 2.5% sample tested at OI between 23-30 vol.-% (b) and between 31-36 vol.-% (c).....	173
Figure 91: PA6/GAS 2.5%/MPP 2.5% UL94 sample and cotton after test	175
Figure 92: DTG curve of PA6/GAS 2.5%/MPP 2.5% and intensity curves of ammonia, CO ₂ and caprolactam recorded during TGA-FTIR experiment	176
Figure 93: Comparison of FTIR intensity curves of ammonia, CO ₂ and caprolactam recorded during TGA-FTIR experiment for PA6/GAS 5% and PA6/GAS 2.5%/MPP 2.5%.....	177
Figure 94: FTIR spectra at 320 °C, 420 °C and 550 °C (corresponding to 32, 42 and 55 min) of gas released during PA6/GAS 2.5%/MPP 2.5% decomposition	177

Figure 95: TIC of PA6, PA6/GAS 5% and PA6/GAS 2.5%/MPP 2.5% corresponding to the main step of decomposition of each formulation	179
Figure 96: ¹³ C CP-DD-MAS NMR spectra of the PA6/GAS 2.5%/MPP2.5% residues obtained after thermal treatment at 20, 270, 320, 410 and 490 °C (*: spinning sideband).....	181
Figure 97: ³¹ P CP-HPDEC-MAS NMR spectra of MPP (*: spinning sideband)	182
Figure 98: ³¹ P CP-HPDEC-MAS NMR spectra of the PA6/GAS 2.5%/MPP2.5% residues obtained after thermal treatment at 20, 270, 320, 410 and 490 °C (*: spinning sideband) .	183
Figure 99: Enlargement of the aliphatic region of the ¹³ C CP-MAS NMR spectra of the PA6 (—) and PA6/AS residues obtained after thermal treatments at 20, 265, 323, 410 and 500 °C..	206
Figure 100: Digital microscope pictures of PA6/nanoGO 1% f1 (a) and f12 (b) formulations, dark dots correspond to nanoGO aggregates.....	207
Figure 101: Particle size distribution of f1 and f12 PA6/nanoGO 1% formulations	208
Figure 102: Mass spectrum of compound a.....	209
Figure 103: Mass spectrum of compound b	209

LIST OF TABLES

Table 1: Suggested notation for polymorphic forms of polyamide 6 [25].....	38
Table 2: Chemical shift assignments for nylon 6 spectra presented in Figure 8	40
Table 3: Band Assignments for Polyamide 6. Position in Wave Numbers (cm^{-1}) [42]	41
Table 4: Properties of PA6.....	42
Table 5: Thermal and fire retardant properties of the most commonly used fibers [55]	47
Table 6: Typical formulations for brominated fire retardants in PA6 [73]	58
Table 7: Limiting oxygen indices (vol.-%) for high molecular weight nylon 6 flame retarded with melamine or its salts [90]	64
Table 8: Cone calorimeter data of nylon-6 and nylon-6 clay nanocomposite [114]	70
Table 9: UL-94 and LOI results for different PA6/halloysite composites [125]	72
Table 10: Properties of PA6 Technyl S-27 BL natural S	82
Table 11: Selected flame retardants to be investigated in PA6.....	83
Table 12: Temperature profile of the extruder from hopper to die	85
Table 13: UL-94 criteria for classification	97
Table 14: Spinnability and PCFC results for commercially available FR solutions	103
Table 15: Spinnability and PCFC results for non-commercial FR solutions.....	107
Table 16: Parameters used for the extrusion of nanocomposite formulations	109
Table 17: Results of particles analysis from images of Figure 45	112
Table 18: Spinnability and PCFC results for NP formulations	114
Table 19: Diameters of PA6 and PA6/AS 5% formulations	123
Table 20: PCFC results for PA6/ammonium sulfamate formulations	124
Table 21: TTI, TTP, pHRR and THR of PA6 and PA6/AS 5%.....	127
Table 22: IR peaks assignment for PA6 and PA6/AS 5% [207]	133
Table 23: PCFC results for PA6/guanidine sulfamate formulations.....	144
Table 24: py-GC-MS degradation products of PA6 and PA6/GAS during the main degradation step, peaks numbers (#) are given on Figure 74	150
Table 25: PCFC results of PA6, PA6/AS 5%, and PA6/AS/MPP formulations.....	158
Table 26: PCFC results of PA6, PA6/GAS 5%, and PA6/GAS/MPP formulations.....	161
Table 27: Characteristic temperatures and enthalpies of the PA6 and PA6/GAS 2.5%/MPP 2.5% formulations	169

Table 28: PCFC results of PA6 and PA6/GAS 2.5%/MPP 2.5% formulations done with microextruder (μ) and large scale extruder	170
Table 29: Cone calorimetry data of PA6 and PA6/GAS 2.5%/MPP 2.5% formulation extruded at large scale (35kW/m ² , 25mm)	171
Table 30: UL-94 results for neat PA6 and for PA6/GAS 2.5%/MPP 2.5% extruded at large scale	174
Table 31: Start and end temperature of the main degradation step of py-GC-MS samples.	178
Table 32: Peak attribution of TIC from Figure 95 (Other attributions available in Table 24 p.152).....	180
Table 33: Results of particles analysis from images of f1 and f12 PA6/nanoGO 1% formulations.....	207

ABBREVIATIONS

APP	Ammonium polyphosphate
ATH	Aluminium tri-hydroxide
BSE	Back scattering electron spectroscopy
CCD	Charge-Coupled Device
CNT	Carbon nanotube
CP	Crossed polarization
CT	Computed tomography
DD	Dipolar decoupling
DSC	Differential Scanning Calorimetry
EDS	Energy-dispersive X-ray spectroscopy
EG	Expandable graphite
EPMA	Electron probe microanalysis
EVA	Ethyl vinyl acetate
FR	Fire retardant
FTT	Fire testing technology
HRR	Heat release rate
IR	Infrared
LOI	Limiting oxygen index
MAS	Magic angle spinning
MLC	Mass loss cone calorimeter
MMT	Montmorillonite
Mw	Molecular weight
MWCNT	Multi-wall carbon nanotube
NMR	Nuclear magnetic resonance
NP	Nanoparticle
OMMT	Organomodified montmorillonite
OMPOSS	OctaMethyl Polyhedral Oligomeric Silsesquioxanes
PA	Polyamide
DiPER	dipentaerythritol
PET	Polyethylene terephthalate
pHRR	Peak of heat release rate
PLA	Polylactic acid
PMMA	Polymethyl methacrylate
POSS	Polyhedral oligomeric silsesquioxanes
PP	Polypropylene
PU	Polyurethane
SEM	Scanning electron microscopy
TGA	Thermogravimetric analysis
TGA-FTIR	Thermogravimetric analysis – Fourier transformation infrared
THR	Total heat release
TIC	Total Ion Chromatogram
TO	Tubular oven
wt.	Weight

GENERAL INTRODUCTION

Since the end of the XIXth century, synthetic polymers have constantly been developed and used in many areas. Nowadays, polymers are found everywhere, mainly because of their relatively low cost, ease of manufacture, and good mechanical properties. They have already replaced many traditional materials, such as wood, stone, leather, metal or glass.

The plastic production has really started to grow fast in the 1950s, just after the Second World War, and has almost never decreased since that time (**Figure 1**). Only the oil shocks of 1973 and 1979 and the 2008 crisis have slowed down or decreased the worldwide production of plastics.

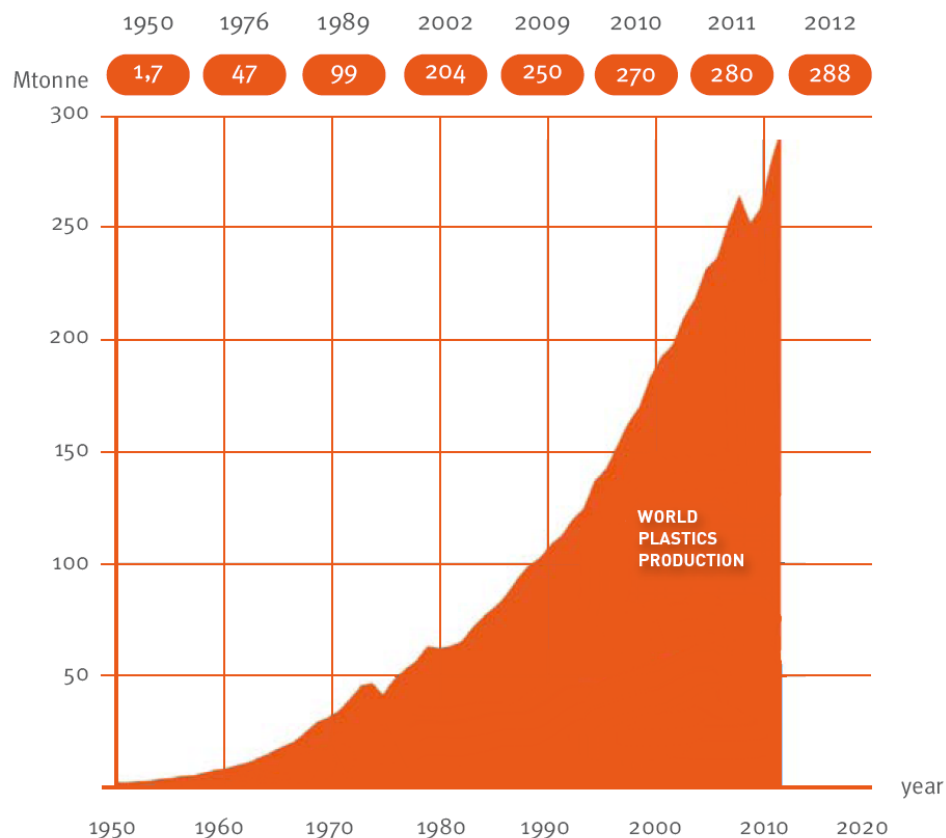


Figure 1: World plastics production 1950-2012, adapted from [1]

However, most polymers, due to their organic nature, will easily burn when submitted to heat or flame. This hazard might slow down the expanding use of plastics in some applications where stringent fire regulations and safety levels must be met.

Statistics in the US report that 1,375,000 fires occurred in 2012 [2]. This corresponds to a fire every 23 s. More tragically, it caused one civilian fire death every 3 hours and 4 minutes. 16,500 civilian injuries and \$12.4 billion in property damage are also reported. Consequently, fire is a major security and economic issue for anyone and everyone.

In order to inhibit, suppress, or delay the production of flames and to prevent the spread of fire, flame retardants can be used. They are usually added to manufactured materials, such as plastics and textiles. Historically, they are used for a long time. As an example in 360 B.C. timbers were coated with vinegar or alum to protect them against fire [3]. Obadiah Wyld received the first patent in Great Britain for developing a flame-retardant mixture of alum, ferrous sulfate and borax in 1735 [4]. Fabrics, textiles and fibers have long been regarded as hazardous materials in case of fire. In 1821, Gay-Lussac published a list of substances found to effectively improve fire resistance of fabrics used for theater curtains [5].

Since the development of polymers, many natural fibers have been replaced by synthetic fibers made from polyolefins, polyesters or polyamides. Polyamide fiber demand in particular is linked to the dynamics of the construction industry, home textiles or automotive industries. In those sectors, flame retardant properties are required and thus polyamide fiber faces strong competition from polyester fiber, for which acceptable flame-retardant solutions already exist. Indeed, one of the classical solutions to flame retard polyester is to incorporate a comonomeric phosphinic acid unit into the PET polymeric chain (trade name Trevira CS). In this context, the global objective of this work is to develop flame retardant composition suitable for use in polyamide 6 (PA6) fibers. Melt-spinning technique is chosen to bring durability of the flame retardant effect. Ultimately, the innovative formulations are expected to have good mechanical properties and to be processable using the traditional processing textile technologies.

First of all, a good knowledge of the materials is required to investigate new solutions for the flame retardancy of PA6 fibers. Consequently, the first chapter reviews the principal methods used for its production (polymerization). Its performances and applications are also discussed, with a focus on its uses as synthetic fibers. The different techniques developed for flame retarding textiles are detailed with respect to the different constraints. In order to

speed-up the selection process of potential flame retardant additives, the fundamentals of flame retardancy of PA6 is also reported.

The second chapter introduces the different materials investigated in this work, the PA6 matrix and the selected FR are detailed. The processing techniques used to melt-spin the different formulations into monofilaments are described, as well as the methods used for their characterization. The tools used to evaluate the thermal and flame retardant behavior of the formulations are finally presented.

In the third chapter, the screening step of the project is presented. According to the literature review, it was proposed to evaluate phosphorus and sulfur based fire retardants, as well as nanoparticles. The effects of the different additives are evaluated; the considered properties are the spinnability of the formulations and their fire behavior. Fire and thermal properties are measured using micro calorimetry and TGA. The dispersion of the nanoparticles is also considered.

Chapter fourth investigates the use of sulfamate salts as fire retardants for polyamide 6 fibers. The mechanical properties of the melt-spun fibers and the additives dispersion are examined. The optimization of the different formulations by varying the FR loadings is also detailed. Eventually, the modes of action of sulfamate salts in the gas phase and in the condensed phase are investigated in order to understand the fire behavior of the formulations.

Finally, in the last chapter, the best candidate studied in the previous chapter is selected for scale-up. The aim of this part is to find a solution allowing the extrusion of a formulation containing a sulfamate salt at large-scale. Indeed, all formulations were, until here, easily microextruded. Scaling-up the process turned out to be difficult as degradation issue occurred. The use of a co-additive appeared to be an interesting way to lower the sulfamate loading while keeping or enhancing the fire properties.

I	STATE OF THE ART: FLAME RETARDANCY OF PA6	
I.1	Introduction.....	29
I.2	Polyamide 6.....	31
I.2.1	Polyamides	31
I.2.2	Polyamide 6 polymerization.....	31
I.2.2.1	High temperature, water-catalyzed melt polymerization _____	32
I.2.2.2	Anionic chain polymerization using base initiators _____	34
I.2.3	Processing and spinning	35
I.2.4	Structure.....	37
I.2.4.1	NMR _____	39
I.2.4.2	FT-IR _____	40
I.2.4.3	Differential scanning calorimetry _____	41
I.2.5	Properties of polyamide 6	41
I.2.6	Applications.....	42
I.2.7	Thermal decomposition and flammability	43
I.2.7.1	Thermal decomposition _____	44
I.2.7.2	Flammability _____	46
I.3	Textile fibers and flame retardancy.....	48
I.3.1	General overview	48
I.3.2	High performance fibers	49
I.3.3	Flame retardant finishings	50
I.3.4	Flame retarding fibers with additives	51
I.4	Polymers flame retardancy.....	52
I.4.1	Combustion and thermal decomposition processes	52
I.4.2	Flame retardants mode of action.....	54
I.4.2.1	Halogen-containing flame retardants _____	56
I.4.2.2	Phosphorus-containing flame retardants _____	58
I.4.2.3	Melamine and its derivatives _____	61
I.4.2.4	Sulfur containing fire retardants _____	64
I.4.2.5	Metal hydroxides _____	65
I.4.2.6	Boron containing compounds _____	66

Chapter 1: State of the Art

I.4.2.7	Nanoparticles _____	68
I.4.2.7.1	1D nanoparticles	68
I.4.2.7.2	2D nanoparticles	72
I.4.2.7.3	3D nanoparticles	74

I.1 INTRODUCTION

Polymers are part of our everyday life; they are widely used because of their unique properties, among them: low weight, low cost and ease of processing. Many parts are made in polymer in general and in polyamide 6 in particular for transportation, electronics & electrical devices, consumer goods, building and construction, packaging or even textile. Its use is due to exceptional properties including flexibility, dimensional stability, abrasion resistance, durability, rigidity, dyeability, recyclability and excellent covering properties [6]. European Union, with 44% share of the total consumption is by far the largest user of polyamide in the World. North America and Asia each account for 25% share [7]. However, polyamide (and polymers in general) has a major drawback: its flammability. In case of fire, polymers will easily burn and often produce toxic smokes, therefore there is a real need to use and develop flame retardants to reduce the risks.

Flame retardants represent a large group of chemicals that consist mainly of inorganic and organic compounds based on bromine, chlorine, phosphorus, nitrogen, boron, metallic oxides and hydroxides. Flame retardant properties can also be achieved by other means than flame retardant chemicals, that is to say, through materials design and barrier technologies. Chemical flame retardants are either additive or reactive. Reactive flame retardants are added during the polymerization process or grafted onto the polymer chain and become an integral part of the polymer. The result is a modified polymer with flame retardant properties but processing a different molecular structure compared to the original polymer. Additive flame retardants are incorporated into the polymer prior to, during, or more frequently after polymerization. Additive flame retardants are molecules that are not chemically bonded to the polymer. They may therefore, in contrast to reactive flame retardants, be released from the polymer and thereby also discharged to the environment.

Among the products made of polyamide 6 a large part are textile fibers, and are used in a variety of industries. Due to these multiple uses, polyamide 6 fabrics must be fire retarded. Some regulations, specifications or standards exist to ensure that materials or products meet certain levels of safety regarding their ignitability and post ignition fire behavior. Among them, the Consumer Protection Act [8] regulates requirements in the UK; in France, NF P.92.507 [9] and NF EN 13501-1 (Euroclasses) [10] must be met in particular cases.

Chapter 1: State of the Art

NFPA 701 [11] is a voluntary industry specification in the US regarding the flammability of fabrics, it is one of the most widely quoted flammability specification for specialty fabric products in the United States.

In this chapter, after an overview of the polyamides and PA6 particularly (Section I.2), we will report the different strategies that can be followed to develop flame retarded fibers and textiles (section I.3). Then, we will review different fire retardants that are or were used in polyamides and focus on PA6 (Section I.4). Finally, we will present the strategies followed in this study.

I.2 POLYAMIDE 6

I.2.1 POLYAMIDES

Polyamide is a family of thermoplastic polymers having a recurring amide group. The amide group can be obtained from the reaction of dicarboxylic acids and diamines (eg. PA6.6) or by the ring opening of lactams (eg. PA6). Development of polyamides is closely linked to the development of two members of this polymer family: polyamide 6 and polyamide 6-6.

The first synthesis of the poly(ϵ -caproamide) was done in 1889 upon heating the ϵ -aminocaproic acid. However, the interest in finding ways to synthesize polyamides grew up only in the 1930s. At that time, two groups, Du Pont and IG Farben, were working on the production of synthetic spinnable polyamides: In the United States, at Du Pont, a lot of works done by the American chemist W. Carothers led to patents about the synthesis of polyamides with aliphatic aminoacids and particularly in 1936 the discovery of the polyamide 6.6 made from adipic acid and hexamethylenediamine [12]. In Germany, at IG-Farbenindustrie, researches by P. Schlack allowed in 1938, the discovery of a way to synthesize polyamide 6 by polymerization of the ϵ -caprolactam with a small amount of water [13].

The industrial development of these two polymers was accelerated during the World War II when the mass production of synthetic fibers was launched to face the shortage of silk used in military equipment. As early as October 1939, nylon (commercial trade name of PA6.6) appeared on the American market, followed in 1940 by PA6 in Germany.

PA6.6 and PA6 continue to be the most popular types, still accounting for more than 90% of nylon use. In recent years there has been increasing interest in polyamides with higher melting points to extend the boundaries of this polymer type and to satisfy more stringent high temperature automotive and electronic applications. This has resulted in the development of PA4.6 and several semi-aromatic nylons [14].

I.2.2 POLYAMIDE 6 POLYMERIZATION

Generally speaking, polyamides can be synthesized by direct amidation where an amine reacts with a carboxylic acid with the removal of water. PA6 is made from ϵ -caprolactam, which is a cyclic amide. This kind of monomer requires other polymerization techniques as

there are no amine and/or carboxylic groups on it. ϵ -caprolactam polymerization (**Figure 2**) starts with the opening of the ring structure followed by condensation and addition [**15, 16**]. The two ways used to produce PA6 will be discussed in the following section.

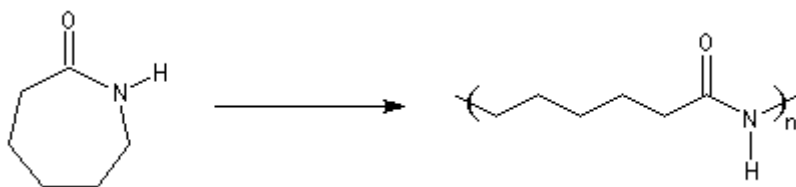


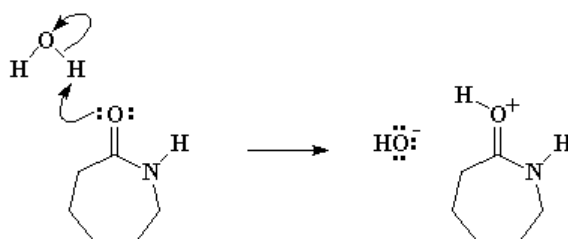
Figure 2: Polyamide 6 synthesis from ϵ -caprolactam

I.2.2.1 HIGH TEMPERATURE, WATER-CATALYZED MELT POLYMERIZATION

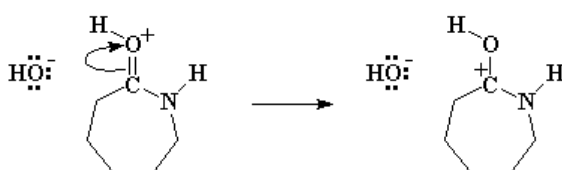
In the industry, the ring opening polymerization of ϵ -caprolactam is initiated by water and typical temperatures applied are 250 - 260°C and the pressure is up to 10 bars. From a mechanistic point of view, this ring-opening polymerization takes place in two main steps, the first being the ring-opening of the caprolactam by water [**17**] and the second is the polycondensation.

In presence of water, the caprolactam carbonyl function is protonated (**Figure 3 – Step 1**), then an electronic rearrangement occurs to form a carbocation (**Figure 3 – Step 2**). The free hydroxyl group attacks the carbocation and gives an unstable cyclic diol (**Figure 3 – Step 3**) which opens its ring to produce a linear amino acid, the ϵ -aminocaproic acid (**Figure 3 – Step 4**).

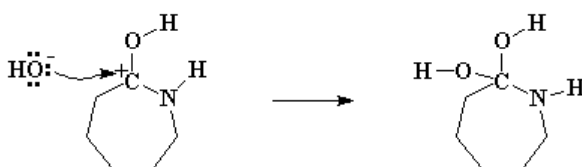
Step 1: Carbonyl protonation from water



Step 2: Electronic rearrangement giving a carbocation



Step 3: Nucleophile attack giving an unstable diol



Step 4: Ring opening rearrangement giving a linear amino acid

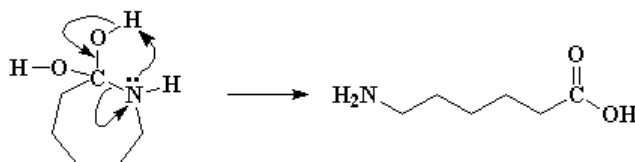
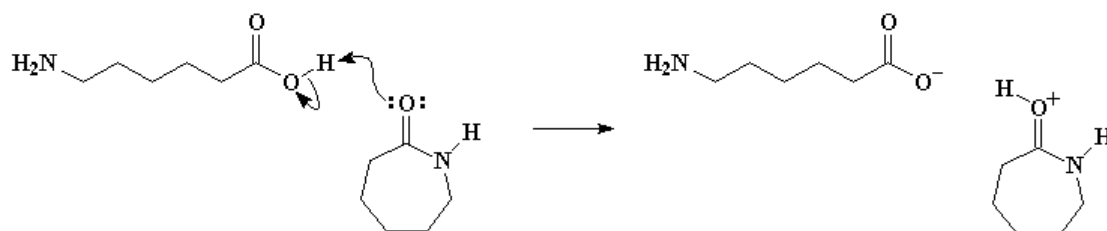


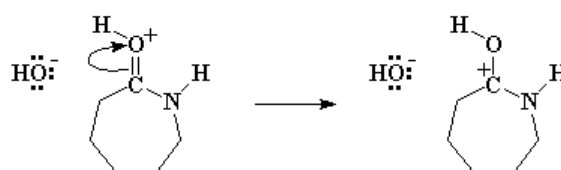
Figure 3: Ring opening of caprolactam by water

The next main step is the ring-opening of the caprolactam by the previously formed amino acid (**Figure 4**). The linear amino acid can react with a caprolactam molecule, like the water molecule did. The caprolactam carbonyl function is protonated (**Figure 4 – Step 1**) then again an electronic rearrangement occurs to form a carbocation (**Figure 4 – Step 2**). This carbocation is attacked by the nucleophilic amino acid that just lost its acid hydrogen and it gives an ammonium specie (**Figure 4 – Step 3**). This specie goes through a ring-opening rearrangement and produces a cationic linear molecule (**Figure 4 – Step 4**). Finally, an intramolecular rearrangement gives the dimer. This ring opening reaction of the caprolactam occurs again and again and finally gives long chains of polyamide 6 polymer.

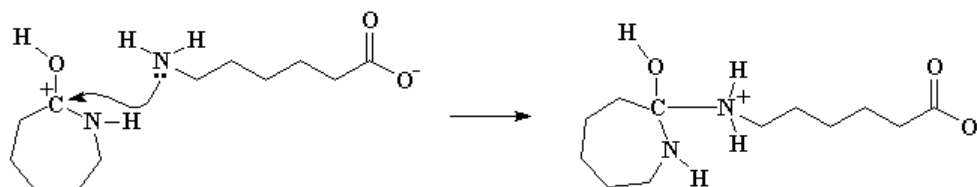
Step 1: Carbonyl protonation from the newly formed amino acid



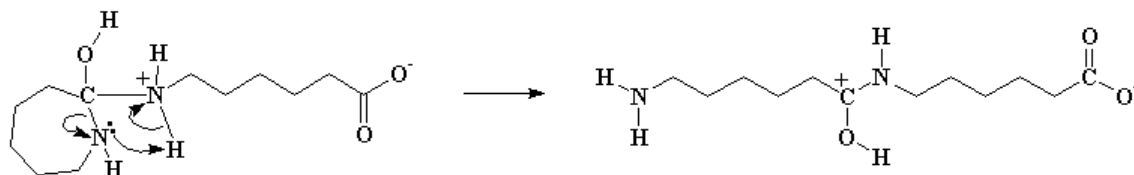
Step 2: Electronic rearrangement giving a carbocation



Step 3: Nucleophile attack giving an ammonium specie



Step 4: Ring opening rearrangement giving a linear molecule



Step 5: Intra-molecular rearrangement giving the dimer

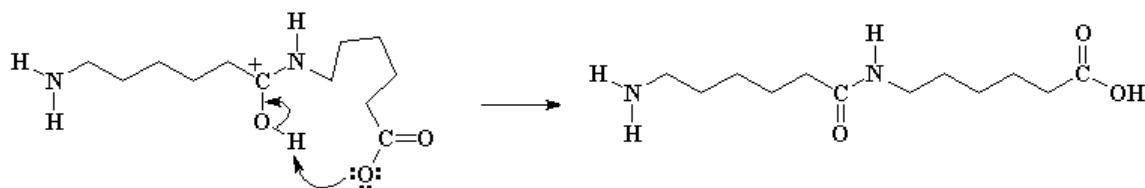


Figure 4: Ring opening of caprolactam by the amino acid

1.2.2.2 ANIONIC CHAIN POLYMERIZATION USING BASE INITIATORS

The anionic chain polymerization requires lower temperatures, around 100°C, and strong base initiators like Na [18]. The initiation of the lactam polymerization occurs in two steps. Caprolactam first reacts with Na to give lactam anion (**Figure 5 – Step 1**). In the second step of the initiation process, the lactam anion (the activated monomer) attacks the carbonyl

function of caprolactam and adds to it. Ring-opening leads to the formation of N-caproylcaprolactam anion (**Figure 5 – Step 2**). Thus another species is generated that can react again in the same manner. This happens over and over to produce a long chain of polyamide 6 (**Figure 5 - Resulting polymer**) [16].

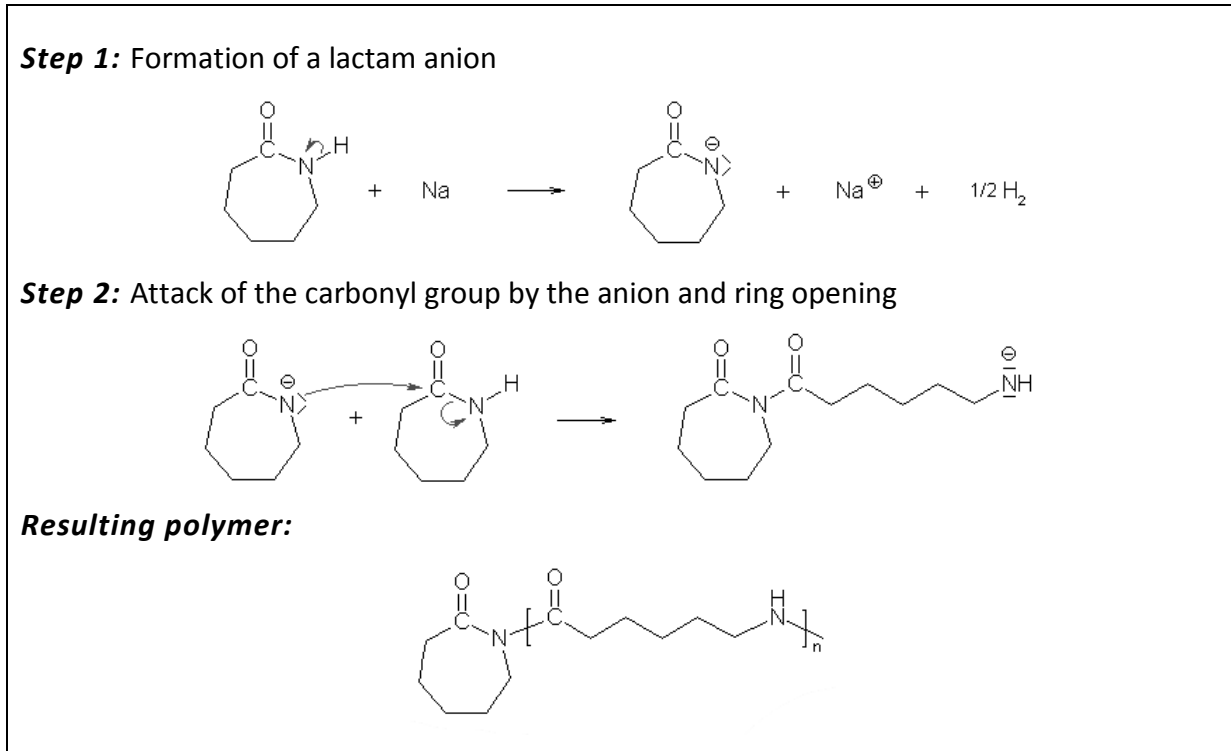


Figure 5: Anionic polymerization

1.2.3 PROCESSING AND SPINNING

There is a large range of PA6 grades and blends available on the market for different applications [19]. Among them we can cite: injection molding, film extrusion, blow molding, wire and cable, extrusion and spinning.

Nylons need to be processed dry to avoid molecular weight loss and processing problems. For example, **Figure 6** indicates both the usable moisture range for nylon-6,6 and nylon-6 in injection molding and the relationship with melt temperature. Extrusion applications require lower moisture contents (max 0.1-0.15% for nylon-6,6 and nylon-6) as do some other nylon types (e.g., max 0.1% for nylon-11 and nylon-12; 0.05% for nylon-4,6). Material that has absorbed some moisture can be re-dried using a vacuum oven at 80°C or a dehumidifier hopper drier [14].

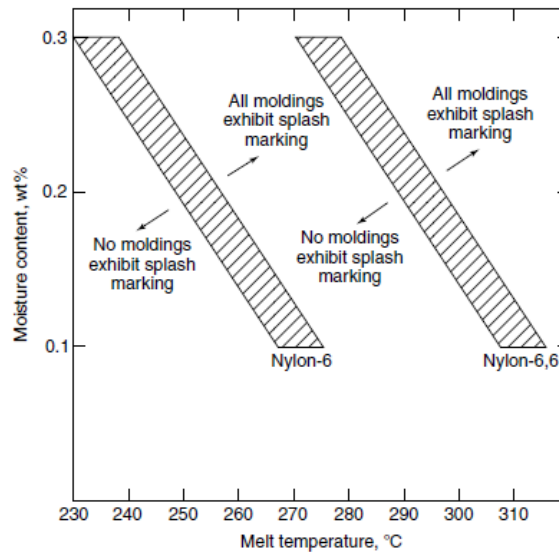


Figure 6: Relationship between moisture content and temperature for an unvented cylinder during injection molding [14].

Material should not be processed at a too high temperature, e.g., preferably not above 290 °C for nylon 6, in order to avoid degradation. Residence times at the higher temperatures should be kept to a minimum. Exposure of molten and hot nylon to air should also be minimized to avoid yellowing of the material.

Melt spinning is the most used process to obtain fibers since it is easy and rather cheap. It is well adapted to thermoplastic polymers having well defined melting temperatures such as polyesters, polyolefins and polyamides. During the process, it is important to control the melt temperature in order to obtain a suitable viscosity for extrusion through the spinneret, while avoiding thermal degradation of the polymer (or of its additives).

Generally, two melt spinning methods can be applied. A two-step method comprising spinning and drawing; the molten polymer is extruded through a spinneret and the melt solidifies into a filament. At this stage, the filaments have little molecular orientation and in order to achieve desirable properties through molecular orientation and crystallinity, the newly formed filaments must be drawn. Nylon can be cold drawn at room temperature. Hot drawing is also frequently used. Nylon filaments are drawn approximately four times their initial length. Drawing PA6 fibers affects physical properties such as elastic modulus (which increases with increasing orientation), density equilibrium, moisture sorption, tenacity and elongation-at-break.

A one-step method also exists: high-speed spinning which is being used increasingly. In high-speed spinning, filament windup speed relative to the extrusion speed is very high and orientation and crystallization occur in elongation flow along the spin line.

Some alternatives to the two conventional melt spinning methods described above exist. Various solution-spinning techniques have been introduced [20, 21]. Solution spinning techniques (gel, wet, dry) enable the spinning of high molecular weight polyamides. New technologies producing micro fibers have also been developed and reported [22]. First, direct spinning is done and then post-spinning processes are applied. Electro spinning [23] is another approach to fiber spinning, it uses electrical forces to produce polymer fibers with nanometer-scale diameters.

I.2.4 STRUCTURE

Polyamide 6 is a semi-crystalline polymer, and thus crystalline arrangements of the polymers exist. A review of the literature shows that a plethora of crystalline, paracrystalline and/or mesomorphic forms have been reported, with different authors sometimes using different notations for the same or very similar forms. The situation has been discussed by Gianchandani *et al.* [24]. Briefly, they suggest that it exists an amorphous phase (I) and two basic types of crystalline or paracrystalline forms, as illustrated in **Table 1**, referred to as α -type (II) or γ -type (III) [25].

Table 1: Suggested notation for polymorphic forms of polyamide 6 [25]

I.	Amorphous (vitrified liquid)
II.	α -phase type <ul style="list-style-type: none"> A. α monoclinic (stable equilibrium phase of Holmes <i>et al.</i> [26]) B. α' monoclinic (paracrystalline α-form of Roldan and Kaufman [27], metastable α form of Parker and Lindenmeyer [28]) C. α^* pseudo-hexagonal (same as Illers <i>et al.</i> [29] γ^* form, low orientation β form of Ziabicki [30], pleated α form of Stepaniak <i>et al.</i> [31, 32], probably same as γ "nematic form" of Roldan and Kaufman)
III.	γ -phase type <ul style="list-style-type: none"> A. γ monoclinic (prototype, stable or metastable phase of Arimoto [33] or Kinoshita [34], same as Bradbury [35, 36] orthorhombic) B. γ^* pseudo-hexagonal (β form of Roldan and Kauffman, γ of Vogelsong [37], high orientation β form of Ziabicki)

The ideal prototype for the α -type structure is the generally accepted equilibrium structure of Holmes *et al.* [26]. This structure is monoclinic with $a = 0.956$ nm, $b = 1.724$ nm (chain axis), $c = 0.801$ nm, and $\beta = 67.5$. The chains are fully extended and arrange in antiparallel hydrogen bonded sheets. The prototype for the γ -type structure is the monoclinic γ -form of Arimoto [33] with $a = 0.933$ nm, $b = 1.688$ nm (chain axis), $c = 0.933$ nm, and $\beta = 59^\circ$. The shortened chain-axis repeat distance is interpreted to correspond to a "kinked" or pleated hydrogen bonded sheet structure in which the hydrogen bonding occurs between parallel rather than antiparallel chains (**Figure 7**). For the α form of nylon-6, the adjacent chains are antiparallel and the hydrogen bonding is between adjacent chains within the same sheet (bisecting the CH_2 angles). For the γ form, the chains are parallel and the hydrogen-bonding is between chains in adjacent sheets.

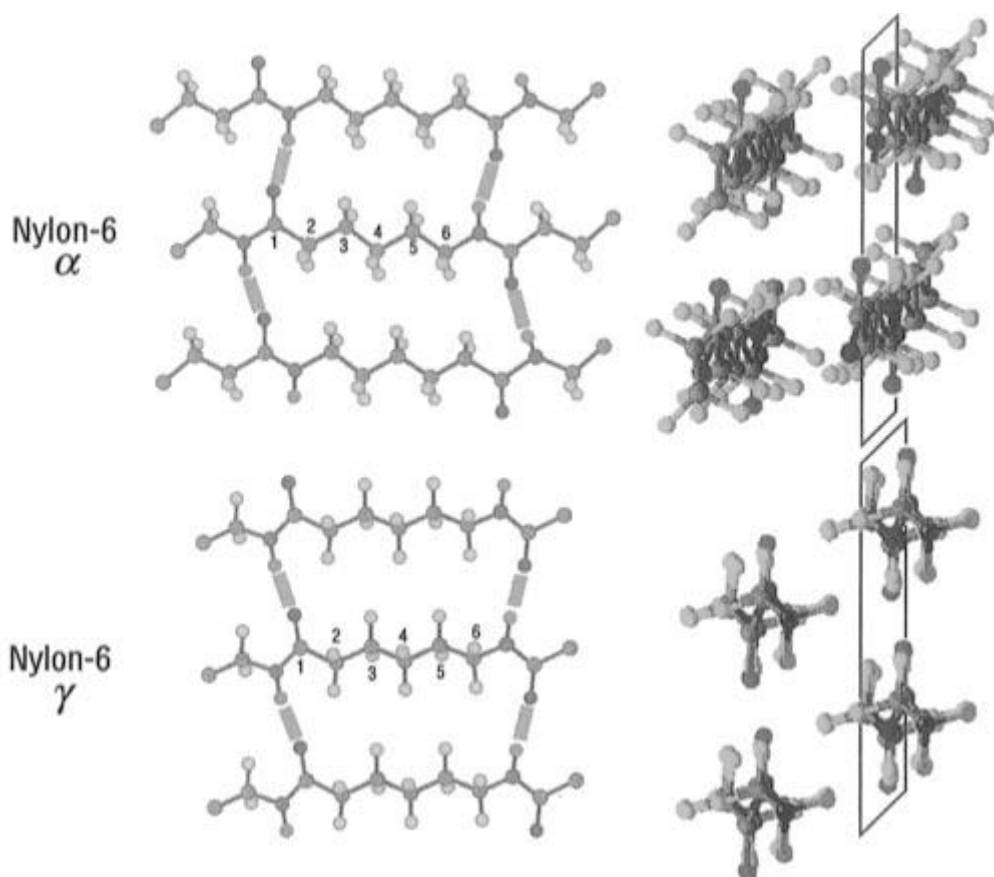


Figure 7: Structures of the α and γ forms of nylon 6 The left side shows the view of the hydrogen-bonding planes, and the right side shows the view down the chain axis [38].

Different techniques have been used to determine the structure of PA6 such as Differential Scanning Calorimetry (DSC) or Wide Angle X-ray Scattering (WAXS), Nuclear Magnetic Resonance (NMR) or even Fourier Transform Infrared Spectroscopy (FTIR).

1.2.4.1 NMR

Solid state NMR can be effective to identify the structure of the crystalline phases of PA6. Moreover, the amorphous phase can be characterized too, using special pulse sequences like BDMAS (Bloch Decay - Magic-Angle Spinning) to obtain spectra of only the amorphous fraction of the sample [39].

Thanks to the ^{13}C and ^{15}N NMR, the morphologic characterization of PA6 can be achieved. **Figure 8** and **Table 2** show the chemical shifts of the different carbons of PA6 depending if it is α or γ phase [40]. It is also reported that the orientational and structural changes in polyamide 6 yarns due to drawing [41] can be investigated using solid state NMR. It appears

that the drawing ratio considerably changes the crystallinity of the PA6 fiber, and thus its mechanical properties.

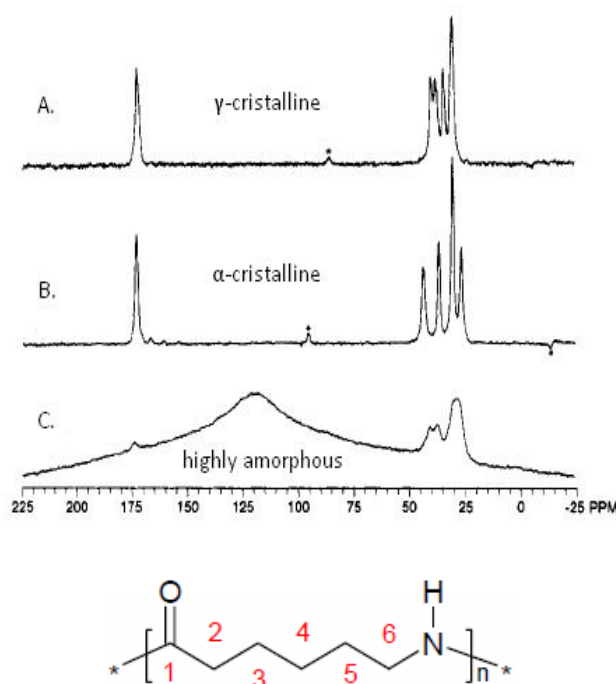


Figure 8: ^{13}C NMR (CP) spectra that discriminate in favor of the crystalline phase for samples that are high in γ crystallinity (A) and high in α crystallinity (B), ^{13}C NMR (BD-MAS) spectra that discriminate in favor of the amorphous phase for samples that were predominantly amorphous(C) [39].

Table 2: Chemical shift assignments for nylon 6 spectra presented in Figure 8

Spectrum	Carbon number and chemical shift (ppm)					
	C1	C2	C3	C4	C5	C6
A	173.4	36.7	26.5	30.4	30.4	43.6
B	173.0	37.8	30.1	30.1	34.1	39.9
C	174.5	36.9	26.2	27.4	30.0	40.3

I.2.4.2 FT-IR

With FT-IR, it is also possible to distinguish the α - and γ -phases according to the wave numbers of the amides functions. The band assignments of α - and γ -phases are reported in **Table 3.** [42].

Table 3: Band Assignments for Polyamide 6. Position in Wave Numbers (cm⁻¹) [42]

α -form	γ -form	Assignments
1305 sh	1306 m	CH ₂ wagg and amide
1295 sh		
1271 m	1274 m	
1214 sh	1214 w	
1202 m		
1170 m	1170 m	CO-NH, skeletal motion (Am)
1124 m	1124 m	C-C stretch (Am)
1076 m	1081 m	
1074 m	1074 m	C-C stretch
1029 m	1029 m	
-	999 w	
983 m	983 m	CO-NH in plane
-	977 m	CO-NH in plane
960 m		CO-NH in plane
951 w		
930 m		CO-NH in plane
833 w		CH ₂ rocking

I.2.4.3 DIFFERENTIAL SCANNING CALORIMETRY

DSC is widely used in polymer science to determine thermal properties of materials. With this technique, we can distinguish the melting temperatures of the two main crystal structures of PA6. Ho *et al.* report that the γ -form and α -form have melting temperatures of 226 °C and 231 °C respectively [43]. In another study, it was shown that γ - and α -forms have melting temperatures of 214 °C and 223 °C respectively [44]. The difference between the two studies is due to the PA6 molecular weight. However, it can be concluded that the γ structure is less stable than the α form.

I.2.5 PROPERTIES OF POLYAMIDE 6

Chemical stability

The chemical reactivity of nylon is a function of the amide groups and the amine and carboxylic acid end groups. The aliphatic segment of the chain is relatively stable. PA6 is particularly resistant to oils and fats, even at high temperatures. However, PA6 is sensitive to some chemical substances (water, acid, amine), to UV radiation and to heat.

Generally, nylon 6 is insoluble in organic solvents, but soluble in formic acid, in some phenolic solvents, and in fluorinated alcohols such as hexafluoro-2-propanol. Dilute solutions of strong mineral acids, such as sulfuric and hydrochloric, weaken nylon fibers and hydrolyze

them at high concentration and elevated temperature. Strong oxidizing agents and mineral acids such as potassium permanganate solution and nitric acid degrade nylon. Nylon, however, can be bleached in most bleaching solutions common to household and commercial mill applications. Nylon can be hydrolyzed by water under pressure at 150°C and above. The amine end group of a nylon fiber can undergo the same reactions as primary amines, such as neutralization, acylation, and dehydrohalogenation of alkylbromides at elevated temperatures. The amine ends can also react with atmospheric contaminants, such as SO₂, nitrogen oxides and ozone, under ambient storage conditions. This phenomenon is referred to as aging and results in reduced acid-dye affinity. Polyamides are not impacted by humidity with temperatures up to 80°C which is not the case in the range of their processing temperature, that is why one needs to dry PA6 before using it. As mentioned above, nylon 6 is insensitive to bases but when heated in presence of amines and acids it results in a quick decrease of its molecular weight [45].

Physical properties

PA6 also has good physical properties such as abrasion resistance, low coefficient of friction, high tensile strength and good creep resistance. These properties are kept on a broad range of temperatures (-50 to 170°C). Some general properties of PA6 are listed in **Table 4**.

Table 4: Properties of PA6

Property	Value
100% elastic under 8% of extension	-
Glass transition temperature	47 °C
Melting point	220 °C
Amorphous density at 25°C	1.08 g/cm ³
Crystalline density at 25°C	1.23 g/cm ³
Moisture regain	4-4.5%

1.2.6 APPLICATIONS

Polyamide 6 is used in a wide range of applications (**Figure 9**); in automotive, door handles and radiator grills can be made from PA6 (**Figure 9 (a)**). In electric and electronic parts, polyamide is found in miniature circuit breakers, residual current devices, fuses, switches and relays, contactors and cabinets (**Figure 9 (b)**). Eventually, polyamide 6 is used in large applications in sport, such as ski bindings and in-line skates (**Figure 9 (c)**). This is because it has excellent fatigue properties and provides high impact and mechanical strength. It can

also be used in gun frames, such as those used by the weapons manufacturer Glock™, which are made with a special composite of nylon 6 and other polymers [46]. But PA6 is also widely used to make synthetic fibers. In 2006, over the global consumption of polyamide, which was about 7 million tons, fibers accounted for 60% [47].

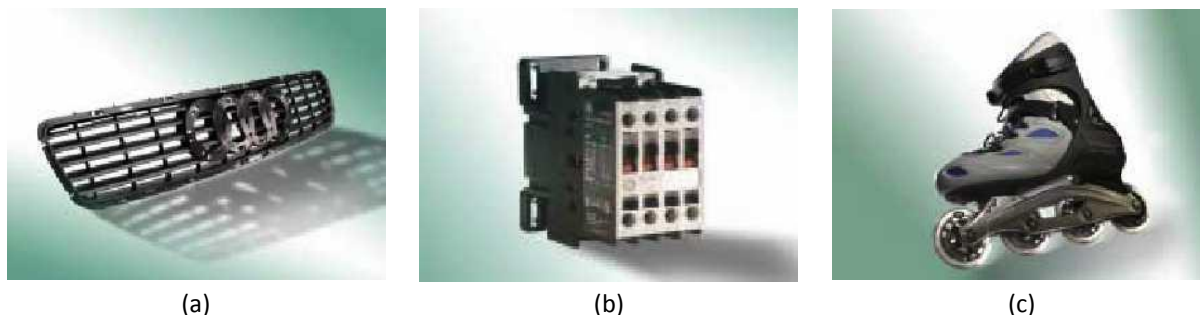


Figure 9: Examples of PA6 applications [48]

The original development of polyamides, initially PA6.6 then PA6, concentrated on their potential as fiber-forming materials where strength, elasticity, and high dye uptake were considered the most important properties, along with the ability to withstand ironing temperatures [14]. Thus, nylon 6 fibers are used in the manufacture of a large variety of threads, ropes, filaments, nets, and tire cords, as well as hosiery and knitted garments. But it is also used as thread in bristles for toothbrushes, surgical sutures, and strings for acoustic and classical musical instruments.

Approximately four million tons of nylon fibers are produced annually worldwide; nylon 6 and nylon 6.6 account for about 98% of the total production [49]. The advantages of nylon fibers over other synthetic fibers are high strength, durability, resilience, ease of dyeability, and low specific gravity [45]. Thus, nylon fibers are used in the flooring, apparel, industrial and transportation industries. However, one of the major drawback of PA6 fibers, and of most other synthetic fibers, is their flammability due to their organic composition. However, in some of the aforementioned applications, strict fire safety levels must be met.

1.2.7 THERMAL DECOMPOSITION AND FLAMMABILITY

As previously discussed, the organic nature of polymers like PA6 might be a problem in terms of flammability risk for certain applications. That is the reason why the material has to comply with strict fire safety requirements in these applications, as mentioned before. In this section, the thermal decomposition and flammability of polyamide 6 will be detailed.

The comprehension of the mechanisms involved in the decomposition of the polymer is very important when dealing with flame retardancy since the flammability is linked to the different gases evolved when the polymer degrades. Knowledge of the fire behavior of the materials also helps bringing solutions to particular problems linked with the burning of the materials.

I.2.7.1 THERMAL DECOMPOSITION

Despite the high level of research activity and the large number of publications in the field, there is no general accepted mechanism for the thermal decomposition of aliphatic nylons, as various experimental conditions might be favorable for one mechanism at the expense of others. The topic has been completely reviewed by Levchik *et al.* [50]. Many molecules and chain end reactive groups have been identified but their quantities and nature depends on multiple factors such as temperature ramp, temperature treatment or presence of a nucleophile as shown by Davis *et al.* [51] etc.

However, some main mechanisms have been identified: **Figure 10** shows that between 200 and 300°C and without nucleophile the thermal degradation of PA6 leads to the formation of the ϵ -caprolactam monomer. This formation often begins at temperatures slightly above 200 °C and primarily occurs by intramolecular endgroup cyclization (end-biting, **Figure 11A** and **B**) and cyclization within the polymer main chain (back-biting, **Figure 11C**). Monomer formation may also occur, but to a lesser degree, via intermolecular aminolysis and acidolysis between two polymer chains (**Figure 11D**).

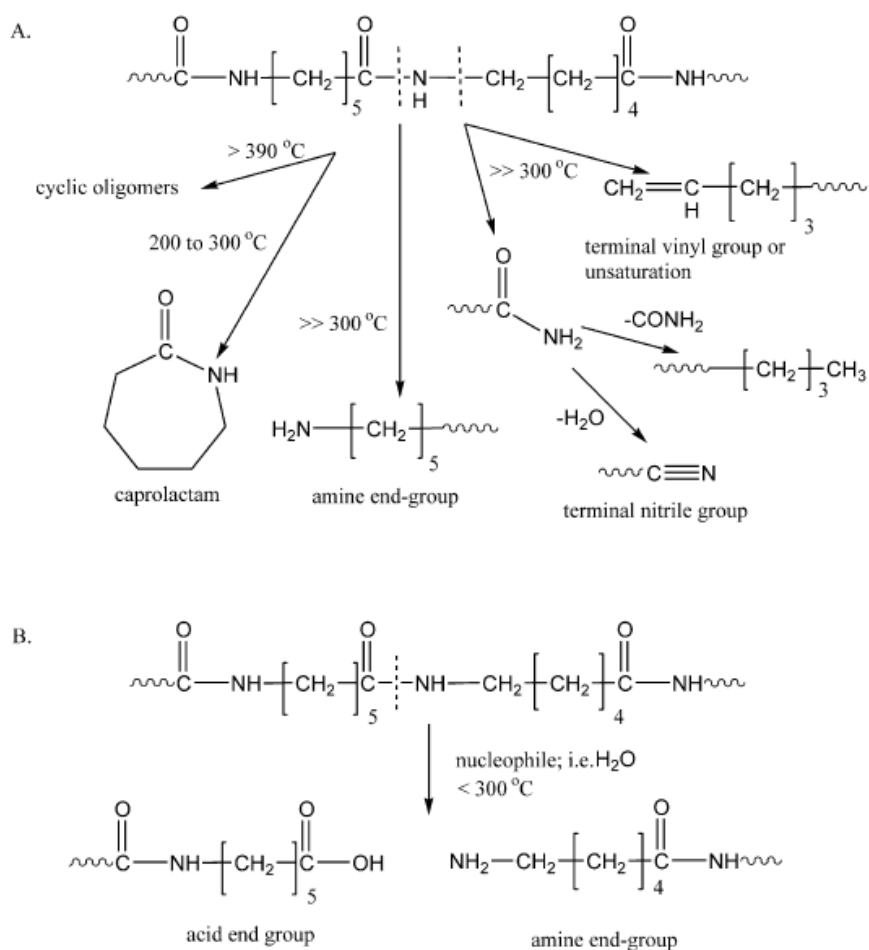


Figure 10: Dominant PA-6 thermal degradation products in the absence of a nucleophile (A) and in the presence of a nucleophile, such as water (B) [51]

Cyclic oligomers are also evolved during the decomposition of PA6 at temperatures above 390 °C. Without the presence of a nucleophile, the products of decomposition are mainly ϵ -caprolactam, cyclic oligomers and small gaseous molecules. Chain scission products are also detected, for instance, the scission of the thermally weakest bond $-\text{NH}-\text{CH}_2-$ leads to the formation of a terminal unsaturation and an amide group; the latter immediately decomposes to a terminal nitrile or methyl group.

In the presence of a nucleophilic molecule such as water or ammonia, or a nucleophilic additive, the decomposition of PA6 is different. Decomposition pathway is changed, and in this situation the weak bond is the $-\text{NH}-\text{CO}-$ (amide), which undergoes hydrolytic scission above 300 °C, and then homolytic scission of alkyl-amide bonds above 500 °C. Hydrolytic scission of the amide bond results in a significant decrease of PA6 molecular weight and an increase in PA6 end-groups.

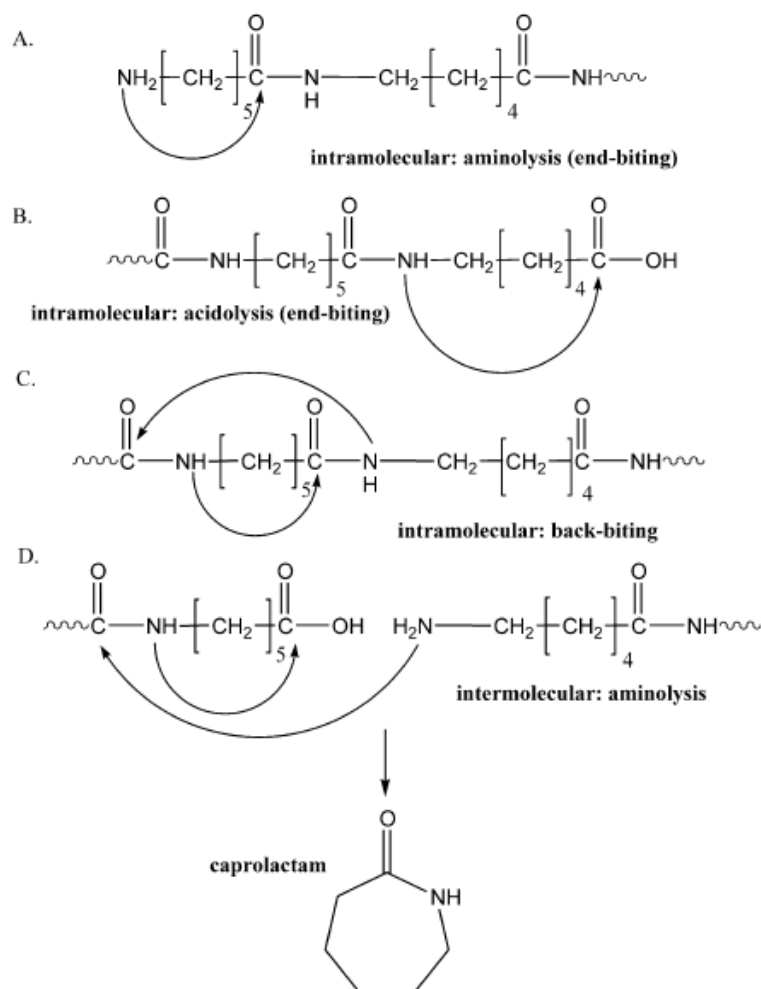


Figure 11: Intra- and intermolecular routes that generate ϵ -caprolactam [51]

1.2.7.2 FLAMMABILITY

Various methods have been used to study the flammability of aliphatic nylons. Reimschuessel *et al.* [52] observed differences between limiting oxygen index (LOI) values for various nylon 6 samples. It was assumed that the flammability of nylon 6 is directly related to the rate at which fuel is produced; therefore, a reciprocal relationship between the LOI and the rate of caprolactam generation should be expected. Furthermore, caprolactam generation was believed to be reciprocal to the molecular weight (intrinsic viscosity η) and proportional to the concentration of amine chain-ends (a) and carboxylic chain-ends (c). In fact, from the series of specially prepared nylons 6 with different molecular weight and different concentration of chain-ends, the **Equation 1** was proposed [52, 53].

$$LOI = 13.5 \times \left(1 + \frac{1}{\eta}\right) + \frac{2050}{(13.5a + ac)}$$

Equation 1

Aliphatic nylons are considered to have low flammability. However, this is an artifact, because low melt viscosity, which may be the result of degradation, contributes to the apparent low flammability. For example, low molecular weight nylon apparel fabric usually drips away when held in flame and does not continue to burn after dripping of the flamed material [54].

The burning behavior of fibers is influenced and often determined by a number of thermal transition temperatures and thermodynamic parameters. **Table 5** lists the commonly available fibers with their glass transition (T_g) and melting (T_m) temperatures, which may be compared with their temperatures of pyrolysis (T_p) and temperatures of ignition (T_c). In addition, LOI and heats of combustion are also compared. Generally, the lower the T_c (and usually T_p) the more flammable is the fiber.

Table 5: Thermal and fire retardant properties of the most commonly used fibers [55]

Fibre	T_g , °C (softens)	T_m , °C (melts)	T_p , °C (pyrolysis)	T_c , °C (ignition)	LOI, %
Wool			245	600	25
Cotton			350	350	18.4
Viscose			350	420	18.9
Nylon 6	50	215	431	450	20–21.5
Nylon 6.6	50	265	403	530	20–21.5
Polyester	80–90	255	420–447	480	20–21
Acrylic	100	>220	290 (with decomposition)	>250	18.2
Polypropylene	–20	165	470	550	18.6
Modacrylic	<80	>240	273	690	29–30
PVC	<80	>180	>180	450	37–39
Oxidised acrylic	—	—	≥640	—	—
Meta-aramid (eg Nomex)	275	375	410	>500	29–30
Para-aramid (eg Kevlar)	340	560	>590	>550	29

In **Table 5**, respective Limiting Oxygen Index (LOI) values are listed, which are measures of the inherent burning character of a material. Fibers having LOI values of 21% or below ignite easily and burn rapidly in air (containing 20.8% oxygen). Those with LOI values above 21% ignite and burn more slowly and generally when LOI values rise above approximately 26%–28%, fibers and textiles may be considered to be flame retardant and will pass most small flame fabric ignition tests in the horizontal and vertical orientations [56]. PA6, with its LOI

value can be described as easily flammable, as for the majority of fibers, except the high performance aramid fibers.

Flammability can also be assessed via other testing methods; UL-94 is a small scale test discriminating materials upon their ability to self-extinguish or spread the flame after ignition of the specimen. Dripping of the samples is also taken into account in this classification. In the literature [57-59] it is found that neat PA6 is non-classified, this means that PA6 burns easily. However in vertical burning test, PA6 is sometimes found autoextinguishable. Indeed, flame can be removed from the sample by dripping of the molten polymer; in this case it is noteworthy to mention that drips are burning.

Cone calorimeter has been used and adapted to the burning of textile fabrics [60]. The major drawback of this tool is the reproducibility and repeatability of the data considering fabrics. It appears that two principal sources influencing the results are coming from the cone itself (heat flux, ceramic backing pads and retaining grid) and from the sample (sample weight, textile construction and relative humidity).

Polyamide 6 burns, and consequently the fibers made from it. In the next section, a literature review describes the solutions that have been found to enhance the reactions to fire of synthetic fibers. The fire retardant strategies used for different kind of fibers are also reported.

I.3 TEXTILE FIBERS AND FLAME RETARDANCY

I.3.1 GENERAL OVERVIEW

The hazard arising from the burning of textiles has been recognized during early civilizations. At that time, natural cellulosic fibers cotton and flax (as linen), were treated with salts like alum to reduce their ignitability and so confer flame retardancy to textile. The fire risks is linked with the high specific surface area of the fiber-forming polymers, which enable maximum access to atmospheric oxygen [61].

The major difference between fibers and bulk polymers is the low thickness of individual fibers, typically 15-30 μm in diameter, yielding yarns of 50–100 μm diameter and fabrics having thicknesses varying from as low as 100 μm to several millimeters.

The burning behavior of fabrics containing a given fiber type or blend of fibers is influenced by a number of factors including the nature of the igniting source and time of its impingement, the fabric orientation and point of ignition (e.g. at the edge or face of the fabric or top or bottom), the ambient temperature and relative humidity, the velocity of the air and last but not least the fabric structural variables [61]. For example, low fabric area density values and open structures make worse burning rate and so increase the hazards of burn severity more than heavier and multilayered constructions as shown by Backer *et al.* [62].

To bring flame retardant properties to fibers, we can cite three methods; the use of high performance fibers, the inclusion of additives or reactive flame retardants into the polymer and the treatment of fibers or fabrics with flame-retardant finishes.

1.3.2 HIGH PERFORMANCE FIBERS

Most of the “everyday” fibers, like polyamide 6 belong to a category known as “commodity fibers”. However it exist a series of fibers called “high performance fibers”, usually referring to fibers with unique characteristics that differentiate them from commodity fibers. High tensile strength, operating temperature, heat resistance, flame retardancy and chemical resistance are among those properties.

Research and development on these fibers was initiated by the strong demand for heat-resistant and flame-retardant materials for space programs or industrial use after World War II [63]. Bourbigot and Flambard have reviewed the subject [64], and gave many examples of these fibers used in aerospace, biomedical, civil engineering, construction, protective apparel, geotextiles or electronic areas.

In order to stay close to the nylon fibers, only the aramids will be discussed. The term aramid is used when amid linkages are attached directly to two aromatic rings and are equal to or greater than 85% aromatic [45]. Meta and para-aramid fibers exist, they are better known under the names Nomex™ and Kevlar™ respectively when commercialized by DuPont. Meta-aramids are naturally nonflammable thanks to their aromatic structures including high carbon/hydrogen ratios and high contents of aromatic double bonds. Nomex™ is used in fire protective clothing, filtration, thermal resistant furnishing. It has a high LOI of 30-32 vol.-% and is thus self-extinguishing.

Even if these fibers present high fire retardant performances, it is out of the scope of this study since the main objective is to develop FR PA6 based fibers.

I.3.3 FLAME RETARDANT FINISHINGS

Flame retardant finishing can also be applied to bring flame retardancy to fibers or textiles. This is particularly useful in the case of natural fibers, where no additives can be directly put into the material during processing of fibers (spinning). Nonetheless, this method can be applied on synthetic fibers as well [65].

Common synthetic fibers like polyamide, polyacrylic and polypropylene have proved difficult to be effectively flame retarded [66] by the additive approach. Indeed, they do not have physical and chemical structures that are compatible with the most common functional flame retardants. During fiber production, the molten polymers are often highly reactive [67, 68] and so have low compatibility with many flame retardant additives. Eventually, the presence of quite high flame retardant concentrations (>20 wt.-%) necessary to confer flame retardant properties, not only creates spinning fluid compatibility problems but also causes serious reductions in ultimate fiber tensile strength and other essential textile properties.

Thus, the use of flame retardant finishes could be one of the solutions to enhance fire behavior of textiles. For polyamide, semi-durable finishes based on thiourea derivatives are often used but usually only on industrial nylon textiles where launderability is not an issue [66]. Durable but stiff flame retardant finishes based upon methylated urea–formaldehyde with thiourea–formaldehyde have been successfully applied to nylon nets for evening wear and underskirts [61]. This finish probably works by stimulating melt flow and dripping. It is or was commercially available as Flamegard® 908 (Sybron Chemicals) [69]. Some durable compounds initially designed for polyester are reported to be also effective for polyamide such as Antiblaze®CU/CT, developed by Albright & Wilson (now Solvay/Rhodia), which is a cyclic oligomeric phosphonate [61]. AFLAMMIT® NY (Thor) is a system of two compounds, comprising NY 1 and NY 2, the first being an organic nitrogen/sulfur FR, and the second a methylolated urea used as a reactive crosslinking component [70].

However, it has to be noted that the existing solutions to flame retard PA6 fibers by finishing of the fibers are rather limited and it implies additional steps in the processing of the materials as presented in **Figure 12**.

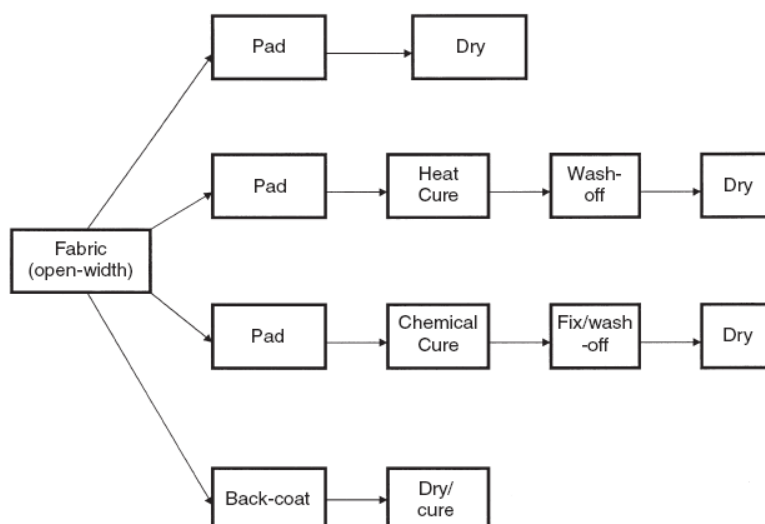


Figure 12: Summary of finishing and coating techniques [61]

The use of fire retardant additives or copolymers for some polymer is thus a more economical way of producing directly flame retarded fibers. Moreover, Drevelle *et al.* [71] studied and compared the use of finishing and the additive approach to flame retard polypropylene. They concluded that the second method is more efficient. This approach will thus be followed in this study and will be discussed in the next section.

1.3.4 FLAME RETARDING FIBERS WITH ADDITIVES

The direct incorporation of flame retardants in the molten polymer during extrusion seems to be the simplest way to make a fiber/textile fire retardant. However, problems of compatibility may occur at the high temperatures used during melt-spinning of polymers like polyamide, polyester and polypropylene [61]. This may prevent the successful incorporation of FR during the process, and consequently, only few fire retarded fibers are commercially available.

Trevira CS (Trevira GmbH, formerly Hoechst); is one of the most successful commercially available FR polyester fibers. It is produced by directly incorporating phosphinic acid units into the PET polymeric chain, forming a copolymer of PET and phosphinic acid. Other FR additives used in polyester to form fibers were reviewed by Horrocks [56] and Levchick and Weil [72], among them bisphenol-S-oligomer derivatives (Toyobo GH), cyclic phosphonates (Antiblaze CU and 1010, Rhodia), and phosphinate salts (Exolit OP950, Clariant). All these FRs do not promote char formation. Phosphonic acid comonomer (Trevira T271), ethoxylated

tetrabromobisphenol A comonomer (Dacron 900F, DuPont), tris(2,3-dibromopropyl) phosphate (TRIS) are also reported.

The high melt reactivity of polyamides [67, 68], and hence poor flame retardant compatibility, has prevented from the commercialization of FR PA6 fibers [61]. Moreover, most fire retardants need to be added in relatively high amounts to be effective in PA6 (they are reviewed in section 1.4.2). The high additive amounts can greatly reduce the strength of the melt-spun fibers. Consequently, no satisfactory solutions have been found yet [69, 73].

I.4 POLYMERS FLAME RETARDANCY

In the previous section, fire retardant finishes for textiles and synthetic fibers have been described. In this section, a general introduction on the burning of polymers is given, followed by a review of the fire retardant solutions developed for polyamides and particularly PA6. The modes of action involved in the enhancement of the fire properties will also be described. Finally the additives used for the flame retardancy of some synthetic fibers will be discussed.

I.4.1 COMBUSTION AND THERMAL DECOMPOSITION PROCESSES

In general it is considered that an external source supplies heat causing the temperature of the polymer to increase. Thus, physical, mechanical, and thermal properties change, it may involve softening in the case of polymers and then upon more heating, bonds begin to break. When the majority of the bonds reach failure point, there is a release of gaseous molecules, called fuel, which differ depending on the material that burns. Then in the presence of oxygen, oxidation of the fuel proceeds rapidly producing heat, flames, and combustion products. When the amount of heat released reaches a certain level, decomposition reactions are induced in the solid phase, and therefore more combustibles are produced. Thus, the combustion cycle, also called the fire triangle (**Figure 13**), is maintained.

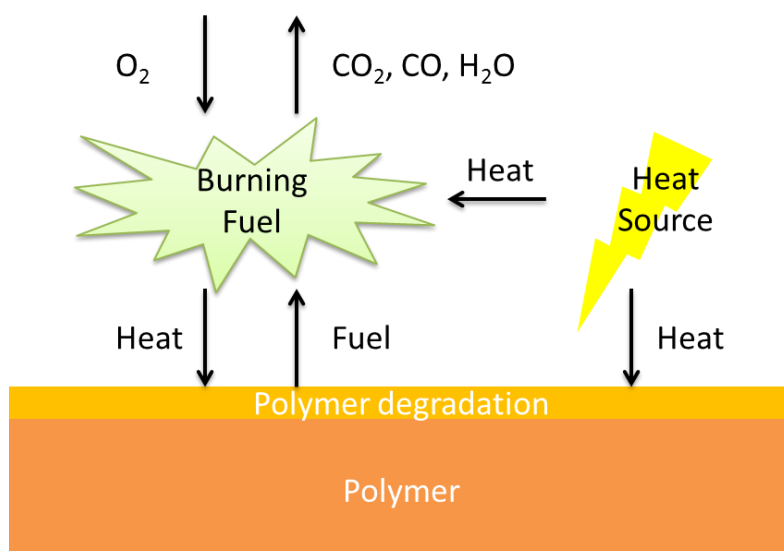


Figure 13: Combustion cycle

Upon thermal decomposition, many phenomena occur in the condensed phase: melting, hydrolyses, crosslinking, charring, dripping, volatile products diffusion and superficial accumulation of materials. Two thermal degradation mechanisms of macromolecules can be distinguished [74]:

- The non-oxidizing thermal degradation consisting in heterolytic or homolytic chain scissions. This degradation, also called pyrolysis, occurs under the simple effect of temperature. Chain scission can occur in two ways:
 - By formation of free-radicals ($R_1-CH_2-CH_2-R_2 \rightarrow R_1-CH_2\cdot + \cdot CH_2-R_2$), in this case, the reaction does not stop at this stage because these radicals start a chain/cascade reaction, which occurs under both oxidizing and non-oxidizing conditions.
 - By migration of hydrogen atoms and formation of two stable molecules one of which having a reactive carbon-carbon double bond ($R_1-CH_2-CH_2-CH_2-R_2 \rightarrow R_1-CH=CH_2 + CH_3-R_2$).
- The oxidizing thermal decomposition wherein the polymer or its degradation products react with oxygen of the air. A variety of products are generated through this mechanism: carboxylic acids, alcohols, ketones, aldehydes, etc. This degradation mechanism also results in the release of radical species (i.e. $H\cdot$ and $OH\cdot$) that are very reactive, particularly in polyolefins. Oxidation can lead to crosslinking through

recombination reactions of the macromolecular radicals. However, bond scission usually remains the dominant reaction.

I.4.2 FLAME RETARDANTS MODE OF ACTION

Flame retardant systems are intended to inhibit or to stop the polymer combustion process described above by acting either physically (cooling, fuel dilution, formation of a protective layer) or chemically (reaction in the solid or gas phase).

A simple schematic representation of the self-sustaining polymer combustion cycle is shown in **Figure 14**. Flame retardants act to break this cycle, and thus extinguish the flame or reduce the burning rate, in a number of possible ways [75]:

- by modifying the pyrolysis process to reduce the amount of flammable volatiles evolved in favour of increasing the formation of less flammable gases or of char ('a')
- by isolating the flame from the oxygen/air supply ('b')
- by introducing into the plastic formulations flame inhibitors compounds ('c')
- by reducing the heat flow back to the polymer to prevent further pyrolysis. This can be achieved by the introduction of a heat sink, e.g. aluminium trihydrate (ATH, $\text{Al}(\text{OH})_3$) which decomposes endothermically or by producing a barrier, e.g. char or intumescent coating, formed when the polymer is exposed to fire conditions ('d')

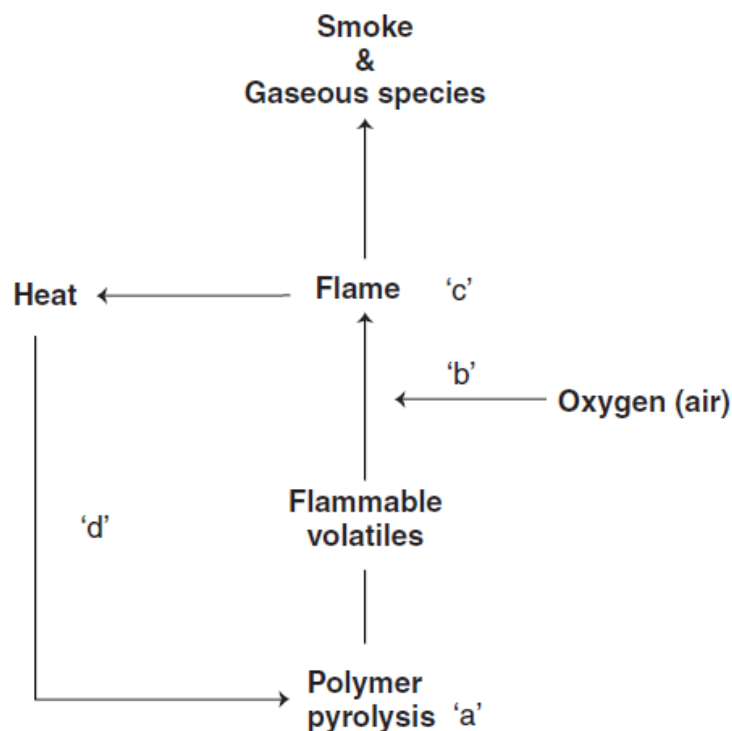


Figure 14: Schematic representation of the self-sustaining polymer combustion cycle; a-d represent potential modes of action of flame retardants [75]

Flame retardants can be classified in two categories:

Additive flame retardants: these are usually incorporated in the material during the polymer transformation process. In this case, the additives have to be thermally stable and of low volatility at the processing temperatures of the particular polymer so as to avoid losses.

Reactive flame retardants: these are incorporated into the polymer during synthesis (as monomer for instance) or during post reaction process such as grafting.

What are the usual flame retardant additives and what is their influence on the flame retardancy of PA6? The next sections aim at answering those questions by describing different classes of fire retardant (according to their chemical nature) and their mode of action. This literature review will mainly focus on additive flame retardants, indeed, this category is usually preferred for the main reason that handling and processing in that case are easier and therefore more cost-effective [74]. The selection of the literature is mainly based on the performance of the FR in polyamide and especially in PA6. With respect to the

special requirements of fiber spinning and as previously described, an emphasis on the FR efficient at low loadings is made. That is the reason why a particular attention will be paid to the use of nanoparticles in the field of fire retardancy.

I.4.2.1 HALOGEN-CONTAINING FLAME RETARDANTS

A wide variety of halogen-containing products have been suggested in the literature as fire retardants for aliphatic nylons. They can be used in combination with synergistic metal oxides, metal salts, phosphorus containing products or charring agents. The main advantage of halogen-based flame retardants is their effectiveness in unreinforced and reinforced nylons [76]. Pearce *et al.* [77] in their review, suggested three basic mechanisms of fire-retardant action of halogen-containing products in aliphatic nylons:

- i. Generation of free-radical and chain inhibitors. (**Figure 15**)
- ii. Promotion of char formation through dehydrogenation reactions
- iii. Formation of a layer of hydrogen halides which acts as a gas barrier between the fuel gas and condensed phases

Thermally induced polymer decomposition releases very reactive free-radical species such as $H\bullet$ and $OH\bullet$, which maintain combustion by a cascade-chain mechanism in the gas phase. Halogenated flame retardants are able to react with these species, stopping the chain decomposition and therefore the combustion of the polymer (**Figure 15**).

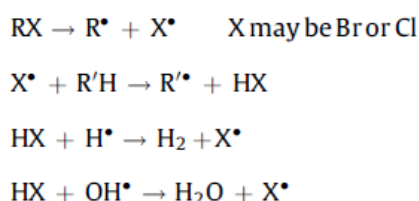


Figure 15: Quenching mode of effective halogen-based species

Cyclooctadiene, bis(hexachlorocyclopentadieno)cyclo-octane is one of the most popular chlorinated flame retardant for aliphatic nylons. It is known under the commercial names Dechlorane 515 or Dechlorane Plus (Oxychem) (**Figure 16**).

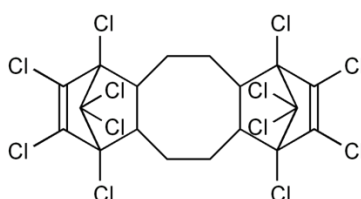


Figure 16: Dechlorane Plus

Flame-retardant nylon formulations typically contain from 15 to 30 wt.-% chlorinated additive and from 4 to 15 wt.-% metal oxide synergist, depending upon the type of nylon and the possible incorporation of glass reinforcement. The choice of synergist is generally made amongst antimony trioxide (Sb_2O_3), ferric oxide (Fe_2O_3), zinc oxide (ZnO) or zinc borates [54]. Ferric oxide is also the most effective single synergist for Dechlorane Plus, giving a UL-94 V0 material for a 1.6 mm thickness with 20% Dechlorane Plus and 5% ferric oxide in nylon 6 [54].

One of the most efficient (and probably most cost-efficient) flame retardant brominated additive for polyamide is decabromodiphenyl ether. However, it is insoluble in the polymer and has negative effects on impact, flexibility and flow. It also tends to darken under UV exposure. A typical loading to reach V0 in polyamide 6 is about 14% bromine in the form of decabromodiphenyl ether with about 6–7% antimony oxide and a small amount (1% or less) of powdered polytetrafluoroethylene (PTFE) to delay the dripping [73].

Another solid additive which may be used as a close alternative to decabromodiphenyl ether is polybrominated phenylindane FR-1808 (DSBG). It has reasonably close properties with respect to thermal stability, compoundability and flow, and has a competitive price. Typical formulations for unreinforced polyamide 6 are shown in **Table 6**.

Table 6: Typical formulations for brominated fire retardants in PA6 [73]

	No Flame Retardant	Decabromo-Diphenyl Ether	Brominated Phenyl Indane FR-1808
Component (%):			
Polyamide 6	100	74.8	73
Flame retardant	–	17.5	19.2
Antimony oxide	–	6.7	6.8
PTFE antidrip	–	1	1
Br content	–	14.6	14.6
Properties:			
Tensile strength (MPa)	66	59	68
Tensile modulus (MPa)	2800	3600	2400
Notched Izod (J/m)	65	59	63
HDT (1.8 MPa) (°C)	na	61	59
UL 94 rating (1.6mm)	NR	V-0	V-0

Data from Dead Sea Bromine Group.

Due to the high loadings of halogenated FR usually needed to flame retard PA6 (> 10 wt.-%), it is unlikely that this class of compounds will be successful in the present work. Moreover, halogenated FRs are being debated concerning their impact on health [78]. The release of such products in environment, especially PBDEs (polybrominated diphenyl ethers), is said to lead to bioaccumulation, and might be a public health issue [79]. Pentabrominated- and octabrominated diphenyl ethers formulations were prohibited in the European Union in the summer of 2004. Eventually, the halogenated systems tend to be abandoned due to market demand of halogen-free products. For those reasons, this class of FR additives will not be investigated in the present work.

1.4.2.2 PHOSPHORUS-CONTAINING FLAME RETARDANTS

The range of phosphorus-based flame retardant products is extremely wide, including phosphates, phosphonates, phosphinates, phosphine oxides and red phosphorus. These phosphorus flame retardant agents can be used as additives or incorporated into the polymer chain during its synthesis, and are known to be active in the condensed and/or gas phase.

In the condensed phase, the phosphorus-based flame retardants are particularly effective with polymers containing heteroatoms (O and N) (polyesters, polyamides, cellulose, etc.). Throughout thermal decomposition in the case of phosphate (e.g. ammonium polyphosphate), phosphoric acid is produced which condenses to form pyrophosphoric acids at fairly low temperature, followed by production of metaphosphoric acid and

polyphosphoric acid at higher temperature. These condensations result in the release of water and through its reaction with the polymer, to the formation of a char that:

- limits the volatilization of fuel and prevents the formation of new free-radicals;
- limits oxygen diffusion, which reduces combustion;
- insulates the polymer underneath from the heat.

Phosphorus-based flame retardants can also volatilize into the gas phase, to form active radicals (HPO_2^\bullet , PO^\bullet and HPO^\bullet), and act as scavengers of H^\bullet and OH^\bullet radicals (**Figure 17**). A third body (M) is required in the reactions involving PO^\bullet radicals.

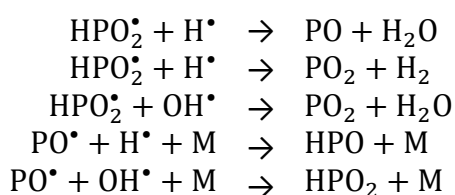


Figure 17: Quenching mode of radical phosphorus-based species [80]

The requirements for nylons are stringent because of high processing temperatures, sensitivity to degradation caused by possible acids and the need for long-term dimensional stability, and avoidance of exudation ('blooming'). These various requirements have eliminated most of the known phosphorus-based flame retardants apart from thermally stable ones [81].

Red phosphorus, is particularly effective in glass-filled polyamides, V0 rating can be achieved with loadings of only 6-12 wt.-% at the UL-94 test. However, traces of phosphine can be found in the formulations [81]. Balabanovich *et al.* [82], have reported the use of red phosphorus alone in neat polyamide 6 at loadings up to 12.5 wt.-%. The basic idea was to cross-link the PA6 matrix by irradiating the samples with ^{60}Co - γ -rays. However, high doses were required and resulted in the loss of the mechanical properties of PA6 due to chemical changes. In order to use lower irradiation doses, they used 5 wt.-% of triallyl cyanurate as cross-linking agent, the fire resistance of PA6 containing 12.5 wt.-% of red phosphorus was then improved, and V0 rating was obtained.

Although salts of dialkylphosphinic acid are only moderately efficient in nylons, they were found synergistic with some nitrogen-containing products like melamine cyanurate [83, 84] melamine phosphate, or melamine polyphosphate [85]. Based on this discovery, Clariant

commercialized the Exolit® OP 1311 for nylon 6 [81]. Exolit® OP 1311 is a non-halogenated flame retardant based on organic phosphinates. The product achieves its flame retardant effect through intumescence, formation of a thin ceramic at the surface of the material and flame inhibition in the gas phase [86]. The thermoplastic polymer with Exolit® OP 1311 foams and crosslinks on exposure to flame and forms a stable char at the surface acting as a barrier. The protective layer provides a heat insulation effect, reduces oxygen access and prevents dripping of molten polymer [87, 88].

Ammonium polyphosphate was also reported as FR for PA6 [89, 90]. APP is an inorganic salt of polyphosphoric acid and ammonia. The chain length (n) of this branched or unbranched polymeric compound is variable; n can be higher than 1000. Short, linear chain APPs (crystalline form I: APP I) ($n < 100$) are more water sensitive (hydrolysis) and less thermally stable than longer chain APPs (crystalline form II: APP II) ($n > 1000$), which exhibit very low water solubility (<0.1 g/ 100 ml). Long chain APPs start to decompose into polyphosphoric acid and ammonia at temperatures above 300°C. Short-chain APPs begin to decompose at temperatures above 150°C. It is therefore very important to adapt the crystalline form (APP I or APP II) of the APP to the polymer decomposition temperature [91]. The effectiveness of APP in PA6 depends on its amount in the polymeric matrix. At relatively low concentration, APP is not efficient in aliphatic polyamides, however, it becomes very efficient at high concentration, e.g. $>10\%$ in polyamide-6,6, $>20\%$ in polyamide-11, -12, -6 (high MW), -10 and $>30\%$ in polyamide-6 (low MW) (Figure 18) [89, 90].

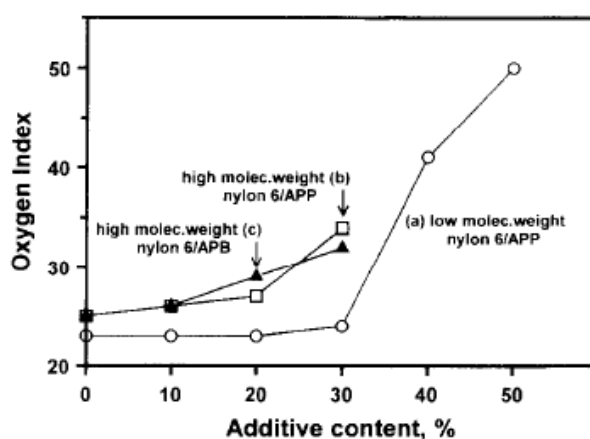


Figure 18: Oxygen index for the PA6 formulations as a function of the APP weight content [90]

APP is also very well known as ingredient for intumescent formulations. The concept of intumescence relies upon the formation of an expanded carbonized layer (char) on the

surface of the polymer during thermal degradation. This layer acts as an insulating barrier, reducing heat transfer between the heat source and the polymer surface. It also limits fuel transfer from the polymer towards the flame as well as the diffusion of oxygen into the material.

In general, the formulation of an intumescent system requires three components:

An acid source: an inorganic acid, an acid salt or other acid such as for example APP that promotes the dehydration of the charring agent.

A charring agent: a carbohydrate that is dehydrated by the acid to form a char. Its effectiveness is related to the number of carbon atoms and reactive hydroxyl sites that contain the carbon source agent molecules. The amount of char produced during thermal decomposition is highly dependent on the number of carbon atoms, whereas the number of reactive hydroxyl sites determines the rate of the dehydration reaction and thus the rate of formation of the carbonized structure [74].

A blowing agent: it decomposes and releases gas, leading to expansion of the polymer and to the formation of a swollen multi-cellular layer. The gas must be released during the thermal decomposition of the carbonizing agent in order to trigger the expansion of the carbonized layer.

The process leading to the formation of the intumescent shield is accepted as follows: the acid released from the acid source catalyzes the dehydration reaction of the charring agent, leading to the formation of a carbonaceous layer. The acid has to be released at a temperature below the decomposition temperature of the carbonizing agent and its dehydration should occur around the decomposition temperature of the polymer.

Phosphorus flame retardants such as red phosphorus, phosphinate salts or APP are effective in polyamide 6 but usually require high loadings (> 10 wt.-%). Others compounds are not thermally stable at the processing temperature of PA6. Thus, the use of phosphorus containing FR might be limited in the present work.

1.4.2.3 MELAMINE AND ITS DERIVATIVES

Melamine is a thermally stable crystalline product characterized by a melting point as high as 345°C that contains 67 wt.-% nitrogen atoms. Melamine sublimates at about 350°C. Upon

sublimation, a significant amount of energy is absorbed, leading to a heat sink effect when dealing with flame retardancy. At high temperature, melamine decomposes with the release of ammonia, which dilutes oxygen and combustible gases and leads to the formation of thermally stable condensates, known as *melam*, *melem* and *melon* (**Figure 19**) [92]

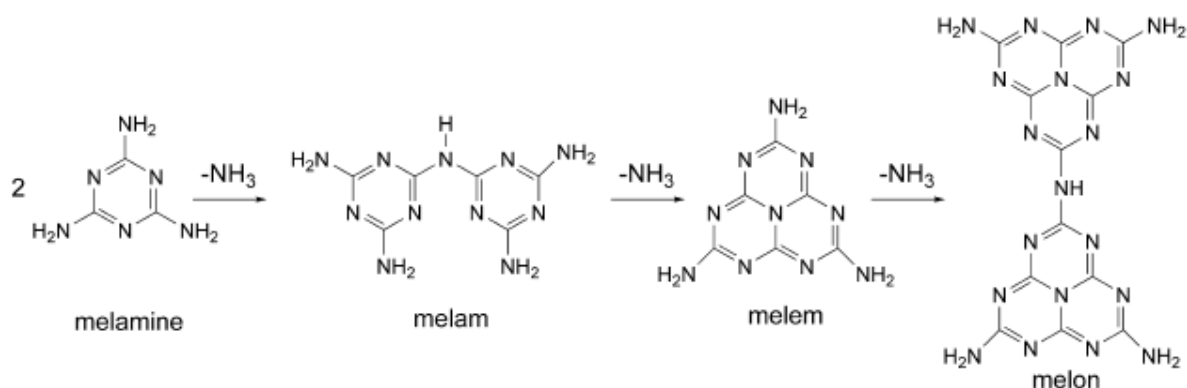


Figure 19: High temperature condensation of melamine

These reactions compete with melamine volatilization and are more pronounced if melamine volatilization is impeded, e.g. by the formation of a protective layer. The formation of melam, melem and melon generates residues in the condensed phase and results in endothermal processes, also effective for flame retardancy.

In addition, melamine can form thermally stable salts with strong acids: melamine cyanurate, melamine phosphate, and melamine pyrophosphate (**Figure 20**). Melamine and melamine salts are characterized by various flame retardant mechanisms. Upon heating, melamine-based salts dissociate and the re-formed melamine can volatilize (like neat melamine) but a large proportion of the melamine undergoes more progressive condensation in the solid phase than in the case of pure melamine [92].

Melamine alone at levels of 5 to 20 wt.% is sufficient to provide V0 performance in nylon 6, 6.6 and 6/6.6 blends. Using melamine in combination with various halogen derivatives, metal oxides, guanidine sulfamate or certain organophosphorus salts, cuprous salts, halogen salts of alkali or alkaline earth metals was found to be advantageous [54, 93].

Melamine cyanurate (MC) is a salt of melamine and cyanuric acid (**Figure 20**). At temperatures above 320°C, it undergoes endothermic decomposition to melamine and cyanuric acid, acting as a heat sink in the process. The vaporized melamine acts as an inert gas source, diluting the oxygen and fuel gases present at the point of combustion. The

cyanuric acid acts to decompose the fuel (polymer), thus removing it from the combustion source very rapidly. It appears thus that MC acts by producing enhanced dripping (with nonburning drips) and also by dissociating endothermically to produce noncombustible vapor [94]. In this case, there are three types of flame-retardant mechanisms [95]. V0 can be obtained at 8-15% loading in unfilled polyamide 6, and at 13-16% in some mineral filled polyamide formulations [73].

Melamine polyphosphate (MPP) is a salt of melamine and polyphosphoric acid. At temperatures above 350°C, it undergoes endothermic decomposition, acting as a heat sink and cooling the combustion source. The phosphoric acid released when MPP degrades reacts with PA6, leading to the formation of a char as previously described in the case of APP. It thus reduces the amount of oxygen present at the combustion source and limits fuel and heat transfers. The melamine released in its gaseous form during the reaction also helps to reduce the oxygen present at or around the combustion source [95].

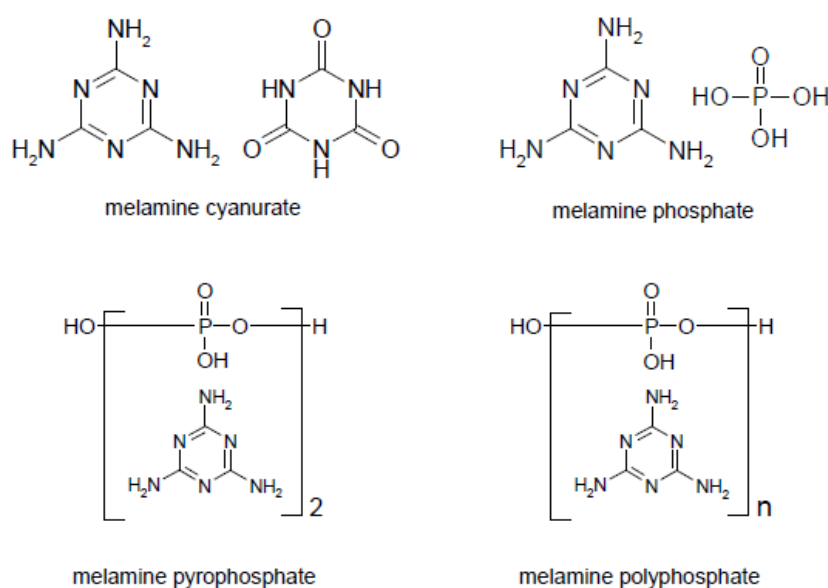


Figure 20: Examples of melamine salts

The main nitrogen compounds of interest as flame retardants for aliphatic nylons are melamine, melamine derivatives and related heterocyclic compounds. Melamine, melamine cyanurate, melamine oxalate and melamine phthalate promote melt dripping of nylon 6, which increases as the additive concentration increases. These formulations self-extinguish very quickly in air and their LOI increases with increasing concentration (Table 7).

The melt dripping effect is very strong in the case of melamine phthalate, where a small amount of the additive (3-10%) leads to large increases in LOI (34% to 53%). The combustion behaviour of melamine pyrophosphate and dimelamine phosphate is different from that of melamine and the other melamine salts. The former are ineffective at low concentrations (< 15%) and become effective at a loading of 20-30% because an intumescent char is formed on the surface of burning specimens [90].

Table 7: Limiting oxygen indices (vol.-%) for high molecular weight nylon 6 flame retarded with melamine or its salts [90]

CONTENT (% WT.)	3	5	10	15	20	30
Additive^a						
Melamine	—	29	31	33	38	39
Dimelamine phosphate	—	23	24	25	26	30
Melamine pyrophosphate	—	24	25	25	30	32
Melamine oxalate	—	28	29	—	33	—
Melamine cyanurate	—	35	37	39	40	40
Melamine phthalate	34	48	53	—	—	—

^aLOI for pure nylon 6 = 24%.

1.4.2.4 SULFUR CONTAINING FIRE RETARDANTS

Although inorganic sulfur derivatives have been known and used since the first century and many formulations have been patented in the last 100 years [96], the use of inorganic sulfur derivatives is still very limited. The sulfur derivatives are used mainly for treating cellulose with ammonium, aluminium, or other metallic sulfates and produce limited, non-durable, flame retardancy [97].

Of particular interest is the sulfation of polyamides to produce reactive durable FR. Numerous diamines and dicarboxylic acids containing phosphorus and/or halogens have been tried since the 1950s to produce reactive modifications of aliphatic polyamide fibers. The problems encountered included the deterioration of the mechanical properties, harsh handle, and the prohibitive cost. However, polyamides treated with low concentrations (1.5-2.5 wt.-%) of ammonium sulfamates (AS) in the presence of dipentaerythritol (0.7 wt.-%) yielded a very high degree of FR with a soft handle and very little deterioration of the mechanical properties [98].

First literature occurrence for polyamide and ammonium sulfamate can be found in a 1995 patent of Lewin [99]. Further studies on this particular system (PA6/ammonium sulfamate)

with the addition of dipentaerythritol were published, once again by Lewin [98, 100]. They show that the addition of a small amount of ammonium sulfamate and dipentaerythritol (2 and 0.7 wt.-% respectively) in PA6 yielded a material rated V0 at the UL-94 test on bars of 1.6 and 0.8 mm thicknesses; the LOI value was 35.7 vol.-%.

The system relies on the sulfation of the primary amino groups of the polyamide at a temperature below 270 °C. At higher temperatures a second sulfation reaction occurs, in which the alkyl amide bonds are severed and upon the degradation of the polymer, there is formation of double bonds and conjugated double bonds that can polymerize into aliphatic and aromatic chars respectively [98]. Since the large-scale extrusion of polyamides is performed at temperatures over 300 °C, the system has limited applications. Nevertheless, it is evident that there is an important potential in utilizing the sulfation reactions and new and improved systems based on sulfation of polymers may be expected in the future [101]. This promising approach will thus be considered in this study.

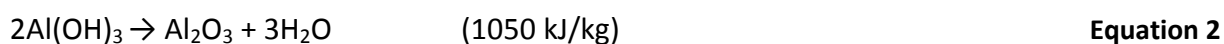
I.4.2.5 METAL HYDROXIDES

Some minerals are more specifically used as flame retardants due to their behavior at high temperature. The most commonly used mineral flame retardants are metal hydroxides (especially aluminum and magnesium hydroxides) and hydroxycarbonates. As the temperature rises, these fillers decompose endothermically and therefore absorb energy. Moreover, they release non-flammable molecules (H₂O, CO₂), which dilute combustible gases, and can also promote the formation of a protective ceramic or vitreous layer [74, 102].

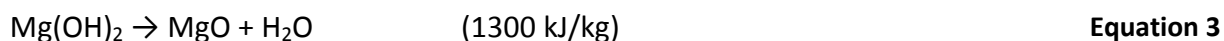
To be used as flame retardants, metal hydroxides need to decompose endothermically and release water at a temperature higher than the polymer processing temperature range, and around the polymer decomposition temperature.

The two most commonly used mineral flame retardants are aluminum tri-hydroxide (ATH) and magnesium di-hydroxide (MDH).

The endothermic decomposition of aluminum tri-hydroxide (Al(OH)₃) occurs between 180 and 200°C and leads to the release of water and to the formation of alumina (Equation 2).



Magnesium di-hydroxide ($\text{Mg}(\text{OH})_2$) acts in the same way as $\text{Al}(\text{OH})_3$ but its endothermic degradation occurs at a higher temperature ($>300^\circ\text{C}$), which is interesting with respect to the extrusion and injection molding processes of some high processing temperature polymers (**Equation 3**).



These mineral compounds are used in polyolefins, TPE, PVC, rubbers, thermosets and can also be used in some engineering polymers such as polyamide. Aluminium trihydroxide (ATH) is selected when the processing temperature is under 200°C . When the processing temperature exceeds 200°C , as for polyamide-6, magnesium dihydroxide (MDH) is then required.

Polyamide 6 can be successfully flame retarded to a V0 standard at UL94 (1.6 mm thickness), using about 60% loading of MDH. However, this product is difficult to process and is rather stiff [103]. Magnesium hydroxide activated with small amounts of catalytic metals, for instance $\text{Mg}_{0.96}\text{Zn}_{0.02}\text{Ni}_{0.02}(\text{OH})_2$, is effective and gives a V0 rating at a loading as low as 33 wt.-% of additives [104]. However, even in that case, the loading is too high if fiber application is required. That is the reason why those additives will not be considered in this study.

1.4.2.6 BORON CONTAINING COMPOUNDS

Borates are a family of inorganic additives with flame retardant properties. Most borates in commercial use are hydrates, among them, zinc borates such as $2\text{ZnO}\cdot 3\text{B}_2\text{O}_3\cdot 5\text{H}_2\text{O}$ are the most frequently used. Their endothermic decomposition (503 kJ/kg) between 290 and 450°C releases their water of hydration (about 13-15%), leading to the formation of boron oxide (B_2O_3).

B_2O_3 softens at 350°C and flows above 500°C leading to the formation of a protective vitreous layer. Moreover, in the case of polymers containing oxygen atom, the presence of boric acid causes dehydration leading to the formation of a carbonized layer [74]. In addition to absorption of heat and dilution of fuel, the release of water serves to blow the char to foam [105]. This layer protects the polymer from the heat of the flame and from the oxygen of the air. The release of combustible gases is also reduced.

Boron containing compounds can be effective in the condensed phase, and in some cases, in the gas phase. A major application of borates is the use of mixtures of boric acids, such as orthoboric acid (H_3BO_3) and borax ($Na_2B_4O_7$) as flame retardants for cellulose and of zinc borate for PVC and some engineering plastics. Zinc borate forms zinc chloride during the pyrolysis of PVC. The latter acts as a Lewis acid suppressing smoke formation [106]. They can take the place of Sb_2O_3 in PVC (2 to 10% gives self-extinguish ability). They can be used in thermoplastic polyesters (PBT), polyolefins, epoxy polymers, and in PA6.

Firebrake ZB, Firebrake 415 and Firebrake 500 (Borax, Rio Tinto) are zinc borates with different chemical compositions that provide flame retardant properties in many polyamides. Their combination with other flame retardants provides unique functionalities. Historically, it has been used with chlorinated flame retardants as a synergist and to increase the resistance against electrical breakdown as determined by the comparative tracking index (CTI). CTI is the maximum voltage for which 50 droplets (electrolyte drops of calibrated volume) can be applied without tracking, that is to say without the formation of a conductive path on the sample and without the appearance of a persistent flame. Today, Firebrake zinc borates also act as synergists with brominated flame retardants to tailor FR properties and CTI. These combinations have also been shown to increase melt stability, and can be used in regrinding processes without a reduction in the original CTI values. In halogen free flame retardant nylon, it has been found that Firebrake zinc borates increase the CTI in glass fiber reinforced systems, illustrating the multi-functional use of these products [107].

Levchik and co-workers [90] studied the fire retardant efficiency of ammonium pentaborate in nylon 6. At concentrations of 10-30 wt.-%, ammonium pentaborate was found to be as efficient as ammonium polyphosphate; however, the mechanism of the fire-retardant action of ammonium pentaborate is different from that of ammonium polyphosphate. The main contribution of ammonium pentaborate is due to its decomposition products, boric acid and boron oxide, which form a glassy protective layer on the surface of the burning polymer [90, 108]. This layer hinders diffusion of the combustible gases to the flame and protects the unstable char formed from oxidation of the decomposing nylon 6 [54]. However, the relatively high amount of boron based fire retardants needed to enhance PA6 properties prevents their use for fiber applications. Thus, this family of FR will not be considered in this work.

I.4.2.7 NANOPARTICLES

Nanometric particles when individualized and properly dispersed in polymer matrices are known to contribute to the enhancement of properties such as thermal, mechanical or fire retardancy. They enable a considerable reduction of the loading rate as the interfacial area between the polymer and the nanofiller is greatly increased.

More precisely, the contribution of each type of nanoparticle to flame retardancy varies and strictly depends on its chemical structure and geometry. Here we will describe and discuss the flame retardant effects of three widely investigated kinds of nanoparticles:

- *layered materials*, such as nanoclays (e.g., montmorillonite: MMT) and layered double hydroxides, which are characterized by one nanometric dimension, referred to as 1D nanoparticles;
- *fibrous materials*, such as carbon nanotubes and sepiolite, which are characterized by elongated structures with two nanometric dimensions and referred to as 2D nanoparticles;
- *particulate materials*, such as polyhedral oligosilsesquioxane (POSS) and spherical silica nanoparticles, which are characterized by three nanometric dimensions and referred to as 3D nanoparticles.

I.4.2.7.1 1D NANOPARTICLES

Nanoclays are nanoparticles of layered mineral silicates. Depending on chemical composition and nanoparticle morphology, nanoclays are organized into several classes such as montmorillonite, bentonite, kaolinite, and hectorite. Organically-modified nanoclays (organoclays) are an attractive class of hybrid organic-inorganic nanomaterials with potential uses in polymer nanocomposites, as flame retardants [109].

Nanoclays are layered materials which consist in stacking of multilayer sheets where each sheet is composed of two outer layers of silica tetrahedra and one central layer containing monovalent, bivalent or trivalent atoms (Al^{3+} , Mg^{2+} , Fe^{3+} , Fe^{2+} , Na^+ , K^+ , etc.) that negatively charge the sheet. The negative charge is compensated by the presence of cations between the stacked sheets (**Figure 21**).

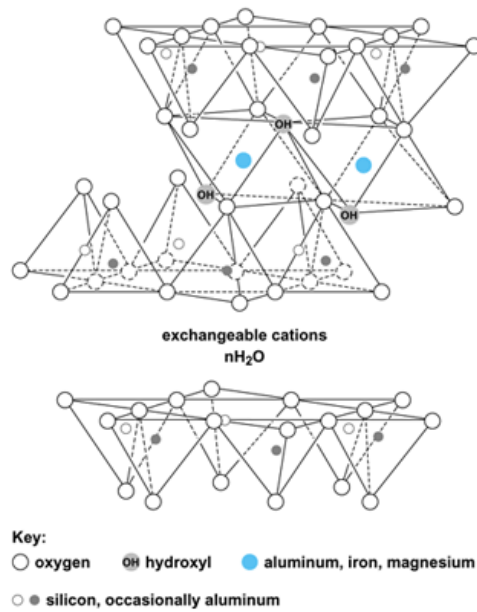


Figure 21: structure of montmorillonite [110]

In order to favor the dispersion of the clay nanolayers within the polymer matrix, a modification of natural clays using organic cations (alkylammonium, alkyl phosphonium and alkyl imidazol(idin)ium cations) is often carried out, leading to the formation of organo-modified nanoclays [111]. Polymer/organoclay nanocomposites bulk can contain three different phases (**Figure 22**): phase separated or microcomposite, intercalated and exfoliated nanocomposite, depending on the compatibility between the polymer matrix and the organic modifier of clays.

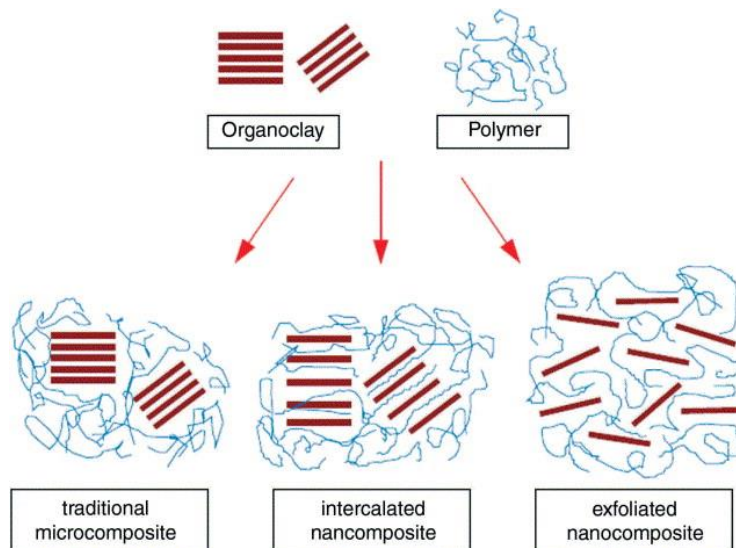


Figure 22: Dispersion of a lamellar filler within a polymer matrix [112]

In the 1980s, nylon 6/clay nanocomposites were firstly synthesized by Toyota Central Research and Development Laboratories and they found that a tiny amount of clay can greatly improve the thermal stability and mechanical properties of this polyamide [113].

Gilman *et al.* [114] have studied the system nylon 6/clay nanocomposite and they found that nanoclays are a very efficient system to flame retard PA6 (Table 8) and it avoids the usual drawbacks associated with other FR additives. The physical properties, such as, for example, the mechanical properties, are not degraded by the clay, but are greatly improved. Furthermore, this system does not increase the carbon monoxide or soot produced during the combustion, as many commercial fire retardants do. The nanocomposite structure appears to enhance the performance of the char through its reinforcement by forming a multilayered silicate structure. This layer may act as an insulator and a mass transport barrier slowing the escape of the volatile products generated as the nylon-6 decomposes.

Table 8: Cone calorimeter data of nylon-6 and nylon-6 clay nanocomposite [114]

Sample	Residue yield (%)	pHRR (kW/m ²) (% decrease)	THR (MJ/m ²)
Nylon-6	0.3	1011	413
Nylon-6 clay nanocomposite 2%	3.4	686 (32%)	406
Nylon-6 clay nanocomposite 5%	5.5	378 (63%)	397

Improved flame retardancy of polymer/ clay nanocomposites is reported, including reduction of the flame spread, of the peak of heat release rate (pHRR) and of the total heat release (THR) [114]. In addition, the melt dripping is inhibited efficiently [105, 114]. Nevertheless, there is no significant increase of LOI and UL-94 rating with addition of MMT alone in polyamide [115, 116].

Addition of conventional FR such as melamine and its derivatives in nylon 6/nanoclays systems can lead to a synergistic effect. However, if the amount of nanoclay reaches a certain level, an antagonist effect is shown [100, 117]. For example in the PA6/MPyP^{*}/MP-MMT[†] system, including 25% of additives, the substitution of 1% of MPyP by MP-MMT leads to a LOI value of 35 vol.-% and a V0 UL-94 rating. However, with 5 wt.-% of MP-MMT, LOI

* Melamine pyrophosphate

† Melamine phosphate modified MMT

decreases to 29 vol.-% and the material is non-classified at UL-94. The same trends are observed with the addition of Na⁺MMT and OMMT[‡].

In the system PA6/OMMT/AS[§]/dipentaerythritol [100], when the amount of OMMT goes from 1% to 5% (with respectively 2 wt.-% of AS and 0.7 wt.-% of DiPER), the pHRR is lowered by 16%, but the LOI decreases from 35.7 vol.-% to 20.2 vol.-%. Concerning the UL-94 rating, 1% OMMT in the formulation gives V0 and 5% OMMT gives a non-classified material. The antagonist effect of 5% OMMT on the UL-94 can be lowered by adding 5 wt.-% of polyvinylpyrrolidone (PVP) to the formulation, or by replacing the 5 wt.-% OMMT by 5 wt.-% Na⁺MMT, giving UL-94 ratings of V2 and V0 respectively.

On the other hand, layered Double Hydroxides (LDHs) have been identified as a promising new additive class for generating polymer nanocomposites with enhanced thermal stability and improved flammability properties. The early report on the flame-retardant application of LDH was published by Miyata *et al.* [118]. Recent advances in the development of LDHs for polymer fire retardancy applications have been reviewed [119].

On the other hand, the flame retardant characteristics of LDH clays originate from their Mg(OH)₂ like chemistry, which involves endothermic decomposition with the release of water and often carbon dioxide. The residue of such combustion is the metallic oxides that impedes the burning process by reducing the oxygen supply to the fresh surface beneath.

The most commonly used LDH is based on the hydrotalcite (Mg₆Al₂(OH)₁₆CO₃·4H₂O, **Figure 23**) structure. The use of natural or organomodified LDH was proved to enhance the fire retardant properties (mainly through reduction of the pHRR) in polymers such as epoxy resins [120] or PA6 [121]. In this last case, 5 wt.-% of MgAl-LDH, exfoliated in PA6, reduced the pHRR in cone calorimetry (35kW/m²) by 40 %. With a loading of 20 wt. %, the LDH were intercalated and the reduction of pHRR was 70 %.

[‡] MMT modified with dimethyl hydrogenated tallow 2-ethylhexyl quaternary ammonium

[§] Ammonium sulfamate

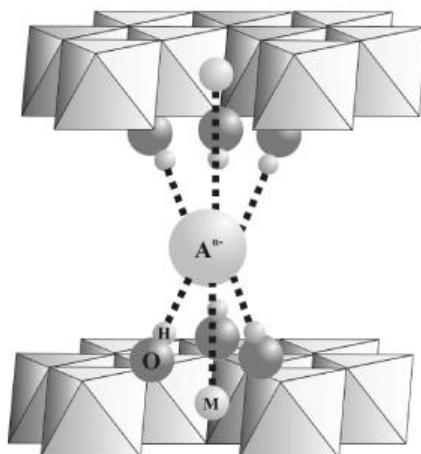


Figure 23: Generic structure of a LDH with A = compensating anion, O = oxygen, H = hydrogen and M = any divalent or trivalent cation [122]

1.4.2.7.2 2D NANOPARTICLES

Halloysite nanotubes (HNTs) are alumino-silicate clays ($\text{Al}_2\text{Si}_2\text{O}_5(\text{OH})_4 \cdot 2\text{H}_2\text{O}$) mined from natural deposits. They are chemically similar to kaolin, but differ by having a predominantly hollow microtubular structure with a high aspect ratio, rather than a stacked plate-like structure [123]. The first report for using HNTs in PA6 comes from NaturalNano Inc. who patented in 2007 its use in PA6 to provide reinforcement and flame retardant properties [124].

Another paper from Marney *et al.* studies the suitability of halloysite nanotubes as fire retardant for nylon 6 [125]. They show that compared to MMT, a much higher amount of HNTs is needed to achieve the same performances (30 wt.-% instead of 2-5 wt.-%). A loading of 15 wt.-% HNTs seems to provide reasonable results, i.e., a 50% reduction in pHRR, V2 UL-94 rating and 23 vol.-% LOI (Table 9).

Table 9: UL-94 and LOI results for different PA6/halloysite composites [125]

HNTs conc. (wt%)	UL 94 rating	t_1^a (s)	t_2^a (s)	Burning of cotton	OI ($\pm 1\%$)
0	V-2 ^b	8	5	Yes	22
5	V-2	2	3	Yes	22
10	V-2	0	7	Yes	21
15	V-2	0	16	Yes	23
20	NR ^c	0	185	Yes	25
30	NR	0	143	Yes	30

^a t_1 and t_2 are a measure of the time that flaming persisted after the burner was removed for the first and second time, respectively.

^b V-2 is the rating given to signify that the material extinguished quickly enough to pass but the cotton indicator below the material ignited.

^c No rating – considered to be a fail.

On the other hand, carbon nanotubes display exceptional properties that can potentially be used in many applications ranging from macroscopic material composites down to nanodevices. Thanks to their high aspect ratio, CNTs percolate to form a network at very low loading in a polymer matrix and lead to substantial enhancement of several functional properties such as mechanical [126], rheological [127-129] and flame retardant [57, 130, 131] properties.

Carbon nanotubes (CNTs) are cylindrical shells made, in concept, by rolling graphene sheets into a seamless cylinder. CNTs exist as either single-wall nanotubes (SWNTs) or multi-walled nanotubes (MWCNTs) (Figure 24).

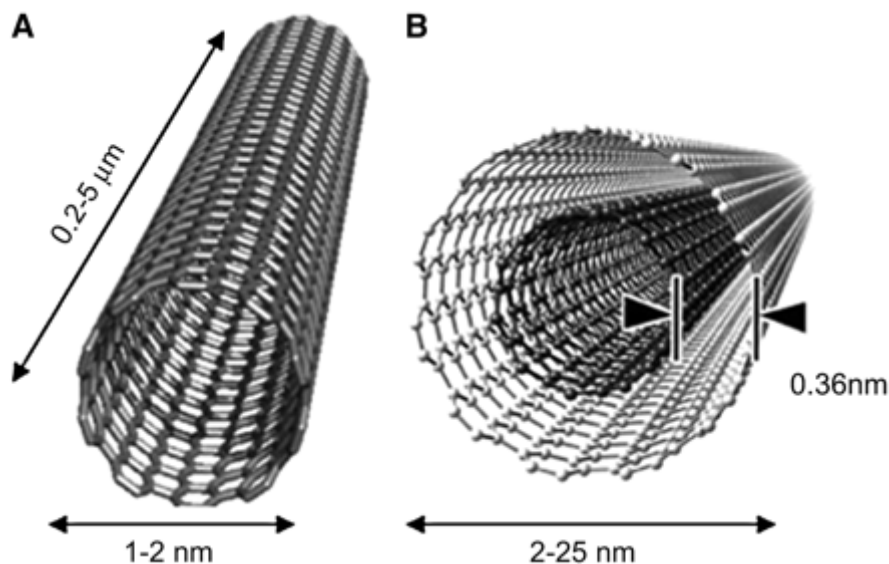


Figure 24: Sketches of CNTs: (A) SWNT (B) MWCNT , showing typical dimensions of length [132]

Schartel *et al.* have studied the system PA6/MWCNTs (5%) [57] and they showed that during burning the MWCNT interconnected network structure remained in the material, since it is thermally stable. Thus, it influenced the melt viscosity. The changed viscosity prevented dripping and flowing, but also hindered the decomposition of volatiles feeding the flame. The percolated structure stabilized the pyrolysis zone and the residue. They say that in principle, these mechanisms were capable of influencing the fire behavior significantly, but the effects were strongly dependent on the fire scenario (external heat flux). The prevention of dripping is known to be necessary to avoid inflammation by dripping, but in other scenarios decreased melt flow results in increasing conversion of the material into fuel, since the heat cannot be removed from the pyrolysis zone by dripping. The stabilization of residue is a key challenge to ensure barrier properties, like the formation of a char, but it can also be

negative for passing flammability tests when low melting hinders heat removal by dripping. It becomes clear that MWCNT may be considered as highly interesting adjuvant in certain distinct systems and scenarios rather than as a general fire retardant.

1.4.2.7.3 3D NANOPARTICLES

POSS is an inorganic silica-like nanocage ((RSiO_{1.5})₈) with a size of about 1-3 nm, surrounded by eight organic groups located at the corners that enhance its compatibility within organic polymers (**Figure 25**). On combustion, POSS acts as a precursor forming thermally stable ceramic materials at high temperature. These inorganic nanocages are also referred to as pre-ceramic compounds.

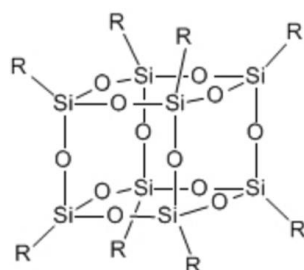


Figure 25: POSS structure

The incorporation of POSS in polymers modifies both the viscosity and the mechanical properties of the molten polymer. In addition, it also affects the thermal stability and fire performances by reducing the quantity of heat released upon combustion. For instance, the incorporation of 10 wt.-% of methyl phenyl polysilsesquioxane in polytetramethylenetherglycol-*b*-polyamide-12 (PTME-*b*-PA) leads to a 70% decrease in peak HRR during cone calorimetry tests carried out at 35 kW/m² [133]. Unfortunately POSS were shown to be rather ineffective in PA6 [134].

Nanoparticles (NP) are known to enhance the polymer properties using low amounts of them. For example, NP can enhance barrier or mechanical properties. Researchers have also managed to enhance thermal and fire properties of polymers using NP. The efficiency of such systems depends on the NP loading, dispersion or even polymer Mw. This kind of additives is thus of interest when working with fibers. Indeed, generally it is mandatory to use low amount of additives in order to keep the spinnability of the material. Different NP should thus be used in this study, to make nanocomposite PA6 fibers.

I.5 FIRE-RETARDANT ADDITIVES FOR FIBERS

In the previous sections, the constraints linked with the spinning process and the flame retardants used in PA6 have been detailed. Taking them into consideration, it is possible to select various additives as potential candidates to flame retard PA6 fibers. This section will thus present systems developed for the flame retardancy of synthetic fibers in general and for PA6 in particular. Synthetic fibers produced with this approach are called inherently FR [67].

Lenzing AG currently produces Lenzing Viscose FR which contains Sandoflam 5060. It has been demonstrated that a wool/viscose FR blend performs better than each fiber alone and this is being used as seat covers in the Airbus 310. The fiber is produced by adding Sandoz 5060 (Clariant 5060, bis(2-thio-5,5-dimethyl-1,3,2-dioxaphosphorinyl) oxide in the formulation. As this additive is phosphorus based, it is similar to other phosphorus-based FRs in terms of mode of action (condensed phase). DuPont and Lenzing AG have jointly developed a special blend consisting of 65% Viscose FR, 30% Nomex and 5% Kevlar for industrial wear under the brand name of Karvin® [135].

Zhang and Horrocks have reviewed different FRs used for polypropylene fibers [136]. In principle, most FRs are effective in rendering PP fire retardant. However, high loadings (usually >20 wt.-%) are needed to achieve the desired level of flame retardancy. Antimony–halogen or tin–halogen formulations exist, but the most common and effective FR for PP fibers is tris(tribromoneopentyl)phosphate (FR 372, ICL) [67]. Flamestab® NOR 116 (Ciba now BASF) is also reported to have some FR properties in PP [137]. Latest development for flame-retarding PP is by nanocomposite-based FRs, which is discussed in detail below.

The previously reported systems are not suitable for PA6, either because their thermal stability is too low or because they are not adapted. Processing of FR additives in polyamides is very difficult because of their melt reactivities [61, 67, 68], furthermore this can lead to a Mw decrease [54]. Butylkina *et al* [138] compared the performance of non-melting type compounds (e.g. lead methylphosphonate and a complex of alkylphosphonic acid and antimony) with highly viscous FR compounds like phosphorylated pentaerythritol (Fostetrol®) and phosphorus-based Borofos® as synergistic additives during melt spinning of nylon 6. An oxygen index value of about 50 vol.% was found in FR nylon 6 having 2 wt.-% of

antimony in an antimony complex of alkyl phosphonic acid but the carbonized residue/char was found to be highest when Borofos® was used as melt additive. In another study, Tyuganova *et al.* [139] have used a ternary system of flame retardant, namely: boric acid, brominated pentaerythritol and antimony oxide, mixed into the polymer melt prior to extrusion and spinning. It has been demonstrated that boron compounds display condensed phase active mechanisms and increase the yield of water and carbonized residue, while halogen-containing compounds are effective inhibitors of free radical reactions in the gas phase. A nylon sample having 2.28 wt.-% Boron, 3.09 wt.-% Br and 2.26 wt.-% Sb gave a LOI value of 29.2 vol.-%. In a recent patent, Bender *et al.* [140] have used DOPO (9,10-dihydro-9-oxa-10-phosphaphenanthrene-10-oxide) to flame retard technical fibers made of PA6 and PA6.6 blends. According to the invention, DOPO and DOPO derivatives were used in the blends at loadings between 7 to 10 % and co additives loadings were 0.01 to 4 %. The mechanical properties of the fibers were good for their application. It has to be noted that even if the potential use as flame retardants of phosphorus and boron based compounds are reported for PA6 fibers, the recent developments for the flame retardancy of polyamides fibers concern mainly the inclusion of nanoparticles [67].

Although there has been considerable amount of research going on in area of polymer nanocomposites, there has been a limited success in developing textile structures with them.

Bourbigot *et al.*, in 2001, reported the first fire performance of PA6 and PA6/MMT fibers made by melt blending and by melt spinning [141]. PA6 nanocomposite exhibited an exfoliated structure and no degradation of the clay was observed after processing. However, the yarns were not uniform because of reagglomeration of the MMT platelets, resulting in poor mechanical properties [68]. The fabrics prepared from these yarns were of 1020 g/m² area density and 2.5 mm thickness. They were tested by cone calorimetry at 35 kW/m² heat flux (Figure 26), where ignition times of 70 and 20 s and pHRR values of 375 and 250 kW/m², respectively, for the normal and nanocomposite polyamide 6 fabrics were recorded. While the latter presents a significant 33.3% reduction in pHRR, ignition resistance was significantly reduced and THR was little affected. It has to be noted that these fabrics have a very high area density; hence this reduction in the peak of heat release rate might not be reflected by fabrics of area densities normally used as apparel fabrics, i.e., 100-200 g/m² [67].

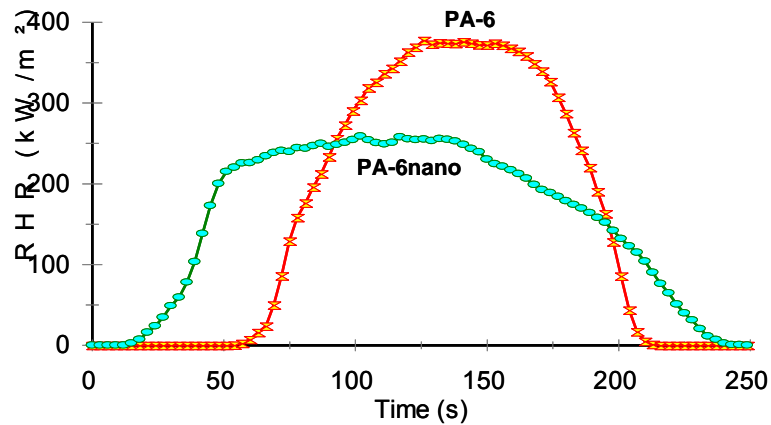


Figure 26: RHR curves of PA6 and PA6/nano fabrics at an external heat flux of 35 kW/m²

In 2008, a study by Shanmuganathan *et al.* [142] reported the spinnability and flammability of PA6/OMMT nanocomposite. 10 wt.-% OMMT is found to be a high concentration with respect to fiber spinnability. Nanocomposites with 8 wt.-% OMMT show better spinnability and the fibers have satisfactory physical properties to be knitted into fabrics. Condensed-phase flame-retardant mechanism of OMMT seems to be effective but to a lesser extent, when the sample geometry is changed from film to fiber and fabric. At a concentration of 8 wt.-% OMMT, the flame-retardant effect depends on fabric geometry as well as test conditions. Char formation kinetics is too slow to protect the material from flame spread in horizontal flame spread tests and hence, the nanocomposite fabrics do not show significant difference in flame spread behavior compared to nylon 6 fabrics. However under radiant heat conditions, the fibers melt and enable formation of a continuous charred surface at very early stages of burning resulting in significant flame retardancy. Fabric tightness factor plays a crucial role in supporting the char formation process, and with higher tightness factor, enhanced flame-retardancy could be achieved (Figure 27).

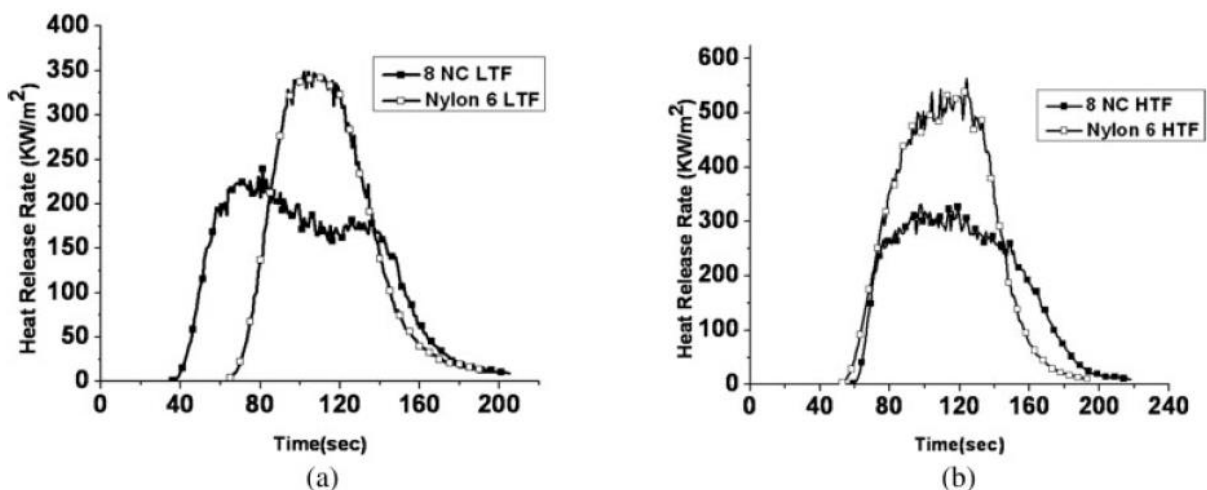


Figure 27: Heat release rate (HRR) curves of (A) nylon 6 and nylon 6/OMMT 8% nanocomposite (8 NC) fabric of low tightness factor (LTF) and (B) nylon 6 and nylon 6/OMMT 8% nanocomposite fabric of high tightness factor (HTF) [142]

With a similar approach to their PA6/MMT fabrics, Bourbigot *et al.* [143] have used poly(vinylsilsesquioxane) (FQ-POSS) in PP (10 wt.-%) to melt spin filaments, which were then knitted into fabrics. POSS was thermally stable and no degradation was detected in the processing conditions. They have tested the flammability of the fabrics using cone calorimetry. POSS had minimal effect on the peak of heat release rate and total heat release values of PP fabric, but delayed the TTI as shown in **Figure 28**. This behavior is opposite to that of layered silicates, which have minimal effect on TTI, but reduce pHRR. Authors claim that POSS does not act as a FR but only as a heat stabilizer via a decrease of the ignitability.

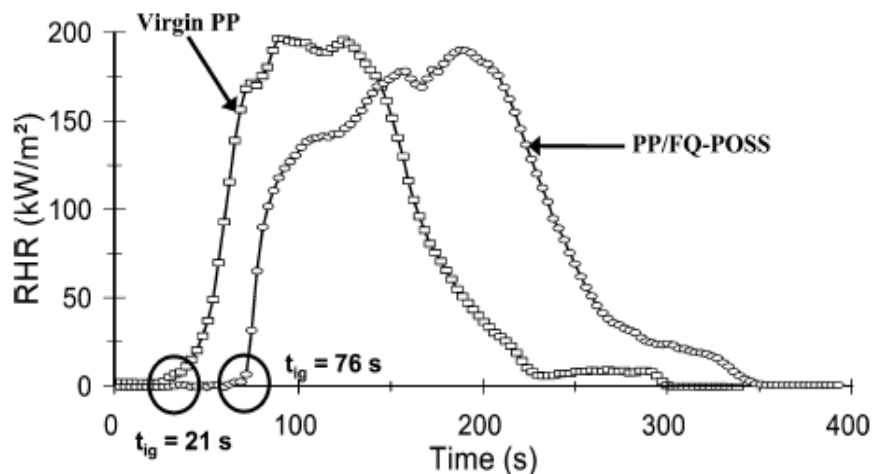


Figure 28: Rate of heat release (RHR) curves of PP and PP/FQ-POSS knitted fabrics at 35 kW/m² [143]

The same group has also successfully prepared yarns from polypropylene/MWCNT (1 wt.-% and 2 wt.-%) nanocomposites [144]. Fabrics knitted from these yarns were tested by cone calorimetry. pHRR is reduced by 50% with a nanotubes loading of only 1 wt.-% but the TTI of the nanocomposite was shorter as depicted in **Figure 29**.

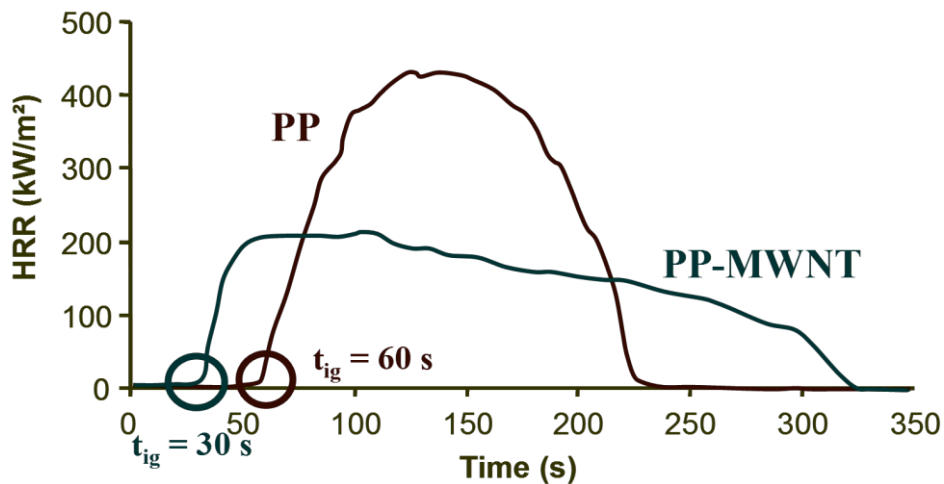


Figure 29: HRR values versus time of PP and PP/MWCNT fabrics at 35 kW/m² [144]

Incorporation of nanoclays in a PP matrix has also been studied by Horrocks group at Bolton University [145-147]. They recognize that one of the difficulties of incorporating nanoclays into polypropylene is the lack of polar groups in the polymer chain, which makes direct intercalation or exfoliation almost impossible. Most often maleic anhydride-grafted polypropylene is used as a compatibilizer, which enhances the interaction between the clay and polymer with strong hydrogen bonding between –OH or –COOH and the oxygen groups of clay. However, the presence of such compatibilizers usually has adverse effects on fiber properties. While this effect is concentration dependent, to keep the rheological properties necessary for extrusion into fiber, lower levels are preferred. Levels between 1% and 3% wt.-% of grafted PP along with sufficient compounding have been shown to improve the dispersion of the clay platelets in the PP matrix [147].

1.6 CONCLUSION

Halogenated flame retardants have been the additive of choice for a long time but the main drawbacks are the recycling of plastics containing halogens and the burning of such materials releasing toxic fumes. Moreover, due to recent directives and market demands, their use is now limited. In the meantime researchers had developed other compounds (phosphorus or nitrogen based, inorganic, etc.), thus halogen-free solutions are available. Mechanisms and modes of action have been widely investigated for bulk polymers with conventional fire retardants and the new trend is the use of “nanoscale” systems (nanocomposite/nanostructured materials).

Chapter 1: State of the Art

For textile applications, it is important to have a durable effect, avoiding the laundering issue. Melt blending the polymer and the FR is one of the solutions as the additives can be completely trapped inside the polymer matrix. In order to draw fibers, the amounts of FRs have to be relatively low (generally a maximum of 10 wt.-%) to keep a good spinnability of the extrudate. Thus, nanoparticles could be a fire retardant of choice because of their size, implying that only small quantities are usually needed to improve the performances. However, due to the burning behavior of fibers, which are thermally thin materials, it is not always easy to reach the desired effect with only nanoparticles.

The state of the art has shown that few solutions exist to flame retard bulk PA6 and PA6 fibers. Some of the fire retardants used in the bulk are not suitable to be used in fibers application due to some processing issues and to the high content required to reach acceptable FR performances. In particular, some phosphorus and sulfur based additives have shown to be particularly effective, even at low loadings. The challenge of this work and the next chapters will thus be focused on finding an innovative system that has enhanced fire properties at low loadings. After a description of the methods and materials used in this study, a first step will consist in the screening of various FR additives and nanoparticles. The selected systems will then be fully investigated in chapters IV and V of this thesis.

II	EXPERIMENTAL TECHNIQUES	
II.1	Introduction	82
II.2	Material Preparation and processing	82
II.2.1	Materials	82
II.2.1.1	Polyamide 6	82
II.2.1.2	Flame retardants and additives	82
II.2.2	Extrusion and fiber spinning	84
II.2.3	Samples processing	85
II.2.3.1	Powders	85
II.2.3.2	Barrels and plates	85
II.3	Materials characterization	86
II.3.1	Mechanical testing	86
II.3.2	Digital microscopy and image processing	86
II.3.3	Electron probe micro analysis	87
II.3.4	Solid-state NMR	88
II.3.5	Differential scanning calorimetry	88
II.4	Thermal degradation and fire testing	89
II.4.1	Thermal degradation	89
II.4.1.1	ThermoGravimetric Analysis	89
II.4.1.2	TGA coupled with FTIR	90
II.4.1.3	py-GC-MS	90
II.4.1.4	Thermal treatments	92
II.4.2	Fire testings	93
II.4.2.1	Pyrolysis Combustion Flow Calorimetry	93
II.4.2.2	Mass Loss Calorimeter	94
II.4.2.3	Limiting Oxygen Index	95
II.4.2.4	UL-94	96
II.5	Conclusion	97

II.1 INTRODUCTION

This chapter aims at describing the materials, techniques and experimental protocols used in this work.

In a first part, the materials, namely the PA6 matrix, the different fire retardants and fillers, will be described as well as the strategy followed to choose them. The processing of the different formulations in order to perform the fire tests will then be presented in a second part. In a third part, the techniques related to the materials characterization will be detailed.

II.2 MATERIAL PREPARATION AND PROCESSING

II.2.1 MATERIALS

II.2.1.1 POLYAMIDE 6

The polyamide used during this study is a standard homopolymer grade of polyamide 6 supplied by Rhodia and referenced by the manufacturer as PA6 Technyl S-27 BL natural S. Properties of this PA6 are reported in **Table 10**.

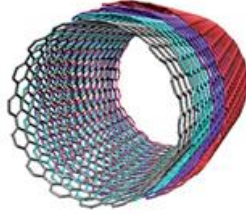
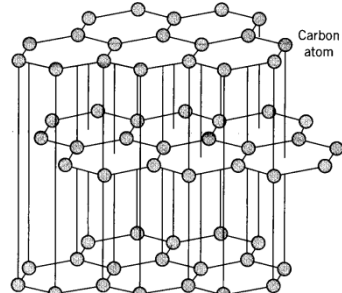
Table 10: Properties of PA6 Technyl S-27 BL natural S

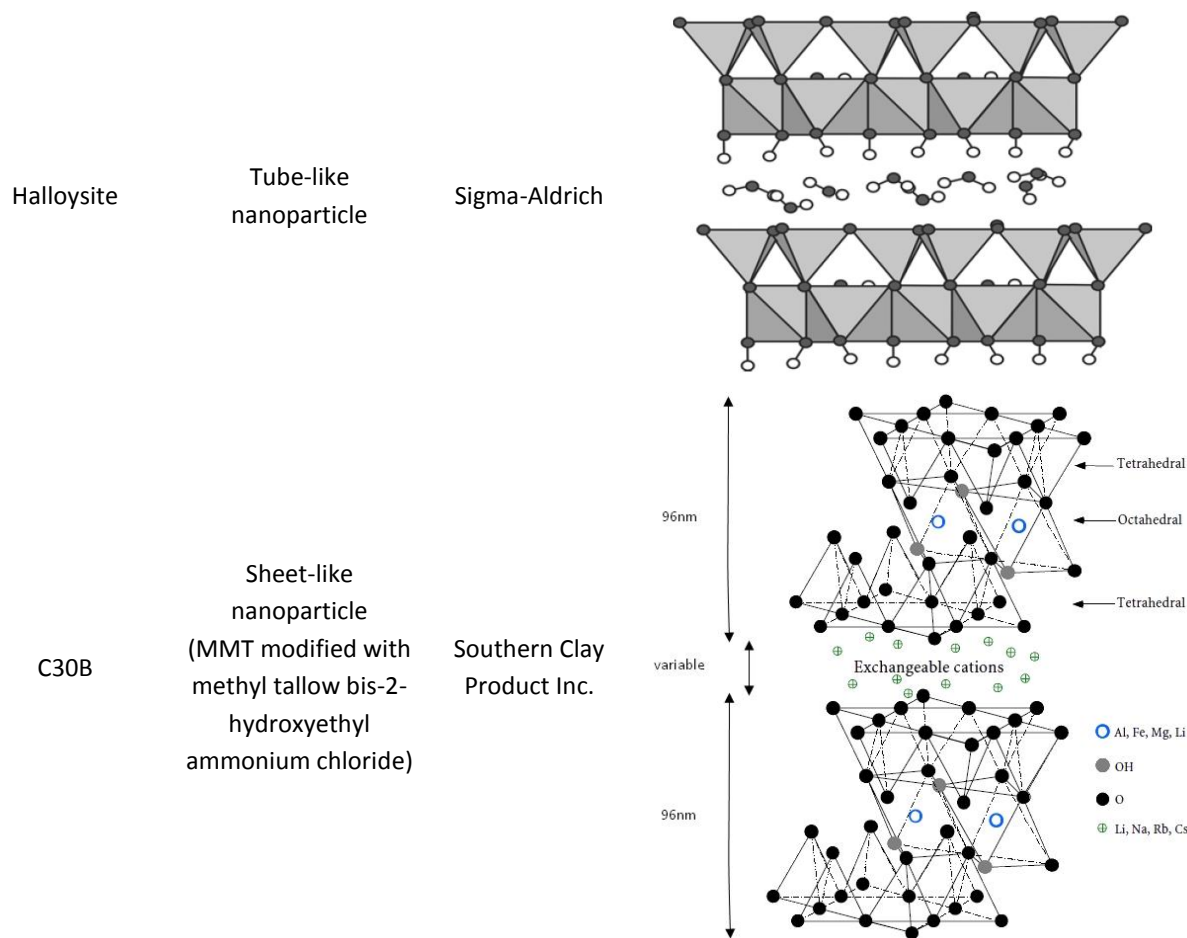
Property	Nominal Value	Unit
Relative viscosity in H ₂ SO ₄ (ISO 307)	2.70	
Viscosity index in HCOOH	140	ml/g
Relative humidity	< 0.2	%
Residual monomer	< 0.8	%
Specific gravity	1.13	g/cm ³
Tensile strength at yield	85	N/mm ²
Tensile strength at break	55	N/mm ²
Elongation at break	> 50	%
Flexural modulus	3000	N/mm ²
Notched Charpy Impact	4.5	kJ/m ²
Melting point	222	°C

II.2.1.2 FLAME RETARDANTS AND ADDITIVES

Fire retardants were selected according to the literature review presented in Chapter 1. Three types of flame retardants additives were selected to evaluate their efficiency in the PA6 matrix: phosphorus fire retardant solutions, sulfur compounds and nanoparticles (**Table 11**).

Table 11: Selected flame retardants to be investigated in PA6

Name	FR type	Supplier	Chemical formula
Exolit® OP 950	Zinc phosphinate (20% P)	Clariant	$\left[\begin{array}{c} \text{O} \\ \parallel \\ \text{R}_1 - \text{P} - \text{O}^- \\ \\ \text{R}_2 \end{array} \right]_2 \text{Zn}^{2+}$
Exolit® OP 1230	Phosphinate salt	Clariant	$\left[\begin{array}{c} \text{O} \\ \parallel \\ \text{---} \text{P} - \text{O}^- \\ \\ \text{---} \end{array} \right]_3 \text{Al}^{3+}$
Aflammit® PCO 900	Proprietary (24% P)	Thor	
Aflammit® PCO 960	Proprietary (24% P)	Thor	
Ammonium sulfamate	Sulfamate salt	Sigma-Aldrich	$\text{NH}_4^+ \quad \text{O}^- - \text{S}(\text{O})_2 - \text{NH}_2$
Guanidine sulfamate	Sulfamate salt	Jinchi Chemicals Co.	$\begin{array}{c} \text{NH} \\ \parallel \\ \text{H}_2\text{N} - \text{C} - \text{NH}_3^+ \\ \text{O}^- - \text{S}(\text{O})_2 - \text{NH}_2 \end{array}$
Melamine polyphosphate Melapur® 200	Nitrogen/phosphorus FR	BASF	$\left[\begin{array}{c} \text{O} \\ \parallel \\ \text{HO} - \text{P} - \text{O} - \text{H} \\ \\ \text{O}^- \\ \\ \text{NH}_3^+ \\ \\ \text{N} \\ / \quad \backslash \\ \text{N} \quad \text{N} \\ \quad \\ \text{H}_2\text{N} \quad \text{NH}_2 \end{array} \right]_n$
MWCNT NC7000 (90% purity)	Tube-like nanoparticle	Nanocyl	
Graphene oxide	Sheet-like nanoparticle	NanoInnova	



II.2.2 EXTRUSION AND FIBER SPINNING

The different formulations were prepared by microextrusion using a DSM Xplore micro 15 device having a volume of 15 cm³. PA6 pellets (Rhodia Technyl S-27 BL) and additives were dried overnight, in an oven at 80°C prior to extrusion. PA6 matrix and additives were extruded under a nitrogen flow at 245°C and 100 rpm (unless otherwise noted). A micro fiber spinning device, also made by DSM (DSM Xplore micro spinning unit), was used to obtain fibers from the formulations. In this case, the microextruder (equipped with a spinneret of 0.75 mm diameter) and the spinning unit were put in series as shown in **Figure 30 (a)**. On the spinning unit, godet and torque speed were set at 30 m/min and 100 m/min respectively.

Larger scale extrusions were also performed on a Thermo Scientific HAAKE PolyLab OS System. It consists in a twin-screw laboratory extruder equipped with feed-dosing elements (**Figure 30 (b)**). Temperature profile of the 10 heating elements was set as reported in **Table 12**.

Table 12: Temperature profile of the extruder from hopper to die

Zone	1*	2	3	4	5**	6	7	8	9	10
Temperature (°C)	300	280	260	260	240	240	235	230	230	210

*PA6 was fed in zone 1, **FR were fed in zone 5

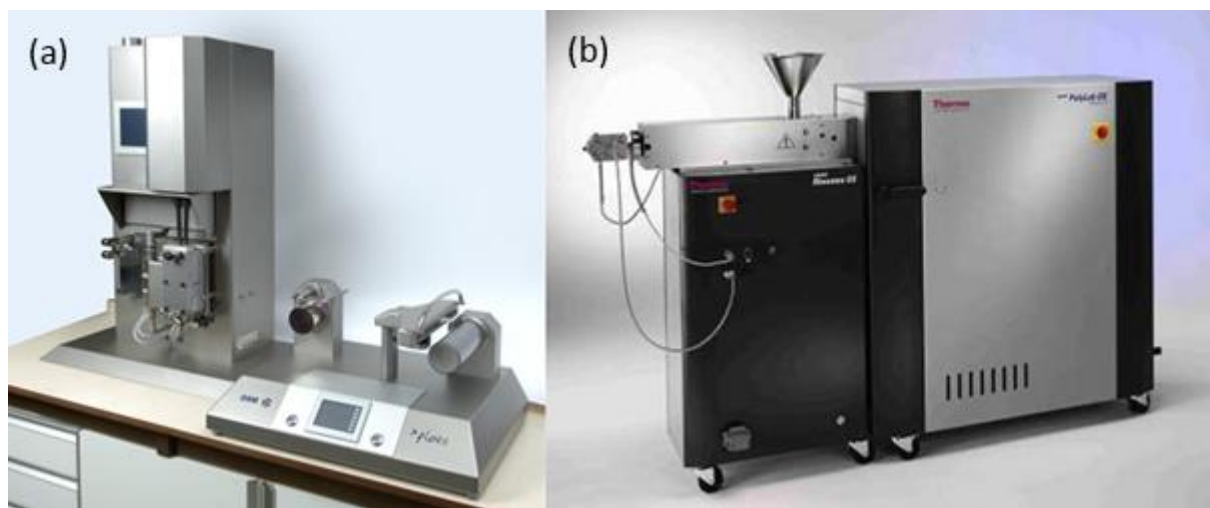


Figure 30: DSM microextruder and spinning unit in series (a) Thermo Scientific extruder (b)

II.2.3 SAMPLES PROCESSING

II.2.3.1 POWDERS

A high speed rotor mill (Retsch - Ultra Centrifugal Mill ZM 200) was used to obtain fine powder from the formulations pellets, or rods, obtained just after spinning. The fed material only remains in the grinding chamber for a very short time and liquid nitrogen was used to cool down the sample, which means that the characteristic features of the sample to be determined are not altered. The powders were used for solid-state NMR, TGA, py-GC-MS and PCFC

II.2.3.2 BARRELS AND PLATES

Samples were obtained by pressing the appropriate mass of material, previously extruded and pelletized, with a hydraulic hot press and specific molds. LOI samples size was 100x10x3 mm³, UL-94 samples were 127x12.7x1.6 mm³ and cone samples were 3x100x100 mm³, according to the different standards [148-150]

II.3 MATERIALS CHARACTERIZATION

II.3.1 MECHANICAL TESTING

Tensile tests were performed using a tensile tester (Mechanical Testing and Simulation - 2M) equipped with a 100N load cell. The fibers were tested on a 100 mm length and with a deformation rate of 100 mm/s. For each formulation, the tensile strength and elongation at break are obtained from an average of 10 measurements.

II.3.2 DIGITAL MICROSCOPY AND IMAGE PROCESSING

Digital microscopes are a variation of traditional optical microscope that uses optics and a charge-coupled device (CCD) camera to output a digital image to a monitor. In this work, the microscope enables to get a clear view of the fibers thanks to the high depth of field. The diameter of the fibers was thus measured with this technique on a Keyence – VHX-1000 digital microscope. Measurements were repeated ten times on randomly chosen parts of the filament, to ensure representative values.

Evaluation of the dispersion was performed on photographs taken with the previously described microscope. ImageJ software was used for image processing. To get the most accurate results, a computer macro analyzing the aggregates was written to ensure that basic steps in the image analysis are the same for each picture (**Appendix A**). Image processing is basically the following: picture is opened in ImageJ software (**Figure 31-a**) and scale bar is fitted to perform measurements. Some pixels are discriminated by adding white to the image (**Figure 31-b**); i.e. dark fibers edges or dark corners due to vignetting effect. Then manual threshold is applied to select (in red) the darkest parts of the image (**Figure 31-c**) (for example, dark dots corresponding to MWCNT aggregates). In the final step, the dark aggregates are counted and their surface measured (**Figure 31-d**). Dark surfaces corresponding to 1 pixel were deselected because they are not representative of aggregates and are due to image noise. In order to characterize the dispersion, six images of a formulation were analyzed following this procedure.

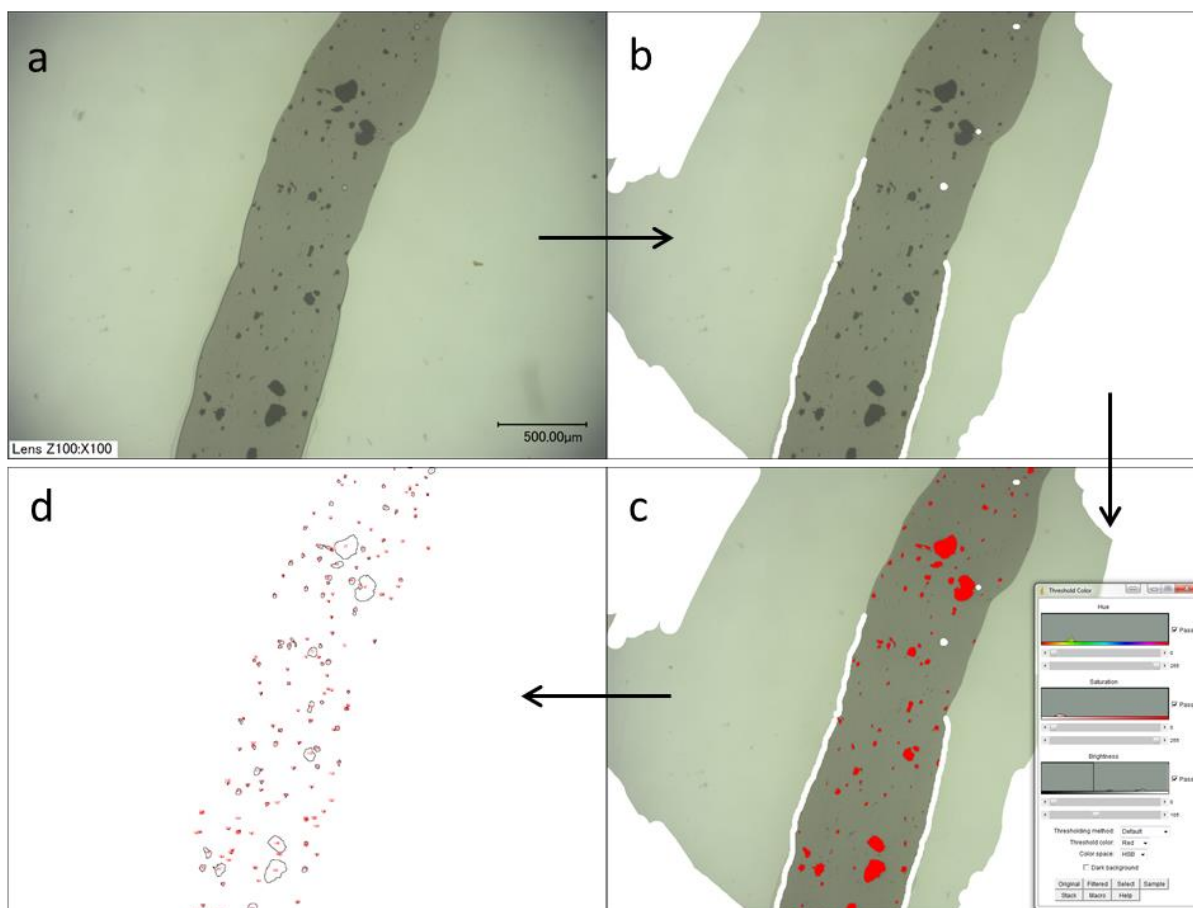


Figure 31: Image processing steps

II.3.3 ELECTRON PROBE MICRO ANALYSIS

Electron probe microanalysis (EPMA) is an analytical technique that is used to establish the composition of small areas on specimens. EPMA is one of several particle-beam techniques. A beam of accelerated electrons is focused on the surface of a specimen using a series of electromagnetic lenses, and these energetic electrons produce characteristic X-rays within a small volume (typically 1 to 9 cubic microns) of the specimen. The characteristic X-rays are detected at particular wavelengths, and their intensities are measured to determine concentrations. All elements (except H, He, and Li) can be detected because each element emits at a specific set of X-rays. This analytical technique has a high spatial resolution and sensitivity. Additionally, the electron microprobe allows obtaining highly magnified secondary- and backscattered-electron images of a sample. In this work EPMA (Cameca – SX 100) was used to characterize the dispersion of FR into the fibers and to get back-scattering electron pictures of the samples. Samples were prepared by plunging the fibers in vertical

position into an araldite resin. Once hardened, the resin is polished and leaves the cross section of the fiber exposed.

II.3.4 SOLID-STATE NMR

Solid-state NMR is a powerful tool for determining the changes of chemical environment in a material.

¹³C NMR measurements were done using a Bruker Avance spectrometer and a 4mm probe, working at 100.6 MHz (9.4 T) with cross polarization (CP) ¹H-¹³C and dipolar decoupling (DD) with magic angle spinning (MAS) (spinning frequency: 10kHz). The Hartmann–Hahn relation matching condition [151] was obtained by adjusting the power on the ¹H channel for a maximum ¹³C FID signal of glycine. All spectra were acquired with contact times of 1 ms and were accumulated with a number of scans varying from 1024 up to 50000.

³¹P NMR measurements were performed on a Bruker Avance II spectrometer, working at 161.9 MHz (9.4 T) and at a spinning rate of 10 kHz. Bruker probe heads equipped with 4 mm MAS assembly were used. Experiments have been carried out using CP because of the long relaxation time of the phosphorus nuclei (10 to 500 s) with ¹H high power dipolar decoupling (HPDEC). A recycle delay of 30 s was optimized and was applied for all samples. H₃PO₄ in aqueous solution (85%) was used as reference for 0 ppm.

II.3.5 DIFFERENTIAL SCANNING CALORIMETRY

Differential scanning calorimetry (DSC) is widely used for the characterization of polymers. Different properties such as glass transition, crystallinity or melting temperatures will be measured. Differential Scanning Calorimetry experiments have been performed on a TA Instrument DSC Q100 and monitored with the TA Universal Analysis software. The samples (5.0 ± 0.5 mg) have been prepared by making powder as previously described. The aluminum pan used is sealed and the nitrogen flow is fixed at 50 mL/min. Experiments are carried out at 10 °C/min, with 3 minutes of isotherm after each heating or cooling phase. The temperature/time ramp is schematized in **Figure 32**.

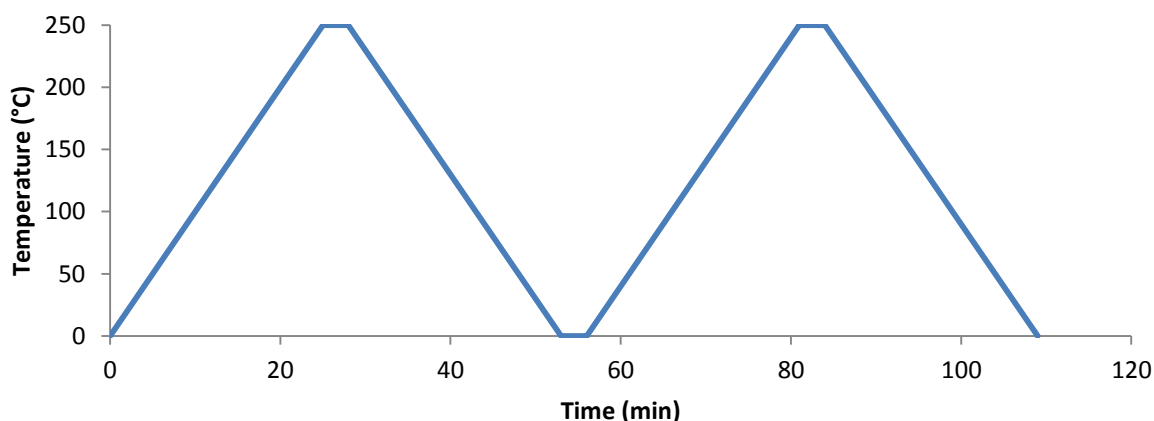


Figure 32: Temperature/time ramp used for DSC experiments

II.4 THERMAL DEGRADATION AND FIRE TESTING

II.4.1 THERMAL DEGRADATION

II.4.1.1 THERMOGRAVIMETRIC ANALYSIS

The ThermoGravimetric Analysis (TGA) is a technique in which the weight loss of a sample is monitored versus temperature while the sample is heated at a defined temperature ramp. The measurements can be carried out in oxidative (air) or inert atmosphere (nitrogen).

TGA measurements were carried out on a TA Instruments TGA Q5000. Samples of about 15 mg (powder form) were put in 250 μ l alumina pans. Balance and purge flow rates were set at 15 and 100 ml/min respectively. For each sample, an isotherm of 50 $^{\circ}$ C was applied for 5 min followed by a heating ramp of 10 $^{\circ}$ C. min^{-1} up to 800 $^{\circ}$ C. Each TG analysis was repeated at least twice to ensure the repeatability of the measurements.

In order to determine potential interactions between polyamide 6 and the flame retardant additives during the thermal degradation, a comparison between experimental and calculated TG curves is performed. The calculated curve is obtained by linear combination of the TG curves of each component (polymer, FR) weighted by their content in the formulation. Weight difference curve $\Delta w(T)$ was determined following **Equation 4**.

$$\Delta w(t) = w_{\text{exp}}(T) - w_{\text{the}}(T)$$

Equation 4

$w_{\text{exp}}(T)$: Experimental TG curve of the PA6/FR formulation

$w_{\text{the}}(T)$: Theoretical TG curve obtained by linear combination of the TG curves of PA6 and FR according to **Equation 5**.

$$w_{\text{the}}(T) = \alpha \times w_{\text{PA6}}(T) + (1 - \alpha) \times w_{\text{FR}}(T) \quad \text{Equation 5}$$

α : PA6 content (wt%) in the formulation

$w_{\text{PA6}}(T)$: Experimental TG curve of PA6

$w_{\text{FR}}(T)$: Experimental TG curve of FR additive

The main objective of this technique is to point out if the addition of the FR will stabilize or destabilize the system. When $\Delta w(t) > 0$, the weight loss is higher than expected, showing that the reactivity of the polymer with the additives leads to a thermal stabilization of the material. On the opposite, when $\Delta w(t) < 0$, the system is thermally destabilized.

II.4.1.2 TGA COUPLED WITH FTIR

Gaseous degradation products were identified coupling a FTIR Nicolet iS10 spectrometer from ThermoScientific, with the TG experiments made on the previously described instrument. A transfer line with an inner diameter of 1 mm was used to connect the TGA and the infrared cell. Both the transfer line and the gas cell were heated to 225 °C to avoid the condensation of the gaseous degradation products, the nitrogen gas flow was also set to 100 ml/min. The IR spectra were recorded between 400 cm^{-1} and 4000 cm^{-1} with the accumulation of 8 scans and an optical resolution of 4 cm^{-1} . For each sample, 15 mg of materials (powder) were positioned in alumina pans. Spectra recording starts at the same time that the 5 min isotherm begins, then a heating ramp of 10 °C/min is applied. This allows to match time and temperature easily, as 1 min corresponds to 10 °C (5 min = 50 °C, 20 min = 200 °C, ...)

II.4.1.3 PY-GC-MS

Pyrolysis-Gas Chromatography-Mass Spectrometry (py-GC-MS) was used in complement to the TGA-FTIR analyses. The device consists of a micro-furnace pyrolyzer (Frontier Lab - PY-2020iD) coupled with a GC-MS device (Shimadzu - GCMS QP2010 SE) (**Figure 33**). Analyses were performed through a thermal desorption mode. In the pyrolyzer furnace, the temperature was initially set at 50 °C and then raised to a defined temperature with a heating rate of 10°C/min. The temperatures of the interfaces between the pyrolyzer and the

GC and between the GC and MS were respectively set at 320 °C and 230 °C. A 30 m-long fused silica capillary column was used and the linear velocity of helium as a carrier gas was 40 cm/s. The GC column temperature was maintained at 35°C during the desorption process of samples in the pyrolyzer and then heated up to 300°C at the rate of 10°C/min, followed by an isotherm of 30 min at 300 °C. Electron-Impact spectra were recorded at 70eV with a mass scan rate of 2 scan/s. For each experiment, sample size is about 200 µg. Pyrograms and mass spectra were treated using the GCMS Post-run Analysis (Shimadzu) and F-Search (Frontier lab). Products are identified using NIST database.

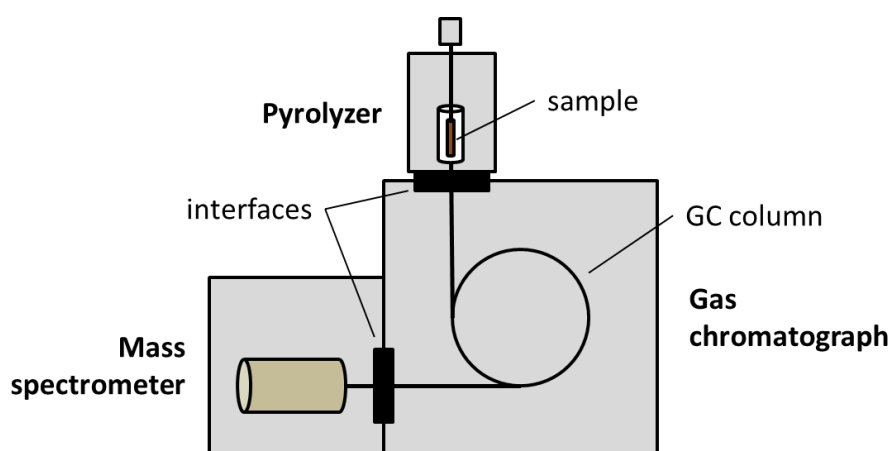


Figure 33: Schematic representation of the pyrolyzer-GCMS

To mimic the degradation of materials obtained by TGA experiments a so called step wise desorption process was used (**Figure 34**). Materials are degraded at 10 °C/min up to their first degradation step and the evolved gases are analyzed after the end temperature of the degradation step is reached. Afterwards the remaining material is heated up to the temperature of the second degradation step and so on. The evolved gases are again analyzed when the desired temperature is reached.

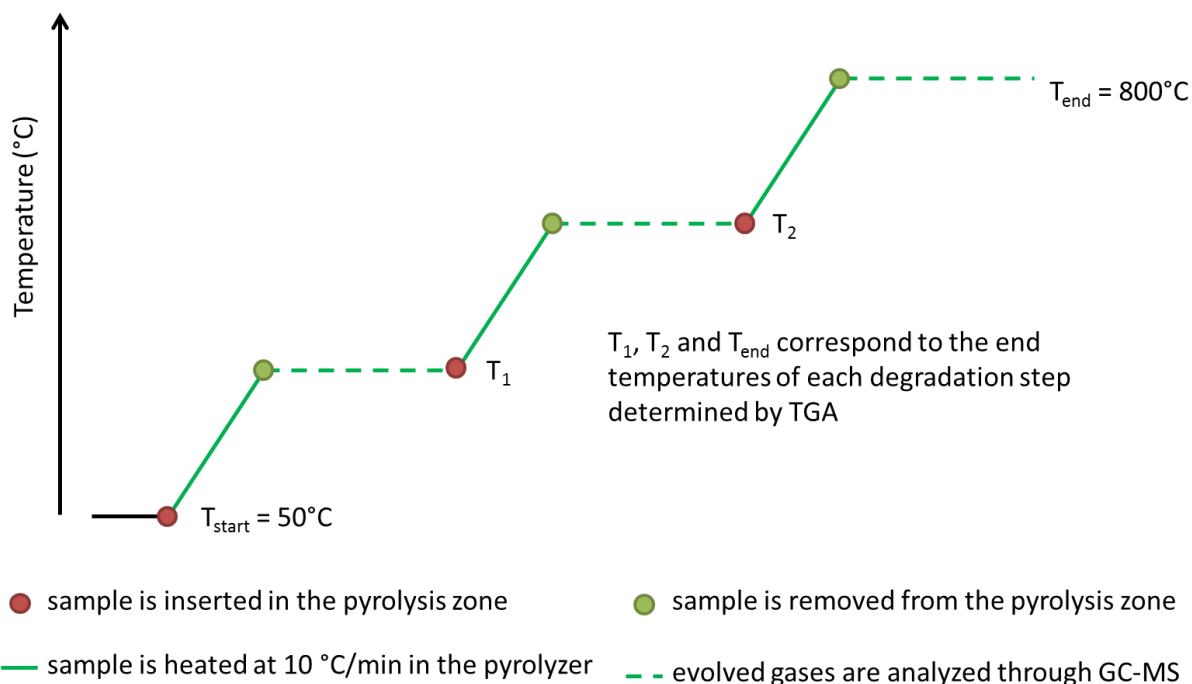


Figure 34: Stepwise method used for py-GC-MS characterization

II.4.1.4 THERMAL TREATMENTS

Thermal treatments consist in heating a sample in a furnace at a defined temperature (Heat Treatment Temperature; HTT). The treatment temperatures were determined according to TG curves as they correspond to the characteristic degradation steps of the systems.

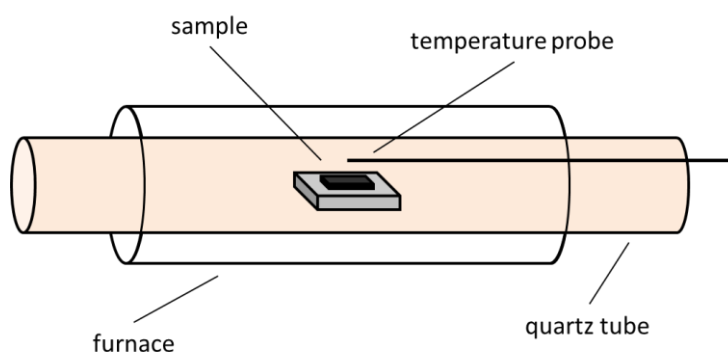


Figure 35: Tubular furnace used for thermal treatments

Samples were heat treated under air at a heating rate of $10^{\circ}\text{C}/\text{min}$ (similar to the one used for the TGA measurements) from ambient to the HTT followed by an isotherm of 1 hour. The samples were then cooled to ambient temperature before being collected. The residues obtained after thermal treatments were stored in a desiccator to avoid hydrolysis of the residues and then analyzed by solid state NMR.

II.4.2 FIRE TESTINGS

II.4.2.1 PYROLYSIS COMBUSTION FLOW CALORIMETRY

The fire-retardant capability was evaluated with a pyrolysis combustion flow calorimeter (PCFC) supplied by Fire Testing Technology Ltd. PCFC was developed by Lyon from FAA and allows measuring the flammability of small samples. **Figure 36** represents the principle of the PCFC device. Samples in the form of powder, were placed in open alumina pans and were degraded in a nitrogen atmosphere (“pyrolyser”) at a heating rate of 1 °C/s and with a nitrogen flow of 80 cc/min. The decomposition gases were then burnt in a nitrogen/oxygen mixture (“combustor”) with 80 cc/min and 20 cc/min flows respectively. The heat release is measured as a function of the temperature using an oxygen analyzer, according to the Huggett relation [152]. Using an heating ramp of 1 °C/s, pHRR value in W/g equals heat release capacity (HRC) in J/(g.K) [153].

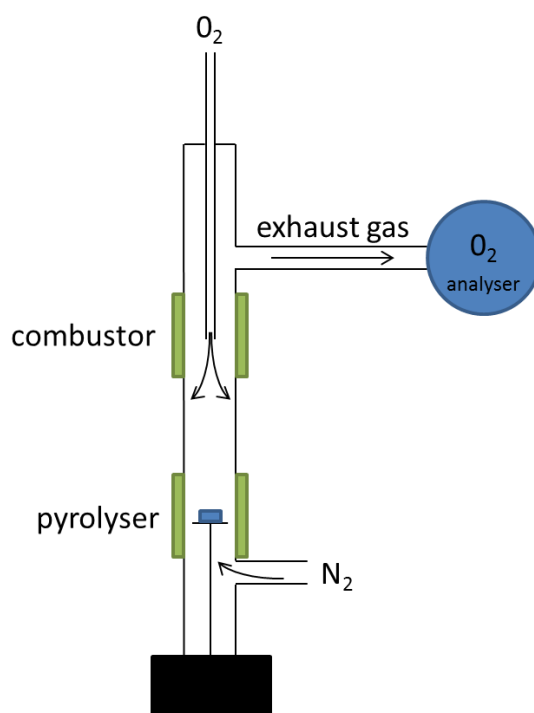


Figure 36: schematic PCFC representation

Determination of the optimal sample mass was performed by testing different amount of powder in the PCFC pan. In order to get the most repeatable measurements, the maximum oxygen consumption has to reach around 50% of the total O₂ in the mixture. That is to say, starting from a mixture containing 20% of O₂, the peak of consumption as to reach 10±3% O₂

II.4.2.2 MASS LOSS CALORIMETER

The mass loss calorimeter (MLC) allows the simulation of the conditions of fire in a small bench scale according to ISO 13927 [149]. A schematic representation of the mass loss calorimeter is given in **Figure 37**. The core of the instrument is a radiant electrical heater in the shape of a truncated cone, irradiating a flat horizontal sample ($100 \times 100 \times 3 \text{ mm}^3$) placed beneath it, at a preset heating flux (35 kW.m^{-2} to simulate a mild fire or 50 kW.m^{-2} for a developed fire). Ignition is provided by an intermittent spark igniter located 13 mm above the sample.

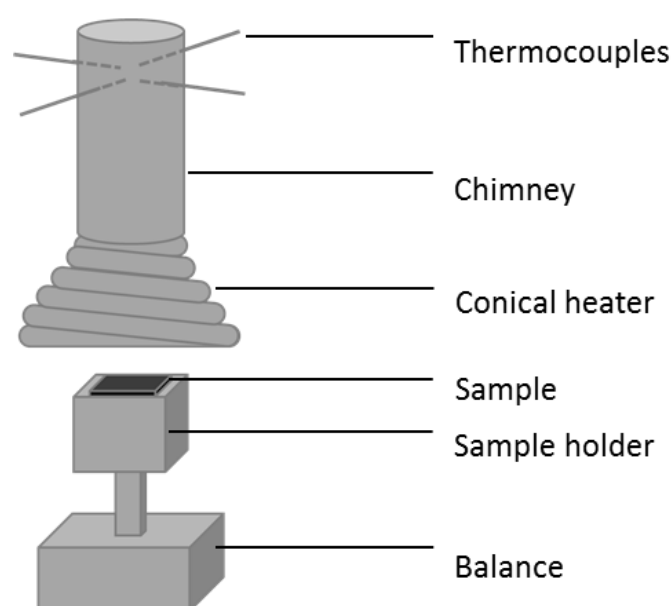


Figure 37: Schematic representation of a mass loss calorimeter

The mass loss calorimeter measures the temperature of the evolved gases using a thermopile located at the top of the chimney. The calibration of the heat release rate (HRR) is performed with methane. A methane flow of 0 to 6.7 ml.min^{-1} is burnt above the sample holder to obtain a calibration curve of the heat release as a function of temperature.

The measured parameters are the Heat Release Rate (HRR), the peak of Heat Release Rate (pHRR), the Total Heat Release (THR) and the Time To Ignition (TTI). These parameters allow the evaluation of the contribution to fire of the material. Another parameter, namely the “Residue Yield” (RY), is determined by subtracting masses of the sample before and after the test. It allows evaluating the propensity of the material to form a carbonaceous char.

The MLC measurements were performed on a Fire Testing Technology mass loss calorimeter device at 35 kW/m^2 , according to the ISO 13927, on specimens of $100 \times 100 \times 3 \text{ mm}^3$. All measurements were repeated at least two times to ensure good repeatability of results. The margin of error is estimated at 10% for the different parameters.

II.4.2.3 LIMITING OXYGEN INDEX

Limiting Oxygen Index (LOI) is a standardized test [148] which allows determining the minimum concentration of oxygen (in vol.-% O_2) in a nitrogen/oxygen mixture that is required for the combustion of a material in vertical position ignited by the top (Figure 38).

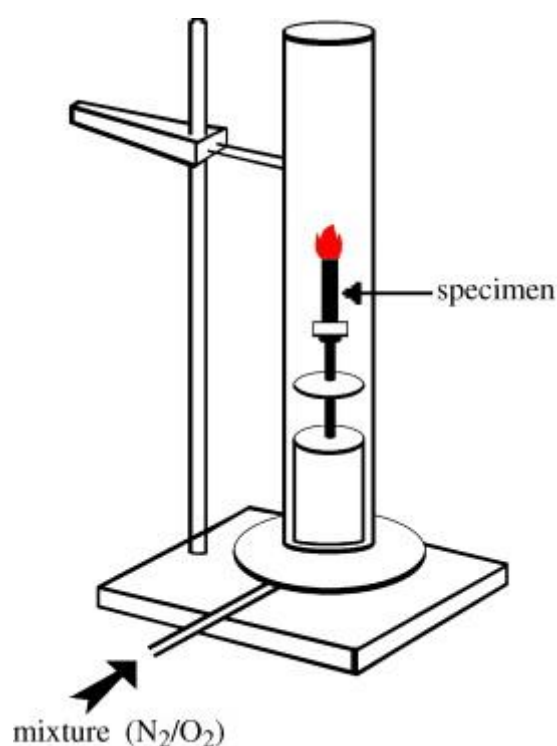


Figure 38: Experimental set-up for LOI measurement [74]

The LOI gives information on the relative flammability of a material. It measures the minimal oxygen concentration in an oxygen/nitrogen mixture that permits either to maintain flame combustion of the material for 3 minutes or lead to a burned length higher than 5 cm of the sample. The top of the test sample is ignited with a burner. Since air contains 21 vol.-% of oxygen, it is agreed that if LOI is lower than 21 vol.-%, the material is a combustible material, and on the contrary if LOI is higher than 21 vol.-%, it is a fire retarded material. LOI was measured using a Fire Testing Technology instrument on samples of $100 \times 10 \times 3 \text{ mm}^3$. LOI values are repeatable within $\pm 1 \text{ vol.-%}$.

II.4.2.4 UL-94

UL-94 is a small-scale test used to classify materials upon their ability either to self-extinguish or to spread the flame after ignition of the specimen. During the test, specimens are clamped vertically and exposed to a defined flame ignition source at the bottom during 10 seconds (**Figure 39**). The flame is applied a second time if the sample self-extinguishes after the first flaming. To evaluate the flammability of the potential drips release during the test, cotton is placed below the sample and may ignite due to burning drips or not.

Three classifications are assigned to materials based on their behavior regarding burning, flame propagation and dripping: V-2, V-1 and V-0, V-0 being the best ranking. If the material does not meet the criteria, it is non-classified (NC) at the UL-94 test. **Table 13** presents the criteria allowing the UL-94 classification.

The UL-94 tests were realized on a Fire Testing Technology Limited equipment on barrels of 127x12.7x1.6 mm³ in accordance with the recommendations of the standard [150]. The barrels are ignited by a blue flame (without cone) of 20 mm. The burner which generates the flame is obtained with methane gas having a flow rate of 105 ml/min with a back pressure lower than 10 mm of water. For each formulation, five bar specimens are tested after they underwent a preconditioning at 23±2°C for a minimum of 48 hours.

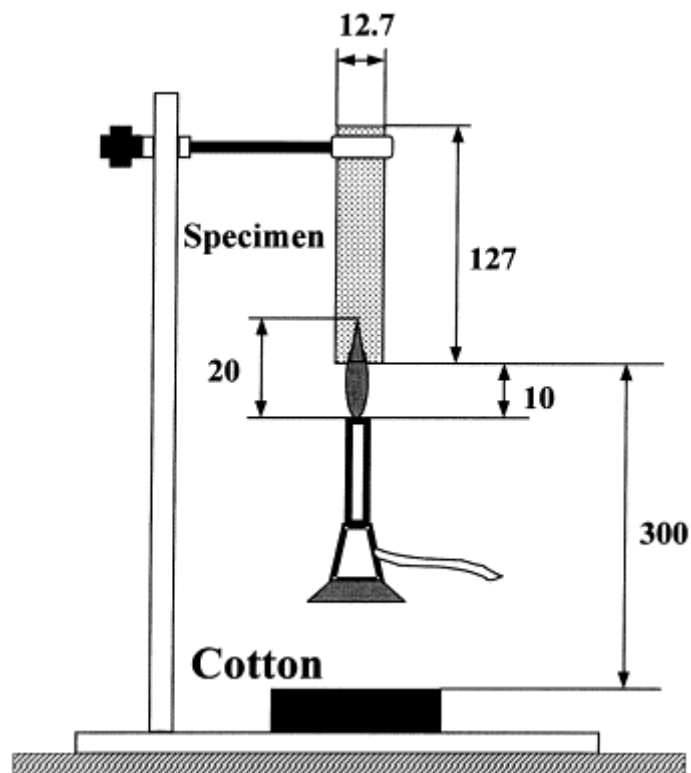


Figure 39: Schematic representation of UL-94 test [154]

Table 13: UL-94 criteria for classification

Criteria	V-0	V-1	V-2
Afterflame time for each individual flaming	≤10s	≤30s	≤30s
Afterflame+afterglow time for each individual specimen, after second flaming	≤30s	≤60s	≤60s
Total afterflame time for any condition set (5 flamings)	≤50s	≤250s	≤250s
Cotton indicator ignited by flaming drops	No	No	Yes
Afterflame or afterglow of any specimen up to the holding clamp	No	No	No

II.5 CONCLUSION

This chapter described the materials, the techniques (in terms of processing and analysis), as well as the protocols used to achieve the main challenge of this project: the development of flame retarded PA6 fibers. In the next chapters, all these techniques will be used to carry out first a screening of different fire retardants. The formulations presenting the most interesting results will be characterized more extensively and the mechanisms of action will then be fully investigated.

III	FLAME RETARDANT SCREENING FOR POLYAMIDE 6 FIBERS	
III.1	Introduction _____	100
III.2	Flame retardant screening _____	101
III.2.1	Selection of flame retardants _____	101
III.2.1.1	Phosphorus based fire retardant _____	102
III.2.1.2	Sulfur based flame retardants _____	102
III.2.1.3	Nanoparticles as fire retardants _____	102
III.2.2	Fire retardant properties and thermal stabilities _____	103
III.2.2.1	Phosphorus based fire retardants _____	103
III.2.2.2	Sulfur based fire retardants _____	106
III.2.1	The use of nanoparticles _____	109
III.2.1.1	Selection of processing parameters _____	109
III.2.1.2	Conclusions on the processing parameters for nanoparticles _____	113
III.2.1.3	Nanoparticles screening _____	114
III.3	Conclusion _____	117

III.1 INTRODUCTION

The aim of the present work is to develop flame retarded PA6 fibers. The challenge is thus to find a system in which the total loading of additives does not exceed 10 wt.-% as discussed in the first chapter. The FRs have also to be stable at the rather high processing temperature of PA6; eventually the spinning ability of the formulation is required. Three types of additives have been chosen, the first are commercial phosphorus fire retardants, the second type consists in sulfur based FR that were found effective at very low loadings in PA6. The last one corresponds to nanoparticles. In a first part, a screening is carried out considering two discriminant properties: the spinnability of the formulation and their flame retardant properties.

The spinnability of the different formulations was determined experimentally using the DSM microextruder and microspinning device described in Chapter 2. During the extrusion process, fibers were drawn, and the formulation is said to be spinnable if a monofilament of at least 50 m can be made.

Pyrolysis-Combustion Flow Calorimetry (PCFC) was chosen as the main fire test to evaluate the different formulations. PCFC is a relatively new method to characterize the potential flame retardancy of polymeric materials. Its main advantage is the possibility to test materials with only milligrams of samples, allowing a quick determination of the materials properties, which is particularly suitable for a screening step where small amounts of materials are available [155]. On the other hand, cone calorimetry requires fabrics and the results may be affected by a number of factors such as the retaining grid, the weight sample and textile construction [60]. PCFC measures the intrinsic properties of the materials and moreover, previous studies have proven the efficiency of PCFC in assessing the burning parameters of textiles and fibers (synthetic or natural) treated with char promoting phosphorus compounds [156, 157]. However, there are in principle strong limitations for correlating microscale with real-scale fire tests. pHRR measured in cone calorimetry has been correlated with pHRR obtained by PCFC in the case of pure polymers [158], but with FR polymers the results are poorly correlated. This difference can be attributed to significant interaction of incomplete gas-phase combustion, gas-phase flame inhibition reactions, char formation, and heat/mass transfer of burning FR compounds in cone calorimetry [159].

Assuming these last assertions, it is legitimate to think that testing nanocomposite in PCFC is non-sense if mechanisms of action related to nanoparticles are mainly the formation of a protective layer preventing from the heat and mass transfer. Indeed, Schartel *et al.* [160], proposed that PCFC does not account for important physical effects occurring on larger scales, such as barrier formation, insulation and flame inhibition. However it is known that NPs are able to change the degradation pathway of polymers, such as MMT (C30B) in PA6 [161], which favors the formation of larger molecules during degradation of the matrix; this has also been reported in EVA [162] and PS [163]. Changes in the degradation pathway of the matrix can lead to different degradation products or ratios, hence affecting the PCFC results. It was also reported that CNT loaded at 0.2 and 1 wt.-% in PA6 and PMMA reduced by 10% the pHRR measured with PCFC [164]. Authors excluded a dilution effect due to the negligible amount of CNT in the formulations, and rather explained the small reduction by radical trapping. It is thus reasonable to use this technique as a first step to evaluate the FR properties of the fibers

This chapter presents the screening of the different fire retardants that have been melt-mixed in PA6. First is described the selection of the different FR used for this work, then formulation containing phosphorus and sulfur based FR are analyzed using the spinning device, the PCFC and the TGA. Eventually, the nanoparticles are also evaluated and discussed. The thermo-oxidative degradation of the different materials was also monitored to get a fast overview of the thermal behavior of the samples. Indeed FR additives are designed to modify the thermal decomposition mechanism of the polymer (e.g. produce less combustible products) [50], this property is thus, also of interest.

III.2 FLAME RETARDANT SCREENING

III.2.1 SELECTION OF FLAME RETARDANTS

The development of a new system to flame retard PA6 fibers requires the selection of potential compounds that can be melt-mixed in the matrix. The selection of FR was function of the “state of the art” presented in Chapter 1, reviewing the previous researches done on flame retardancy of PA6.

Three types of flame retardants additives were selected to evaluate their potential efficiency in the PA6 matrix: commercial phosphorus based fire retardant, sulfur based compounds and nanoparticles.

III.2.1.1 PHOSPHORUS BASED FIRE RETARDANT

Phosphorus based FR products including Exolit® OP 950, Exolit® OP 1230, Aflammit® PCO 900, Aflammit® PCO 960 were evaluated at a loading of 5wt.-% in PA6.

Clariant's Exolit® OP 950 and Exolit® OP 1230 are phosphinate salts, these salts are known to be effective in PA6 [85]. Although OP 950 was initially designed to be used in PET [165], this additive was selected because it melts, which is a great benefit when drawing fibers as it allows to obtain good dispersion of the fire retardant. OP1230 is described as a highly stable phosphinate flame retardant for high temperature nylons, and moreover, suitable for use in fibers applications [166].

Thor products Aflammit® PCO 900 and Aflammit® PCO 960 (which is a non micronised version of the PCO 900) were chosen as they are flame retardants with melting point of 245°C (which is in the processing temperature range of PA6). They are said to have good thermal stability up to 270-280°C and to be effective in a wide range of polymers, especially fibers, non-wovens and very thin walled articles [167].

III.2.1.2 SULFUR BASED FLAME RETARDANTS

Sulfur based FR compounds such as ammonium sulfamate were chosen due to their ability to raise LOI values in PA6 and improve the UL-94 rating at very low content [98]. The addition of a small amount of ammonium sulfamate and dipentaerythritol, 2 and 0.7 wt.-% respectively in PA6, yielded a V0 at UL-94 rating on bars of 1.6 mm thickness, and a LOI value of 35.7 vol.-% [168]. Ammonium sulfamate alone in PA6 also leads to a V0 with 2 wt.-% loading [98]. Ammonium and guanidine sulfamate will thus be evaluated.

III.2.1.3 NANOPARTICLES AS FIRE RETARDANTS

Nanoparticles and nanocomposites have gained more and more attention in the past few years, as only small amounts of NP can dramatically enhance the materials properties; this is particularly true for mechanical properties [169, 170]. Moreover, NP were shown to lower

pHRR and slow down combustion processes in many polymers [171]. This approach has also been validated in the literature for fiber applications [68, 172, 173]. Carbon (graphene oxide and MWCNT) and silicate (halloysite and MMT) based NP were chosen in this study and both types have sheet-like and tubular shapes.

III.2.2 FIRE RETARDANT PROPERTIES AND THERMAL STABILITIES

III.2.2.1 PHOSPHORUS BASED FIRE RETARDANTS

Phosphorus based flame retardants were incorporated at 5 wt.-% in the polyamide matrix (Table 14) and appear to have nearly no effect on the pHRR measured by PCFC. The best results were obtained with OP 1230 and PCO 900 with a reduction of 6.3% of the pHRR. These results could be attributed to a dilution effect of the matrix also noticeable by the reduction of 5% of the THR. However, the results are too close to the margin of error of the instrument and thus no improvement of the FR properties could be observed.

Table 14: Spinnability and PCFC results for commercially available FR solutions

Formulation	Spinnable*	pHRR (W/g)	Δ pHRR/PA6 (%)	THR (kJ/g)	Δ THR/PA6 (%)
PA6	Y	588	-	30.0	-
PA6/OP950 5%	Y	593	0.8	27.0	-10.0
PA6/OP1230 5%	Y	551	-6.3	28.5	-5.0
PA6/PCO900 5%	Y	552	-6.3	28.5	-5.0
PA6/PCO960 5%	Y	591	0.4	26.9	-10.3

* Y: yes, N: no

Thermal stability of the different samples was evaluated using TGA in thermo oxidative conditions (Figure 40 and Figure 41). A three-step decomposition is obtained for neat PA6. From ambient to 320 °C a small weight loss of 2% is attributed to moisture evolution. The main step of degradation (between 320 °C and 480 °C with a maximum rate at 449 °C) corresponds to 88 % wt. loss. The last step, from 480 to 540°C, corresponds to a 10 % wt. loss and is due to the oxidation of the transient residue. The major decomposition step corresponds to the volatilization of monomer and chain fragments while the second step corresponds to oxidation of the charred residues with emission of CO and CO₂ as reviewed in the literature [50, 54].

When 5 wt.-% OP950 is added in PA6, similar behavior is observed. From ambient to 320 °C a small weight loss of 3.6 % is attributed to moisture evolution. The main step of degradation occurs between 320 and 478 °C and a weight loss of 84 % is observed, the maximum

degradation is reached at 445 °C. The final step from 478 °C to 560 °C corresponds to the oxidation of the residues (11 %).

Finally is the case of PA6/OP1230 5%, from ambient to 328 °C a small weight loss of 4.2 % is attributed to moisture and water evolution. The main step of degradation occurs between 328 °C and 475 °C and a weight loss of 79 % is observed, the maximum degradation is reached at 442 °C. The final step from 478 °C to 675 °C corresponds to the oxidation of the residues (15 %).

As a conclusion, it is observed that the major step of degradation occurs at the same temperature for each sample including neat PA6. The major difference is seen during the last degradation step, which is attributed to the oxidation of the transient residues. For the OP1230 formulation, one can note that more residue is oxidized than for the other two samples, namely PA6 and PA6/OP950 5%. The presence of a decomposition step before 400 °C is not seen, probably because of the low loading of phosphinate salts (5 wt.-%) used in the present work and their relatively high thermal stability [174].

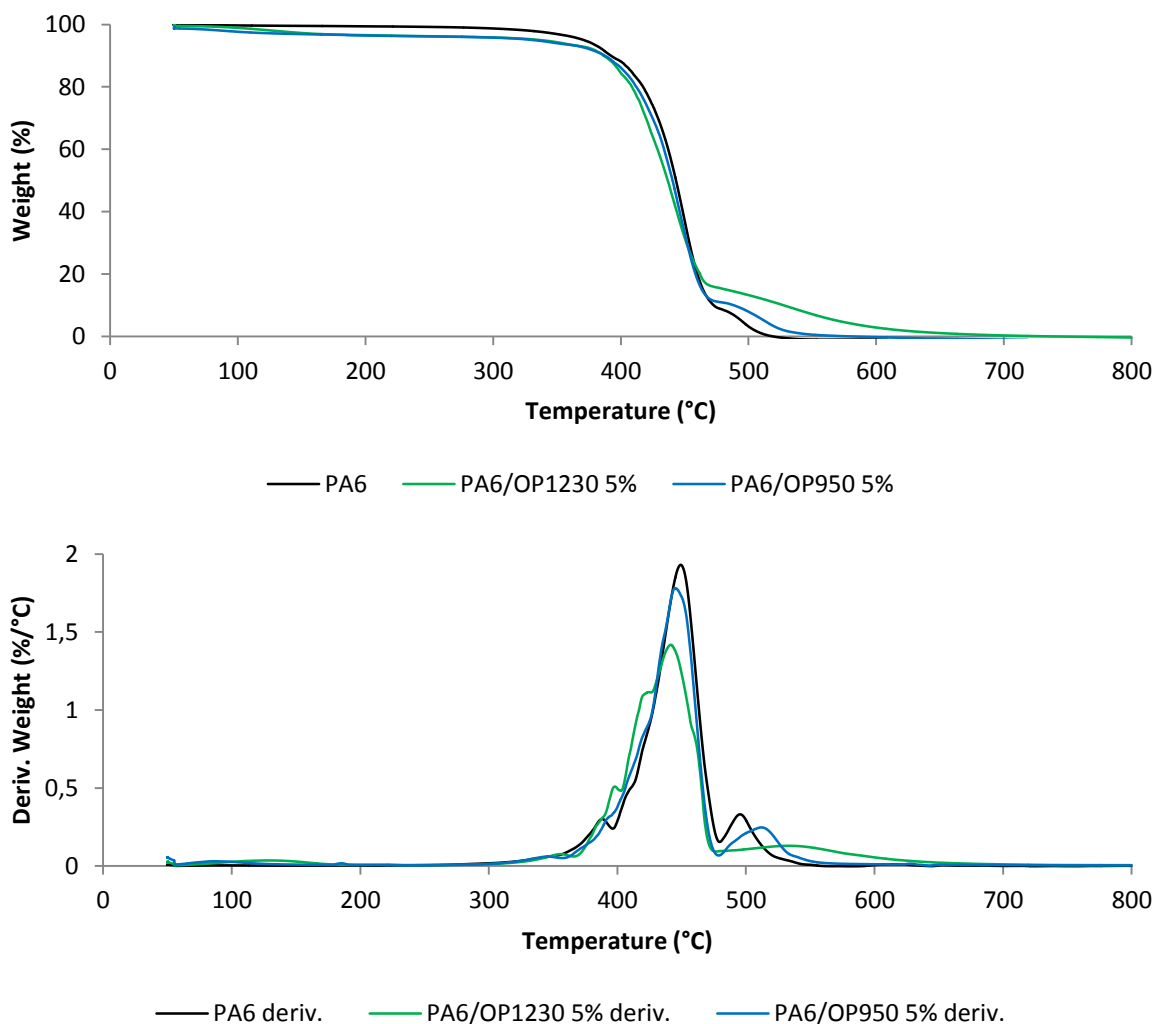


Figure 40: TG and DTG curves of neat PA6 and PA6 containing commercial products PA6/OP1230 5% and PA6/OP950 5% (10 °C/min, air)

Considering the products from Thor, a three step degradation process is observed for PA6/PCO900 5% and PA6/PCO960 5% (**Figure 41**). From ambient to 270 °C, a weight loss of 3.5 wt.-% is attributed to water and moisture evolution. The main step of degradation starts at 270 °C and ends at 430 °C, with a weight loss of 78 %. Then from 430 to 483 °C, a small weight loss of 8 wt.-% is observed followed by a char oxidation occurring from 483 to 620 °C with a weight loss of 10 %.

Thor products, PCO900 and PCO960 lead to a significant destabilization of the matrix as both formulation starts to degrade at a temperature around 50 °C lower than neat PA6. One can note the very good repeatability of the extrusions and TGA. Indeed, PCO900 is a micronized version of PCO960 and thus, they correspond to the same compound and by extent they give the same formulations, in terms of matrix and additives chemistry. This explains why the two

TG curves are superimposed. Transient residues from the PCO formulations are more resistant towards oxidation, as shown by the last step of degradation occurring on a broader range of temperature.

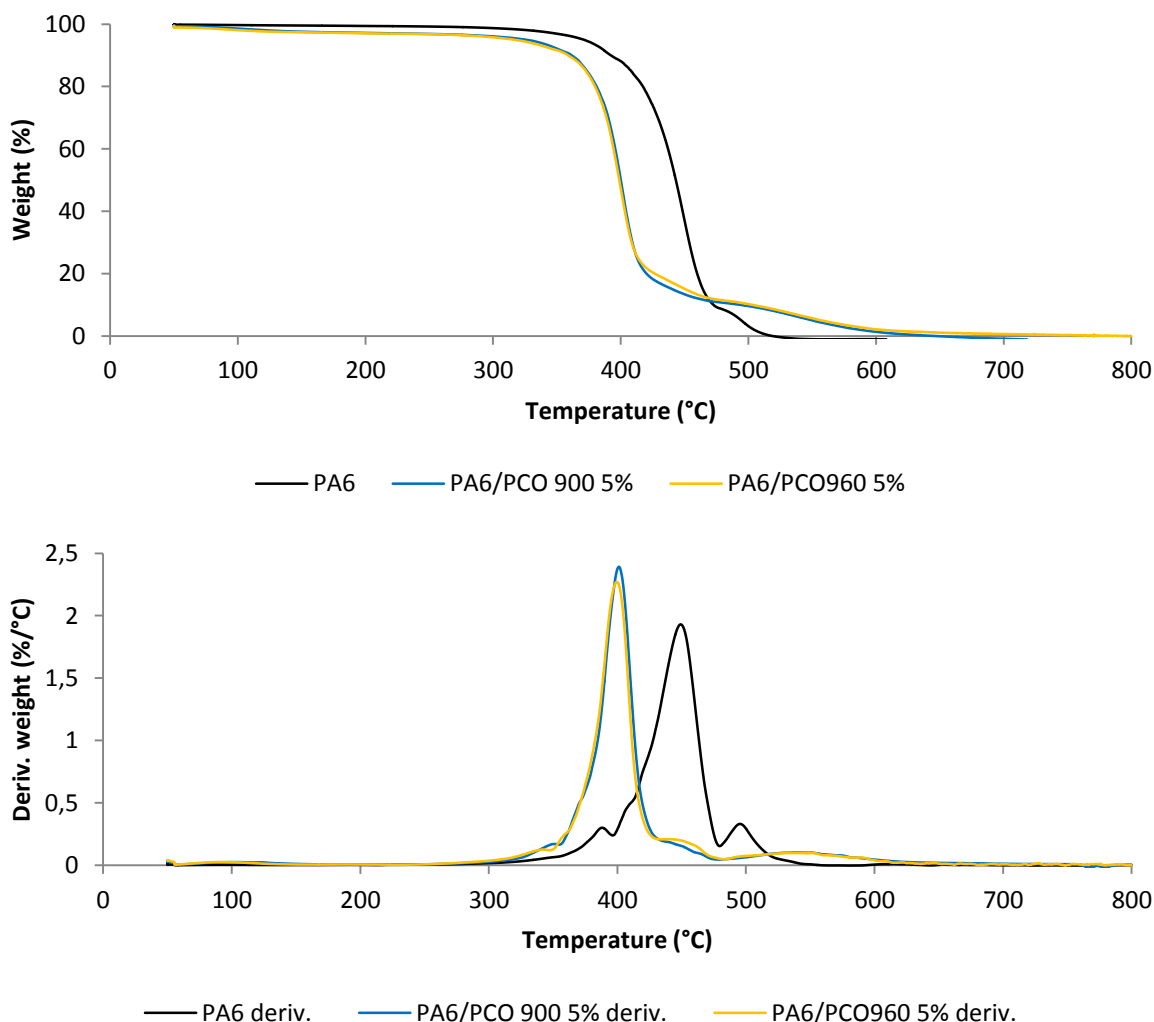


Figure 41: TG and DTG curves of neat PA6 and PA6 containing commercial products PA6/PCO900 5% and PA6/PCO960 5% (10 °C/min, air)

III.2.2.2 SULFUR BASED FIRE RETARDANTS

Ammonium sulfamate and guanidine sulfamate were evaluated as FR in PA6 at various loadings (5 and 10 wt.-%). Those additives gave the most interesting results in terms of pHRR decrease (**Table 15**). A Δ pHRR/PA6 of -21.6 % is obtained with a formulation containing 5 % of AS. However, the formulation containing 10 wt.-% of AS could not be spun. Guanidine sulfamate appears to be easier to process and could be spun with loadings of 10 wt.-%. In this case, pHRR was reduced by 25.4 %. AS and GAS formulations show a decrease in pHRR values with increasing content of FR. THR value of all formulations is decreased compared

with pure PA6. Moreover, this decrease is higher than the amount of additives in the formulations, meaning that not only a diluting effect is shown by PCFC.

Table 15: Spinnability and PCFC results for non-commercial FR solutions

Formulation	Spinnable*	pHRR (W/g)	Δ pHRR/PA6 (%)	THR (kJ/g)	Δ THR/PA6 (%)
PA6	Y	588	-	30.0	-
PA6/AS 5%	Y	461	-21.6	27.1	-9.7
PA6/AS 10%	N	-	-	-	-
PA6/GAS 5%	Y	500	-14.9	27.4	-8.7
PA6/GAS 10%	Y	439	-25.4	25.7	-14.3

* Y: yes, N: no

The thermal stability of the materials containing 5 wt.-% of AS and GAS and 10 wt.-% of GAS was investigated by TGA (**Figure 42**). Concerning PA6/AS 5%, apart from a small weight loss of 2 % between 50 and 260 °C due to the release of moisture and water adsorbed on the material, PA6/AS 5% sample exhibits three steps of degradation. The first one starts at 260°C, and corresponds to a weight loss of 7 %. Lewin et al. [98, 168] reported sulfation reaction in the temperature range of 200-270 °C as well as dimerization of AS into diammonium imidobisulfonate, both reactions releasing ammonia. Between 310 and 490 °C, the main degradation step corresponds to a weight loss of 77 % with a maximum rate at 447 °C. The last weight loss of 14 wt.-%, from 490 to 600 °C, is assigned to the oxidation of the transient residue.

Similarly, PA6/GAS 5% presents a three step degradation process, apart from a small weight loss of 1.5 % between 50 and 268 °C due to the release of moisture. The first step starts at 268°C and ends at 368 °C, it corresponds to a weight loss of 8.5 %. Between 368 °C and 483 °C, the main degradation step corresponds to a weight loss of 75 % with a maximum rate at 437 °C. The last weight loss of 15 wt.-%, from 483 to 610 °C, is assigned to the oxidation of the transient residue.

Overall behavior of PA6/GAS 10% is similar to that of PA6/GAS 5% and exhibits three steps of degradation, apart from a small weight loss of 3 % between 50 and 263 °C due to the release of moisture. The first step starts at 263°C and ends at 360 °C, it corresponds to a weight loss of 14 %. Between 360 °C and 486 °C, the main degradation step corresponds to a weight loss of 64 % with a maximum rate at 430 °C. The last weight loss of 19 wt.-%, from 483 to 650 °C, is assigned to the oxidation of the transient residue.

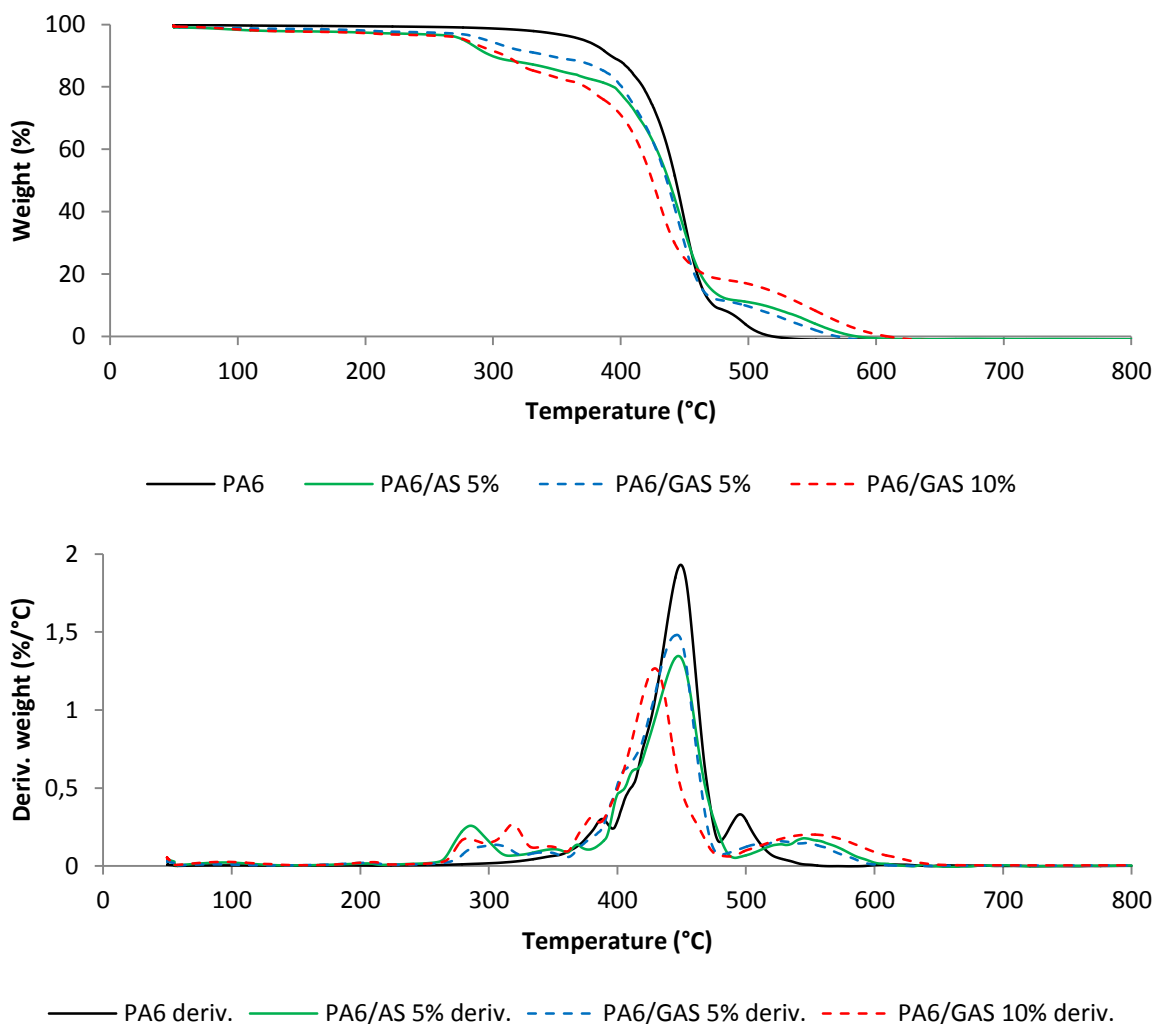


Figure 42: TG and DTG curves of neat PA6 and PA6 containing sulfamate salts PA6/AS 5%, PA6/GAS 5% and PA6/GAS 10% (10 °C/min, air)

It can thus be concluded that in thermo-oxidative conditions, neat PA6 decomposes in two steps while the formulated polymers undergo a three-step degradation. The additional step is believed to be due to decomposition/interaction of the FR or its decomposition products with the PA6 matrix, thus the addition of FR leads to a decrease of the thermal stability of PA6. It can be seen with the guanidine sulfamate containing formulations that the higher the amount of GAS in PA6, the more important the first step of degradation. Adding 10 wt.-% of GAS in the PA6, the temperature of maximum mass loss rate is decreased to 430 °C while for the other formulations and neat PA6 this temperature is between 446 and 448 °C.

III.2.1 THE USE OF NANOPARTICLES

Nanoparticles and the resulting nanocomposites often work by the formation of a protective layer at the top of the burning material, acting as a heat shield and barrier for pyrolysis gases [125, 129, 130, 175]. Moreover, it is widely reported that nanoscale morphology influences the fire performance of nanocomposite [176]. The dispersion has a significant influence on the HRR and flammability [177], thus, in order to improve the fire retardancy of polymers and in particular polyamide, it is in general required that nanoparticles are well dispersed (nanodispersed) [178-180]. This allows creating an homogeneous barrier without cracks in order to avoid bubbling when submitted to heating. The dispersion of the NP is thus of importance when dealing with nanocomposites and should therefore be studied. In a general way “true” nanocomposite have better results in terms of HRR and pHRR can even be an indication that a nanocomposite structure has been obtained [181].

III.2.1.1 SELECTION OF PROCESSING PARAMETERS

Unlike with polystyrene, TGA cannot give any information on the state of dispersion of the nanoparticles in PA6 [182], thus other means methodologies have to employed to investigate the dispersion of nanoparticles in the matrix. The most common techniques used to study the morphology of nanocomposites are scanning electron microscopy and transmission electron microscopy [183]. Solid state NMR can also be used to characterize the dispersion of clay in PA6 by measurement of the T_1^h relaxation times [184, 185]. In the case of carbon nanotubes, electrical measurements can serve as a good indicator of the state of dispersion as they are conductive nanoparticles [186].

In this study, the optimization of the processing parameters in the case of PA6/MWCNT was first considered. Investigation of the multiwall carbon nanotubes dispersion was done on two formulations extruded with different parameters described in **Table 16**. Four factors were selected according to their ability to influence the dispersion. These factors are all processing parameters of the microextruder.

Table 16: Parameters used for the extrusion of nanocomposite formulations

Parameters	Temperature (°C)	Screws speed (RPM)	Residence time (s)	Screws type
f1	245	50	180	standard
f12	275	100	540	“nano”

First, it is known that melt temperatures influence the melt viscosity of the polymer [187] and thereby the level of dispersion and the magnitude of generated shear stresses for agglomerate dispersion [188].

Dispersion of agglomerates during extrusion also depends on the shear stress intensity thus on screw speed as demonstrated in the literature [189]. It was demonstrated by Pötschke *et al.* [186] that in microcompounder, higher screw speed enhanced the dispersion of agglomerated CNT; a dielectric measurement performed on the nanocomposite samples was used to characterize the dispersion.

An extended residence time is bound to result in polymer degradation while short residence times may not provide the desired level of dispersion. Moreover over-mixing could cause reagglomeration of nanoparticles [188, 190]. While processing carbon nanotubes, long mixing times can also cause a decrease of the NP aspect ratio and therefore modify the barrier forming properties of this FR [191].

Standard or “nano designed” (Figure 43) screws were available for the microextruder in the laboratory. The difference between the two designs is the presence of notches in the screw thread of the “nano” screws. Standard screws are not equipped with mixing elements, and consequently cannot create complex flow types which are more efficient in dispersive mixing. As a result of similar geometrical design of the two screws, the melt conveying characteristics are similar; therefore, despite twin screws, the flow type of the melt of extruder is similar to that of a single screw extruder without having any mixing elements [192]. On the contrary, with “nano” screws, during the process, the polymer melt is forced to flow through the notches, hence this enforces elongational flow and thus promotes dispersion [193].



Figure 43: Standard and "nano" screws used with the microextruder, the red circle on the zoomed part shows the notch on the "nano" screws

f12 parameters corresponds to the more severe conditions: PA6 is extruded for 9 minutes at 275 °C and 100 rpm. This could lead to chain breakage and degradation of the polymer due to high mixing rate and long residence time (thermo-mechanical degradation). Moreover, small amounts of moisture left after drying may hydrolyze the molten polymer [194]. Eventually, mechanical properties of the materials, and fibers, might be impacted. f1 parameters gives the “softest” conditions of extrusion, and should have less impact on the fibers than f12.

PA6/MWCNT 1% formulations were prepared with the conditions described as f1 and f12, and fibers were drawn according to the method described in Chapter 2. Fibers were cryo-fractured in liquid nitrogen and their cross sections were observed by Scanning Electron Microscopy (SEM). **Figure 44** shows two pictures of the formulations f1 and f12, the white objects on both of them correspond to MWCNT. Only a few MWCNT have been observed despite the high number of observations. Literature shows that well dispersed MWCNT are rather easy to see using SEM [57, 195]. Thus, it suggested that the dispersion in f1 and f12 formulations is not optimal. The materials may rather be microcomposites than nanocomposites. This explains why only a few nanoparticles are observed, as most of them are regrouped in big aggregates.

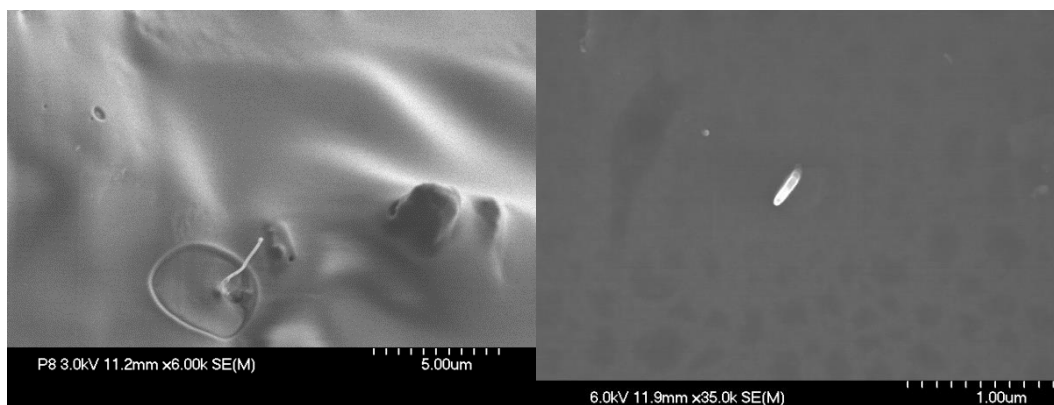


Figure 44: SEM pictures of a cross section of PA6/MWCNT 1% f1 (left) and f12 (right) formulations

Observations with a digital microscope on fibers are shown in **Figure 45**. It confirms the low dispersion observed with SEM.

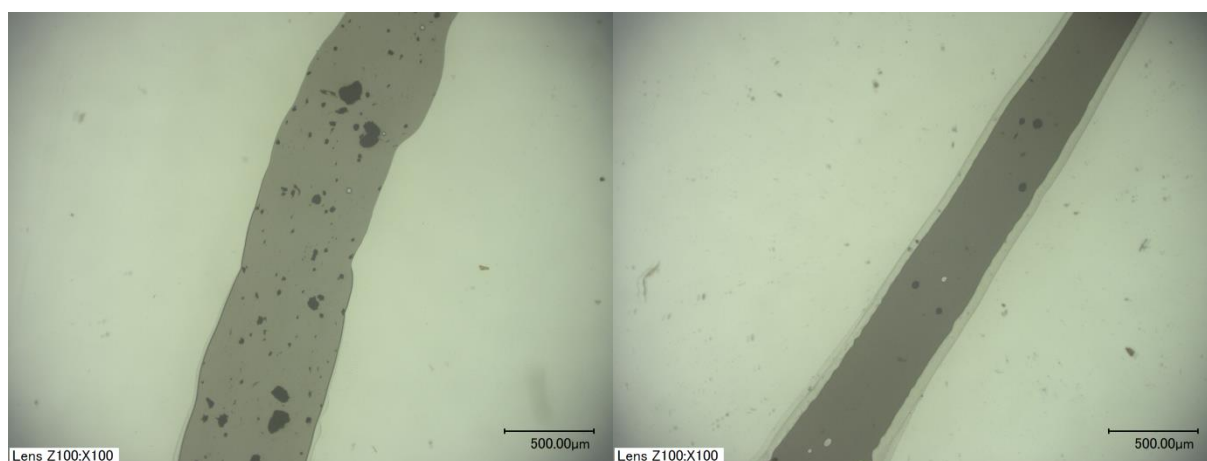


Figure 45: Digital microscope pictures of PA6/MWCNT 1% f1 (left) and f12 (right) formulations, dark dots correspond to MWCNT aggregates

Using digital microscopy, it can be seen that MWCNT aggregates are present in both formulations, however it seems that f1 fibers contains aggregates of smaller and bigger size. In order to characterize the dispersion of the nanotubes, image processing was done on pictures of the two extreme formulations using imageJ software to get the count and average particle size of the aggregates, with the method described in part II.3.2. Results of image analysis are summarized in **Table 17** and **Figure 46**.

Table 17: Results of particles analysis from images of Figure 45

Formulation parameters	Average particles count	Average size (μm^2)
f1	103	534.36
f12	16	1280.02

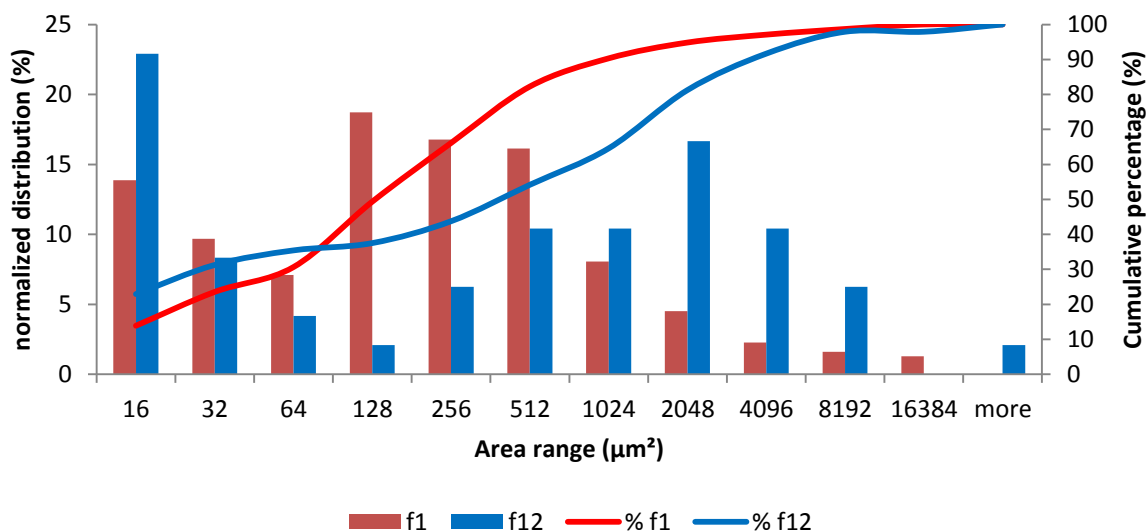


Figure 46: Particle size distribution of f1 and f12 formulations

From the results of image analysis it is possible to show that microdispersion is achieved with both parameters as the average particle size is in the range of 500-1300 μm^2 . With **Table 17**, it can be concluded that f1 parameters enhance the dispersion as more particles are counted and the average aggregate size is lower than for f12 formulation. Analyze of the particle size distribution also indicates that f1 parameters gives smaller aggregates size (between 128 and 512 μm^2) whereas f12 has more big particles. The cumulative percentage curves shown in **Figure 46**, shows that 80% of the aggregates from f1 are 512 μm^2 wide or less, whereas, 50 % of the f12 aggregates are at least 512 μm^2 wide.

III.2.1.2 CONCLUSIONS ON THE PROCESSING PARAMETERS FOR NANOPARTICLES

The investigation carried out on four different processing parameters allowed to quickly determine the influence on the dispersion of MWCNT using the “extreme” parameters with two formulations. It appears that in the range of selected temperatures, residence times, RPM and screw designs, the resulting formulations are microcomposites. Indeed, each set of parameters gives particle size in the range of μm^2 area, and none of the two give significantly different results. The same study was done on nano graphene oxide and the same trends are observed (**Appendix C**).

It was eventually decided to standardize the parameters for all other works using levels from both f1 and f12. A rotational screw speed of 100rpm was kept to allow a better feeding of the PA6 pellets in the microextruder. The use of “nano screws” was maintained in order to get the best mixings as possible with regard to an eventual use of NP in future formulations.

The temperature of extrusion was set to 245 °C to avoid melt reactivity or degradation with the incorporation of FR and the residence time was also kept low (3 minutes).

III.2.1.3 NANOPARTICLES SCREENING

Carbon based NPs were introduced at 1 wt.-% in the matrix while silicate based were filled at 5 wt.-% (**Table 18**). All nanoparticles formulations were spinnable, as previously reported in various studies [**141**, **196**]. With 5% of organomodified nanoclay (C30B), pHRR is reduced by 6.1 % compared to neat PA6. These results can be attributed to a polymer dilution, and is in the margin of error of the measurements. Similarly with the other NP, no real decrease in pHRR was observed.

Table 18: Spinnability and PCFC results for NP formulations

Formulation	Spinnable	pHRR (W/g)	Δ pHRR/PA6 (%)	THR (kJ/g)	Δ THR/PA6 (%)
PA6	Y	588	-	30.0	-
PA6/MWCNT 1%	Y	568	-3.4	28.9	-3.7
PA6/nano GO 1%	Y	569	-3.2	29.6	-1.3
PA6/halloysite 5%	Y	572	-2.7	28.7	-4.3
PA6/C30B 5%	Y	552	-6.1	27.9	-7

Thermal stability of the different samples was investigated by TGA in thermo-oxidative conditions; results can be seen in **Figure 47** for carbon-based NP and **Figure 48** for silicate-based NP.

A two-step degradation is recorded for PA6/MWCNT 1%. The main step of degradation occurs between 320 °C and 480 °C and a weight loss of 86 % is observed, the maximum degradation is reached at 446 °C. The final step from 480 °C to 590 °C corresponds to the oxidation of the transient residue (12 %). A two-step degradation is similarly observed for PA6/nanoGO. The main step of degradation occurs between 310 °C and 477 °C and a weight loss of 84 % is observed, the maximum degradation is reached at 444 °C. The final step from 477 °C to 645 °C corresponds to the oxidation of the residue (13 %). It is observed that for both carbon based NPs, there is no residue at the end of the TG analysis. Moreover, the presence of either MWCNT or nanoGO does not significantly affect the thermal stability of PA6.

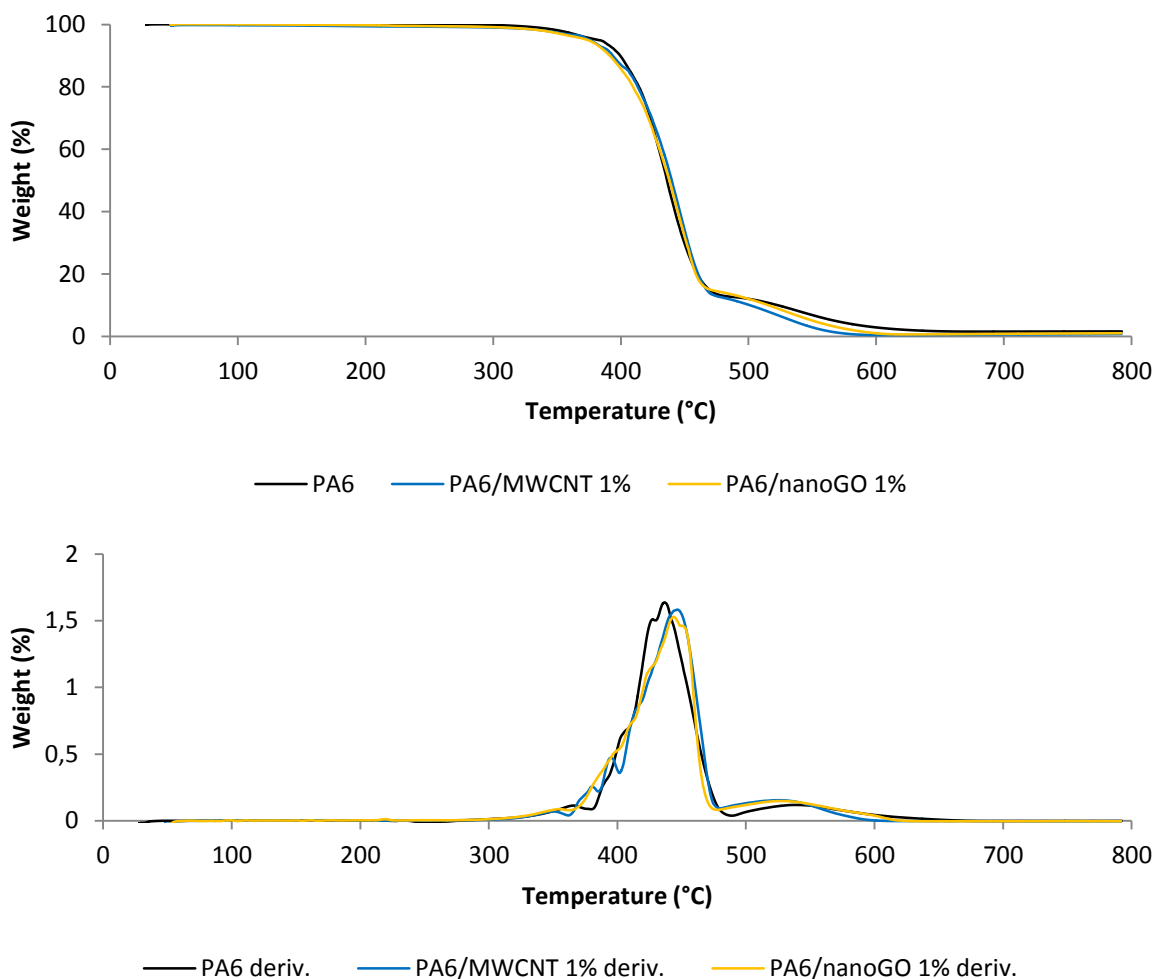


Figure 47: TGA and DTG curves of neat PA6 and PA6 containing carbon-based nanoparticles PA6/MWCNT 1% and PA6/nanoGO 1% (10 °C/min, air)

For PA6/HNT 5%, from ambient to 320 °C a small weight loss of 2 % is attributed to moisture and water evolution. The main step of degradation is observed between 320 and 478 °C and a weight loss of 80 % is observed, the maximum degradation is reached at 445 °C. The final step from 478 °C to 563 °C corresponds to the oxidation of the residues (12 %). A stable residue of 5.9 wt.-% is left at the end of the experiment, and corresponds, within the margin of error, to the HNT content of the formulation.

Similar behavior is observed for PA6/C30B 5%. From ambient to 320 °C, a small weight loss of 1.3 % is attributed to moisture and water evaporation. The main step of degradation occurs between 320 and 482 °C and a weight loss of 82 % is observed, the maximum degradation is reached at 446 °C. The final step from 482 °C to 610 °C corresponds to the oxidation of the residues (12 %). A stable residue of 4.7 wt.-% is left at the end of the experiment, it is proposed that the residues corresponds approximately to the C30B loading,

without its surfactant, and to a small amount of char. Indeed it was observed that Cloisite® 30B could promote the char formation of PA6 films [173, 197]. It is assumed that the same phenomena occurs in this formulation.

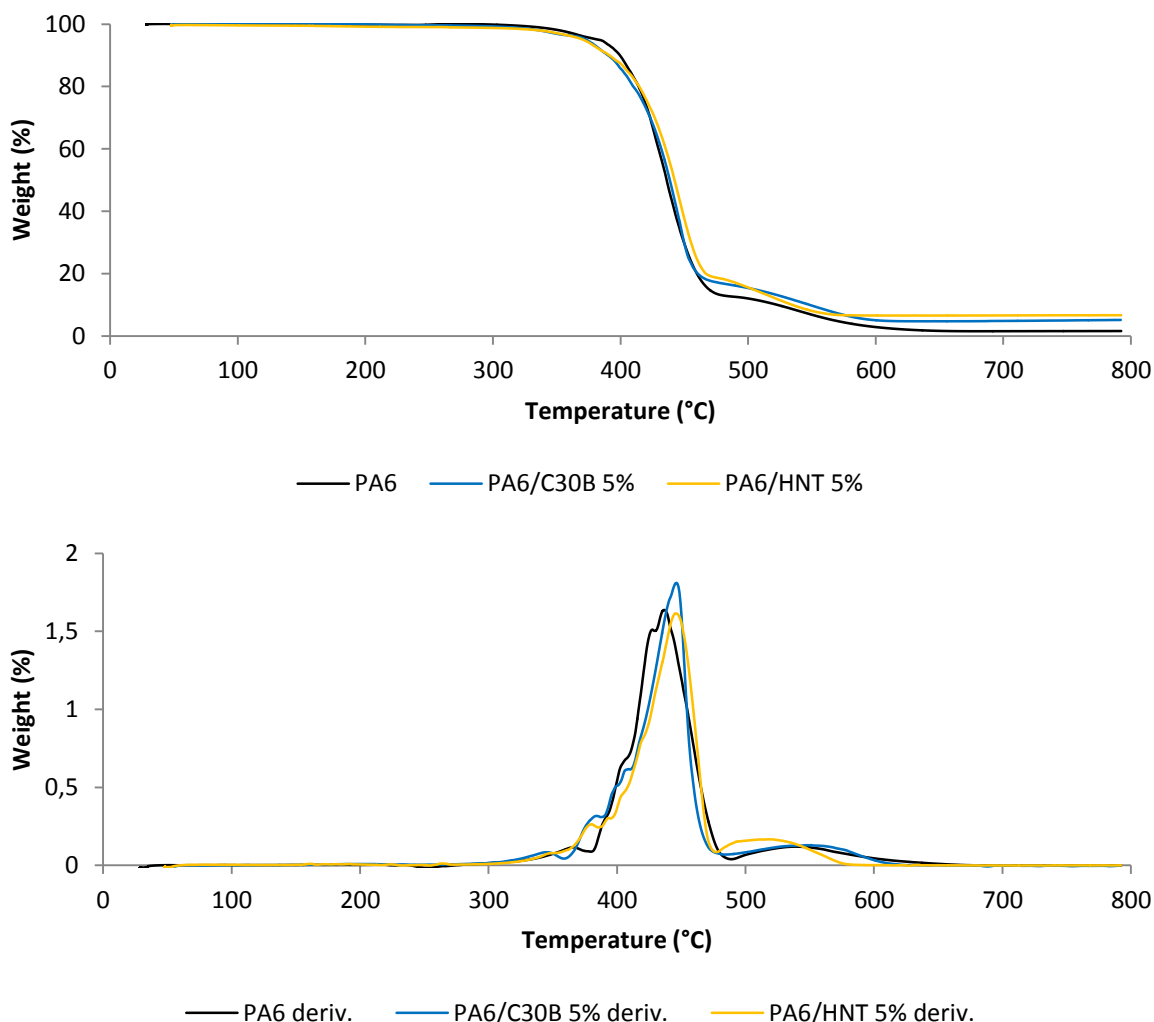


Figure 48: TG and DTG curves of neat PA6 and PA6 containing silicate-based nanoparticles PA6/C30B 5% and PA6/HNT 5% (10 °C/min, air)

For each of the five samples (the four NP and neat PA6), a two-step degradation is observed, the thermal stability of nanocomposites does not vary significantly from that of neat PA6 as all curves are similar. The literature reports that with some polymers containing nanoparticles, the onset temperature of degradation is significantly increased (e.g., polystyrene [198]) while with PA6, there is no change in the TG parameters as already demonstrated by Morgan *et al.* [182]. However, in the present study, a difference in the temperature of maximum mass loss rate was observed. Indeed, for neat PA6 the temperature corresponding to the maximum rate of mass loss is 436°C, whereas for all the

other formulations the value is between 444 and 446 °C, showing a slight improvement of the thermal stability for PA6/NP formulations.

III.3 CONCLUSION

Screening of materials is a very important phase of the work when trying to find new FR solutions. PCFC requires only milligrams of sample and is adapted to work along with microextruder, which only allows the production of small batches (usually 10 g with the microextruder used). Moreover, the properties can be measured on the fiber whereas larger FR tests usually require textile structures.

Phosphorus based fire retardants such as Exolit® OP 950 and OP 1230 or PCO 900 and PCO 960 were designed to be used in fibers. Therefore these compounds were evaluated in the PA6 fibers. The screening results obtained with PCFC do not show any improvement on the curves of heat release rate. That is to say that the pHRR were not significantly decreased, however the total heat release is generally decreased. It indicates either that less material is burned or that the combustion of the fuels is less efficient. TG investigation on the different formulations shows a clear destabilization of the PA6 matrix when PCO 900 and PCO 960 are used, since the main step of degradation occurs 50 °C before that of pure PA6. An interesting fact is that for each formulation, the char formation is enhanced as the oxidation of the transient residues involves higher weight loss than for PA6 alone. These oxidation steps also occur in larger temperature ranges. Thus, it can be assumed that the formed char is more resistant to oxidation and eventually of a different nature than the char of neat PA6.

Sulfur based additives allowed getting the best results of the screening. Indeed, formulations containing sulfamate salts show the lower values of peak of heat release rate. It is possible to reach a decrease of more than 20 % of the pHRR with only 5 % of ammonium sulfamate. However, AS leads to a degradation of the matrix when higher loadings (>10 wt.-%) are incorporated. Another sulfamate salt having a guanidinium molecular counterion has allowed to draw fibers with 10 wt.-% of additives and overcome the degradation issue. However, in this case the pHRR reduction was not as important as with AS (while keeping the same amount of FR in the PA6). Guanidine sulfamate and ammonium sulfamate containing formulations both starts to degrade earlier than neat PA6, but, as for the phosphorus based

FR, TG curves also show a different char oxidation. Thus, it is assumed that the sulfamate salts might as well enhance the char formation and modify its nature.

Finally, nanoparticles (MWCNT, nanoGO, HNT, C30B) have been melt-mixed in PA6 with different sets of parameters. Severe and soft conditions both gave microdispersions, as shown by SEM and optical microscopy. The different formulations were analyzed using the PCFC and TGA. No significant reductions of pHRR or THR were recorded as the results are within the margin of error of the instruments. The slight decrease of the pHRR and THR, are attributed to a dilution effect as the order of magnitude is similar to the loadings of NP in the formulations.

According to this first part of the work, some interesting results have emerged. Indeed, sulfamate salts seem a promising way to achieve the aim of this work: find an innovative system to flame retard PA6 fibers. The next step could thus consist in investigating the flame retardant mechanisms of the sulfamate salts. Elucidating the modes of action should then allow enhancing the fire retardant effect of these compounds. The next chapter will deal with the investigation of the mode of action of the ammonium sulfamate and guanidine sulfamate. Other aspects such as mechanical properties of the fibers and additives dispersion will also be considered.

IV Sulfamate Salts as Flame Retardant for Polyamide 6 Fibers

IV.1	Introduction.....	120
IV.2	The use of ammonium sulfamate	120
IV.2.1	Mechanical properties of the PA6/AS fibers.....	122
IV.2.2	Additive dispersion in the fiber	123
IV.2.3	Fire tests on PA6/ammonium sulfamate formulations.....	124
IV.2.3.1	Pyrolysis combustion flow calorimetry _____	124
IV.2.3.2	Mass-loss calorimetry_____	125
IV.2.4	Comprehension of the modes of action	127
IV.2.4.1	Thermal stability of PA6/AS _____	127
IV.2.4.1.1	Thermo-oxidative degradation	127
IV.2.4.1.2	Pyrolysis	129
IV.2.4.2	Gas phase analysis _____	131
IV.2.4.2.1	TGA-FTIR.....	131
IV.2.4.2.2	Pyrolysis-GC-MS.....	136
IV.2.4.2.3	Conclusion.....	138
IV.2.4.3	Solid phase analysis _____	138
IV.2.5	Conclusion	140
IV.3	The use of guanidine sulfamate	140
IV.3.1	Processing issues solved?.....	140
IV.3.2	Mechanical properties of the PA6/GAS fibers	142
IV.3.3	Fire tests on PA6/guanidine sulfamate formulations	143
IV.3.4	Additive dispersion.....	145
IV.3.5	Degradation mechanism	147
IV.3.5.1	Gas phase analysis _____	147
IV.3.5.1.1	TGA-FTIR.....	147
IV.3.5.1.2	py-GC-MS	149
IV.3.5.2	Solid phase analysis _____	150
IV.4	Conclusion	152

IV.1 INTRODUCTION

The previous chapter described the flame retardant screening of FR for PA6 fibers according to PCFC and to the thermal behavior of the different formulations. The results allowed focusing on a particular family of molecules: sulfamate salts. Indeed, it was noticed that the pHRR is decreased by 21.6% with only 5 wt.-% of AS and by 25.4% using 10 wt.-% of GAS, which is of particular interest when dealing with formulations for fiber applications. In order to understand these results, this chapter aims at describing the sulfamate systems. Their mode of action as FR in PA6 will be fully investigated.

First, the mechanical properties of the fibers will be considered. During melt processing, thermal, oxidative, and hydrolytic processes may contribute to the degradation of the PA6 matrix, and therefore to a change of the mechanical properties [15]. Moreover, it was found in the literature that ammonium sulfamate/dipentaerythritol systems has potential instability within the processing temperature range of 240-260 °C [199]. In the previous chapter, it was shown that formulations containing 10 wt.-% of ammonium sulfamate were not spinnable due to the matrix degradation. It is thus important to, not only consider the thermal and fire behavior of the samples, but also control the mechanical properties of the fibers.

In a second part, the modes of action involved in the flame retardancy of the sulfamate systems will be examined, investigating both the gas phase and the solid phase. In the solid phase, the dispersion of the additives will be evaluated. Heat treatments of the materials will permit the investigation of the chemical changes occurring in the condensed phase when the materials degrade. Evolved products from the decomposition of the fibers could also be modified and should therefore be analyzed.

IV.2 THE USE OF AMMONIUM SULFAMATE

Ammonium sulfamate is a white crystalline solid, its molecular formula is $H_6N_2O_3S$, the molecule is represented in **Figure 49**.

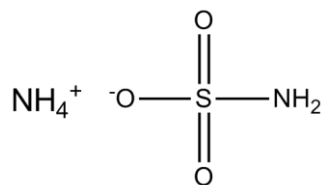


Figure 49: Molecular structure of ammonium sulfamate

Ammonium sulfamate as a flame retardant additive for PA6 combined with dipentaerythritol was studied by Lewin, those results were published in 2002 [98]. However his work on the subject is older. Indeed, Lewin patented its work in 1994 that has now expired [99]. In this work, the system and its fire performances in PA6 are described. The FR system was investigated in the bulk; ammonium sulfamate was used with addition of dipentaerythritol as charring agent at loadings of 2.0 and 0.7 wt.-% respectively. PA6 formulations yielded a V0 rating at the UL-94 test on bars of 1.6 and 0.8 mm thickness, the LOI value was 35.7 vol.-%. The very low amount of ammonium needed to flame retard PA6 makes it a strong candidate to flame retard fibers made of the same polymer. To our knowledge, this additive was never used as a flame retardant additive for synthetic fibers or thin applications (films). However, a patent from 1956 report the use of AS as flameproofing agent in coating for cotton or rayon fabrics, but decomposition issues led to the loss of the mechanical properties of the fabrics and to their yellowing [200]. Later, in 1974, AS was used in the form of aqueous solutions to treat PA6 fabrics [201], it is reported that such coatings function mainly by “melting point depression”, in other words, the dripping was promoted.

The innovative aspect of this work is thus to add this FR in the polymeric matrix during the extrusion-spinning process. Recently in 2013, Kandola and Horrocks team published their work, also based on Lewins previous studies, and mentioned the possibility to develop such systems for films and fibers but they faced processing difficulties [199]. In the present work, it was possible to spin fibers containing 5 wt.-% of AS. However formulations containing higher amounts of AS were barely spinnable or even unspinnable with “high” loading (10 wt.-%). It was assumed that degradation of the matrix occurred during extrusion, leading to a dramatic decrease of the melt viscosity which do not permit the spinning of these PA6/AS formulations.

IV.2.1 MECHANICAL PROPERTIES OF THE PA6/AS FIBERS

The mechanical properties of the fibers are first investigated in order to measure the impact of the sulfamate salt on the polyamide 6 fibers. During the screening, processing issues were encountered with the formulations containing 7 wt.-% or higher content of ammonium sulfamate. Addition of 7 wt.-% of FR resulted in very brittle fibers whereas it not possible to obtain fiber with 10 wt.-%. It is assumed that the increase of AS content lead to an increase of the degradation of the PA6 matrix and thus to a decrease of the mechanical properties of the fibers. In order to verify this hypothesis, mechanical properties of the fibers were evaluated through tensile testing. **Figure 50** presents the tensile strength and the elongation at break for pure PA6, PA6/AS 3% and PA6/AS 5 % formulations. No data could be recorded for the PA6/AS 7% fibers because the samples were too brittle.

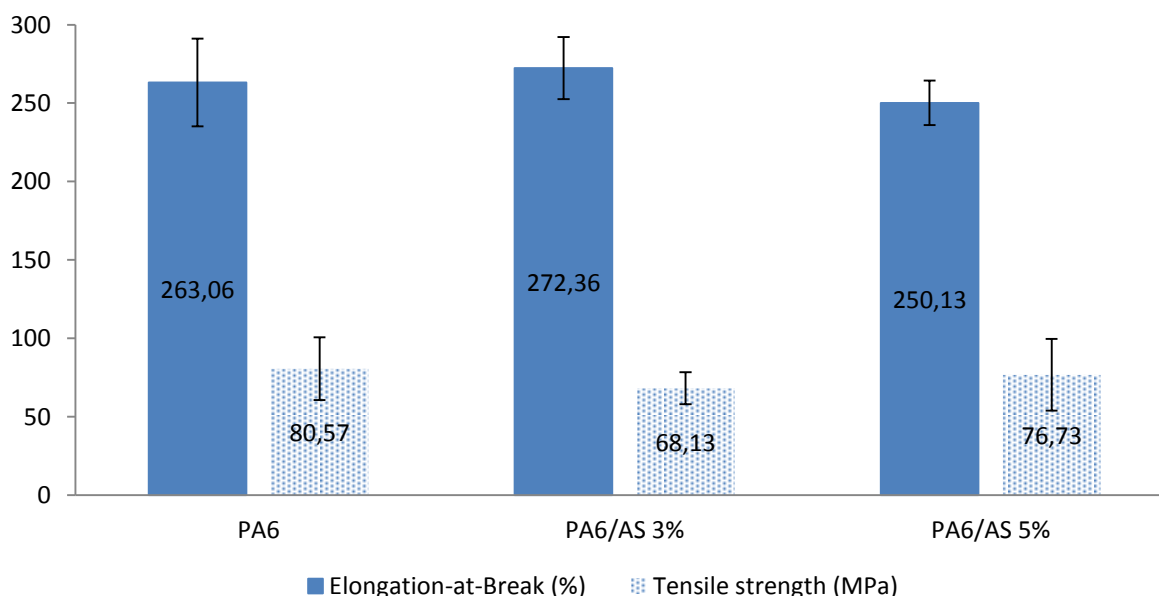


Figure 50: Elongation-at-break (%) and tensile strength (MPa) of PA6, PA6/AS 3% and PA6/AS 5 % formulations

The results show that the tensile strength of PA6 is around 80 MPa. The addition of low amounts of AS does not affect in an important way the mechanical properties of the fibers. The tensile strength of the two AS formulations decreases slightly compared to the neat PA6 fibers but the change is not significant considering the calculated standard deviation. The two formulations containing AS have also an elongation at break value (around 260 %) similar to that of pure PA6. It can be concluded that the incorporation of AS up to 5 wt.-%

loading does not change the tensile strength and elongation at break of formulated PA6 compared with neat PA6.

IV.2.2 ADDITIVE DISPERSION IN THE FIBER

Considering the mechanical and flame retardant properties of the fibers, PA6/AS 5% was chosen as the optimal formulation, and thus our studies will focus on this particular formulation.

Table 19 and **Figure 51** report the fiber diameter obtained for pure PA6 and for PA6/AS 5%. The fibers have a homogeneous diameter and an average standard deviation of 10 % is calculated.

Table 19: Diameters of PA6 and PA6/AS 5% formulations

Material	Average diameter (μm)	Standard deviation (μm)
PA6	108.9	10.8
PA6/AS 5%	85.0	9.0

The diameter of both fibers is close to 100 μm considering the standard deviation, but the fiber is thinner in the case of the formulated PA6. The decrease could be attributed to a difference in the melt viscosity induced by the presence of AS as well as the instruments set up and precision.

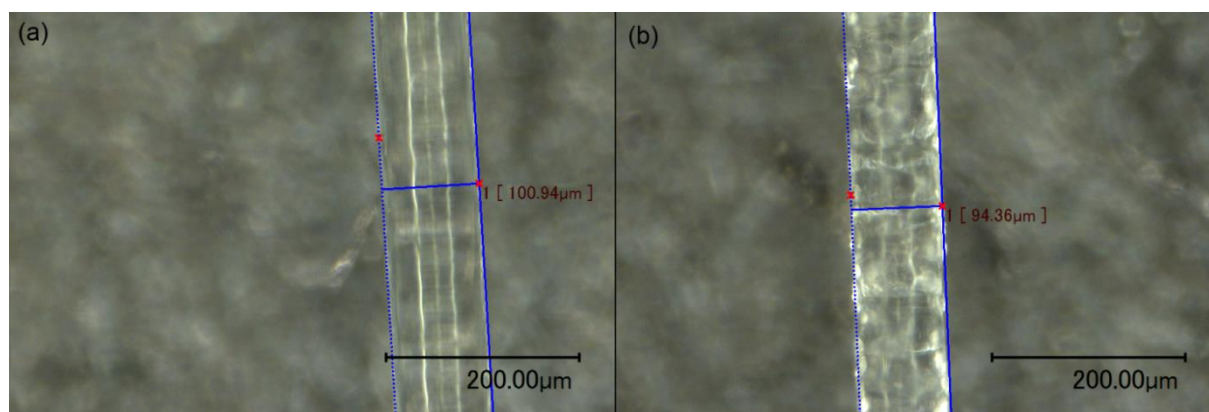


Figure 51: Digital microscope photographs of PA6 (a) and PA6/AS 5% (b) fibers

In order to assess the distribution of ammonium sulfamate, back-scattering electron pictures (BSE) and EPMA cartographies were used to examine the cross section of PA6/AS 5% fibers, the resulting pictures are presented in **Figure 52**. **Figure 52(a)** shows black dots on the cross-section of the fibers. They are due to the beam of the EPMA which degrades the sample during the analysis. EPMA cartography of sulfur on PA6/AS 5% fibers, **Figure 52(b)**, shows

that the formulation does not contain any agglomerate of sulfur and so, the dispersion of AS in the material is homogeneous. In fact, AS melts around 130°C [168] and thus AS is in the molten state at the extrusion temperature of the formulation allowing to obtain a good dispersion of the FR.

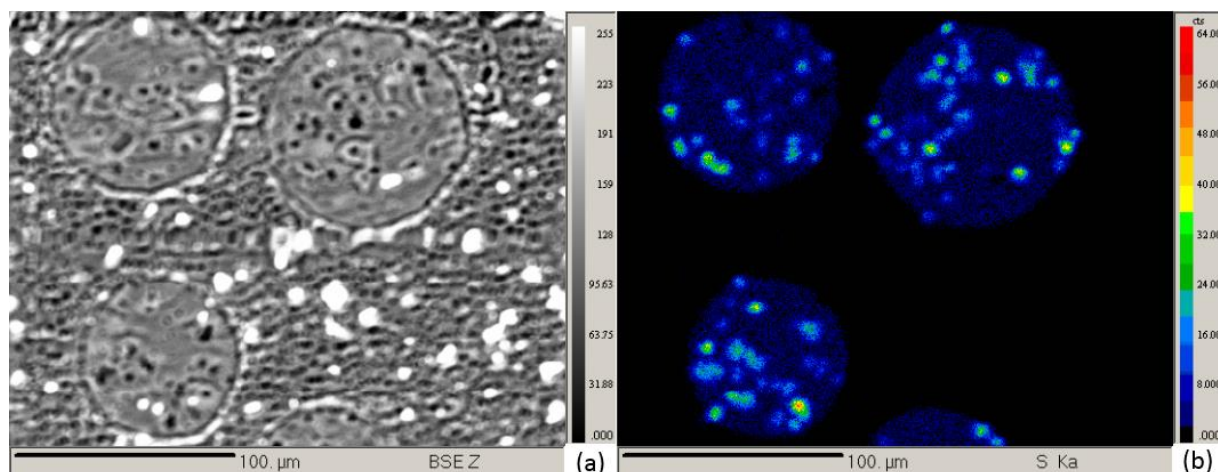


Figure 52: BSE picture (a) and EPMA sulphur cartography (b) of the cross section of PA6/AS 5% fibers

IV.2.3 FIRE TESTS ON PA6/AMMONIUM SULFAMATE FORMULATIONS

IV.2.3.1 PYROLYSIS COMBUSTION FLOW CALORIMETRY

PCFC is particularly suitable to assess fire properties of materials when only small amounts are available. This test is very helpful for determining if a flame retardant modifies the degradation pathway towards less flammable species. PCFC permits to measure the heat released by the burning of combustible compounds and the temperatures at which they are released. In **Table 20** and **Figure 53** are presented characteristic data obtained with this technique for different formulations containing from 3 wt.-% to 10 wt.-% of AS in the PA6 matrix.

Table 20: PCFC results for PA6/ammonium sulfamate formulations

Formulation	pHRR (W/g)	Δ pHRR/PA6	THR (kJ/g)	Δ THR/PA6
PA6	588		30.0	
PA6/AS 3%	504.6	-14.1 %	27.9	-7
PA6/AS 5%	461.4	-21.6 %	27.1	-9.7
PA6/AS 7%	409.3	-30.4 %	25.6	-14.7
PA6/AS 10%	-	-	-	-

Two effects can be observed from the **Table 20**. The first is that ammonium sulfamate is effective in reducing the pHRR of PA6. The second is that the higher the AS content in the

formulation, the lower the pHRR value. However, it was impossible to make fibers with a formulation containing 10 wt.-% of this FR as the material coming out from the extruder was partially degraded and brownish. Therefore, no measurements were performed with PCFC on this last formulation. When the AS loading is 7 wt.-%, the fibers can be spun but they are very brittle as previously discussed.

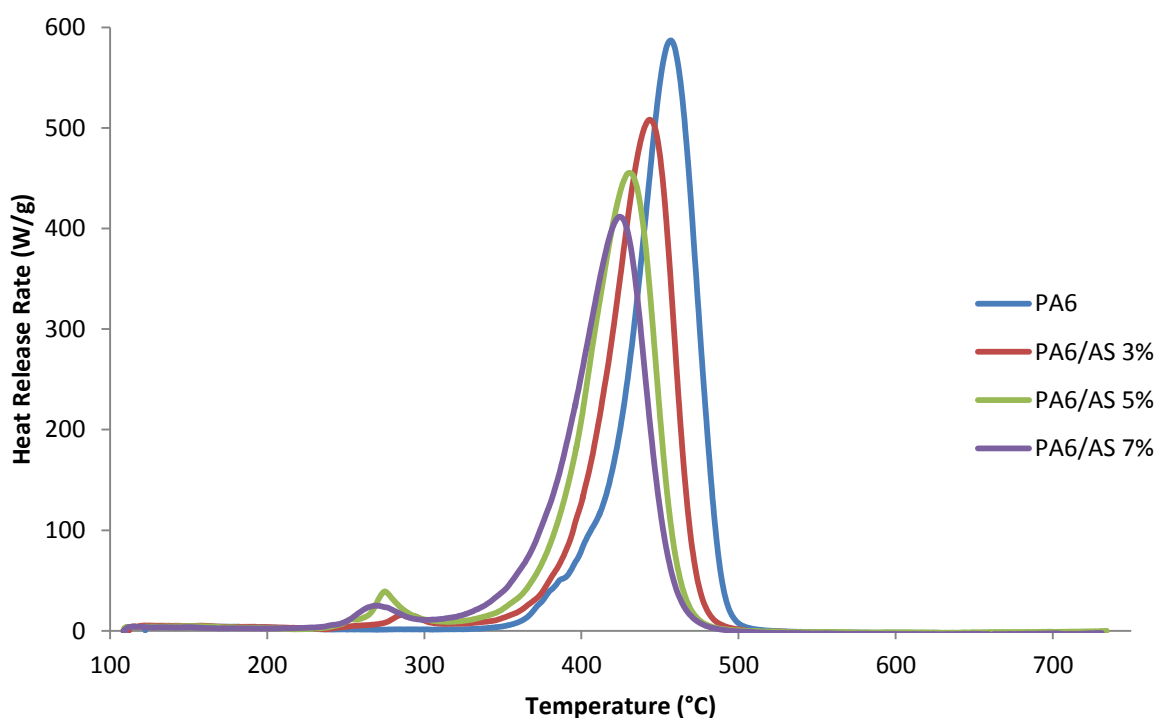


Figure 53: Heat release rate curves versus temperature for PA6 and PA6/AS formulations obtained with PCFC

On **Figure 53**, it can be noticed that the temperature at which the pHRR occurs is lowered with the increase of AS amount in the formulations. The shift of the peaks towards lower temperatures may be attributed to a destabilization effect induced by AS. The smaller peaks around 270 °C may be attributed to release of flammable ammonia. This effect and the release of ammonia around 270 °C will be further investigated in this chapter.

IV.2.3.2 MASS-LOSS CALORIMETRY

The reaction to fire of PA6 and PA6/AS 5% formulations was characterized with mass-loss calorimetry. The heat release rate as a function of time for the two materials is presented in **Figure 54** and characteristic data are reported in **Table 21**. Surprisingly, at the opposite to what is observed using PCFC, the curves show that the incorporation of 5 wt.-% AS in PA6

leads to an increase of the pHRR. For the formulated PA6, an increase of 11 % of the pHRR is observed. The time to ignition and time to peak (TTp - time corresponding to the highest heat release rate) are both shortened for the PA6/AS 5% formulation.

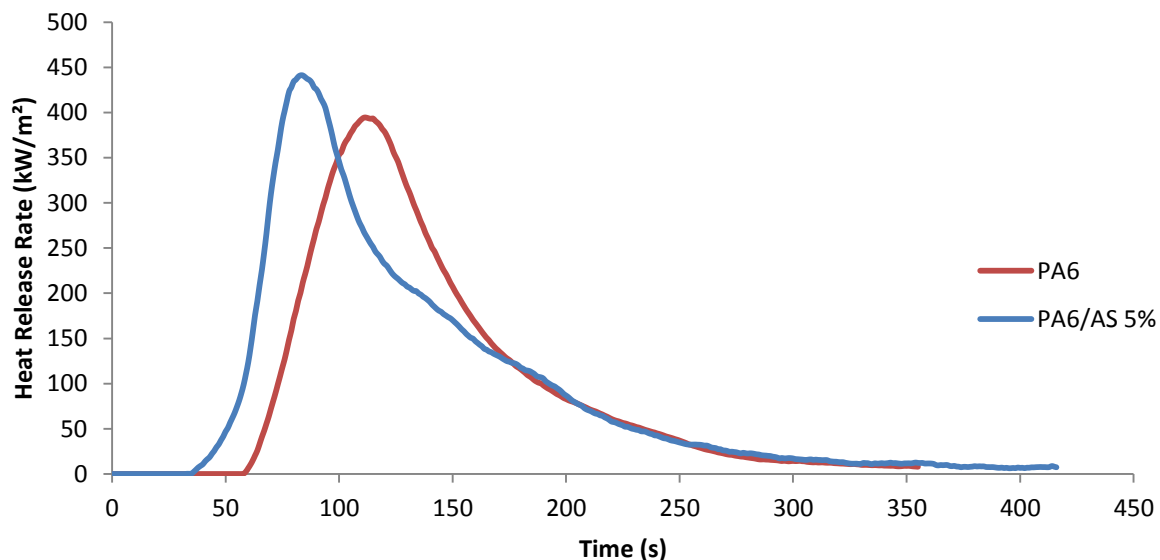


Figure 54: Heat release rate versus time for PA6 and PA6/AS 5%

A decrease of 38 % and 25 % of the TTI and TTp respectively are observed. However, the THR is the same for both samples (42 MJ/m²). These results confirm those of Lewin *et al.* [168]. They explained this behavior by the decomposition of the sulfated PA6 into sulfuric acid, which oxidizes, dehydrates and carbonizes the polymer very rapidly with a relative high HRR. In this case, shorter TTI and TTp can be explained by the degradation, promoted by AS. Fuel is released earlier and thus TTI is decreased. Consequently, TTp is also decreased.

As discussed in Chapter 3, PCFC and cone calorimeter results do not always correlate. Indeed, the scale and the heating rates are different. In PCFC milligrams sample is linearly heated (1 °C/s) whereas in cone calorimetry experiment, the sample is directly impacted by a heat flux of 35 kW/m². It can be found in the literature that polyamides competitively decompose into nitrile/vinyl chains end products and lactams, depending on the experimental parameters (i.e. temperature) and/or presence of FR [202, 203]. Consequently, the orientation of the degradation reactions can be different between cone calorimeter and PCFC, hence, changing the decomposition products and/or their ratio. It is also known that atmosphere can change the degradation products of polyamide [204]. In PCFC, the sample is

degraded in nitrogen whereas cone calorimetry is done under air in the present study. Thus, the fuel composition might also be different.

Table 21: TTI, TTP, pHRR and THR of PA6 and PA6/AS 5%

Material	TTI (s)	TTP (s)	pHRR (kW/m ²)	THR (MJ/m ²)
PA6	58	111	394	42
PA6/AS 5%	36	83	441	42

IV.2.4 COMPREHENSION OF THE MODES OF ACTION

In order to elucidate the mode of action of AS as flame retardant for PA6, the degradation products of PA6/AS formulation were analyzed in the gas phase and condensed phase by different techniques. Gas phase analysis included TGA-FTIR and py-GC-MS to identify the composition of the evolved degradation gases. Condensed phase was characterized with solid-state NMR.

IV.2.4.1 THERMAL STABILITY OF PA6/AS

IV.2.4.1.1 THERMO-OXIDATIVE DEGRADATION

TG and DTG curves of PA6, AS and the combination of the two in the PA6/AS 5% formulation are presented in **Figure 55**. The description of the degradation steps of PA6 and PA6/AS 5% was done in part III.2.2.2.

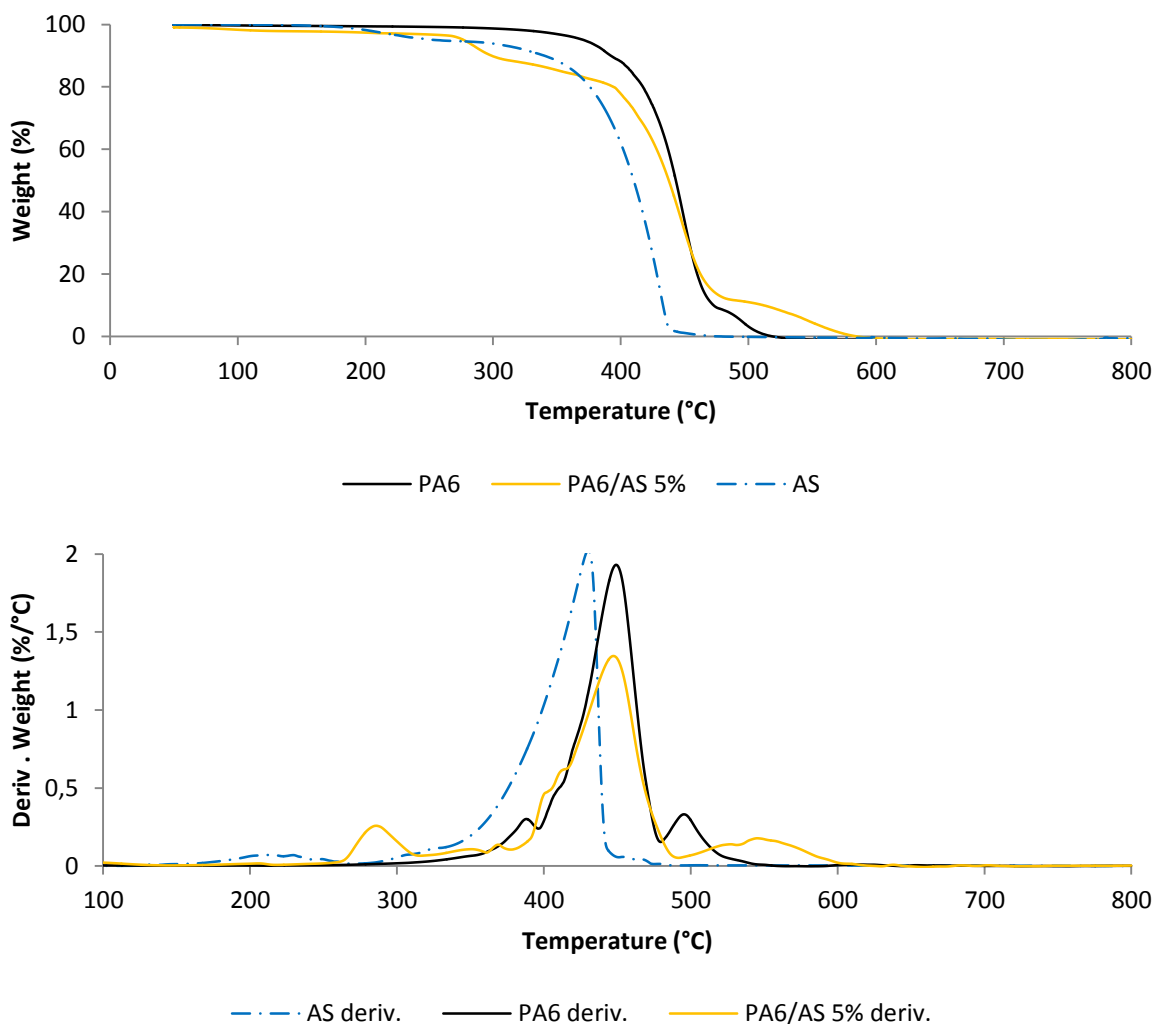


Figure 55: TG and DTG curves of PA6, AS and PA6/AS 5% (10 °C/min, air)

Ammonium sulfamate decomposes in two steps. The first weight loss (between 170 and 270 °C) corresponds to the dimerization of AS associated to the release of ammonia [98]. The second step begins at around 270 °C and the maximum degradation rate is reached at 430 °C.

In **Figure 56**, experimental and calculated TG curves have been plotted for the PA6/AS 5% formulation (in thermo-oxidative conditions) as well as the resulting difference weight loss curve. The main objective is to point out if the incorporation of the FR leads to an increase or a decrease in the thermal stability of the system. The difference weight loss curve of PA6/AS 5% formulation shows two distinct zones: (i) the first one between 260 and 450 °C where $\Delta w(t) < 0$ meaning that the thermal stability of the formulation is decreased and (ii) the second zone between 450 and 600 °C where $\Delta w(t) > 0$ corresponding to a thermal stabilization.

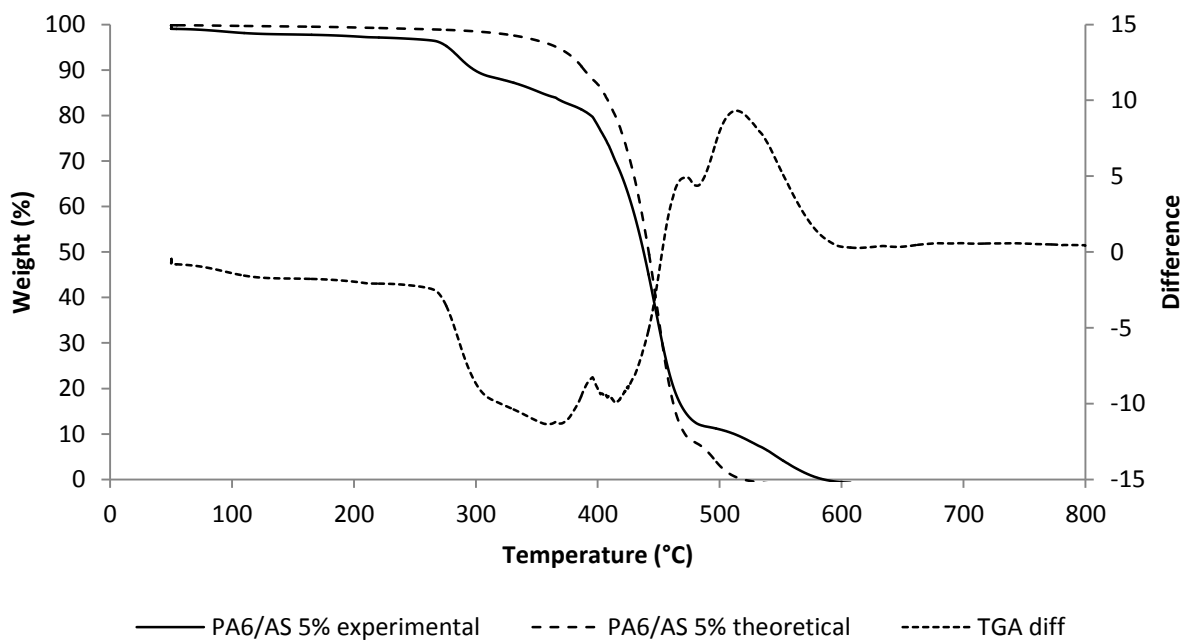


Figure 56: Calculated and experimental TG curves and difference weight loss curve of the PA6/AS 5% formulation

PA6/AS starts to degrade at lower temperature than PA6 and the presence of significant stabilization and destabilization zones suggest that interactions between AS and PA6 and/or their degradation products should occur during the thermo-oxidative degradation of the sample.

IV.2.4.1.2 PYROLYSIS

Samples were also analyzed in nitrogen atmosphere to examine the differences between pyrolysis and thermo-oxidative decomposition of PA6 and PA6/AS 5%. TG curves are shown in **Figure 57**.

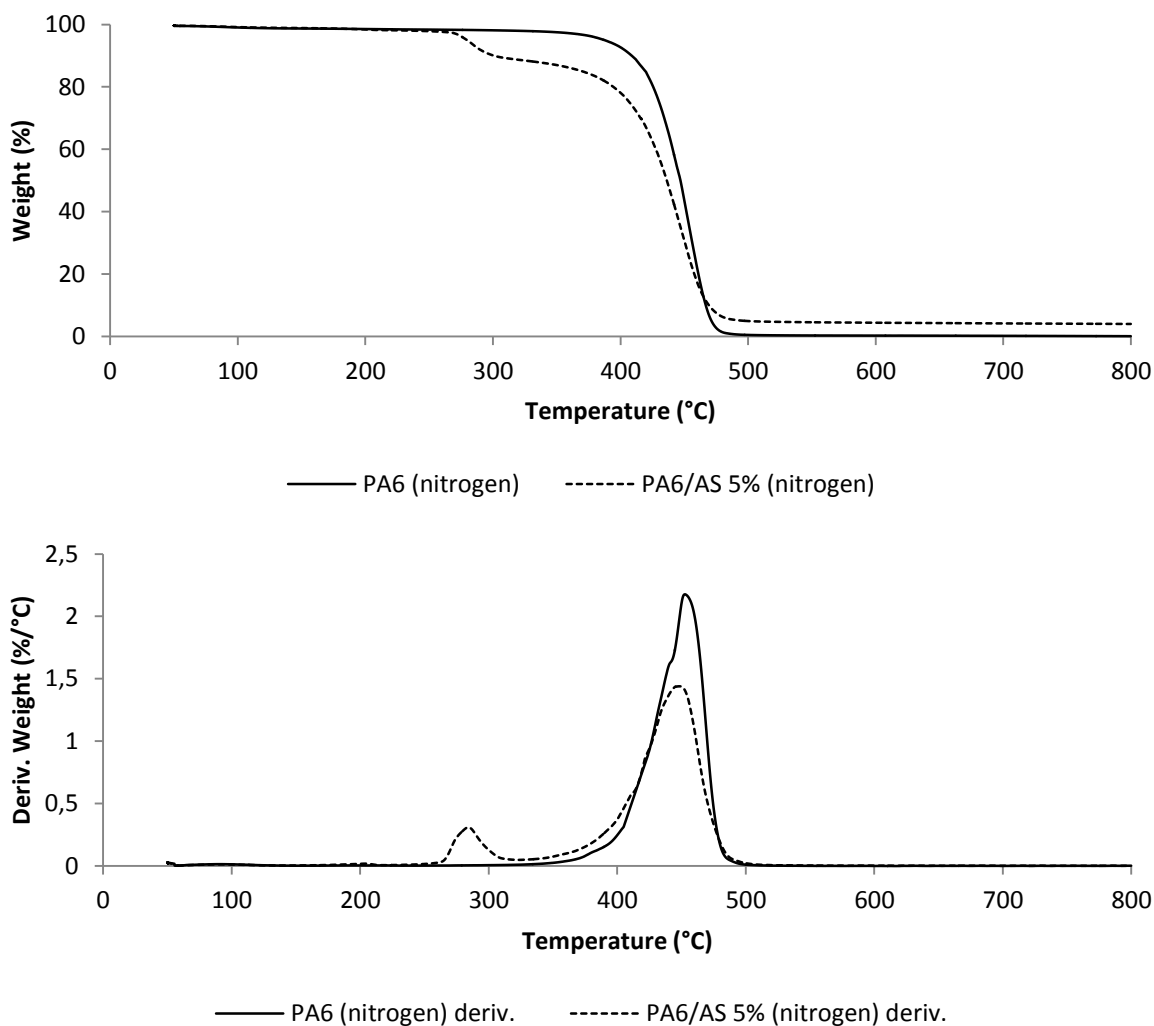


Figure 57: TG and DTG curves of PA6 and PA6/AS 5% (10 °C/min, nitrogen)

For PA6, a one-step decomposition is observed. The decomposition starts at 350 °C and ends at 490 °C with the total degradation of the sample.

Concerning PA6/AS 5%, a two-step decomposition is recorded. The first weight loss starts at 260 °C and is of 9 wt.-%. The second loss of 84% begins at 323 °C and stops at 490 °C, leaving a 5 wt. % residue at the end of the degradation.

TG curves of PA6 and PA6/AS 5%, under air and under nitrogen, exhibit the same degradation steps, occurring at comparable temperatures. The main difference is observed at high temperature, under air, where an additional oxidation step occurs for PA6 and PA6/AS 5%. Another major difference is the amount of residue at the end of the TGA experiment for the formulated PA6. A 5% residue is obtained at the end of the experiment under nitrogen while the residue is completely oxidized under air. However, if the

temperatures of the different decomposition steps are similar in both atmospheres, the products of degradation may be different. Indeed, as reviewed in the literature [204], it is found that, a general reduction in the quantities of heavier hydrocarbons occurs in air atmosphere. An increase in the production of CO and CO₂ is also observed as the oxygen content of the atmosphere is increased.

IV.2.4.2 GAS PHASE ANALYSIS

In order to understand what occurs during the degradation process, degradation products of PA6 and PA6/AS formulations have been analyzed, first by TGA coupled with FTIR spectrometer. This technique is efficient for small decomposition products, such as CO₂, H₂O, NH₃ or CH₄ or hydrocarbon decomposition products with a high symmetry and therefore unambiguous vibration spectra [205]. In the previous section, it is discussed that hydrocarbons of different molecular weight might be evolved according to the experimental parameters. Thus, in a second-step py-GC-MS was considered to precisely detect the different products of thermal decomposition.

IV.2.4.2.1 TGA-FTIR

The spectra corresponding to the characteristic degradation temperatures of PA6 and PA6/AS 5% are shown in **Figure 58**. Characteristic temperatures of the main degradation steps (320, 449, 500 °C and 260, 447, 550 °C for PA6 and PA6/AS 5% respectively) were selected according to the TG curves presented in **Figure 55**. They correspond to the beginning of the first degradation step, then the maximum of degradation during the main step and finally the end of the oxidation step.

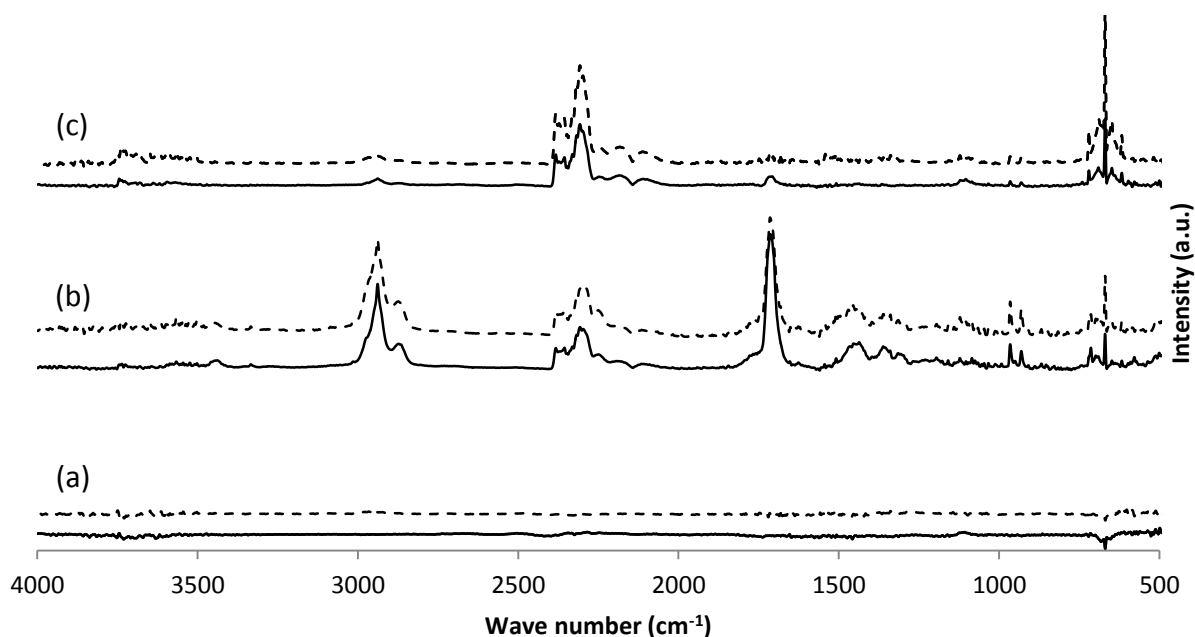


Figure 58: FTIR spectra of the gases evolved during the thermo-oxidative degradation of PA6 (—) and PA6/AS 5% (--) at characteristic temperatures of degradation (PA6: (a) 320 °C; (b) 449 °C; (c) 500 °C, PA6/AS 5%: (a) 260 °C; (b) 447 °C; (c) 550 °C)

On the FTIR spectra, for the beginning of the first degradation step of PA6 and PA6/AS 5%, at 320 °C and 260 °C respectively (**Figure 58(a)**), only peaks of water are detected around 3600 cm^{-1} and 1500 cm^{-1} . Peaks of water are also present during the whole experiment (at 449, 447, 500 and 550 °C) due to the formation of water during the degradation of PA6 and PA6/AS 5% [50, 98]. Around 450 °C (**Figure 58(b)**), the main degradation product is ϵ -caprolactam exhibiting characteristic peaks at 2938 and 1713 cm^{-1} corresponding respectively to the δ vibration of CH_2 groups and ν vibration of the carbonyl group of CONH [206]. Other major evolved gas products are CO_2 (669 cm^{-1} , 2349 cm^{-1}), CO, hydrocarbons and NH_3 (930 cm^{-1} , 965 cm^{-1}). At 500 and 550 °C (**Figure 58(c)**), mainly CO_2 and CO are released, and traces of ϵ -caprolactam and ammonia are found. In **Table 22** is given the full assignment of the peaks of the different spectra [207-211]. The spectra are similar for both PA6 and PA6/AS suggesting that AS does not significantly modify the gas phase during the decomposition of PA6 in a large extent.

Table 22: IR peaks assignment for PA6 and PA6/AS 5% [207]

Functional group or component	Wave number (cm ⁻¹)	Vibration type	Additional ref.
CO ₂	669	δ	
	2354	v _{as}	
NH ₃	930	δ	
	965	δ	
	1626		[211]
	3332	v	
CH ₂	2873	δ	
	2938	δ	
	1440		
N-CH ₂	1440		
Amide I (prim., sec.)	1713	v	[208]
Amide II (sec.)	1508	δ, v	[208]
Amide III (prim.)	1340	δ, v	[208]
-C≡N	2250	v	[210]
H ₂ O	1400-1700	δ	
	3400-3700	v _{as}	

IR spectra recorded during the degradation of the two samples in pyrolysis conditions (**Figure 59**) show that the same gases, except CO, are detected but the amount CO₂ is less important than in the thermo-oxidative conditions. It makes sense because no oxidation can occur during the pyrolytic decomposition and only a few amounts of CO₂ can be evolved.

On the FTIR spectra, for the beginning of the first degradation step of PA6 and PA6/AS 5%, at 350 °C and 260 °C respectively (**Figure 59(a)**), peaks of water are detected around 3600 cm⁻¹ and 1500 cm⁻¹ for both samples. For PA6/AS, ammonia is also detected (peaks at 930 cm⁻¹, 965 cm⁻¹). During the main degradation step (**Figure 59(b)**), ε-caprolactam (2938 and 1713 cm⁻¹), ammonia and CO₂ (669 cm⁻¹, 2349 cm⁻¹) are detected. However, the intensity of carbon dioxide is very low compared to the other peaks and to the spectra recorded in thermo-oxidation conditions. Finally at 500 °C (**Figure 59(c)**), the spectra show peaks corresponding to ε-caprolactam. However, CO₂ is now almost invisible, which is consistent with the absence of oxygen and thus oxidation of the transient residue could not occur.

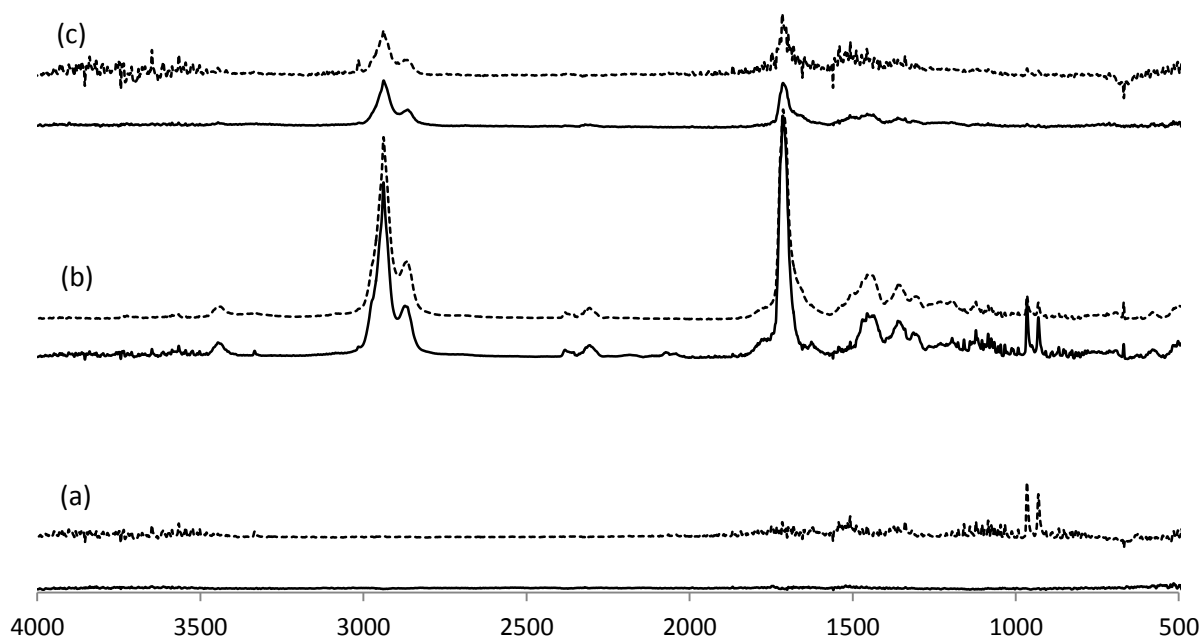


Figure 59: FTIR spectra of the gases evolved during the pyrolytic degradation of PA6 (—) and PA6/AS 5% (--) at characteristic temperatures of degradation (PA6: (a) 350 °C; (b) 449 °C; (c) 500 °C, PA6/AS 5%: (a) 260 °C; (b) 450°C; (c) 500 °C)

Additional information can be obtained from the FTIR spectra. Indeed, even if the spectra are similar at selected temperatures, it does not necessarily mean that the same phenomena occur at the same time. As a consequence, the intensities of the main peaks corresponding to ϵ -caprolactam ($\bar{\nu} = 2938 \text{ cm}^{-1}$), CO_2 ($\bar{\nu} = 2354 \text{ cm}^{-1}$) and NH_3 ($\bar{\nu} = 965 \text{ cm}^{-1}$) are plotted as a function of time (**Figure 60**) in the case of the thermo-oxidative degradation. For ϵ -caprolactam and NH_3 , the maximum of intensity (related to the maximum emission of gases) is reached at shorter times (also meaning lower temperatures) in the case of the PA6/AS 5% formulation. This indicates that the degradation of PA6 is promoted by the presence of AS and could explain the results obtained in PCFC.

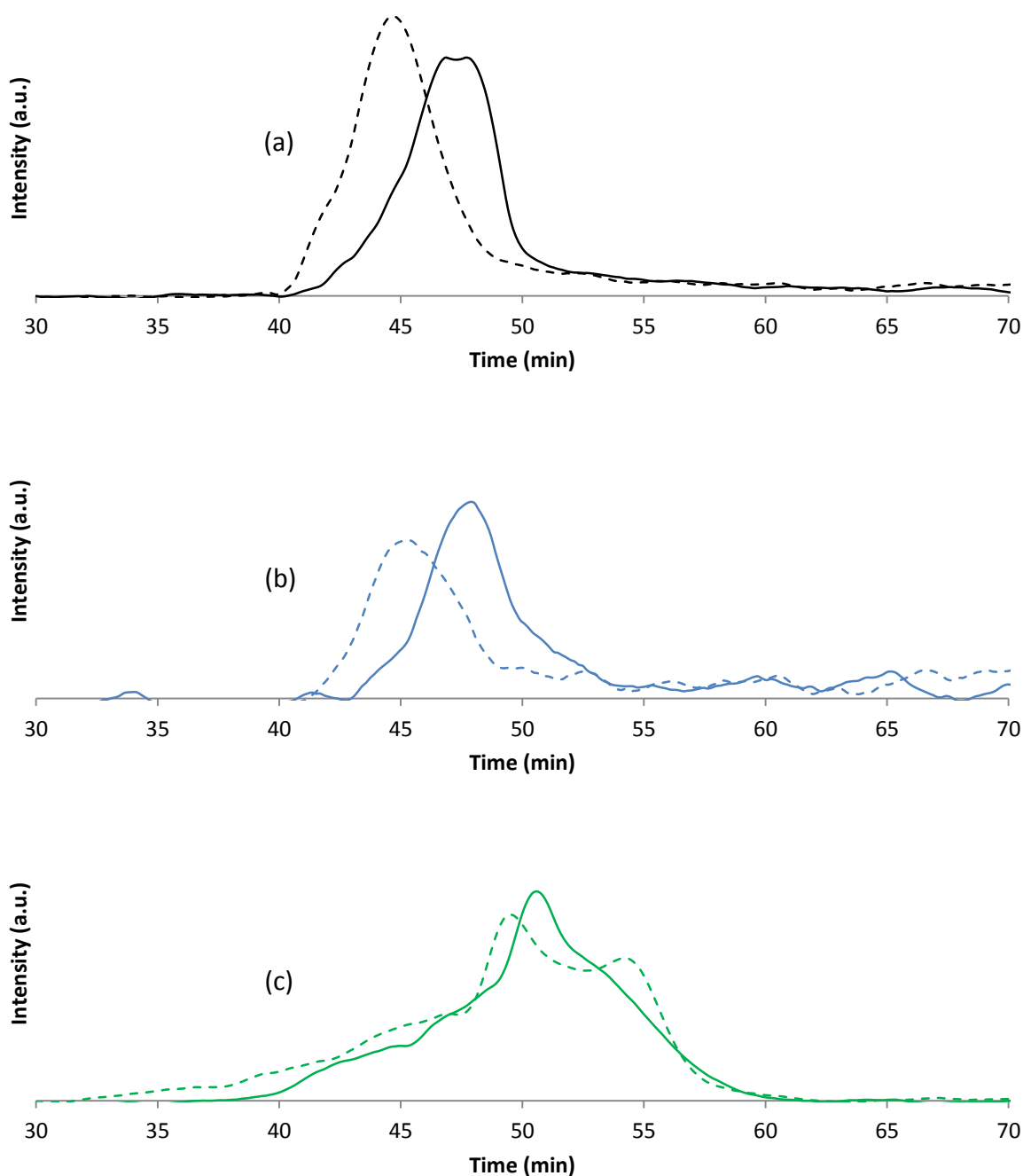


Figure 60: Intensity of the caprolactam (2938 cm⁻¹, (a)), NH₃ (965 cm⁻¹, (b)) and CO₂ (2354 cm⁻¹, (c)) peaks versus time (— : PA6, --- : PA6/AS 5%)

Figure 60(c) allows a comparison of CO₂ emission between PA6 and PA6/AS formulations. An additional peak is observed at the end of the degradation process at 55 min (namely around 550 °C) for the PA6/AS formulation compared to neat PA6. It shows that oxidation of the residue occurs at higher temperature for the fire retarded formulation. It indicates that the residue of the FR formulation exhibits higher oxidation resistance than that obtained in the

case of PA6 alone. It thus explains the increase of the thermal stability observed at temperatures higher than 450 °C on the difference weight loss curve (**Figure 56**).

In order to understand the role of AS in the formulation, TGA-FTIR experiment was done on the pure AS and the intensity of the evolved ammonia is plotted on **Figure 61**. Two peaks can be distinguished: (i) the first one corresponds to the first degradation step observed in TGA (**Figure 55**) and is attributed to the dimerization of AS with the corresponding release of ammonia (**Equation 6**) [98] and (ii) the second one corresponds to the decomposition of the dimer and unreacted AS (second degradation step of the TG curve).



It is observed that ammonia is released at shorter times, about 20-25 min, which corresponds to 200-250 °C, compared to the FR formulation. Indeed, no ammonia peak was detected on **Figure 60** before 30 min (300 °C). The ammonia formed by the dimerization of AS was not detected in the gas phase during the PA6/AS 5% analysis. Two hypothesis can be drawn. Either the amount of NH₃ is too low to be detected or ammonia reacts with the polymeric PA6 chains through aminolysis, leading to an accelerated decomposition of PA6 (**Figure 55**). The second hypothesis is favored since degradation of PA6 is observed at lower temperature in presence of AS.

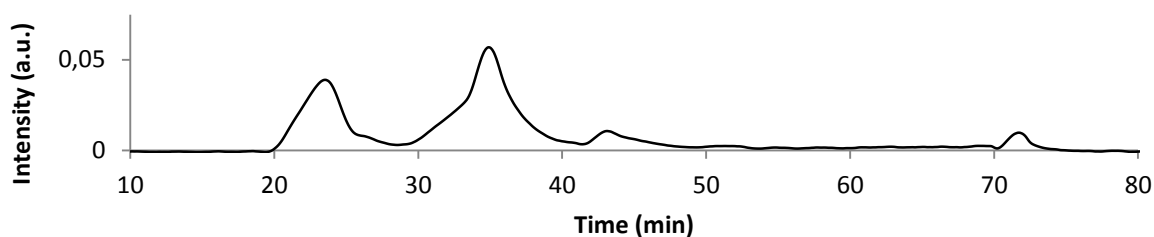


Figure 61: Intensity of the NH₃ (965 cm⁻¹) peak versus time for AS alone

IV.2.4.2.2 PYROLYSIS-GC-MS

In order to differentiate overlapping compounds in FTIR and to detect potential additional molecules, PA6 and PA/AS 5% formulation were analyzed with py-GC-MS using a stepwise method (described in **Figure 34** in part II.4.1.3). The temperatures were selected according

to the TG curves presented in **Figure 57**. Total Ion Chromatograms (TIC) of neat and formulated PA6 shown in **Figure 62** correspond to the main degradation step of each sample

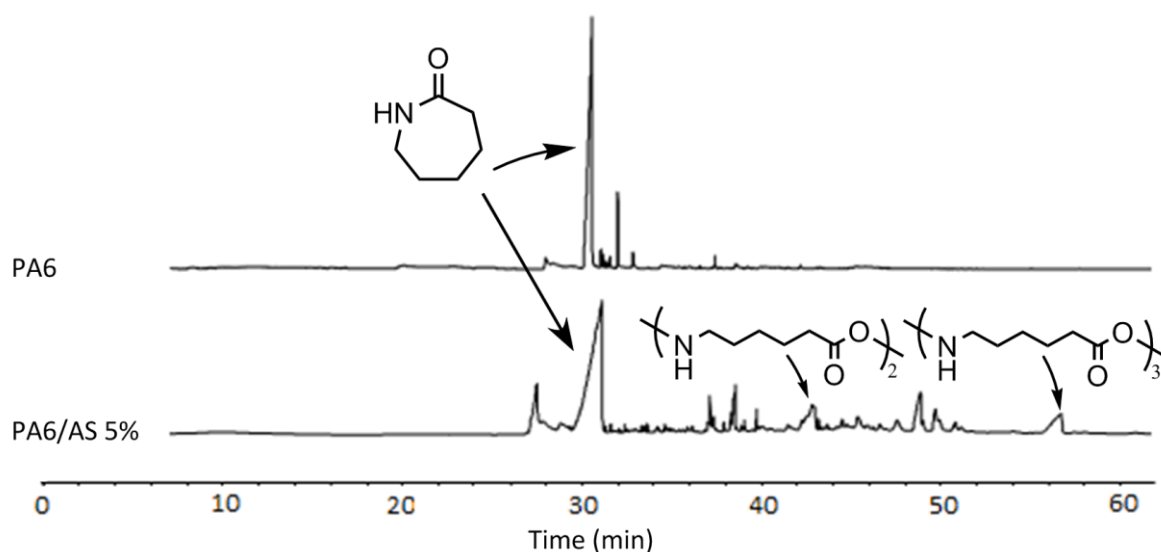


Figure 62: TIC corresponding to the pyrolysis of PA6 between 350 °C and 490 °C, and PA6/AS 5% between 323 °C and 490 °C

For both materials, the main decomposition peak corresponds to caprolactam (with m/z of 113) as already shown by TGA-FTIR and in accordance with the literature. On both chromatograms, a less intense peak is visible before the one of ϵ -caprolactam, and is located around 29 min. These peaks correspond to 6-aminohexanenitrile. For neat PA6, the main degradation product is caprolactam [212] but additional minor compounds can be also identified. On the PA6 Total Ion Chromatogram, the second intense peak at 32 min corresponds to 1-(cyclohex-1-en-1-yl)piperidine.

In comparison with neat PA6, a series of less intense peaks appear at longer times for the PA6/AS 5%. Those additional peaks are assigned to dimers and trimers (with characteristic maximum m/z of 226 and 339) as well as random chain scission products, containing from 1 to 3 repeating units of the PA6 matrix. This indicates that the gas phase composition is changed between neat PA6 and the formulation containing AS. As reported in the literature [50, 51], the presence of a nucleophilic molecule changes the decomposition thermodynamics, and the amide bond is more easily broken, leading to a dramatic decrease of the PA6 MW. In this study, it was shown that ammonia is released by AS, thus the decomposition pathway of PA6 is modified. The minor peaks detected at 37, 39 and 49 min

are assigned to azepane-2-thione, N-(5-cyanopentyl)pent-4-enamide and 6-acetamido-N-(5-cyanopentyl)hexanamide respectively.

IV.2.4.2.3 CONCLUSION

Analysis of the gas phase by coupling the FTIR spectrometer to the TGA showed that the decomposition gases were the same for PA6 and PA6/AS5 % in air and nitrogen, except that the intensity of the CO and CO₂ peaks were lowered in pyrolytic conditions. To get further information on the gas phase, py-GC-MS was used to differentiate the decomposition gases of the samples based on their retention time, and to some extent their molecular weight. This approach shows that AS modifies the degradation pathway of PA6, and promotes the formation of hydrocarbon molecule and chains of higher molecular weight. The composition of the gas phase is thus modified by the incorporation of AS.

IV.2.4.3 SOLID PHASE ANALYSIS

TG curve of PA6/AS in nitrogen (**Figure 57**) shows a stable residue at high temperature and TGA difference (**Figure 56**) also proves a stabilization of the system above 450 °C. It can thus be assumed that interactions between PA6 and AS also occur in the condensed phase. Thus, analyses of the condensed phase by solid state NMR were conducted to detect potential chemical reactions between the degradation products of AS and PA6. The ¹³C CP-DD-MAS NMR spectra of the residues obtained after the thermal treatment, at characteristic temperatures, of PA6 and PA6/AS 5% formulations are given in **Figure 63**. From 20 to 323 °C, the spectra of PA6 and PA6/AS formulations are similar exhibiting peaks between 20 and 45ppm assigned to aliphatic carbons (details on this chemical shift range are given in **Figure 99 Appendix B**) and at 170 ppm attributed to C=O groups [213]. At 410 °C, peaks between 13-17 ppm corresponding to CH₂-CH₃ groups appear. The aliphatic region of the FR formulation broadens and it suggests a disordered structure. At the same time, a broad band centered at 130 ppm appears, attributed to unsaturated carbon bonds (aromatic species forming char). For pure PA6, the aromatic peak is not observed and the aliphatic region still shows well defined bands. At 410 °C, the PA6/AS 5% formulation is thus more degraded (formation of a charred structure) than the neat PA6. This is in good agreement with previous results suggesting a destabilization of PA6 by AS. At 500 °C, PA6 is almost completely degraded (only a small amount of residue after heat treatment) and no band could be detected. On the contrary, PA6/AS 5% formulation exhibits a relatively intense

broad band centered at 130 ppm while the peaks corresponding to aliphatic carbon bonds and to the carbonyl groups have almost disappeared. It is noteworthy that the aromatic carbons begin to oxidize at such a high temperature. The broadness of the band indicates the presence of the oxidized aromatic carbons because of the shoulder located at about 155 ppm.

It can thus be concluded that the incorporation of AS in the formulation leads to the formation of unsaturated carbon bonds and thus to the formation of charred residue. This was also visually observed after the thermal treatment of the different samples. The ^{13}C NMR experiments on the residues after thermal treatments indicate that PA6 begins to degrade at lower temperatures in the presence of AS. However, AS also promotes the formation of aromatic char which is more resistant at high temperature and to oxidation (i.e. 500 °C, **Figure 63**) than the residues produced for pure PA6 at the same temperature.

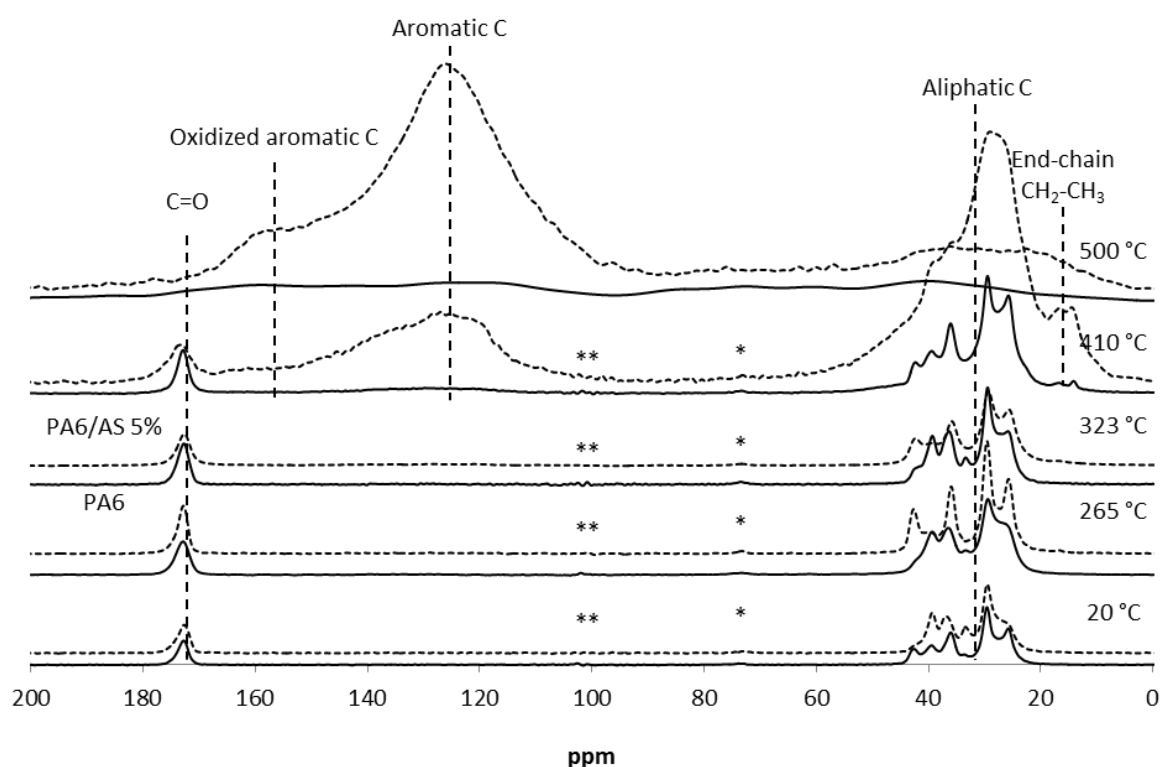


Figure 63: ^{13}C CP-DD-MAS NMR spectra of the PA6 (—) and PA6/AS 5% (--) formulations residues obtained after thermal treatment at 20, 265, 323, 410 and 500 °C (*: spinning sideband, **: frequency carrier)

IV.2.5 CONCLUSION

The decomposition pathway of PA6/AS has been investigated. The pHRR measured in microcalorimeter is reduced by 30% when incorporating 7 wt.-% of ammonium sulfamate. At this loading, the fibers exhibit poor mechanical properties but at 5 wt.-%, they are unchanged compared to neat PA6 fibers. The results show that AS modifies the decomposition pathway of PA6 by promoting char formation and a modification of the nature of the gaseous degradation products was also observed. The formation of a charred material and the changes of the evolving decomposition gases explain the modification of the reaction to fire of PA6/AS.

However, the release of ammonia by AS in the temperature range of 200-220 °C leads to an aminolysis of the PA6 matrix. Thus, a maximum loading of 5% was found which limits the enhancement of the fire properties. In order to overcome this limitation, another sulfamate salt was considered: the guanidine sulfamate.

IV.3 THE USE OF GUANIDINE SULFAMATE

Guanidine sulfamate (GAS) is a white crystalline solid, its molecular formula is $H_6N_2O_3S$ and the molecule is represented in **Figure 64**. It has a melting point of 130 °C

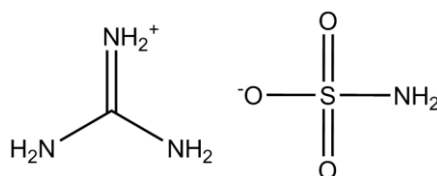


Figure 64: Molecular structure of guanidine sulfamate

IV.3.1 PROCESSING ISSUES SOLVED?

In the case of AS fibers, it was noticed that an early release of ammonia during processing lead to aminolysis of the PA6 and to its degradation. This issue limit the production of fibers for the formulation containing more than 5 wt.-% of AS. Thus, another sulfamate salt was investigated in order to overcome the limitations of AS, in terms of loading in the matrix. With GAS, it is possible to incorporate 10 wt.-% of additive in the PA6 and spin the fibers without any problem. In order to understand this result, TGA-FTIR was performed on the guanidine sulfamate to characterize its thermal behavior.

Figure 65 represents the TG and DTG curves corresponding to the thermo-oxidative degradation of ammonium sulfamate and guanidine sulfamate. Both FR begin to degrade around 200 °C but the main steps of weight loss are separated by 56 °C, $DTG_{max}(AS)$ is equal to 430 °C whereas $DTG_{max}(GAS)$ is equal to 374 °C. However at the processing temperature of PA6 (245 °C) the weight loss is similar for both FR (7%).

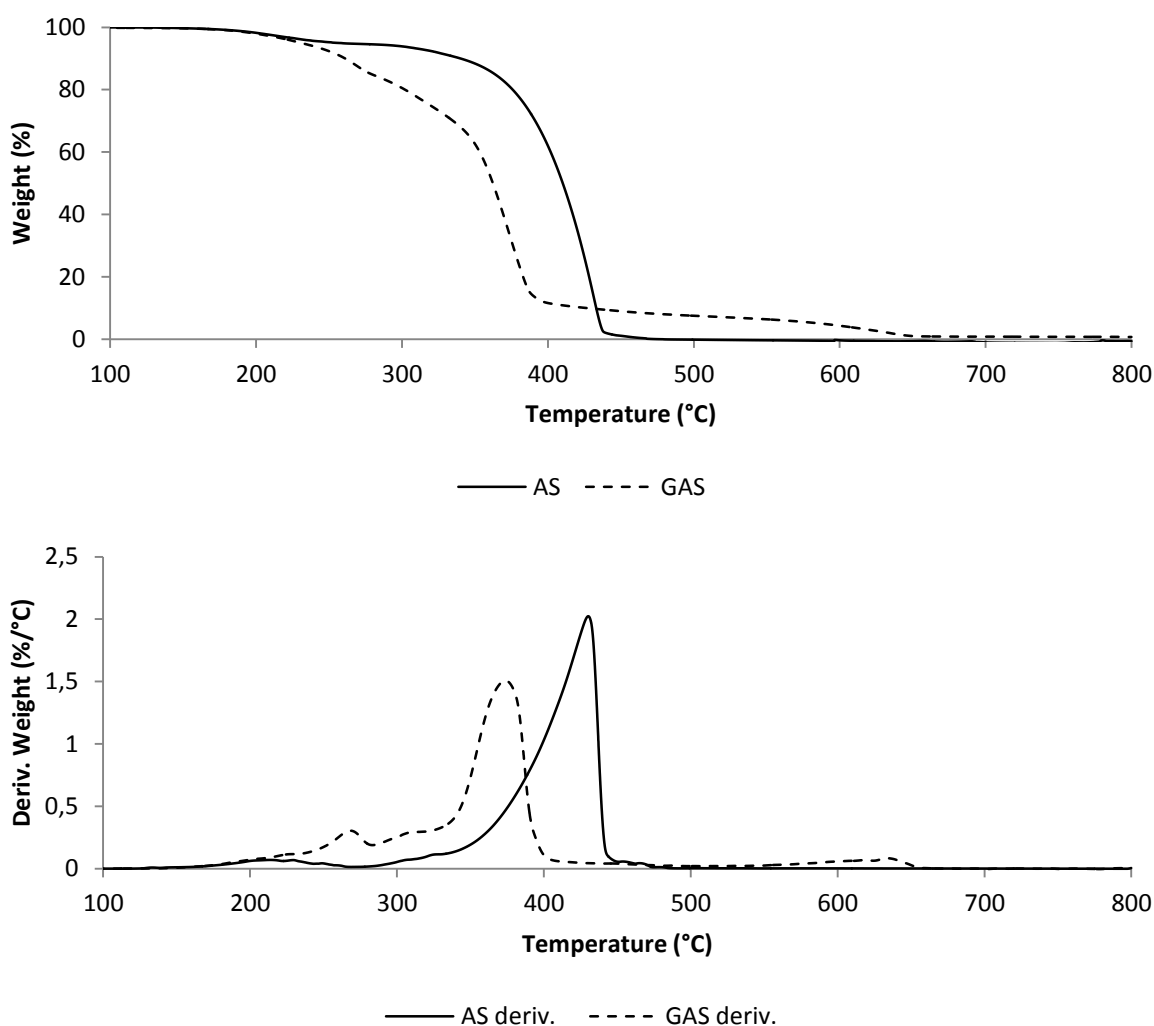


Figure 65: TG and DTG curves of AS and GAS

An analysis of the evolved gases of the degradation of GAS was done and compared to the results obtained with AS. **Figure 66** represents the intensity of a characteristic peak corresponding to ammonia ($\bar{\nu} = 965 \text{ cm}^{-1}$) as a function of time obtained during the decomposition of AS and GAS. In part IV.2.4.2.1, it was demonstrated that the first peak of ammonia release, by AS, was due to its dimerization, this reaction occurring at the processing temperature of PA6, it leads to a degradation of the matrix (aminolysis). For GAS, it can be noticed that a very small amount of NH_3 is released before 245 °C (corresponding to

24 min (1min = 10 °C)). The peak of evolved ammonia is located at 350 °C (35 min) for both FR.

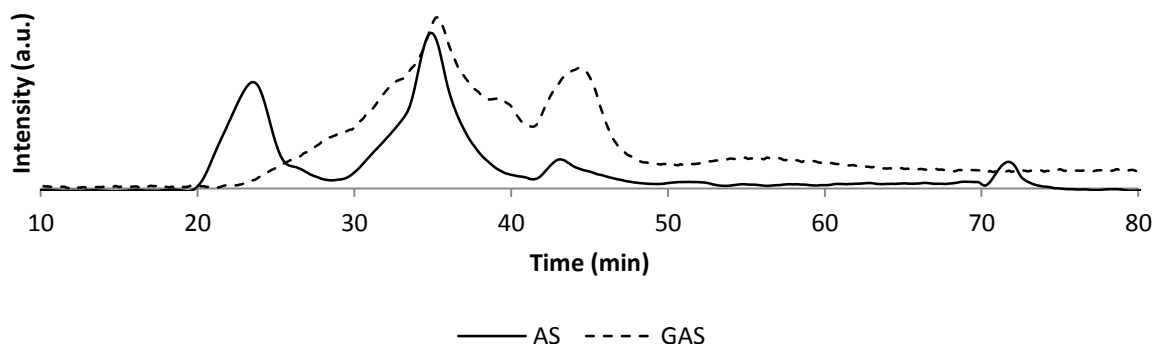


Figure 66: Intensity of the NH_3 peak (965 cm^{-1}) versus time for GAS and AS.

These results explain the reason why GAS is easier to process with PA6 than AS at 245 °C. The release of ammonia is limited and therefore no significant degradation of the matrix occurs. Thus, it is assumed that, as for ammonium sulfamate, there is an upper limit of GAS weight ratio for the formulation to be spinnable. But this value is higher in the case of GAS compared to AS.

IV.3.2 MECHANICAL PROPERTIES OF THE PA6/GAS FIBERS

Figure 67 reports the elongation-at-break and tensile strength of PA6/GAS 5% and 10% fibers. No significant change occurs on the elongation-at-break compared to neat PA6 fibers, both formulations have similar values, around 260 %. Concerning the tensile strength, a decrease of the value is observed for the PA6/GAS 5% fibers but considering the margin of error, this change is not relevant. It is thus assumed that guanidine sulfamate has no influence on the mechanical properties of the fibers, up to 10 wt.-% loading. A formulation containing 20 wt.-% of GAS was prepared, but no fibers could be drawn out of it because of an advanced degradation.

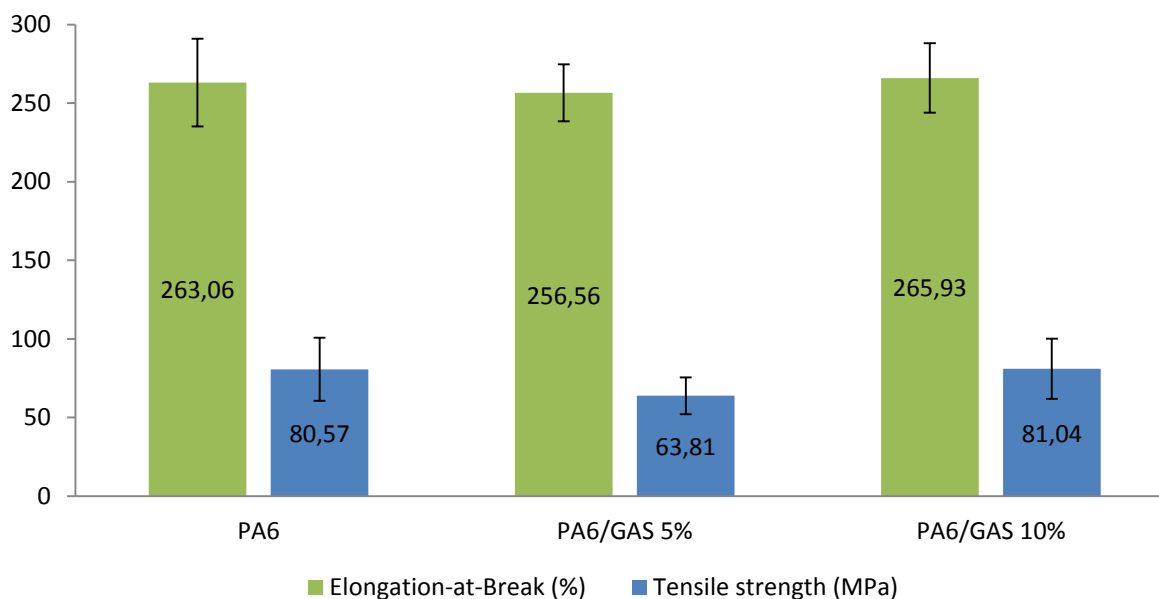


Figure 67: Elongation-at-break (%) and tensile strength (MPa) of PA6, PA6/GAS 5% and PA6/GAS 10% formulations

IV.3.3 FIRE TESTS ON PA6/GUANIDINE SULFAMATE FORMULATIONS

Heat release rate curves versus time obtained with PCFC for three formulations containing guanidine sulfamate are presented in **Figure 68**. The curves are similar to those obtained for the ammonium sulfamate formulations, that it to say that the higher the GAS content in the formulation, the lower the pHRR. A shift to lower temperatures of the pHRR is observed when the loading of GAS increases. A smaller peak is also observed, however contrary to what was observed for the AS containing formulation, this peak appears around 300 °C.

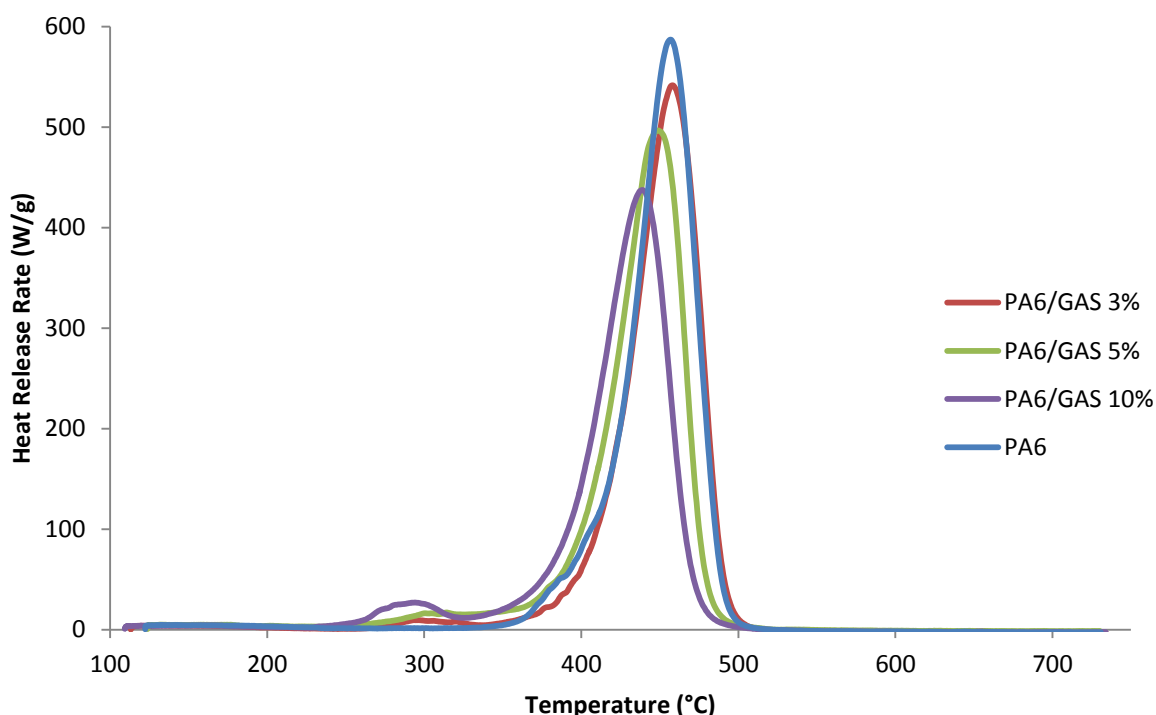


Figure 68: HRR curves versus temperature obtained with PCFC for PA6 and PA6/GAS formulations

The results of spinnability and PCFC tests are summarized in **Table 23**. All formulations, except that containing 20 wt.-% of GAS, were spinnable and the maximum of decrease (-25 %) of the pHRR was obtained for the PA6/GAS 10% formulation. THR decrease is also a function of the additive loading, and may be related to the formation of small amount of char observed in the sample cups at the end of the experiment. In order to achieve better PCFC results, a formulation containing a high loading of GAS was done (20 wt.-%) but it leads to processing issues due to PA6 degradation. This means that maximum GAS weight ratio, allowing to keep the formulation spinnable was reached.

Table 23: PCFC results for PA6/guanidine sulfamate formulations

Formulation	Spinnable*	pHRR (W/g)	Δ pHRR/PA6 (%)	THR (kJ/g)	Δ THR/PA6 (%)
PA6	Y	588	-	30.0	-
PA6/GAS 3%	Y	537	-8.7 %	28.9	-3.7
PA6/GAS 5%	Y	500	-14.9 %	27.4	-8.7
PA6/GAS 7%	Y	477	-18.9 %	27.6	-8.0
PA6/GAS 10%	Y	439	-25.4 %	25.7	-14.3
PA6/GAS 20%	N	-	-	-	-

*Y: yes, N: no

These results reflect a same overall behavior compared with AS. However, the amount of GAS needed to reach the same level of fire retardancy as with AS is higher. This is illustrated

in **Figure 69** where the pHRR of each formulation is plotted against its FR content in PA6. Calculations show that GAS needs to be incorporated at a ratio 1.7 times higher than AS to have the same level of pHRR reduction.

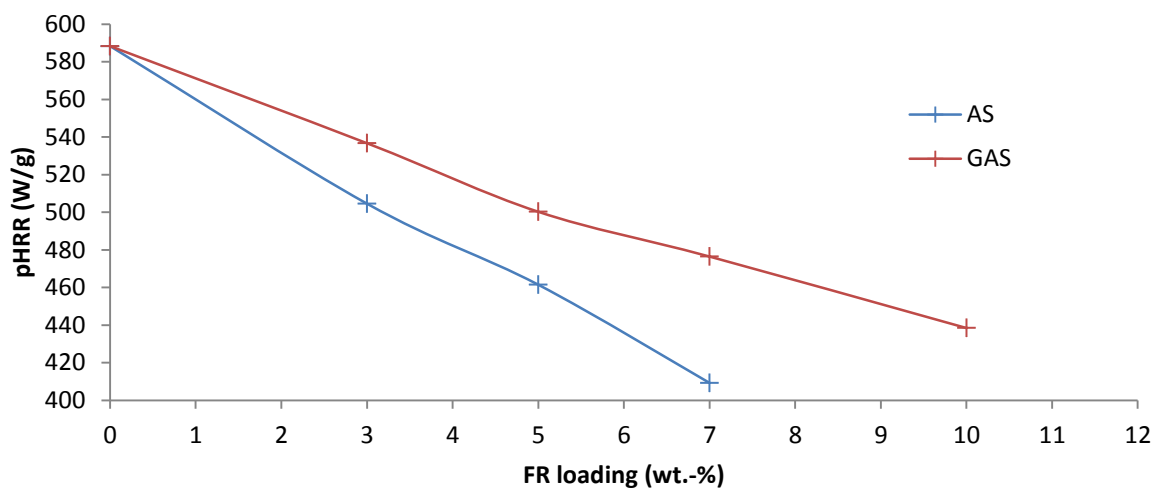


Figure 69: pHRR of AS and GAS containing formulations in function of their loading

IV.3.4 ADDITIVE DISPERSION

EPMA was used to investigate the dispersion of GAS in formulations containing 5 wt.-% (**Figure 70**) and 10 wt.-% (**Figure 71**) of this additive. BSE pictures and sulfur cartographies of each sample are shown, cross section of the fibers have been encircled in yellow. The diameter of the fibers varies between 100 and 120 μm for both samples and the cartographies of sulfur show that GAS is well dispersed in the PA6 matrix.

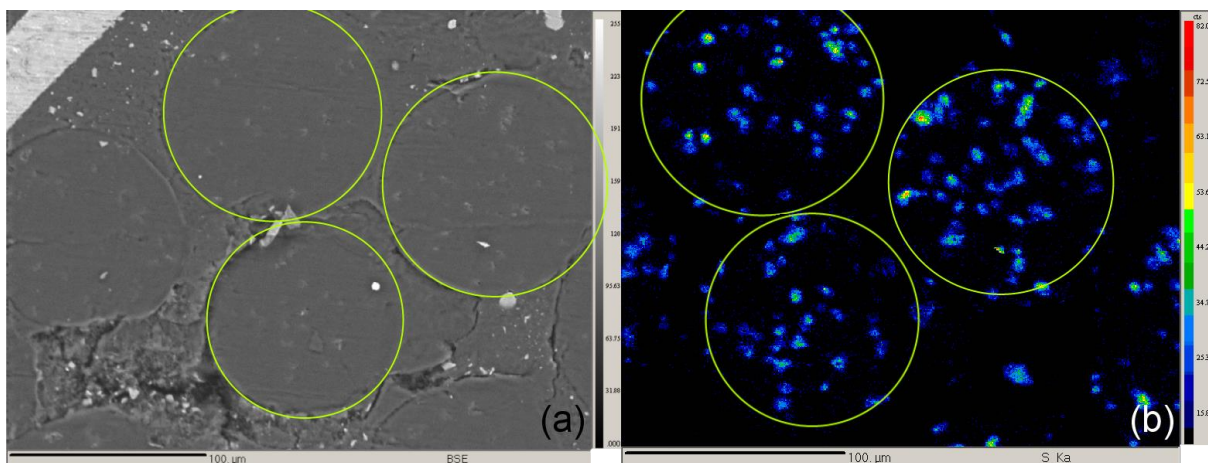


Figure 70: BSE picture (a) and EPMA sulfur cartography (b) of the cross section of PA6/GAS 5% fibers (circled in yellow)

On the BSE pictures, the white dots correspond to SiC (silicon carbide) grains that were used to polish the cross-section surface of the samples before analysis.

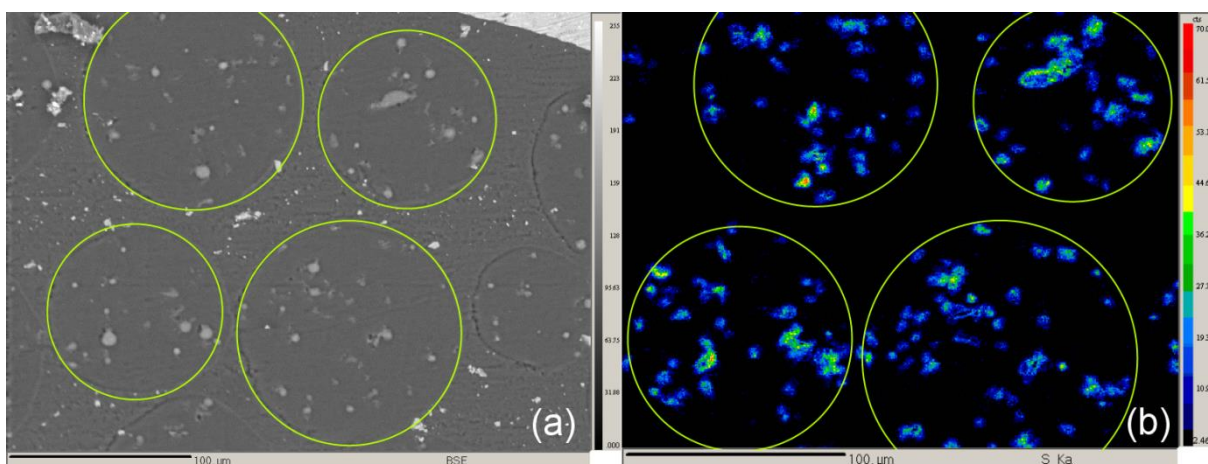


Figure 71: BSE picture (a) and EPMA sulfur cartography (b) of the cross section of PA6/GAS 10% fibers (circled in yellow)

The overall dispersion is similar for both samples, even if the GAS loadings are different (5 wt.-% and 10 wt.-%). Guanidine sulfamate is a melting additive (melting point : 130 °C) at the process temperature, moreover, no blooming effect has been detected, hence GAS seems compatible with the matrix, this permits the achievement of good dispersions. As reported in section IV.3.2, mechanical properties of the fibers containing 5wt.-% and 10 wt.-% of GAS are similar to pure PA6.

IV.3.5 DEGRADATION MECHANISM

IV.3.5.1 GAS PHASE ANALYSIS

IV.3.5.1.1 TGA-FTIR

Figure 72 represents the experimental and theoretical TG curves of PA6/GAS 5% and PA6/GAS 10% formulations. The description of the different degradation steps was previously detailed in part III.2.2.2. TGA difference curves confirm the information given by the TGA. That is to say, that the degradation of PA6 starts at lower temperature than in the presence of GAS, with an additional weight loss step. Moreover, the char oxidation lasts on a broader temperature and weight loss range. The intensity of the difference curves in the destabilization zone (from 265 °C to 450 °C) and in the stabilization zone (from 450 °C to around 600 °C), has increased between the formulation containing 5 and 10 wt.-% of GAS. However, the shape of the two curves is similar. This result indicates that the ratio of GAS greatly influence the different effects of this additive. In one hand, the stabilizing effect is enhanced but in the other hand the destabilization is also increased when more GAS is added to PA6.

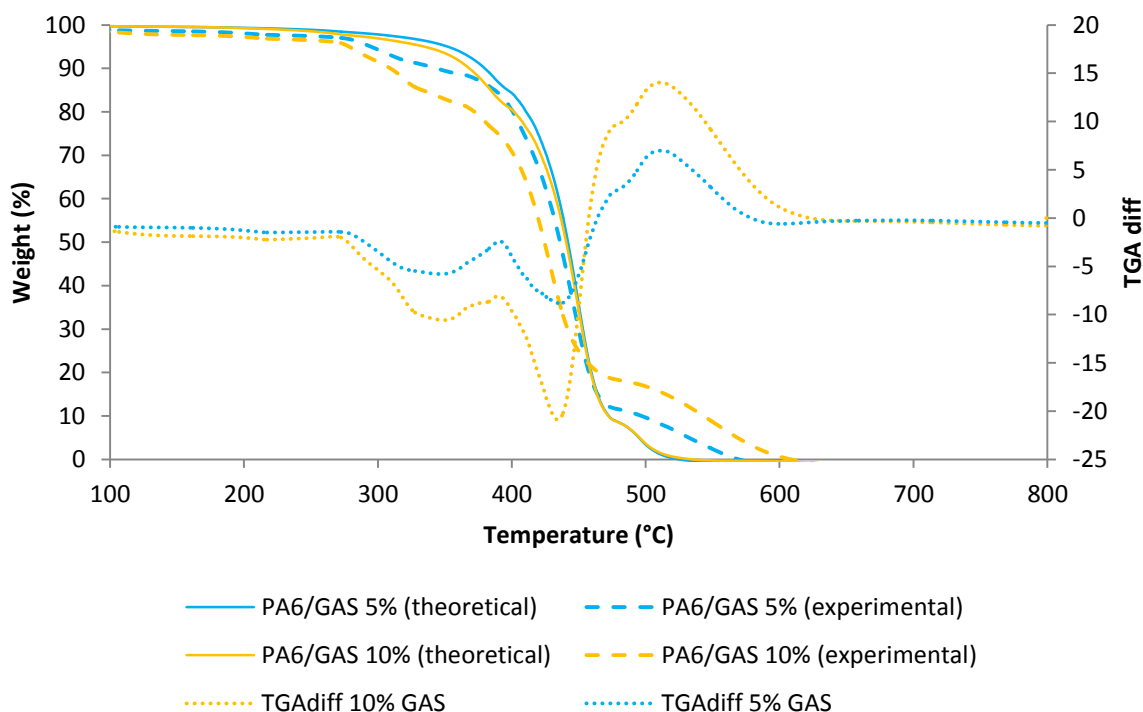


Figure 72: Experimental and theoretical TG curves of PA6/GAS 5% and PA6/GAS 10%, and their TGA difference curves (10 °C/min, air)

The spectra of the gases evolved during the thermo-oxidative degradation of PA6/GAS formulations from TGA-FTIR are presented in **Figure 73**. They correspond to the characteristic temperatures of degradation, obtained from the TG curves. 300 °C corresponds to maximum of weight loss rate of the first degradation step, 430 °C is the maximum degradation rate and 500 °C corresponds to the oxidation of the transient residues. Spectra for both formulations show the same peaks for each temperature.

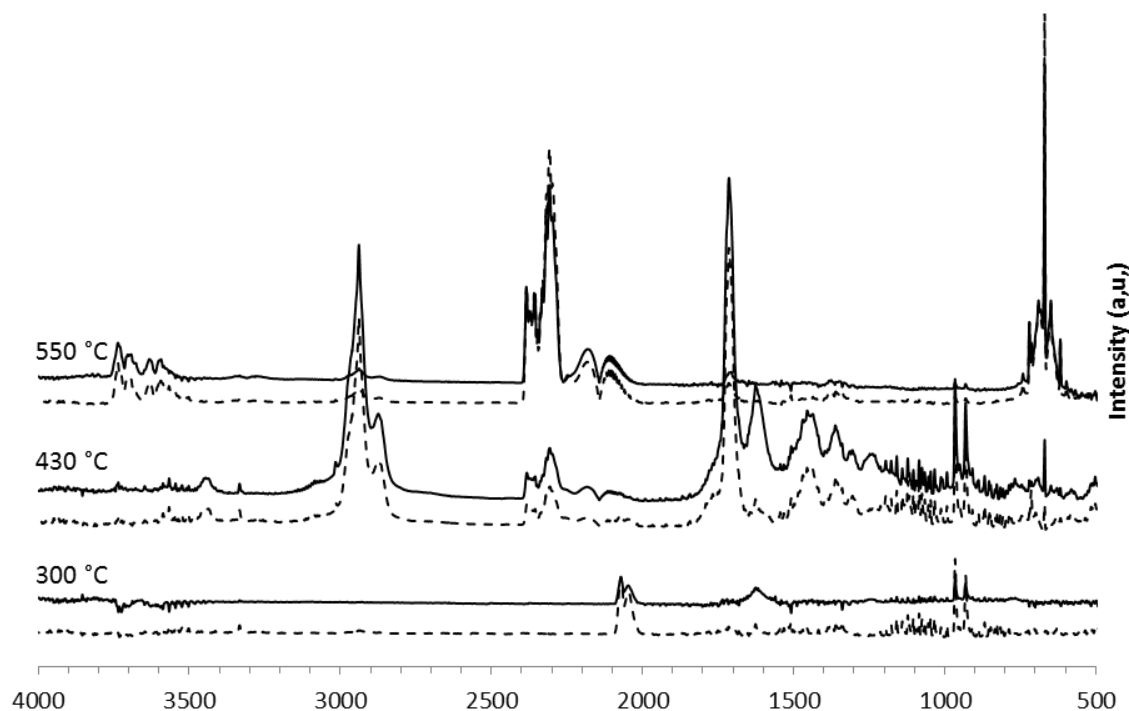


Figure 73: FTIR spectra of the gases evolved during the thermo-oxidative degradation of PA6/GAS 5% (—) and PA6/GAS 10% (--) at characteristic temperatures of degradation.

At 300 °C peaks corresponding to ammonia are visible (930, 965, 1626 and 3332 cm^{-1}), water is also detected with peaks around 3600 cm^{-1} and 1500 cm^{-1} . Compared to the spectra of the first degradation step of neat PA6 and PA6/AS 5% a new double peak has appeared at $\bar{\nu} = 2070$ and 2045 cm^{-1} (the peak is not found during the whole experiment on PA6 and PA6/AS 5%). This double peak has not been found in the literature concerning the degradation products of polyamide, however, using NIST database of infrared spectra [207], it is often attributed to $\text{C}\equiv\text{N}$ and/or $\text{C}-\text{C}\equiv\text{N}$ bonds. The spectra was recorded at 300 °C, at this temperature it is known that PA6 can decompose into nitrile end-group products [51]. It is thus assumed that GAS promotes the decomposition of PA6 into small molecules having nitrile end-groups.

When the temperature is increased to 430 °C, during the main degradation step, the major evolved gases are ammonia and caprolactam with the corresponding characteristic peaks, at 930, 965 cm^{-1} and 2938, 1713 cm^{-1} respectively. Water is also released during the degradation and low intensity peaks of CO and CO₂ are present (669 and 2000-2200 cm^{-1})

Eventually, at 550 °C char oxidation occurs and mainly CO and CO₂ are produced, however traces of caprolactam can be identified.

IV.3.5.1.2 PY-GC-MS

PA6 containing 5 wt.-% of GAS was analyzed with py-GC-MS using a stepwise method. In **Figure 74** presents the chromatogram corresponding to the main degradation step (between 368 °C and 483 °C). The products assignments are detailed in **Table 24**. Compared with neat PA6, it can be seen that there are many more peaks, indicating that the matrix has another degradation pathway. At 30 min, for PA6 and PA6/GAS 5%, the most intense peak corresponds to the cyclic monomer of PA6: ϵ -caprolactam. On both chromatograms, a less intense peak is visible before the one of ϵ -caprolactam, and is located around 29 min. These peaks correspond to 6-aminohexanenitrile.

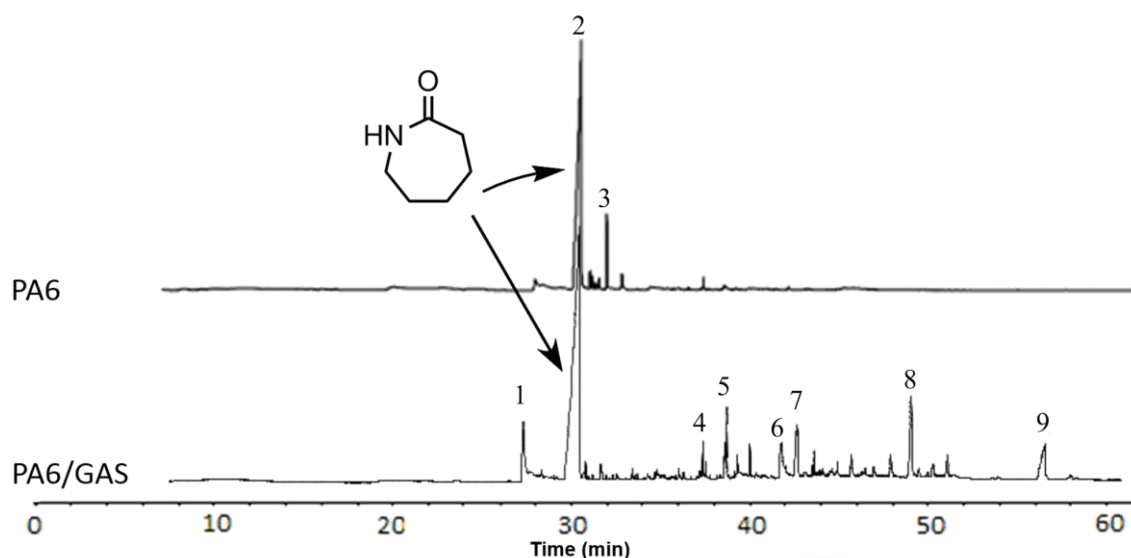
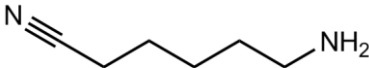
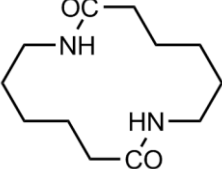
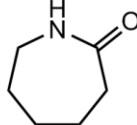
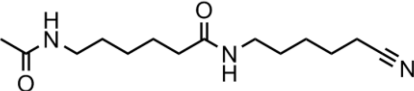
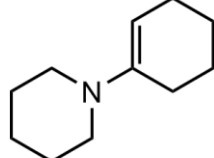
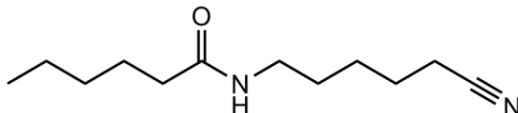
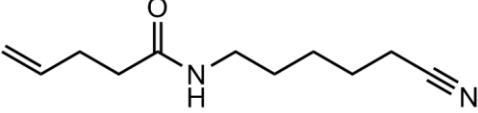
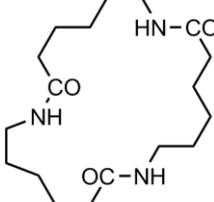
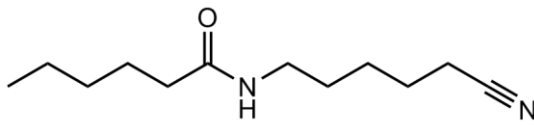


Figure 74: TIC curves corresponding to the pyrolysis of PA6 between 350 °C and 490 °C, and PA6/GAS 5% between 366 °C and 490 °C

For the PA6/GAS formulation a series of less intense peaks is visible. As for AS, the products of degradation evolved during the main weight loss of PA6 and PA6/GAS are very different; neat PA6 mainly depolymerize and forms ϵ -caprolactam while the presence of GAS

promotes the formation of numerous chain scission products. These chain scission products have higher molecular weights and dimers and trimers of caprolactam are detected. This indicates that GAS acts in the same way as AS by changing the degradation pathway of PA6.

Table 24: py-GC-MS degradation products of PA6 and PA6/GAS during the main degradation step, peaks numbers (#) are given on Figure 74

#	product	#	product
1	 6-aminohexanenitrile	6	 1,8-diazacyclotetradecane-2,9-dione
2	 azepan-2-one (caprolactam)	7	 6-acetamido-N-(5-cyanopentyl)hexanamide
3	 1-(cyclohex-1-en-1-yl)piperidine	8	 <i>N</i> -(5-cyanopentyl)hexanamide
4	 <i>N</i> -(5-cyanopentyl)pent-4-enamide	9	 1,8,15-triazacyclohencicosane-2,9,16-trione
5	 <i>N</i> -(5-cyanopentyl)hexanamide		

IV.3.5.2 SOLID PHASE ANALYSIS

The ^{13}C CP-DD-MAS NMR spectra of the residues obtained after the thermal treatment of PA6/GAS 5% formulations, at the previously defined characteristic temperatures, are given in **Figure 75**. From 20 to 320 °C, the spectra of PA6/GAS formulation are similar. Peaks

between 20 and 45 ppm are assigned to aliphatic carbons and at 170 ppm attributed to C=O groups [213]. From 320 °C, peaks between 13-17 ppm corresponding to CH₂-CH₃ groups appear. The aliphatic region broadens and it suggests a disordered structure. At the same time, a broad band centered at 125 ppm appears that can be attributed to unsaturated carbon bonds (aromatic species forming char). At 500 °C a relatively broad band centered at 130-140 ppm is predominant while the peaks corresponding to aliphatic carbon bonds and to the carbonyl groups have almost disappeared. At such a high temperatures (410 and 500 °C) the aromatic carbons begin to oxidize. The broadness of the band indicates the presence of the oxidized aromatic carbons because of the shoulder located around 140 and 160 ppm. The incorporation of GAS in the formulation leads to the formation of unsaturated carbon bonds and thus to the formation of charred residue.

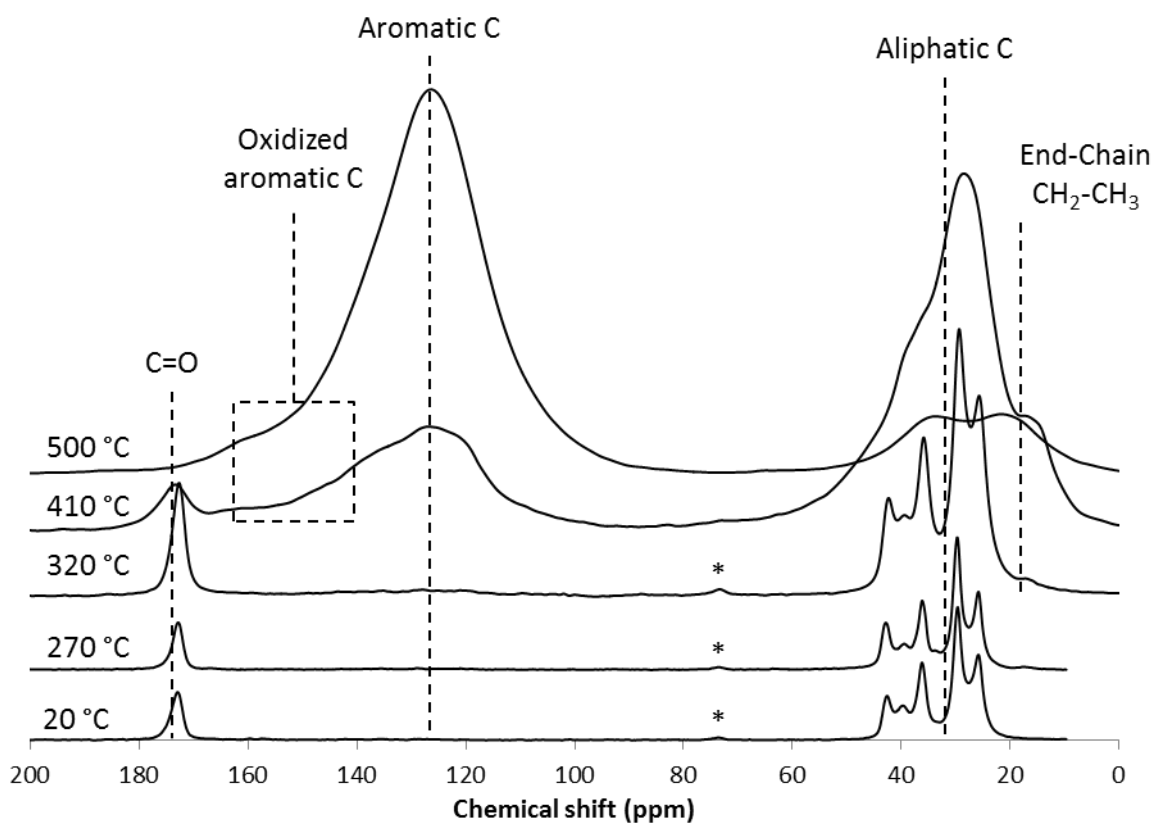


Figure 75: ¹³C CP-DD-MAS NMR spectra of the PA6/GAS 5% formulation residues obtained after thermal treatment at 20, 270, 320, 410 and 500 °C (*: spinning sideband)

Guanidine sulfamate is a carbon containing salt, and thus carbon signal should be visible on the ¹³C NMR spectra, however the relatively low amount of GAS in the formulation prevents the apparition of intense peak. However, if a zoom is made on the C=O area a peak located at 158 ppm should appear [214]. On **Figure 76** a zoom has been made on the 150-200 ppm

region, a very little peak appears beside the C=O peak, around 159 ppm, this peak corresponds to GAS. The guanidine peak is not present on all spectra as it may be hidden by the noise of the signal.

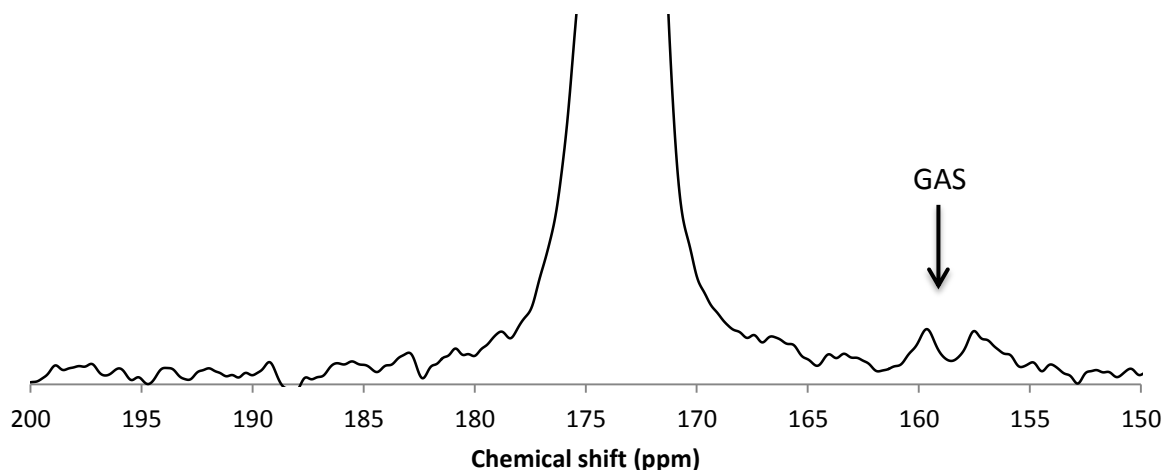


Figure 76: Zoom made between 150 and 200 ppm on the ^{13}C CP-DD-MAS NMR spectra of the PA6/GAS 5% formulation obtained at room temperature

IV.4 CONCLUSION

In this chapter, the fire behavior of the formulations containing the two selected sulfamate salts, namely ammonium sulfamate and guanidine sulfamate, were investigated. It has been demonstrated that both FR acted in a similar way. PCFC results show a decrease of the peak of heat release rate for all formulations, and it appears that the efficiency of the FR is related to its weight content in the formulation, THR is also decreased.

AS and GAS act similarly modifying the degradation pathway of PA6. In the solid phase, TGA difference curves indicate a stabilizing effect of AS and GAS at high temperatures ($T > 450\text{ }^\circ\text{C}$). Solid state NMR proves the formation of aromatic carbons, meaning that a certain amount of char is not converted into fuel. The characterization of the condensed phase confirms the TGA results showing a more important char oxidation over a broader temperature range. PCFC suggested an action in the gas phase, and py-GC-MS shows that the products of degradation are different between neat PA6 and PA6 formulated with AS or GAS. Mainly depolymerization (caprolactam) is observed for PA6, while for the formulated PA6, a gas composition containing heavier molecules (with caprolactam dimers, trimers and in between chain scission products) is detected. Since it was previously reported that ϵ -caprolactam

release control the fire behavior of PA6, this is consistent with an improvement of the fire behavior.

From a mechanical point of view, the use of ammonium sulfamate is subjected to some limitations. Indeed, TGA-FTIR shows that in the range of processing temperature of PA6, AS releases ammonia. With loadings higher than 5 wt.-% of AS, the aminolysis of the PA6 matrix lead to a degradation of the matrix and thus limit the spinning process. GAS was used as an alternative to AS, however, the fire performances are not as good as AS.

It is known that the presence of a nucleophile promotes the breakage of the amide bonds and favors the formation of chain fragments instead of ϵ -caprolactam. This behavior was also revealed by the py-GC-MS experiments. Ammonia and guanidine do not have the same nucleophilicity, thus, it is proposed that their action is different. Ammonia is more nucleophile than guanidine, consequently, more chain fragments and oligomers are produced. In other words, AS is more efficient because it promotes the formation of more oligomers than GAS.

During this study, both sulfamate salts were extruded at large scale. However, it resulted in brownish and degraded materials. All formulations presented until here were done with the help of a microextruder, allowing the preparation of 10 g samples. It is important to ensure that the formulation is able to go through a larger extruder, where the temperature profiles are different and usually more aggressive towards the polymer and its additives. As a consequence, the next chapter will aim at finding a system compatible with a larger scale extrusion process. Spinnability and fire results, should in the same time, be enhanced of at least equal to what was obtained with microextrusion.

V	SCALE-UP OF THE SULFAMATE SALTS SYSTEMS	
V.1	Introduction.....	156
V.2	Potential synergy between sulfamate salts and melamine polyphosphate.....	157
V.2.1	AS/MPP.....	157
V.2.1.1	PCFC Results and spinnability _____	157
V.2.1.2	Thermogravimetry _____	158
V.2.2	GAS/MPP	160
V.2.2.1	PCFC Results and spinnability _____	160
V.2.2.2	Thermogravimetry _____	161
V.2.3	Conclusion	162
V.3	Scale-up with the PA6/GAS/MPP system	163
V.3.1	Materials characterizations.....	164
V.3.1.1	Spinnability and additives dispersion _____	164
V.3.1.2	Thermogravimetric analysis _____	166
V.3.1.3	Differential scanning calorimetry (DSC) _____	167
V.3.1.4	PCFC _____	169
V.3.2	Fire performance of large-scale PA6/GAS/MPP.....	170
V.3.2.1	Cone calorimetry _____	170
V.3.2.2	UL-94 and LOI _____	173
V.3.3	Analysis of the decomposition gases	175
V.3.3.1	TGA-FTIR _____	175
V.3.3.2	py-GC-MS _____	178
V.3.4	Analysis of the condensed phase	180
V.4	Conclusion	183

V.1 INTRODUCTION

This chapter aims at scaling-up the extrusion process of the fibers. Indeed, in the previous chapter, it was shown that formulations containing a high amount of ammonium sulfamate and guanidine sulfamate (>7 wt.-% and >10 wt.-% respectively) were hardly processable due to the release of ammonia at the extrusion temperature. This issue may also intensify during scale-up as it requires the use of a different temperature profile. For microextrusion, the temperature was set to 245 °C from hopper to die; at larger scale, the process and the conditions are changed. It is mandatory to heat the matrix at higher temperature: the PA6 is heated at 300 °C in the feeding zone and the temperature is gradually decreased along the screws till the die.

In order to limit the risks of matrix degradation, it is proposed to substitute a part of the sulfamate salts by another compound and to develop a synergistic effect. The co-additive should therefore have no negative effect on the fire properties and mechanical properties. Finding a synergist of the sulfamate salts should therefore allow to enhance the fire properties and to decrease the amounts of AS or GAS used in the formulations. Using less of these FR while maintaining the FR properties should allow the up-scaling of the process.

It was found in the literature that sulfur compounds may act as synergists with ammonium polyphosphate [15] but the literature on this subject is very limited. Ammonium polyphosphate is widely used in intumescent systems as an acid source. High amounts of APP (generally >30 wt.-%) are usually needed to efficiently flame retard PA6 [203]. However, APP has a relatively low thermal stability and requires fast processing to avoid degradation [54]. Melamine polyphosphate (MPP) is thermally stable at the processing temperature of PA6, and thus, was chosen to replace APP. In this chapter, MPP will be used as a potential synergist with sulfamate salts. MPP is widely used in the fire retardancy of polyamides, it has applications in PA6 and glass fiber reinforced PA6.

In this work, MPP will be mixed with both AS and GAS. The ratio of FR additives will be varied in order to obtain the best FR properties and a synergistic effect. Then, scale-up of the most effective formulation will be carried out. Eventually, the microscale and large-scale formulations will be compared to verify if the scale-up influences the properties of the materials.

V.2 POTENTIAL SYNERGY BETWEEN SULFAMATE SALTS AND MELAMINE

POLYPHOSPHATE

V.2.1 AS/MPP

V.2.1.1 PCFC RESULTS AND SPINNABILITY

PCFC curves of the formulations containing various ratios of AS and MPP are presented in **Figure 77**. In order to compare the results, PA6 and PA6/AS 5% curves were also added. Compared to neat PA6, the temperature of pHRR is decreased, as well as the pHRR itself. The pHRR temperatures (T_{pHRR}) of the different formulations are given in **Table 25**. T_{pHRR} decreases with the increase of the MPP content in the formulations. Indeed, when 20% of AS is replaced by MPP, the shift of the T_{pHRR} is negligible compared to the formulation containing 5 wt.-% of AS. However, when 50% of AS is substituted by MPP the impact on the temperature of pHRR intensifies, and becomes maximal when 100% of AS is replaced by MPP. The decreases compared to PA6/AS 5% are respectively 18 and 59 °C. On the curves, a small peak is also present from 270 to 300 °C; it is attributed to the release of small combustible gases such as ammonia. It was previously shown with TGA-FTIR that this compound could evolve from the PA6/AS formulations in this temperature range.

pHRR and THR values of the PA6, PA6/AS 5%, PA6/MPP 5% and PA6/AS/MPP formulations are also reported in **Table 25**. All the formulations containing AS and/or MPP have decreased pHRR, T_{pHRR} and THR values. In the formulations containing both FR (AS and MPP), it is observed that the higher the amount of MPP, the higher the pHRR. Comparing the formulation containing 1 wt.-% MPP and 4 wt.-% AS with the PA6/AS 5% formulation, a decrease of both pHRR and THR can be seen (411 w/g and 461 w/g respectively). The PA6/AS 4%/MPP 1% has a pHRR reduction of 30.1% compared to neat PA6. This last result is better than with AS or MPP alone at 5wt.-% in the PA6, which have a 21.6 and 9.9% pHRR reduction respectively. Thus, a synergistic effect between AS and MPP is obtained for this ratio.

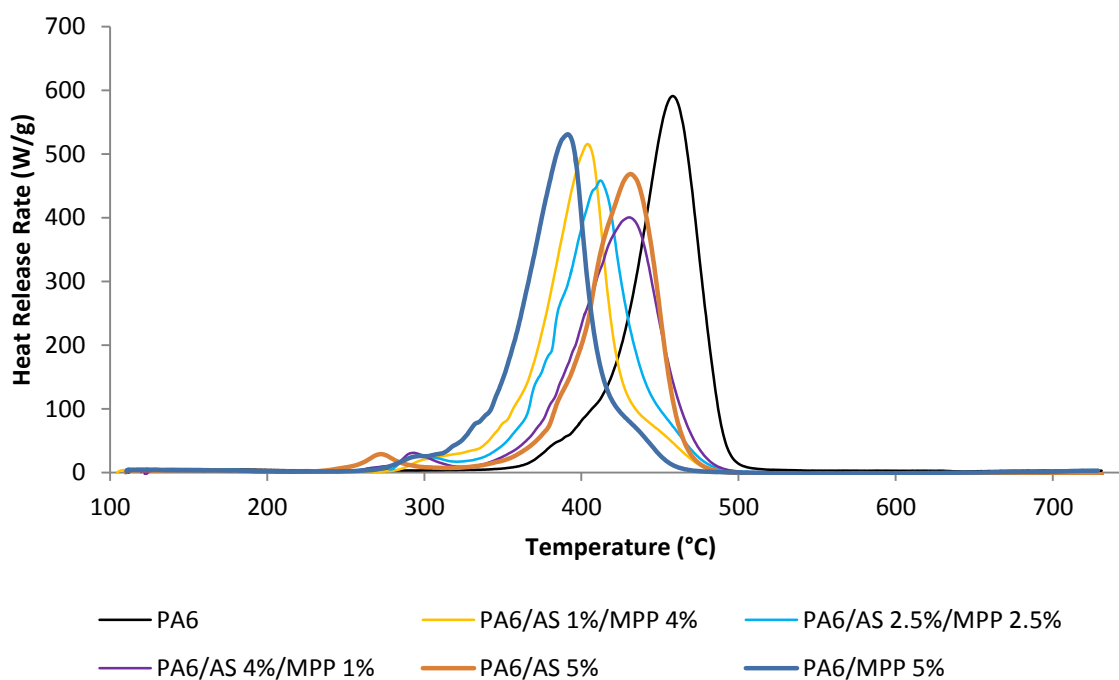


Figure 77: HRR curves versus temperature obtained with PCFC of PA6, PA6/AS/MPP formulations and PA6/AS 5%

Table 25: PCFC results of PA6, PA6/AS 5%, and PA6/AS/MPP formulations

Formulation	Spinable*	pHRR (W/g)	Δ pHRR/PA6	T_{pHRR} (°C)	THR (kJ/g)	Δ THR/PA6
PA6	Y	588	-	456	30.0	-
PA6/MPP 5%	Y	530	-9.9	371	29.7	-1.0
PA6/AS 1%/MPP 4%	Y	508	-13.6	404	28.0	-6.7
PA6/AS 2.5%/MPP 2.5%	Y	458	-22.1	412	27.7	-7.7
PA6/AS 4%/MPP 1%	Y	411	-30.1	429	26.8	-10.7
PA6/AS 5%	Y	461	-21.6	430	27.1	-9.7

* Y: yes, N: no

V.2.1.2 THERMOGRAVIMETRY

TG and DTG curves of the three PA6/AS/MPP formulations are given in **Figure 78**. From this curves, it is evident that a higher amount of AS in the formulation, leads to a higher weight loss during the first step of degradation. This is consistent with the fact that this first step corresponds to the degradation of AS (dimerization with ammonia evolution). On the other hand, the AS/MPP ratio plays an important role on the destabilization of the matrix during the main decomposition step.

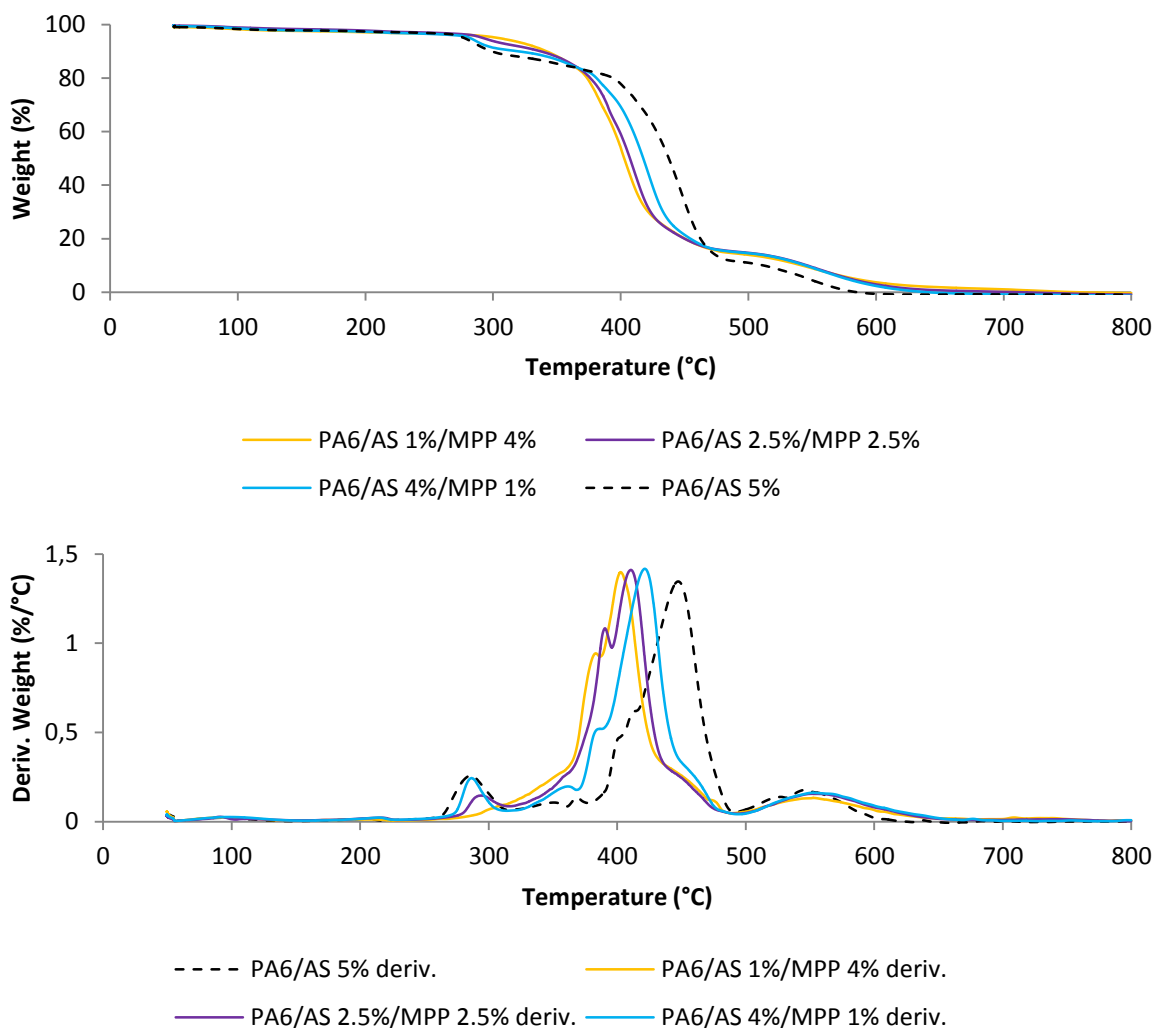


Figure 78: TG and DTG curves of PA6/AS/MPP formulations and PA6/AS 5% (10 °C/min, air)

It is observed that the higher the MPP content in the formulation, the lower the temperature of maximum mass loss rate. This behavior could be linked with the previously described decrease of T_{pHRR} observed in PCFC experiment. It is thus assumed that MPP promotes PA6 degradation. Eventually, the last degradation step, which begins at 500°C, is the same for all three formulations and it ends at higher temperature than for PA6/AS 5%.

These results support those from PCFC, where a shift of the pHRR to lower temperature with increased MPP content occurred. In fact, by promoting PA6 degradation, MPP favors the emission of combustible fuel, thus shifting the pHRR. The earlier degradation of PA6 due to the presence of melamine salts was reported in the literature [203, 215, 216] and a severe depolymerization is reported. It is found that melamine may interact with the H bonds network of PA6, which favors its thermal degradation. Aminolysis due to ammonia release by melamine may also contribute to the degradation [215].

V.2.2 GAS/MPP

V.2.2.1 PCFC RESULTS AND SPINNABILITY

PCFC curves of the formulations containing various ratios of GAS and MPP are presented in **Figure 79** and **Table 26** summarizes the PCFC results for the formulations containing guanidine sulfamate or/and MPP. For all the formulations containing MPP, a shift of the pHRR to lower temperature is measured, compared to neat PA6 and PA6/GAS 5%. As for the PA6/AS/MPP formulations, the temperature of the pHRR is highly decreased when 4 wt.-% of GAS are substituted by MPP in the PA6/GAS formulation. With the formulations containing 1 wt.-% and 2.5 wt.-% of MPP the decrease is comparable. It is thus assumed that MPP in the formulations favors the volatilization of combustible gases.

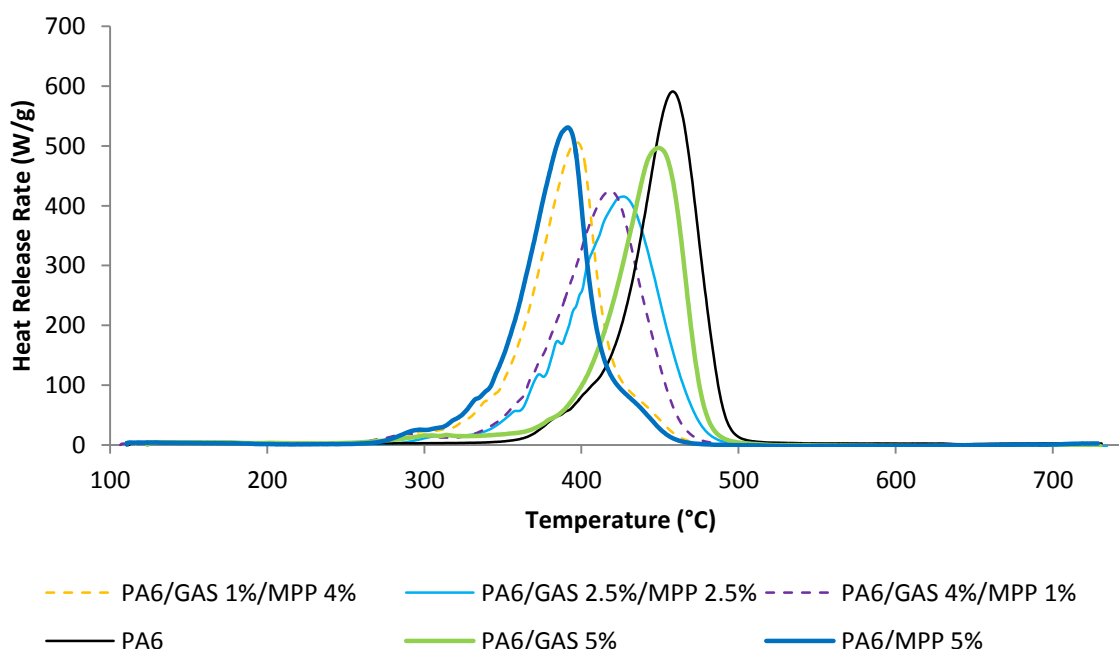


Figure 79: HRR curves versus temperature obtained with PCFC of PA6 and PA6/GAS/MPP formulations

The gradual substitution of GAS by MPP enhances the fire behavior of PA6/GAS, when 1 or 2.5 wt.-% of GAS are substituted. Reductions of 27.0 and 30.1 % of the pHRR are observed respectively. However, when 80% of GAS are substituted (4 wt.-%), the results are the same as for the formulation containing 5 wt.-% GAS alone, in terms of pHRR. Based upon these results, the ratio 50/50 for GAS/MPP is found to be the most efficient in reducing the pHRR. Keeping the same ratio, a formulation containing a higher amount of FR additives, namely 5 wt.-% of GAS and 5 wt.-% of MPP, was thus extruded. In fact, it was previously observed

that adding more GAS to the formulation resulted in an enhancement of the pHRR reduction. However, it was found that PA6/GAS 5%/MPP 5% is less efficient than PA6/GAS 2.5%/MPP 2.5%: pHRR is decreased by 20.6 % versus 30.1%. The pHRR decrease of PA6/GAS 2.5%/MPP 2.5% is higher than the decrease measured with GAS and MPP alone at 5 wt.-%, thus a synergistic effect occurs between these two compounds.

Table 26: PCFC results of PA6, PA6/GAS 5%, and PA6/GAS/MPP formulations

Formulation	Spinnable*	pHRR (W/g)	Δ pHRR/PA6	T _{pHRR} (°C)	THR (kJ/g)	Δ THR/PA6
PA6	Y	588	-	456	30.0	-
PA6/MPP 5%	Y	530	-9.9	371	29.7	-1.0
PA6/GAS 1%/MPP 4%	Y	498	-15.3	400	28.1	-6.3
PA6/GAS 2.5%/MPP 2.5%	Y	411	-30.1	428	28.7	-4.3
PA6/GAS 4%/MPP 1%	Y	429	-27.0	420	28.1	-10.0
PA6/GAS 5%	Y	500	-15.0	449	27.4	-8.7
PA6/GAS 5%/MPP 5%	Y	467	-20.6	397	27.0	-31.3

* Y: yes, N: no

V.2.2.2 THERMOGRAVIMETRY

Figure 80 presents the TG and DTG curves of PA6/GAS/MPP formulations. Overall, the same trends as those found for the PA6/AS/MPP formulations can be observed. A first decomposition step occurs between around 270°C to 320 °C for the formulations containing 4 and 2.5 wt.-% of GAS, while no decomposition step is observed in that temperature range for the formulation containing 1 wt.-% of GAS. In this temperature range, the behavior is similar to that of PA6/GAS 5%. At higher temperature, during the main decomposition step, the incorporation of an increasing amount of MPP in the formulation leads to a progressive shift of the maximum weight loss rate to lower temperatures. This indicates that MPP promotes the degradation of PA6 into gaseous products. However, contrary to the PA6/AS/MPP formulations, the last decomposition step is different for the formulation containing 4 wt.-% of MPP, less transient residue is formed and then oxidized. The same general behavior was previously observed with the AS/MPP formulations, and is also attributed to MPP promoting PA6 degradation.

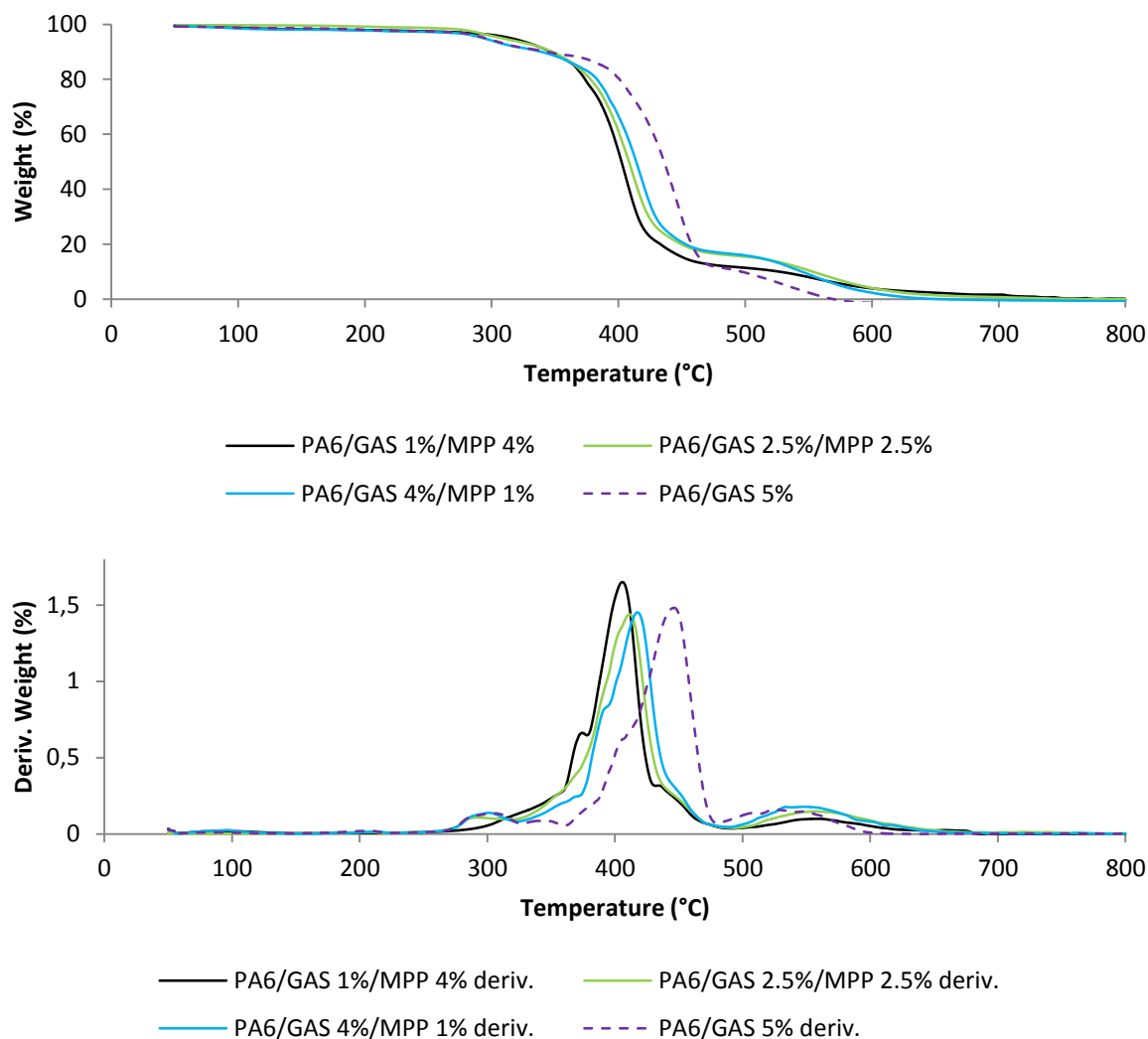


Figure 80: TG and DTG curves of PA6/GAS/MPP formulations and PA6/GAS 5% (10 °C/min, air)

V.2.3 CONCLUSION

In the literature, phosphorus compounds are proposed to be potential synergists with sulfur based compounds. In this study, it was proposed to substitute a part of the sulfamate compounds by melamine polyphosphate. This approach has two objectives; first it was intended to find an effective synergism between sulfur and phosphorus compounds. The second objective was to find a solution for scaling up the extrusion process. Indeed, some effective formulations made with the microextruder and containing only the sulfamate salts could not be processed at larger scales due to degradation of the matrix.

Basically, the idea was to reduce the amount of sulfamate salts in the formulations by substituting guanidine or ammonium sulfamate by melamine polyphosphate. This reduction

should allow a better processability of the formulation. The potential synergism between the two compounds should also allow obtaining better FR properties.

PCFC results show that the substitution of 50 to 80% of AS by MPP in the PA6/AS 5% formulation has a negative impact on the FR performances. The pHRR is either unchanged or increased which means that the flame retardancy level is decreased. Moreover, the pHRR temperature is decreased for both formulations. However, the PA6/AS 4%/MPP 1% shows improved results. Concerning the work on guanidine sulfamate, the same overall behavior is observed. “High” amounts of MPP lead to higher pHRR when substituting GAS. In this case, the temperature of the pHRR is also decreased. PA6/GAS 4%/MPP 1% and PA6/GAS 2.5%/MPP 2.5% have similar results but this last formulation appears to be more efficient in terms of pHRR decrease and pHRR temperature.

TGA show that the formulations containing the highest ratios of MPP (with either AS or GAS) have a main degradation step occurring at lower temperature, due to MPP promoting the PA6 degradation. This supports the PCFC results indicating that MPP has a negative impact on the pHRR and by extent, on the matrix.

The highest pHRR decrease obtained using sulfamate salts and MPP was 30.1% compared no neat PA6, which is similar to the decrease recorded with the PA6/AS 7% formulation. However, spinning fibers with this last formulation using the microextruder led to very fragile fibers (section IV.2.1). The two formulations allowing a 30.1% reduction of the pHRR are PA6/AS 4%/MPP 1% and PA6/AS 2.5%/MPP 2.5%. Thus, they are the two best candidates for the up-scaling step of the project. However, it was demonstrated that it is easier to process GAS than AS, thus PA6/GAS 2.5%/MPP 2.5% will be selected for large scale extrusion. Moreover, the amount of sulfamate salt is lower with this formulation and it is expected that the risk of degradation during the processing is minimum.

V.3 SCALE-UP WITH THE PA6/GAS/MPP SYSTEM

In a scaling up step of a process, any issue that seemed insignificant while running on a small laboratory extruder can become a very large problem on bigger machines [217]. In chapters III and IV, it was mentioned that sulfamate salts alone in PA6 were processable in the microextruder, up to 7 wt.% for AS and 10 wt.% for GAS. However, when scaling up the

process with these formulations, different processing parameters were required (e.g. higher temperatures) and degradation issues occurred, certainly due to the release of ammonia by the FR.

Using MPP as a co-additive, it was possible to extrude a formulation containing 2.5 wt.-% of guanidine sulfamate and 2.5 wt.-% of melamine polyphosphate with a larger scale extruder. The next step consists in verifying that scaling up using different processing parameters does not affect the polymer properties.

V.3.1 MATERIALS CHARACTERIZATIONS

V.3.1.1 SPINNABILITY AND ADDITIVES DISPERSION

The morphology of the fibers obtained for PA6/GAS 2.5%/MPP 2.5% at micro-scale and large scale extrusion are first compared. Figure 81(a) present the BSE picture of the cross section of PA6/GAS 2.5%/MPP 2.5% fibers. It can be seen that the diameter of the fibers is around 100 μm , as obtained previously. EPMA phosphorus and sulfur cartographies are shown in Figure 81(b) and (c) respectively. The two additives appear to be homogeneously dispersed in the PA6 matrix. Surprisingly, it appears that aggregates of sulfamate are generally also composed of MPP. It is assumed that the melting sulfamate salt might “trap” a part of the MPP during processing. Consequently, GAS is often found with MPP in the aggregates. An optical micrograph of the fiber is shown in Figure 81(d). The diameter measured (96.6 μm) is in the range of 100 μm considering the calculated mean diameter and standard deviation (96.6 \pm 9.1 μm).

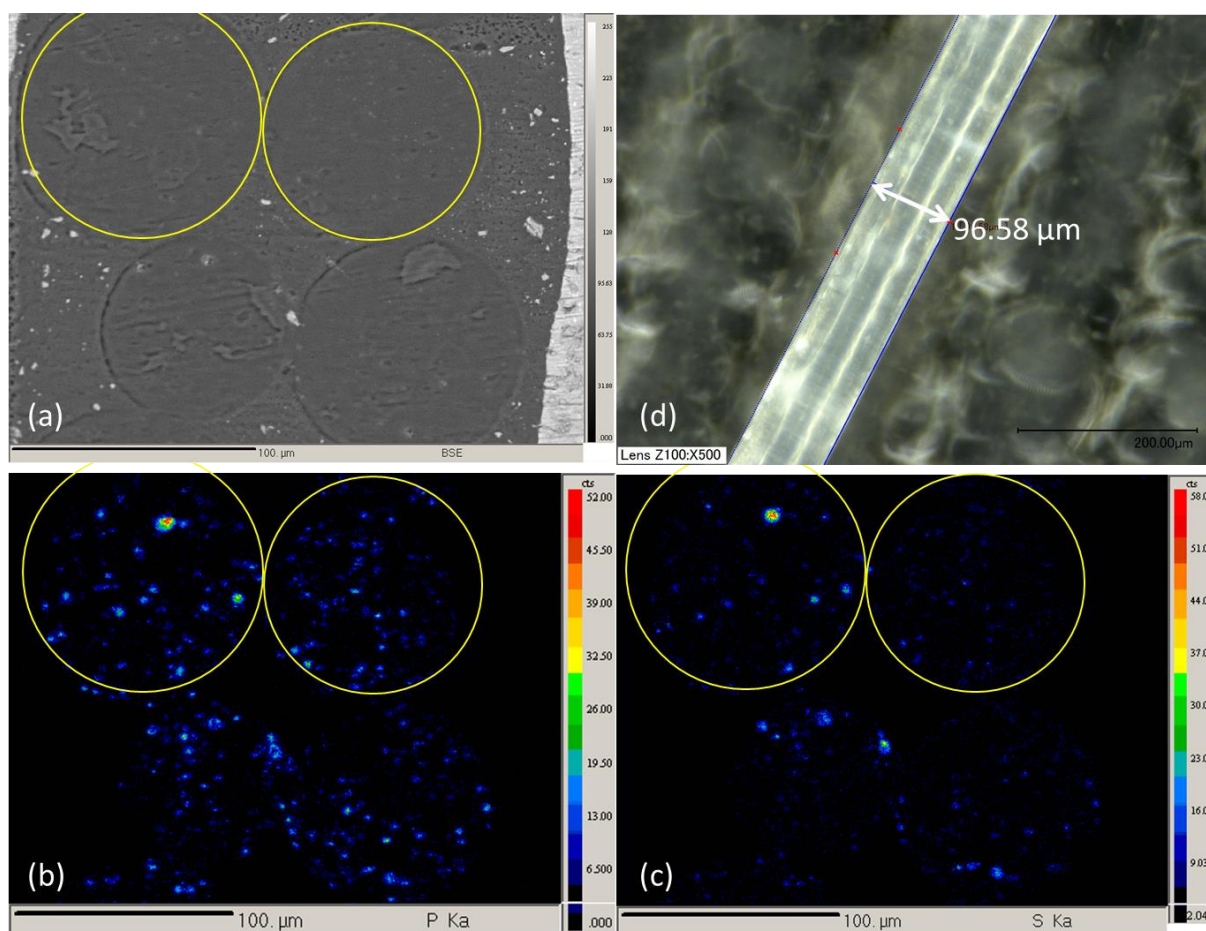


Figure 81: BSE picture (a), EPMA phosphorus cartography (b), EPMA sulfur cartography (c) of the cross section of PA6/GAS 2.5%/MPP 2.5% fibers (circled in yellow), and optical micrograph of the fiber (d) from microextrusion

Concerning the upscaled formulation, extruded material was pelletized in order to perform different experiments. Spinnability was accessed via direct microextrusion-spinning as no specific large scale spinning device was available. Pellets of the PA6/GAS 2.5%/MPP 2.5% formulation were introduced into the micro extruder and usual parameters described in section II.2.2 (p.84) were used. However, the “direct” method implies no circulation of the material in the recycling channel, thus it is directly extruded without further mixing. It also needs to be noted that a second heating cycle is performed, which might lead to some degradation of the polymer. On **Figure 82(a)** is shown the BSE picture of the cross section of PA6/GAS 2.5%/MPP 2.5% fibers. EPMA phosphorus cartography and sulfur cartography are shown in **Figure 82(b)** and **(c)** respectively. The two additives are less homogeneously dispersed than in the microextruded formulation, since the presence of a few big aggregates (in red) is observed. An optical micrograph of the fiber is shown in **Figure 82(d)**. The

diameter measured (120.9 μm) is close to the range of 100 μm considering the calculated mean diameter and standard deviation (103.4 \pm 14.7 μm).

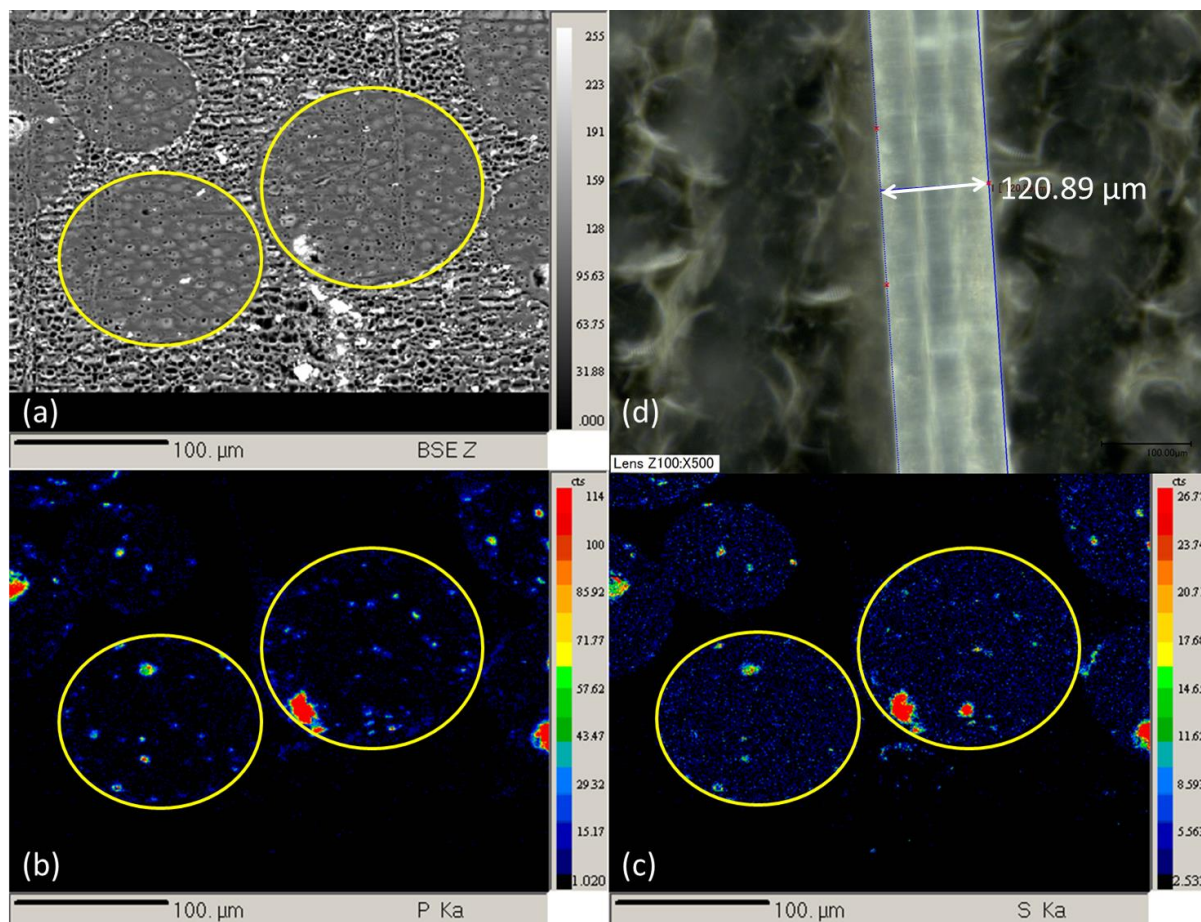


Figure 82: BSE picture (a), EPMA phosphorus cartography (b), EPMA sulfur cartography (c) of the cross section of PA6/GAS 2.5%/MPP 2.5% fibers (circled in yellow), and optical micrograph of the fiber (d) from upscale

V.3.1.2 THERMOGRAVIMETRIC ANALYSIS

Figure 83 compares the TG and DTG curves of the formulation containing 2.5 wt.-% of GAS and MPP in the case of the micro-scale and large scale extrusion. Both curves have the same overall shape, the part of the curves corresponding to the first decomposition step (between 270 and 320 $^{\circ}\text{C}$) are superimposed. Concerning the main step, the weight loss rate temperature is slightly lower for the large-scale extruded material, a difference of 7 $^{\circ}\text{C}$ is observed (411 $^{\circ}\text{C}$ for the microextruded material versus 404 $^{\circ}\text{C}$ for the large-scale extrusion). The difference, might not be significant, however it could be attributed to a molecular weight (Mw) difference between the two formulations. The influence of the molecular weight was studied by different groups. A correlation between the temperature of maximum

rate of decomposition and Mw was found in polystyrene [218] and polybutadiene [219]. Mw also influences the degradation pathway of aliphatic polyesters and eventually their weight loss rate [220]. For large-scale extrusion, the conditions are more severe, as the temperature in the feeding zone is higher (300 °C versus 245 °C for microextrusion) and the shear stress is also higher because of the screw design. These different parameters can lead to a decrease of the molecular weight. Eventually, the step of oxidation of the transient residues is similar, with respect to the previously reported shift of decomposition temperature.

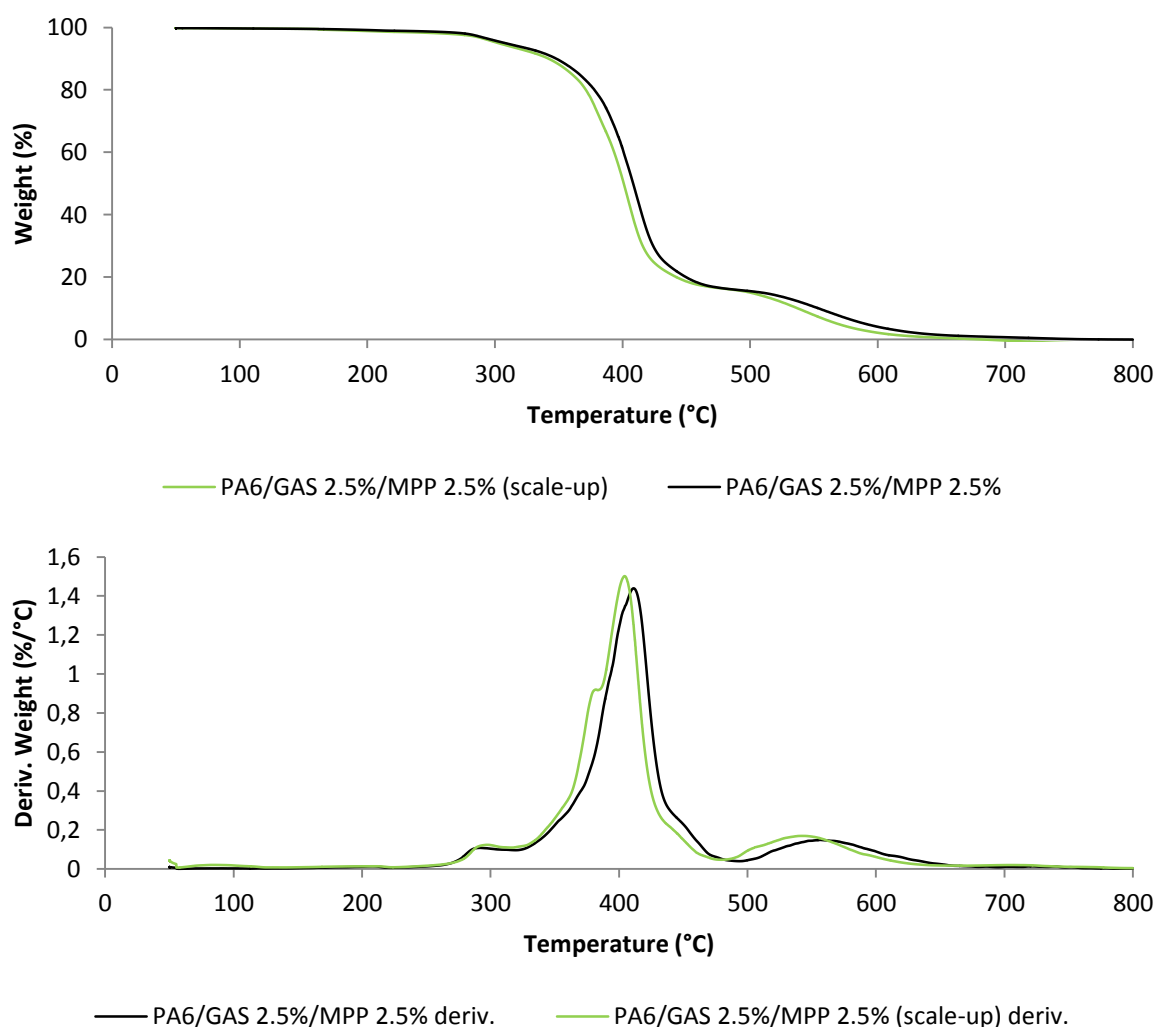


Figure 83: TG and DTG curves of PA6/GAS 2.5%/MPP 2.5% extruded at micro scale and larger scale (scale-up) (10 °C/min, air)

V.3.1.3 DIFFERENTIAL SCANNING CALORIMETRY (DSC)

Thermal and mechanical properties depend on the structure of the polyamide 6. To study the influence of additives on the crystalline structure of the formulation, differential scanning calorimetry (DSC) has been realized. The DSC thermograms of PA6 and PA6/GAS

2.5%/MPP 2.5% extruded at micro scale and larger scale are shown in **Figure 84**. First of all, it is worth to mention that after all DSC experiments, samples were collected and no color change was observed. The powder just changes into a more or less compact layer due to melting and cooling cycles. Measurements are performed on the second temperature cycle of the DSC experiment. Data obtained from the DSC curves are reported in **Table 27**.

For the neat PA6, the thermogram corresponds to a typical semi-crystalline polymer. It shows a T_g , followed by the melting of the crystalline phases during heating. Upon cooling, a crystallization peak is observed.

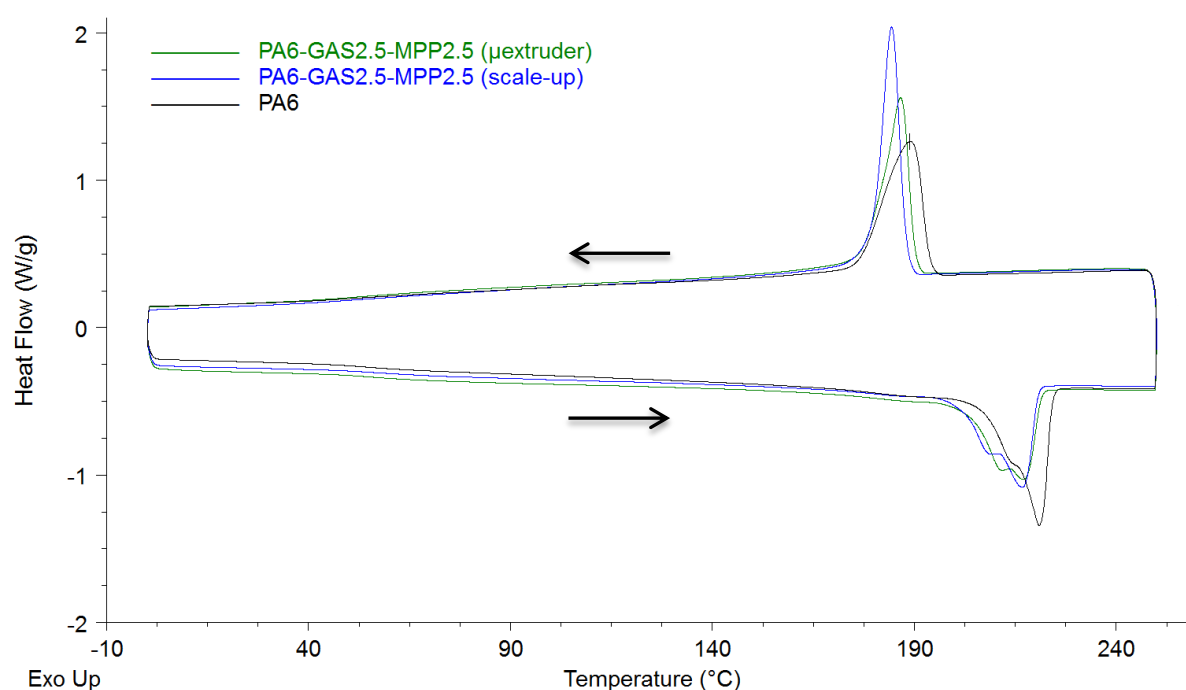


Figure 84: DSC thermograms of PA6 and PA6/GAS 2.5%/MPP 2.5% extruded at both scales

During heating, T_g and two melting temperatures (T_m) are observed for each sample. The two T_m correspond to the melting of the γ and α phases. The data corresponds to what is found in the literature [44]. A shift to lower temperature is observed for the melting temperature of the two PA6/GAS 2.5%/MPP 2.5% formulations. This shift is also observed for the crystallization temperature (T_c). It is attributed to a small degradation of the matrix during the processing [221]. The larger shift (5 °C) for the up-scaled formulation might indicate a slightly more degraded matrix. However, no significant change in the glass transition temperature is observed. This is consistent with the literature that reports change of only 1 °C between two different PA6 having \bar{M}_w of 65200 g/mol and 11600 g/mol [222].

Table 27: Characteristic temperatures and enthalpies of the PA6 and PA6/GAS 2.5%/MPP 2.5% formulations

Formulation	T_g (°C)	$T_{m\gamma}$ (°C)	$T_{m\alpha}$ (°C)	ΔH_m (J/g)	T_c (°C)	ΔH_c (J/g)
PA6	55	215	221	55	189	57
PA6/GAS 2.5%/MPP 2.5% (μ extruder)	55	212	217	56	187	56
PA6/GAS 2.5%/MPP 2.5% (scale-up)	56	209	217	49	184	54

T_g : glass transition temperature

$T_{m\gamma}$: melting temperature of γ phase crystallites

$T_{m\alpha}$: melting temperature of α phase crystallites

ΔH_m : enthalpy of fusion

T_c : crystallization temperature

ΔH_c : enthalpy of crystallization

V.3.1.4 PCFC

PCFC measurements were performed on the PA6/GAS 2.5%/MPP 2.5% formulations that have been extruded at large-scale and with the microextruder (**Figure 85**). For both formulations, the FR performance are similar; pHRR obtained with scale-up is 436 W/g versus 411 W/g for microextruder. T_{pHRR} of the material obtained at large scale is lowered by 15 °C and THR is decreased by 2.7% compared to the microextruder. The results are summarized in **Table 28**.

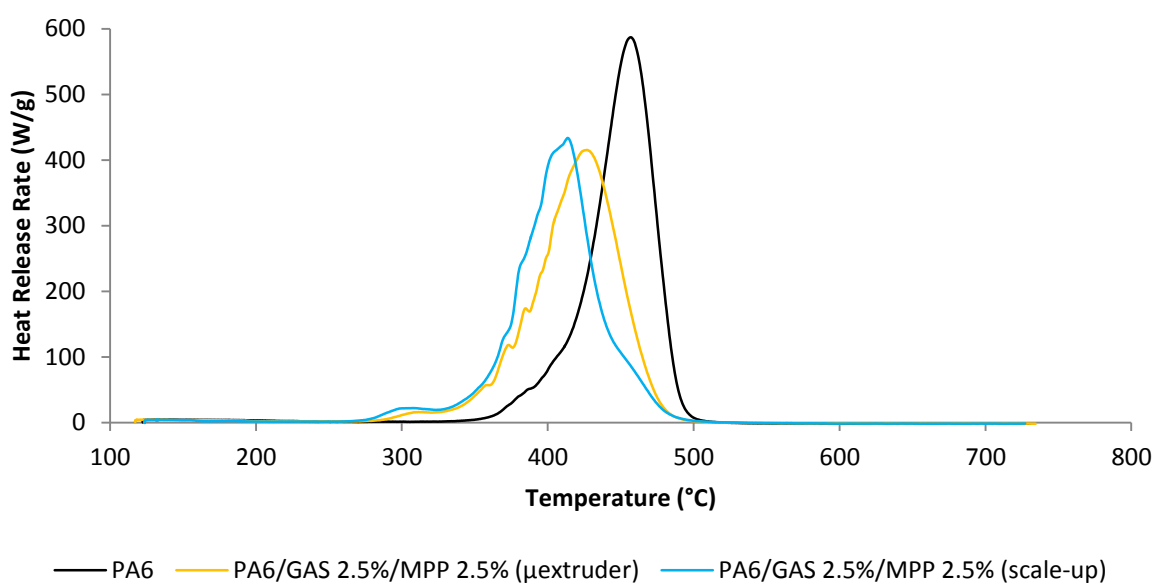


Figure 85: HRR curves versus temperature obtained with PCFC of PA6 and PA6/GAS 2.5%/MPP 2.5% formulations done with microextruder (μ extruder) and large scale extruder (scale-up)

The PCFC data indicate that taking into account the margin of error of the PCFC (5%), the results are similar.

Table 28: PCFC results of PA6 and PA6/GAS 2.5%/MPP 2.5% formulations done with microextruder (μ) and large scale extruder

Formulation	T_{pHRR} ($^{\circ}\text{C}$)	pHRR (W/g)	$\Delta pHRR/PA6$ (%)	THR (kJ/g)	$\Delta THR/PA6$ (%)
PA6	456	588	-	30.0	-
PA6/GAS 2.5%/MPP 2.5% (μ)	428	411	-30.1	28.7	-4.3
PA6/GAS 2.5%/MPP 2.5% (scale-up)	413	436	-25.9	27.9	-7.0

V.3.2 FIRE PERFORMANCE OF LARGE-SCALE PA6/GAS/MPP

Since the material was extruded at large scale, it was possible to evaluate the fire performance of the material using other fire testing methods (MLC, LOI and UL-94). However, it has to be noted that the experiments were done on plates or barrels and should therefore not be relevant for textile application.

V.3.2.1 CONE CALORIMETRY

The reaction to fire of the different formulations was tested by mass-loss calorimetry. HRR versus time of neat PA6 and of the fire-retardant formulation are presented in **Figure 86**. Data calculated from the curves are summarized in **Table 29**. The calculated standard deviation indicates good repeatability of the experiments. Similar values for pHRR, time to pHRR and THR are recorded for PA6 and flame retarded PA6, according to the margin of error (10 %). The results concerning neat PA6 are comparable to what was reported in the literature [180].

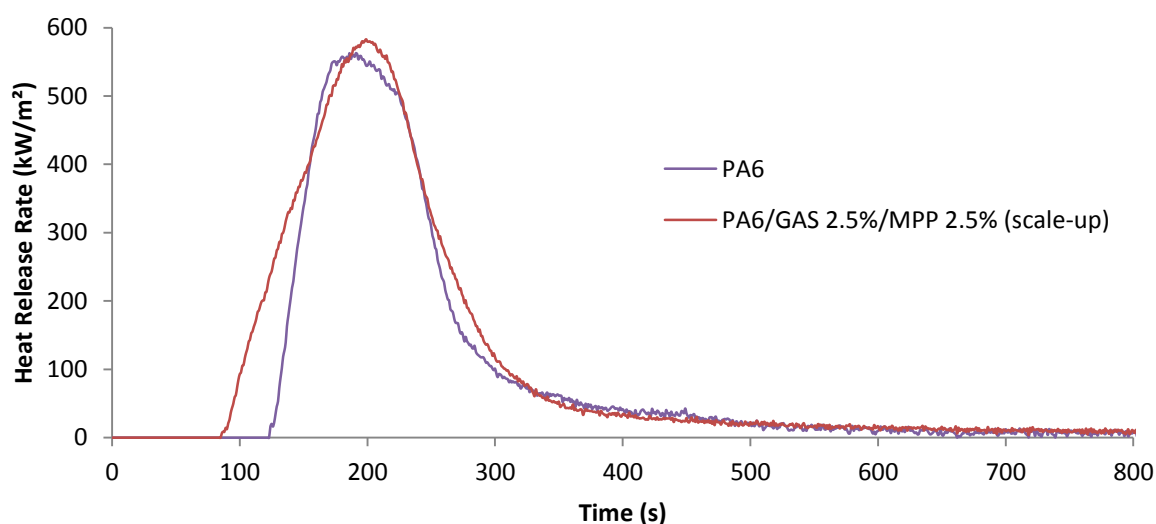


Figure 86: Cone calorimetry curves of PA6 and PA6/GAS 2.5%/MPP 2.5% formulation extruded at large scale (35kW/m², 25mm)

Time to ignition is the only parameter presenting a significant variation when comparing the FR formulation with the neat PA6. In the test conditions (heat flux: 35 kW/m², distance: 25 mm), neat PA6 has a TTI of 124±13 s whereas PA6/GAS 2.5%/MPP 2.5% has a TTI of 87±2 s. This behavior could be brought by the thermal stability of the flame retarded material that is lower to that of pure PA6. Indeed, it is proposed that time to ignition is decreased because PA6 degradation is promoted in the presence of GAS and MPP as observed on TGA and PCFC. The rapid accumulation of combustible fuels underneath the char skin favors the appearance of cracks. Hoffendahl *et al.* [223] have observed the same behavior with EVM in the presence of melamine phosphate (MP). They measured quantitatively the evolved gas of degradation, and they attributed the TTI decrease to the release of flammable ammonia from MP. It is assumed that the same phenomenon occurs in this case.

Table 29: Cone calorimetry data of PA6 and PA6/GAS 2.5%/MPP 2.5% formulation extruded at large scale (35kW/m², 25mm)

Property	PA6	PA6/GAS 2.5%/MPP 2.5%	Δ/PA6 (%)
peak HRR (kW/m ²)	603±13	582±20	-4
time peak HRR (s)	218±16	213±9	-2
TTI (s)	124±13	87±2	-30
Total heat release (MJ/m ²)	73±2	79±1	+8

It is also important to describe what occurs during the test. For the PA6 samples, when the cone shutter is opened, the material begins to heat and rapidly melts, with high bubbling. Then a thin char skin is gradually formed at the top of the bubbling surface and begins to swell. At this time TTI is not reached yet. Eventually, the swollen char skin, containing a lot of gas, breaks and releases its fuel that instantaneously burns (TTI) with the huge increase of the HRR. All the material burns and nearly nothing is left at the end of the test (**Figure 87**).



Figure 87: Cone calorimetry residues of PA6 viewed from above

Concerning the PA6/GAS 2.5%/MPP 2.5% when the cone shutter is opened, the material also melts with high bubbling. However, contrary to PA6, the surface of the sample becomes very dark. A thin char skin is also gradually formed at the top of the bubbling surface and swells. Like for PA6, the swollen char skin breaks and releases its fuel, ignition occurs with the increase of the HRR. When HRR starts to decrease, a new charred surface gradually appears and swells thanks to the fuel beneath it (**Figure 88**). However, the intumescent char formation occurs around 250 s during the cone calorimeter experiment, that is to say after the pHRR. Thus it is too late to protect the polymer, as most of it is already burnt.



Figure 88: Char formation during the cone calorimetry experiment on PA6/GAS 2.5%/MPP 2.5%

Figure 89(a) shows the char formed during the cone calorimetry experiment with the PA6/GAS 2.5%/MPP 2.5% sample. On **Figure 89(b)** a cut on the cross section was done to observe the internal structure of the char. It can be seen that it is composed of many small bubbles that form a foam-like char.

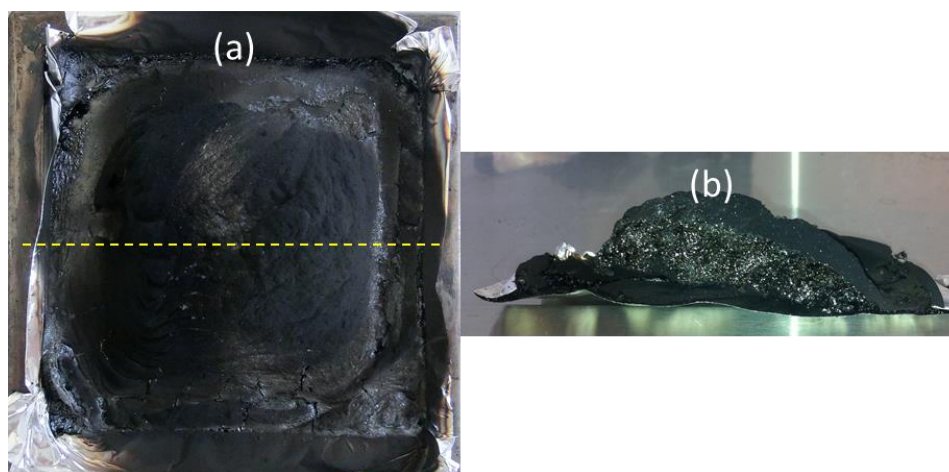


Figure 89: Cone calorimetry residues of PA6/GAS 2.5%/MPP 2.5% viewed from above (yellow line: cross-section) (a) and view of the char cut in the cross section (b)

V.3.2.2 UL-94 AND LOI

LOI values were determined; surprisingly, a LOI value of 28 vol.-% was obtained for neat PA6. Some high LOI values were already reported for neat PA6 [57, 86]. Below its LOI value, PA6 self-extinguished by moderate dripping (Figure 90(a)), and by visual observation, drips seemed rather viscous. PA6/GAS 2.5%/MPP 2.5% has a LOI of 37 vol.-% and was hardly ignited between 23 and 30 vol.-% of O₂ (Figure 90(b)). In this case, the small flame extinguished by moderate dripping. When oxygen content is raised between 31 and 36 vol.-%, a heavy dripping occurred as shown on Figure 90(c), removing the flame. In that case, drips seemed to have a lower viscosity as they flowed rapidly until the bottom of the LOI sample.



Figure 90: PA6 sample tested at OI below 28 vol.-% (a) PA6/GAS 2.5%/MPP 2.5% sample tested at OI between 23-30 vol.-% (b) and between 31-36 vol.-% (c)

By visual observation of the burning behavior of the samples during the LOI test, it is assumed that MPP and AS change the melt viscosity of PA6. Thanks to a lower melt viscosity, heavy dripping could remove material and flame from the top of the sample and allow a quick extinction of the flame, virtually raising the LOI to high value. This behavior was observed by Levchik *et al.* [215] in PA6 containing melamine, melamine oxalate, melamine phthalate and melamine cyanurate.

UL-94 tests were performed to characterize the burning behavior of PA6 and PA6/GAS 2.5%/MPP 2.5%. Detailed results are reported in **Table 30**. It is observed that PA6 burns easily but quickly flames out by dripping. The cotton is ignited for all samples and second ignition is shorter than the first. PA6 is rated V2.

Table 30: UL-94 results for neat PA6 and for PA6/GAS 2.5%/MPP 2.5% extruded at large scale

Formulation	t_1/t_2 * (s)	Dripping **	Cotton ignition **	rating
PA6	3.6/2.4	Y	Y	V2
PA6/GAS 2.5%/MPP2.5%	1.6/1.9	Y	N	V0

* t_1 and t_2 , average combustion times after the first and the second application of the flame

** Y: Yes, N: No

For the fire retarded PA6, samples are easily ignited and they extinguish, by dripping, more rapidly than neat PA6. For these samples, cotton remains unburned after each test. PA6/GAS 2.5%/MPP 2.5% is thus rated V0.

As also detailed for LOI, PA6 drips appear more viscous than drops from the fire retarded PA6. This behavior is attributed to the FRs that promote the PA6 degradation. In fact, after ignition of the neat PA6, a large flaming droplet falls and ignites the cotton. Generally, one or two other droplets extinguished the materials by removing the flame from the burning sample. Concerning the FR PA6, the flame of the burning sample is removed by the first droplet. This small droplet is then extinguished during its fall and does not ignite the cotton (**Figure 91**).



Figure 91: PA6/GAS 2.5%/MPP 2.5% UL94 sample and cotton after test

It is assumed that the difference in viscosity changes the size of the burning droplets. Large burning drops are not easily extinguished during the fall, whereas small droplets are.

Kandola *et al.* have investigated the melt dripping of thermoplastic polymers [224]. They showed that, increasing PA6 temperature, from 425 °C to 630 °C produces drops with decreasing mass and diameter. Moreover, viscosity is a function of both temperature and molecular weight. Thus, if the FRs promote the PA6 degradation, molten material will quickly have shortened chains and low viscosity, which in the end produced smaller drops that are more easily extinguished.

V.3.3 ANALYSIS OF THE DECOMPOSITION GASES

It was previously demonstrated that PA6/GAS 2.5%/MPP 2.5% presents good FR properties according to PCFC, UL-94 and LOI. The last part of this chapter is dedicated to the study of the mechanism of action of GAS/MPP mixture into the PA6 matrix.

V.3.3.1 TGA-FTIR

The DTG curve of PA6/GAS 2.5%/MPP 2.5% is represented in **Figure 92(a)**. It is compared with the intensity versus time curves of the peaks corresponding to the main degradation products of the material: ammonia, carbon dioxide and caprolactam (**Figure 92(b)**). The

curves were plotted using characteristic peaks at $\bar{\nu} = 965 \text{ cm}^{-1}$ (NH_3), 669 cm^{-1} (CO_2) and 2938 cm^{-1} (ϵ -caprolactam). Three main degradation steps are observed around 29, 41 and 55 min ($290 \text{ }^\circ\text{C}$, $410 \text{ }^\circ\text{C}$ and $550 \text{ }^\circ\text{C}$ respectively) corresponding to the maximum weight loss rate of the three degradation steps described previously. These steps fit perfectly with the maximum intensity of the curves.

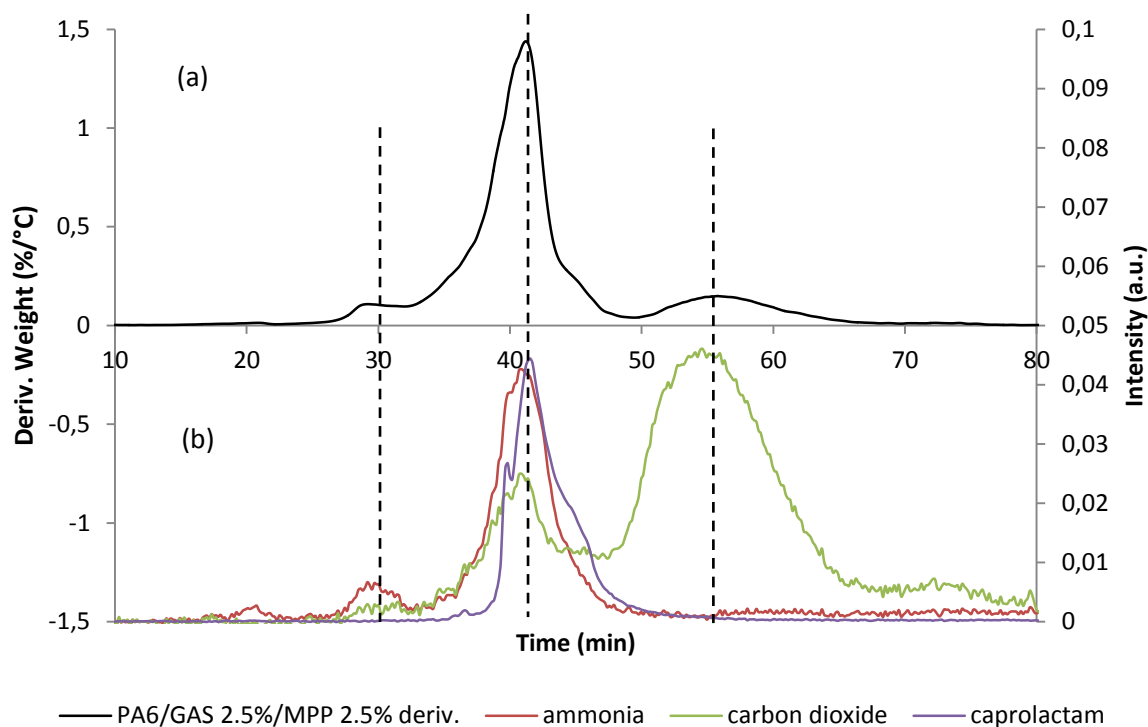


Figure 92: DTG curve of PA6/GAS 2.5%/MPP 2.5% and intensity curves of ammonia, CO_2 and caprolactam recorded during TGA-FTIR experiment

It is observed that NH_3 is released during the first two degradation steps while ϵ -caprolactam is only released during the main degradation step (2nd step). Carbon dioxide is evolved mainly during the second and third degradation steps. This last step corresponds to the oxidation of the transient residues. The curves are similar to those obtained with the PA6/GAS 5% formulation (**Figure 93**). However, it can be seen that ammonia and ϵ -caprolactam are released earlier for the MPP containing formulation. This is consistent with the results of TGA indicating a fastest weight loss for the main degradation step of PA6/GAS 2.5%/MPP 2.5% compared with the PA6/GAS formulations containing no or a little amount of MPP. Ammonia may also be released from the MPP condensation to melon phosphate derivatives [225], especially in the range of $250\text{--}380 \text{ }^\circ\text{C}$ where evaporation of melamine competes with condensation to melam, melam and melon occurring with

elimination of ammonia [226]. However no major difference can be observed between the two formulations. Eventually, concerning the oxidation of the transient char (last degradation step), the formulation containing MPP has higher weight loss, meaning that MPP enhances the formation of transient residues. This step also occurs on a broader temperature range, explaining the wide CO₂ peak for the PA6/GAS/MPP formulation.

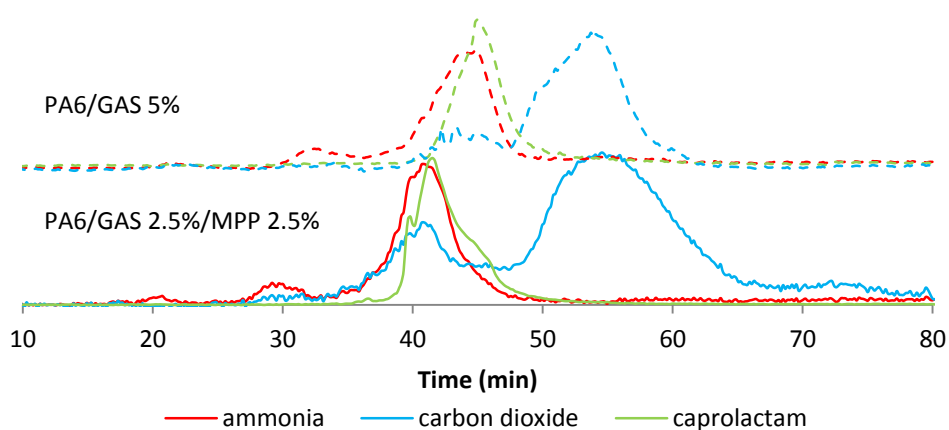


Figure 93: Comparison of FTIR intensity curves of ammonia, CO₂ and caprolactam recorded during TGA-FTIR experiment for PA6/GAS 5% and PA6/GAS 2.5%/MPP 2.5%

FTIR spectra of the gas evolved during the TGA experiments performed on the PA6/GAS 2.5%/MPP 2.5% are shown in **Figure 94**. They correspond to temperatures around the maximum of weight loss rate of each degradation step, according to the DTG curve of **Figure 92(a)**.

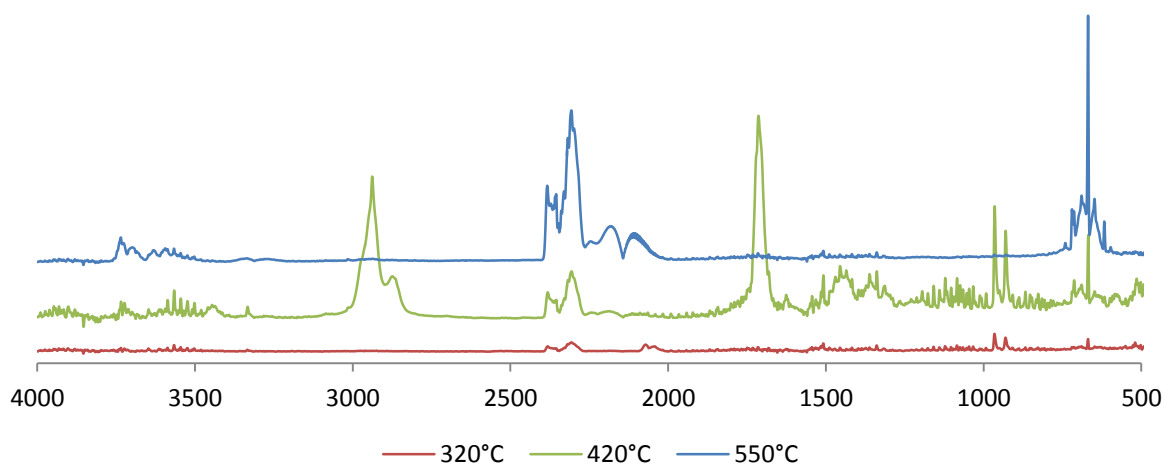


Figure 94: FTIR spectra at 320 °C, 420 °C and 550 °C (corresponding to 32, 42 and 55 min) of gas released during PA6/GAS 2.5%/MPP 2.5% decomposition

At 320 °C, CO₂ ($\bar{\nu} = 669 \text{ cm}^{-1}, 2349 \text{ cm}^{-1}$), NH₃ ($\bar{\nu} = 930 \text{ cm}^{-1}, 965 \text{ cm}^{-1}$) and water (bands around 1500 and 3600 cm⁻¹) are released. At the maximum weight loss rate of the main degradation step (420 °C), the same gases (NH₃, CO₂, H₂O) are released along with CO and ϵ -caprolactam ($\bar{\nu} = 1713, 2938 \text{ cm}^{-1}$). However, as previously demonstrated, not only ϵ -caprolactam corresponds to these vibration bands, and other scission products of PA6 may appear within those wavenumbers. This is proved by the appearance of a low intensity peak corresponding to nitrile-ends at $\bar{\nu} = 2245 \text{ cm}^{-1}$. Nitrile compounds are known as PA6 degradation products [54]. In the last step, mainly CO and CO₂ are released, and this step corresponds to the transient char oxidation. The evolved gases, detected using TGA-FTIR, are the same as for the PA6/AS or PA6/GAS formulations described in chapter IV. Additional decomposition products of MPP, such as isocyanic acid, are not seen [227], but might overlap with other compounds.

V.3.3.2 PY-GC-MS

In order to overcome the limitations of FTIR to identify the evolving products of decomposition from PA6/GAS 2.5%/MPP2.5%, py-GC-MS was used. It permits to differentiate the overlapping compounds in FTIR. However, this experiment was carried out under N₂ (pyrolysis conditions). The temperature range of the main degradation step of each formulation was determined using their DTG. The ranges used for the stepwise method of py-GC-MS are listed in Table 31. The resulting chromatograms, compared with those of neat PA6 and PA6/GAS 5% are shown in Figure 95.

Table 31: Start and end temperature of the main degradation step of py-GC-MS samples

Sample	Main decomposition step temperature range	
	Start temperature (°C)	End temperature (°C)
PA6	320	480
PA6/GAS 5%	368	483
PA6/GAS 2.5%/MPP 2.5%	320	491

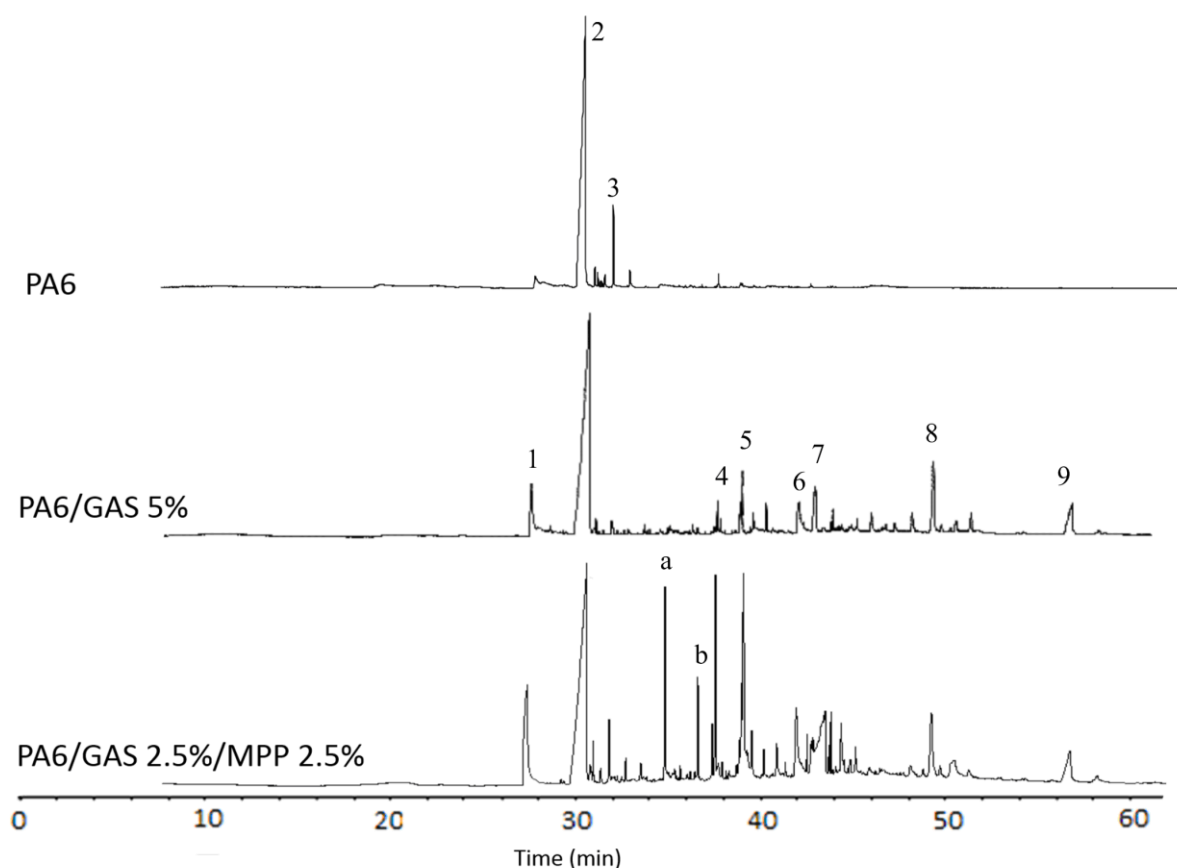
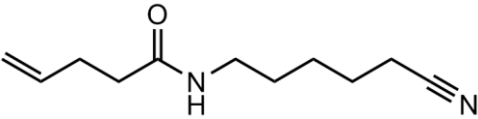
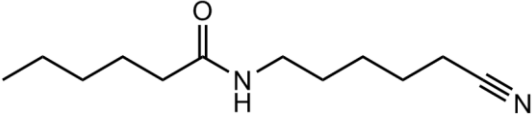
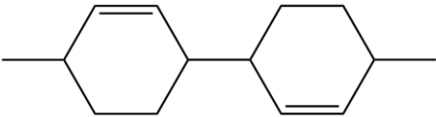


Figure 95: TIC of PA6, PA6/GAS 5% and PA6/GAS 2.5%/MPP 2.5% corresponding to the main step of decomposition of each formulation

The evolved gases have been identified in section IV.3.5.1.2 (p.149) for PA6 and PA6/GAS. The overall chromatogram of PA6/GAS 2.5%/MPP 2.5% is similar to that of PA6/GAS 5%. However, the intensity of peaks 4 and 5 (corresponding molecules are reported in **Table 32**) is higher, especially for 4 and 5 that are almost as intense as the peak of ϵ -caprolactam (peak 2, relative intensity 100%). This means that higher amounts of these products are formed during the decomposition of the formulation containing GAS and MPP.

Table 32: Peak attribution of TIC from Figure 95 (Other attributions available in Table 24 p.150)

#	Attribution
4	 <i>N</i> -(5-cyanopentyl)pent-4-enamide
5	 <i>N</i> -(5-cyanopentyl)hexanamide
a	Melamine containing product.?
b	 4,4'-dimethyl-[1,1'-bi(cyclohexane)]-2,2'-diene

Two new peaks, called a and b, have also appeared on the chromatogram of **Figure 95**. Their identification is not clear, however it is assumed that “a” might be a product from the reaction of MPP with PA6, GAS or their degradation products since it was not observed for the degradation of PA6 and PA6/GAS 5%. Product b could be attributed to 4,4'-dimethyl-[1,1'-bi(cyclohexane)]-2,2'-diene, an unsaturated carbon product from PA6 decomposition/recombination. More details on a and b compounds mass spectrum are given in **Appendix D**.

V.3.4 ANALYSIS OF THE CONDENSED PHASE

Solid state NMR was chosen to study the condensed phase. The ^{13}C solid state NMR spectra of the PA6/GAS 2.5%/MPP 2.5% at ambient temperature and treated at different temperatures are presented in **Figure 96**. The temperatures were selected according to the TG curves. 270 °C corresponds to the beginning of the first degradation step; 320°C is the maximum of weight loss rate of the first step. 410 °C is around the maximum weight loss rate of the second (main) step of degradation. 490 °C corresponds to the beginning of oxidation of the transient residues.

There is no change in the ^{13}C solid state NMR spectra between 20 and 320 °C: the aliphatic carbons are seen from 20 to 45 ppm, the carbonyl group is located at 170 ppm. From 410 to 490 °C, the spectra change; namely C=O peak disappears and the aliphatic region broadens.

At 490 °C, the aliphatic carbons have almost disappeared and a broad band centered at 130 ppm can be distinguished, corresponding to unsaturated carbon bonds (i.e. aromatic species). Because of the high temperature, oxidized aromatic carbons appear characterized by the shoulder observed between 150-160 ppm.

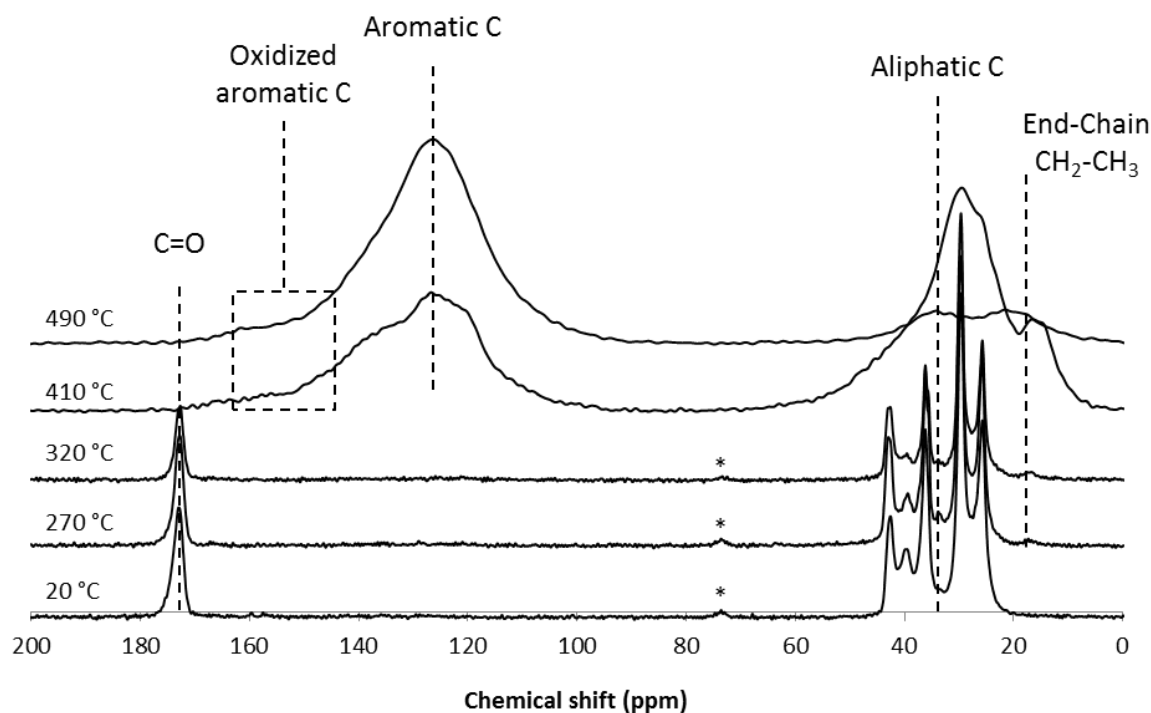


Figure 96: ^{13}C CP-DD-MAS NMR spectra of the PA6/GAS 2.5%/MPP2.5% residues obtained after thermal treatment at 20, 270, 320, 410 and 490 °C (*: spinning sideband)

The formulation contains melamine polyphosphate, thus it is possible to perform ^{31}P solid state NMR. First, NMR spectrum of pure MPP was recorded (**Figure 97**). It exhibits three main signals; a double peak at -21.5 and -24.2 ppm corresponding to linear polyphosphates, another peak at -11 ppm attributed to pyrophosphates and eventually, at 0 ppm a peak characteristic of H_3PO_4 . The other peaks are spinning sidebands (stars on top of each on **Figure 97**).

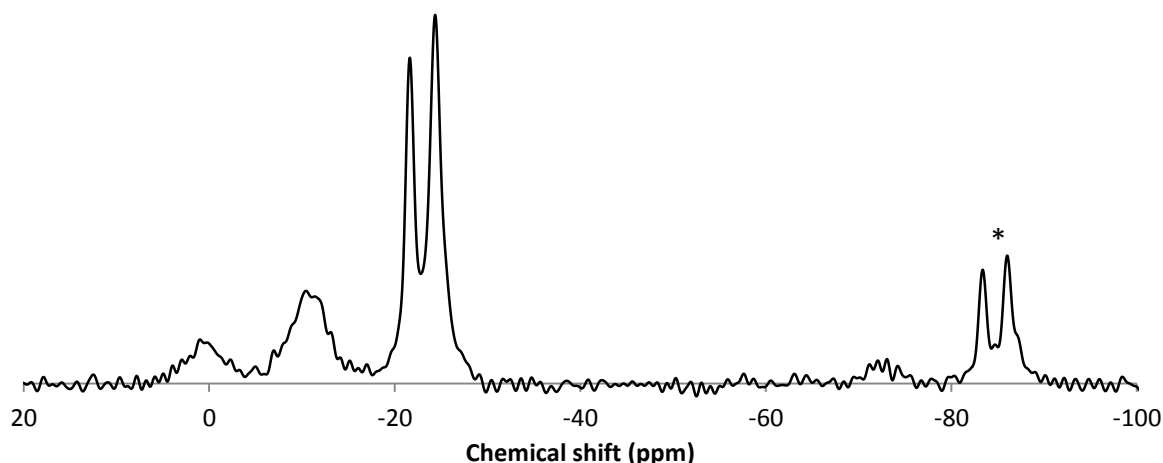


Figure 97: ^{31}P CP-HPDEC-MAS NMR spectra of MPP (*: spinning sideband)

The NMR experiments were done on the same thermally treated samples used for ^{13}C NMR. The spectra are presented in **Figure 98**. It is possible to distinguish the three previously described phosphate signals. For ease of comprehension, the groups have been highlighted. At 20 °C mainly polyphosphates are found but a few ortho and pyrophosphates are also present. At 270 °C, the same spectrum is obtained, meaning that MPP is not degraded. According to the work of Chen and Wang [228], pure melamine phosphate condenses on itself to form melamine pyrophosphate in the range of 260-300 °C, these data are consistent with the presented results which show no depolymerized MPP at 270°C. As the temperature continues to increase to 320 °C, the pyrophosphate peak becomes predominant but the polyphosphate peak is still visible. It is thus assumed that MPP has started to degrade but is not completely depolymerized. At higher temperatures (410 and 490 °C) the orthophosphate peak is the highest. However, particular attention should be paid with the attribution of the peaks. At 0 ppm the peak can correspond not only to H_3PO_4 but may also be attributed to $-\text{PO}_4$ units in R_2HPO_4 , RH_2PO_4 (with R = alkyl). At -11 ppm the peak could also be attributed to $-\text{PO}_4$ units in $\phi_2\text{RPO}_4$ (with ϕ = aromatic group), and/or $\phi_2\text{HPO}_4$ and/or polyphosphate chain end groups [229]. At these temperatures, the peak at -11 ppm can also indicate $\phi_2\text{RPO}_4$ and/or $\phi_2\text{HPO}_4$ which constitute a charred structure, and is consistent with the ^{13}C NMR spectra of **Figure 96** at 410 and 490 °C.

MPP is well known in intumescent systems [230], it is used as an inorganic acid source. Upon heating it produces, in situ, phosphoric acid, which catalyzes the char formation process, and melamine acts as a blowing agent. Cone calorimetry experiments have shown an

intumescent behavior of the PA6/GAS/MPP formulation (Section V.3.2 p.170). ^{31}P NMR shows that not all MPP is degraded into H_3PO_4 . It is assumed that reactions of the ortho and pyrophosphates with the PA6 chain lead to the formation of $\phi_2\text{RPO}_4$, $\phi_2\text{HPO}_4$ with R being parts of the PA6 polymeric chain.

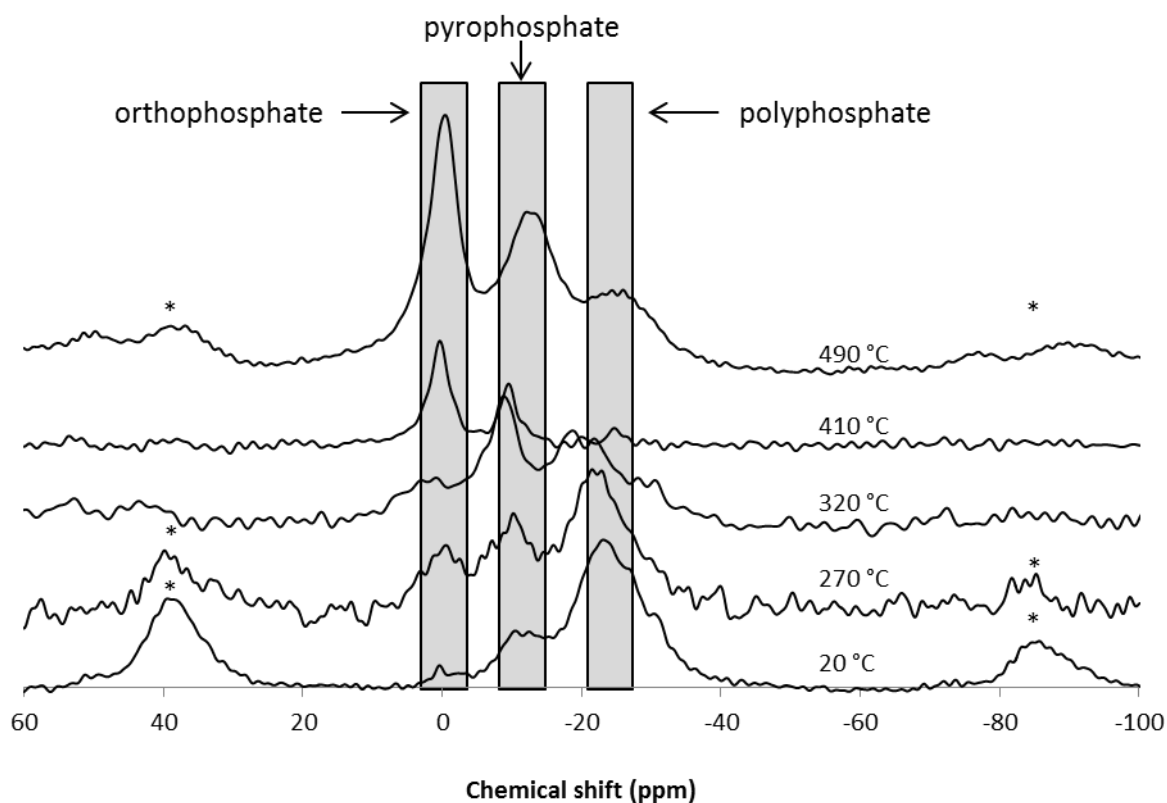


Figure 98: ^{31}P CP-HPDEC-MAS NMR spectra of the PA6/GAS 2.5%/MPP2.5% residues obtained after thermal treatment at 20, 270, 320, 410 and 490 °C (*: spinning sideband)

V.4 CONCLUSION

In the previous chapter, the work on sulfamate salts allowed understanding the process leading to better PCFC results. Moreover, it was demonstrated that using sulfamates at small scale (e.g. microextrusion) is an easy process, if the loading is not too high. However, scaling-up was difficult because of processing issues. The aim of this chapter was to find a solution to overcome the problems encountered when large scale extrusion was used. MPP was found to be an effective co-additive for AS and GAS. Indeed, by varying the ratio AS/MPP or GAS/MPP and keeping a total FR loading of 5wt.-%, PCFC results could be enhanced. For a formulation containing 5 wt.-% of AS, pHRR was reduced by 21.6%, using 4 wt.-% of AS with 1 wt.-% MPP allowed a further reduction of 8.5 percentage points, compared with neat PA6.

Concerning GAS, alone at 5 wt.-% a reduction of 15.0 % of the pHRR was obtained, its combination with MPP using a 50/50 ratio, also gave a reduction of 30.1%. This formulation was thus selected and then successfully extruded at large scale.

PCFC results indicate that formulations obtained either with micro or large-scale extrusion give similar results in terms of pHRR and THR. However cone calorimetry does not show any improvement of the FR properties with this formulation, even though char formation occurs at the end of the experiment. TTI is significantly decreased compared with neat PA6. It is assumed that GAS and MPP promote PA6 degradation and consequently speed up fuel formation and release. Further tests have shown enhancements of the fire behavior: LOI jumps from 28 vol.-% for neat PA6 to 37 vol.-% for the PA6/GAS 2.5%/MPP 2.5% formulation and UL-94 classification is also improved and goes from V2 to V0. In both tests, it was proposed that enhanced dripping is responsible for the results. For LOI, flame is removed from the burning zone by the heavy dripping and the same phenomena is observed in UL-94 test; drips remove heat.

Analysis of the gas phase and of the condensed phase shows that GAS and MPP change the degradation pathway of PA6 in a similar way as GAS does. For PA6, caprolactam is the main degradation product, as seen by py-GC-MS. When GAS and MPP are added to the formulation, a large number of heavier molecules are produced during the degradation (i.e. dimers and trimers). It is assumed that these compounds burn less efficiently, leading to enhancement of the PCFC results. On the other hand, GAS promotes char formation at high temperature, the presence of MPP in the formulation enhances this process as demonstrated by solid state NMR.

GENERAL CONCLUSION

Polyamide 6 fibers may be used in sectors like construction, home textiles or automotive, and therefore need to comply with severe requirements to limit flammability risks. This work aimed at developing new formulations for the flame retardancy of polyamide 6 fibers. Indeed, no satisfactory solutions have been found yet to protect these fibers in case of fire. Moreover, it faces strong concurrence from polyester fibers for which FR systems are well established (i.e. use of comonomeric phosphinic acid unit).

Extrusion followed by melt-spinning was chosen as the main process. Indeed, it allows incorporating the fire retardant additives directly in the melted polymeric matrix and thus, avoids the durability issue of the FR properties, usually met with finishing. The ultimate goal was to be able to process fibers at large-scale. In order to achieve the scale-up, the work was divided into two main tasks. The first step was dedicated to find an innovative system, processed at the micro scale, allowing good spinnability and having enhanced fire properties. The second task concerned the upscaling.

The screening of different fire retardants was thus performed using the microextruder to process the formulations. Pyrolysis combustion flow calorimetry was used as the main fire test to select the best candidates. Spinnability was also a discriminant factor. Phosphorus based and sulfur based FR additives were melt-mixed in PA6. Different kinds of nanoparticles were also considered. While NP and phosphorus FR did not allow enhancing the FR performance of the fibers, sulfur based FR had good results. Indeed, ammonium sulfamate (AS) and guanidine sulfamate (GAS) were found to be efficient in very low amounts (<10 wt.-%). This particularity is very important in fibers applications because higher loadings usually results in the loss of the mechanical properties of the fibers.

The understanding of flame retardant mechanisms was also an important concern of this work. Based on the screening results, two systems were selected for an in-depth study of the modes of actions. Analyzing the decomposition gases of polymers is essential for the understanding of the thermal behavior of polymers. Therefore analyzing techniques like thermogravimetry coupled with Fourier Transformed Infra-Red spectroscopy was used. The method is efficient for decomposition products, such as CO₂, H₂O, NH₃. However, when complex mixtures of hydrocarbon decomposition products are released to the gas phase, the

General Conclusion

results of this technique are not easily interpreted because of overlapping signals. Pyrolysis gas chromatography coupled with mass spectrometry (py-GC-MS) allowed identifying the decomposition products of the different formulations and understanding the effects of the sulfamate salts on the decomposition of PA6. Indeed, PCFC results showed a reduction of more than 30% of the pHRR using 7 wt.-% of AS. At the same time no apparent change on the decomposition gases was detected with TGA-FTIR. The pHRR reduction could be explained using the py-GC-MS. This technique has indicated that, in fact, the evolving decomposition products are different, and consequently the decomposition pathways of neat and fire retarded PA6 are not the same. Indeed, while ϵ -caprolactam was mainly released in the case of neat PA6, heavier decomposition products were obtained for the flame retarded formulation. In the condensed phase, solid state NMR spectroscopy has demonstrated that an aromatic structure was formed at high temperatures. This charred structure does not seem to protect the material from heat or mass transfers since it is formed too late, but it does not contribute to the flame. It was proposed that sulfamate salts are transformed in sulfuric acid at high temperature. The formed acid oxidizes, dehydrates and carbonizes the polymer.

From a processing point of view, fibers containing a maximum of 7 wt.-% AS and 10 wt.-% GAS could be spun. However, fibers with 7 wt.-% AS were very fragile and a formulation containing only 5 wt.-% was more easily processable. Mechanical testings showed that the additives did not change the properties (elongation at break and tensile strength) of the fibers compared to neat PA6. With higher loadings, processing issues appeared certainly due to aminolysis of the matrix by ammonia released from the additives. A scale-up was performed on formulations using only the sulfamate salts at 5 wt.-% but it failed due to more severe parameters compared to micro-scale processing. For example, the feeding zone had to be set at 300 °C to rapidly melt the PA6, in order to use the extruder properly. The change in processing scale and processing parameters prevented the use of formulations found to be effective at the micro scale.

In order to perform the scale-up, it was considered to use phosphorus containing FR as synergists of the sulfamate salts. MPP was chosen because of a good thermal stability at the processing temperature. The investigation of the potential synergy between the two FR was first performed using the microextruder to quickly optimize the ratios of the different

General Conclusion

additives. MPP alone appear to greatly promote the matrix degradation and formulations containing high MPP ratios also released fuels at lower temperature. Eventually, the two best results, in terms of pHRR decrease, were obtained using PA6/AS 4%/MPP 1% and PA6/GAS 2.5%/MPP 2.5%. Both gave reduction of 30.1 % of the pHRR compared to pure PA6. GAS being more easily processed at the microscale, it was assumed that it would also be easier at larger-scale. Consequently, it was decided to perform the scale-up using the PA6/GAS 2.5%/MPP 2.5% formulation. A rod was successfully extruded. Using the extruded pellets, it was possible to directly melt-spin the formulation with the microextruder coupled with the micro-spinning device in “direct method”. PCFC gave very similar results in terms of pHRR decrease and pHRR temperature.

Further fire retardant properties were also evaluated. Cone calorimetry (MLC) results do not show improvements on the pHRR or THR compared to PA6. A decrease of the time to ignition was even recorded. It is assumed that the promotion of the PA6 decomposition induced by the FR additives favors the formation of fuels. Thus the minimum concentration of fuels needed for inflammation is reached earlier. Nonetheless, a major difference is the formation of a structured char after that pHRR is reached, but its late formation cannot protect the material. On the other hand, LOI was improved and jumped from 28 to 37 vol.-%, mainly by a dripping effect, removing the heat and the material from the combustion zone. UL-94 classification is also improved and goes from V2 for the neat PA6 to V0 for the PA6/GAS 2.5%/MPP 2.5% formulation.

OUTLOOKS

Many perspectives have emerged along this work. The FR mode of action of ammonium sulfamate and guanidine sulfamate were described in-depth, but the synergistic effect of AS/MPP and GAS/MPP still remains to be explained. Some ratios were found to be more efficient than others: for GAS/MPP, the 50:50 ratio at 5 wt.-% total loading obtained the best pHRR decrease. However, when the total loading was increased up to 10 wt.-% the PCFC results were worse. Finding the best ratios and loadings could be achieved through the use of an experimental design. Further investigation on the GAS/MPP synergism should also be done to know if the effect comes from the “melamine” or the “polyphosphate”. Formulations containing only melamine and GAS could be tested. Other compounds known to enhance dripping could also be used in combination with sulfamate salts, such as melamine cyanurate to compare the effect to MPP.

About the chemistry of the fire retardants, two sulfamate salts were used as fire retardant and their mode of action was detailed. However, many counter-anion could be used to enhance the FR properties. In particular, metallic salts could be considered. In the case of dialkylphosphinates, the use of different metallic cations led to enhanced fire behavior, and the development of the famous Exolit OP® at Clariant. Different metal salts in combination with APP have already shown improvement of the fire performance with cotton fabrics [231] or in PP [232]. In particular $MnSO_4$ and $ZnSO_4$ were found effective. It seems to be an advantage to use sulfur compounds in combination with polyphosphates, as also shown in the present work. The literature on this subject is also limited and therefore it could be an interesting field of research.

The system GAS/MPP that was developed is efficient at low loadings, and could be up-scaled. Obviously, the main outlook is to make a fabric with the PA6/GAS 2.5%/MPP 2.5% formulation to test its fire properties and performances. Although primarily designed to be used in PA6 fibers applications, it could also be used in the bulk. In this case, further experiments should be considered, in particular for electrical applications. Indeed, the material is rated V0 at the UL-94 which is required in such applications. Glow wire values, mechanical properties and CTI should, of course, be determined.

REFERENCES

1. PlasticsEurope. *Plastics – the Facts 2013*. An analysis of European latest plastics production, demand and waste data. 2013; Available from: <http://www.plasticseurope.org/cust/documentrequest.aspx?DocID=59108>.
2. National Fire Protection Association. *Fires in the U.S. 2013* [cited 2014 2014-04-28]; Available from: <http://www.nfpa.org/research/reports-and-statistics/fires-in-the-us>.
3. Lowden L.A. and Hull T.R., *Flammability behaviour of wood and a review of the methods for its reduction*. *Fire Science Reviews*, 2013. **2**(1): p. 1-19.
4. Wyld O., British Patent No. 551, 1735,
5. Gay-Lussac J.L., *Note sur la propriété qu'ont les matières salines de rendre les tissus incombustibles*. *Annales de chimie et de physique*, 1821. **18**: p. 211-216.
6. Rhodia. *Rhodia Group: Polyamide fibers*. [cited 2011 July]; Available from: http://www.rhodia.com/en/markets_and_products/product_ranges/polyamide_fibers.tcm.
7. Plastemart. *Special polyamides are expected to grow much faster than polyamide 6 & 6.6*. [cited 2011 July]; Available from: http://www.plastemart.com/upload/Literature/special_polyamides.asp.
8. *Consumer Protection Act, 1987(a). Furniture and Furnishings (Fire) (Safety) Regulations 1988*, in *S.I. 1988/1324*, HMSO, Editor 1988: London, UK.
9. Association Française de Normalisation (AFNOR), *NF P92-507 Sécurité contre l'incendie - Bâtiment - Matériaux d'aménagement - Classement selon leur réaction au feu*, 2004: France.
10. Association Française de Normalisation (AFNOR), *NF EN 13501-1 Classement au feu des produits et éléments de construction - Partie 1 : classement à partir des données d'essais de réaction au feu*, 2013: France.
11. National Fire Protection Association, *NFPA 701: Standard methods of fire tests for flame-resistant textiles and films (revised 2010)*, 2010: USA.
12. Carothers W.H., *Linear condensation polymers*. Us Patent 2071250, DuPont 1937, United States.
13. Schlack P., *Verfahren zur Herstellung verformbarer hochmolekularer Polyamide*. German Patent 748253, Farbenindustrie A.G., 1938,
14. Palmer R.J., *Polyamides, Plastics*, in *Encyclopedia of Polymer Science and Technology* 2002, John Wiley & Sons, Inc.
15. Yang H.H., *Polyamide Fibers*, in *Handbook of Fiber Chemistry, Third Edition*, Lewin M., Editor 2006, CRC Press.
16. Roda J., *Polyamides*, in *Handbook of Ring-Opening Polymerization* 2009, Wiley-VCH Verlag GmbH & Co. KGaA. p. 165-195.
17. Odian G., *Principles of Polymerization (4th edition)* 2004, New York: John Wiley and Sons.
18. Alger M.S.M., *Polymer science dictionary*, ed. Springer 1997: Chapman & Hall.
19. BASF. *Ultramid®; Polyamides: PA6 (Nylon 6) - BASF Corporation Plastics Portal*. 2011 [cited 2011 June]; Available from: <http://www.plasticsportal.com/products/ultramidpa6.html>.
20. Smook J., Vos G.J.H. and Doppert H.L., *A semiempiric model for establishing the drawability of solution-spun linear polyamides and other flexible chain polymers*. *Journal of Applied Polymer Science*, 1990. **41**(1-2): p. 105-116.

References

21. Cho J.W., Lee G.W. and Chun B.C., *Mechanical properties of nylon 6 fibers gel-spun from benzyl alcohol solution*. Journal of Applied Polymer Science, 1996. **62**(5): p. 771-778.
22. Mukhopadhyay S. and Ramakrishnan G., *Microfibres*. Textile Progress, 2008. **40**(1): p. 1-86.
23. Darrell H.R. and Iksoo C., *Nanometre diameter fibres of polymer, produced by electrospinning*. Nanotechnology, 1996. **7**(3): p. 216.
24. Gianchandani J., Spruiell J.E. and Clark E.S., *Polymorphism and orientation development in melt spinning, drawing, and annealing of nylon-6 filaments*. Journal of Applied Polymer Science, 1982. **27**(9): p. 3527-3551.
25. Salem D.R., *Structure formation in polymeric fibers* 2001: Hanser.
26. Holmes D.R., Bunn C.W. and Smith D.J., *The crystal structure of polycapromide: Nylon 6*. Journal of Polymer Science, 1955. **17**(84): p. 159-177.
27. Roldan L.G. and Kaufman H.S., *Crystallization of nylon 6*. Journal of Polymer Science Part B: Polymer Letters, 1963. **1**(11): p. 603-608.
28. Parker J.P. and Lindenmeyer P.H., *On the crystal structure of nylon 6*. Journal of Applied Polymer Science, 1977. **21**(3): p. 821-837.
29. Illers K.H., Haberkorn H. and Simák P., *Untersuchungen über die γ -struktur in unverstrecktem und verstrecktem 6-polyamid*. Die Makromolekulare Chemie, 1972. **158**(1): p. 285-311.
30. Ziabicki A., *Über die mesomorphe β -Form von Polycapronamid und ihre Umwandlung in die kristalline Form α* . Colloid & Polymer Science, 1959. **167**(2): p. 132-141.
31. Stepaniak R.F., Garton A., Carlsson D.J. and Wiles D.M., *The characterization of nylon 6 filaments by x-ray diffraction*. Journal of Applied Polymer Science, 1979. **23**(6): p. 1747-1757.
32. Stepaniak R.F., Garton A., Carlsson D.J. and Wiles D.M., *An examination of the crystal structures present in nylon-6 fibers*. Journal of Polymer Science: Polymer Physics Edition, 1979. **17**(6): p. 987-999.
33. Arimoto H., Ishibashi M., Hirai M. and Chatani Y., *Crystal structure of the γ -form of nylon 6*. Journal of Polymer Science Part A: General Papers, 1965. **3**(1): p. 317-326.
34. Kinoshita Y., *An investigation of the structures of polyamide series*. Die Makromolekulare Chemie, 1959. **33**(1): p. 1-20.
35. Bradbury E.M. and Elliott A., *Infra-red spectra and chain arrangement in some polyamides, polypeptides and fibrous proteins*. Polymer, 1963. **4**: p. 47-59.
36. Bradbury E.M., Brown L., Elliott A. and Parry D.A.D., *The structure of the gamma form of polycapromide (Nylon 6)*. Polymer, 1965. **6**(9): p. 465-482.
37. Vogelsohn D.C., *Crystal structure studies on the polymorphic forms of nylons 6 and 8 and other even nylons*. Journal of Polymer Science Part A: General Papers, 1963. **1**(3): p. 1055-1068.
38. Dasgupta S., Hammond W.B. and Goddard W.A., *Crystal Structures and Properties of Nylon Polymers from Theory*. Journal of the American Chemical Society, 1996. **118**(49): p. 12291-12301.
39. Hatfield G.R., Glans J.H. and Hammond W.B., *Characterization of structure and morphology in nylon 6 by solid-state carbon-13 and nitrogen-15 NMR*. Macromolecules, 1990. **23**(6): p. 1654-1658.
40. Casanovas J. and Alemán C., *Calculated NMR chemical shifts of nylon 6: a comparison of the α and γ forms*. Journal of Materials Science, 2002. **37**(17): p. 3589-3594.

References

41. Schreiber R., Veeman W.S., Gabriëlse W. and Arnauts J., *NMR Investigations of Orientational and Structural Changes in Polyamide-6 Yarns by Drawing*. *Macromolecules*, 1999. **32**(14): p. 4647-4657.
42. Vasanthan N. and Salem D.R., *FTIR spectroscopic characterization of structural changes in polyamide-6 fibers during annealing and drawing*. *Journal of Polymer Science Part B: Polymer Physics*, 2001. **39**(5): p. 536-547.
43. Ho J.-C. and Wei K.-H., *Induced $\gamma \rightarrow \alpha$ Crystal Transformation in Blends of Polyamide 6 and Liquid Crystalline Copolyester*. *Macromolecules*, 2000. **33**(14): p. 5181-5186.
44. Liu T.X., Liu Z.H., Ma K.X., Shen L., Zeng K.Y. and He C.B., *Morphology, thermal and mechanical behavior of polyamide 6/layered-silicate nanocomposites*. *Composites Science and Technology*, 2003. **63**(3-4): p. 331-337.
45. Anton A. and Baird B.R., *Polyamides, Fibers*, in *Encyclopedia of Polymer Science and Technology* 2002, John Wiley & Sons, Inc.
46. TGSCOM. *The Glock FAQ*. 2009 [cited 2011 August 19th]; Available from: http://www.glockfaq.com/content.aspx?ckey=Glock_FAQ_General_Glock_Info.
47. Plastemart. *Global scenario of polyamide looks quite challenging*. [cited 2011 July]; Available from: <http://www.plastemart.com/upload/Literature/marketscenarioofpolyamide.asp>.
48. British Plastics Federation. *Nylons (Polyamide)*. 2010 [cited 2011 2011-07-15]; Available from: <http://www.bpf.co.uk/Plastipedia/Polymers/Polyamides.aspx>.
49. IHS. *Nylon Fibers*. 2011 [cited 2011 2014-03-04]; Available from: <http://www.ihs.com/products/chemical/planning/ceh/nylon-fibers.aspx?pu=1&rd=chemihs>.
50. Levchik S.V., Weil E.D. and Lewin M., *Thermal decomposition of aliphatic nylons*. *Polymer International*, 1999. **48**(7): p. 532-557.
51. Davis R.D., Gilman J.W. and VanderHart D.L., *Processing degradation of polyamide 6/montmorillonite clay nanocomposites and clay organic modifier*. *Polymer Degradation and Stability*, 2003. **79**(1): p. 111-121.
52. Reimschuessel H., Shalaby S. and Pearce E., *J Fire Flamm*, 1973(4): p. 299.
53. Pearce E., *Contemporary topics in polymer science*. Vol. 5. 1984, New York: Plenum Press.
54. Levchik S.V. and Weil E.D., *Combustion and fire retardancy of aliphatic nylons*. *Polymer International*, 2000. **49**(10): p. 1033-1073.
55. Horrocks A.R., *An Introduction to the Burning Behaviour of Cellulosic Fibres*. *Journal of the Society of Dyers and Colourists*, 1983. **99**(7-8): p. 191-197.
56. Horrocks A.R. and Price D., *Fire Retardant Materials*, ed. Horrocks A.R. and Price D. 2001: Woodhead Publishing.
57. Schartel B., Pötschke P., Knoll U. and Abdel-Goad M., *Fire behaviour of polyamide 6/multiwall carbon nanotube nanocomposites*. *European Polymer Journal*, 2005. **41**(5): p. 1061-1070.
58. Song L., Hu Y., Lin Z., Xuan S., Wang S., Chen Z. and Fan W., *Preparation and properties of halogen-free flame-retarded polyamide 6/organoclay nanocomposite*. *Polymer Degradation and Stability*, 2004. **86**(3): p. 535-540.
59. Levchik S.V., Levchik G.F., Balabanovich A.I., Weil E.D. and Klatt M., *Phosphorus oxynitride: a thermally stable fire retardant additive for polyamide 6 and*

References

- poly(butylene terephthalate)*. Die Angewandte Makromolekulare Chemie, 1999. **264**(1): p. 48-55.
60. Tata J., Alongi J., Carosio F. and Frache A., *Optimization of the procedure to burn textile fabrics by cone calorimeter: Part I. Combustion behavior of polyester*. Fire and Materials, 2011. **35**(6): p. 397-409.
 61. Horrocks A.R., *Textiles*, in *Fire Retardant Materials*, Horrocks A.R. and Price D., Editors. 2001, Woodhead Publishing. p. 128-181.
 62. Backer S., *Textile fabric flammability* 1976: MIT Press.
 63. Mera H. and Takata T., *High-Performance Fibers*, in *Ullmann's Encyclopedia of Industrial Chemistry 2000*, Wiley-VCH Verlag GmbH & Co. KGaA.
 64. Bourbigot S. and Flambard X., *Heat resistance and flammability of high performance fibres: A review*. Fire and Materials, 2002. **26**(4-5): p. 155-168.
 65. Bajaj P., *Heat and flame protection*, in *Handbook of Technical Textile*, Horrocks R., Editor 2000, Wood Head Publishing. p. 223-263.
 66. Horrocks A.R., *Developments in flame retardants for heat and fire resistant textiles--the role of char formation and intumescence*. Polymer Degradation and Stability, 1996. **54**(2-3): p. 143-154.
 67. Kandola B.K., *Flame Retardancy Design for Textiles*, in *Fire retardancy of polymeric materials*, Wilkie C.A. and Morgan A.B., Editors. 2010, CRC Press. p. 725-757.
 68. Bourbigot S., *Flame Retardancy Of Textiles: New Approaches*, in *Advances in Fire Retardant Materials*, Horrocks A.R. and Price D., Editors. 2008, Woodhead Publishing. p. 9-40.
 69. Weil E.D. and Levchik S.V., *Flame Retardants in Commercial Use or Development for Textiles*. Journal of Fire Sciences, 2008. **26**(3): p. 243-281.
 70. Thor. AFLAMMIT® NY - Durable Textile Flame Retardant. 2011 [cited 2011 2014-07-13]; Available from: <http://www.thor.com/>.
 71. Drevelle C., *Conception et développement de systèmes retardateurs de flamme pour fibres synthétiques*, 2005, Université Lille I: Lille, Nord, France.
 72. Levchik S.V. and Weil E.D., *A review on thermal decomposition and combustion of thermoplastic polyesters*. Polymers for Advanced Technologies, 2004. **15**(12): p. 691-700.
 73. Weil E.D. and Levchik S., *Current Practice and Recent Commercial Developments in Flame Retardancy of Polyamides*. Journal of Fire Sciences, 2004. **22**(3): p. 251-264.
 74. Laoutid F., Bonnaud L., Alexandre M., Lopez-Cuesta J.M. and Dubois P., *New prospects in flame retardant polymer materials: From fundamentals to nanocomposites*. Materials Science and Engineering: R: Reports, 2009. **63**(3): p. 100-125.
 75. Price D., Anthony G. and Carty P., *Introduction: polymer combustion, condensed phase pyrolysis and smoke formation*, in *Fire Retardant Materials 2001*, Woodhead Publishing.
 76. Williams I.G., *Flame retarded polyamides - development, types and applications*. Plastics and Rubber Processing and Applications, 1984. **4**(3): p. 239.
 77. Lewin M., Atlas S.M. and Pearce E.M., *Flame-retardant polymeric materials*, ed. Lewin M., Atlas S.M. and Pearce E.M. 1975, New York: Plenum Press.
 78. Shaw S.D., Blum A., Weber R., Kannan K., Rich D., Lucas D., Koshland C.P., Dobraca D., Hanson S. and Birnbaum L.S., *Halogenated flame retardants: do the fire safety benefits justify the risks?* Reviews on Environmental Health, 2010. **25**(4): p. 261-305.

References

79. Talsness C.E., *Overview of toxicological aspects of polybrominated diphenyl ethers: A flame-retardant additive in several consumer products*. Environmental Research, 2008. **108**(2): p. 158-167.
80. Levchik S.V., *Introduction to Flame Retardancy and Polymer Flammability*, in *Flame Retardant Polymer Nanocomposites 2006*, John Wiley & Sons, Inc. p. 1-29.
81. Levchik S.V. and Weil E.D., *A Review of Recent Progress in Phosphorus-based Flame Retardants*. Journal of Fire Sciences, 2006. **24**(5): p. 345-364.
82. Balabanovich A.I., Levchik G.F., Levchik S.V. and Schnabel W., *Fire retardance in polyamide-6. The effects of red phosphorus and radiation-induced cross-links*. Fire and Materials, 2001. **25**(5): p. 179-184.
83. Jenewein E., Kleiner H.-J., Wanzke W. and Budzinsky W., *Synergistic flame protection agent combination for thermoplastic polymers*. US Patent 6,365,071, Clariant GmbH, 2002, Germany.
84. Leutner B., Klatt M., Fisch H. and Nam M., *Flame-retardant polyester molding compositions containing flame retardant nitrogen compounds and diphosphinates*. US Patent 6,503,969, BASF Aktiengesellschaft, 2003, Germany.
85. Schlosser E., Nass B. and Wanzke W., *Flame-retardant combination*. US patent 6,255,371, Clariant GmbH, 2001, Germany.
86. Samyn F., *Compréhension des procédés d'ignifugation du polyamide 6*, 2007, Université Lille I: Lille, Nord, France.
87. Clariant. *Exolit® OP 1311 - Product Data Sheet*. 2011; Available from: <http://www.additives.clariant.com/>.
88. Hörold S., Nass B., Schacker O. and Wanzke W. *A New Generation of Flame Retarded Polyamides Based on Phosphinates*. in *8th International Flame Retardants Conference*. 2004. London, UK: Interscience Communications.
89. Levchik S.V., Costa L. and Camino G., *Effect of the fire-retardant ammonium polyphosphate on the thermal decomposition of aliphatic polyamides. Part III-- Polyamides 6.6 and 6.10*. Polymer Degradation and Stability, 1994. **43**(1): p. 43-54.
90. Levchik S.V., Levchik G.F., Balabanovich A.I., Camino G. and Costa L., *Mechanistic study of combustion performance and thermal decomposition behaviour of nylon 6 with added halogen-free fire retardants*. Polymer Degradation and Stability, 1996. **54**(2-3): p. 217-222.
91. Liu G. *Ammonium Polyphosphate-An Overview with Respect to Its Properties, Environmental and Toxicological Aspects*. in *4th International Conference on Bioinformatics and Biomedical Engineering (iCBBE)*. 2010.
92. Costa L., Camino G. and Luda di Cortemiglia M.P., *Mechanism of Thermal Degradation of Fire-Retardant Melamine Salts*, in *Fire and Polymers 1990*, American Chemical Society. p. 211-238.
93. Weil E.D. and Choudhary V., *Flame-Retarding Plastics and Elastomers with Melamine*. Journal of Fire Sciences, 1995. **13**(2): p. 104-126.
94. Casu A., Camino G., De Giorgi M., Flath D., Morone V. and Zenoni R., *Fire-retardant mechanistic aspects of melamine cyanurate in polyamide copolymer*. Polymer Degradation and Stability, 1997. **58**(3): p. 297-302.
95. Mukherjee A., *Melamine derivatives - An alternative to traditional flame retardants*. Plastics Engineering, 2001. **57**(2): p. 42-43.
96. Weil E.D., Lewin M. and Barinov V. *Recent advances in flame retardancy of polymeric materials*. in *BCC*. 2002. Norwalk, CT.

References

97. Lewin M., *Flame Retarding of Polymers with Sulfamates. I. Sulfation of Cotton and Wool*. Journal of Fire Sciences, 1997. **15**(4): p. 263-276.
98. Lewin M., Brozek J. and Martens M.M., *The system polyamide/sulfamate/dipentaerythritol: flame retardancy and chemical reactions*. Polymers for Advanced Technologies, 2002. **13**(10-12): p. 1091-1102.
99. Lewin M., *Flame retardant polyamide compositions*. US Patent 5,424,344, E. I. DuPont de Nemours and Company, 1995, United States.
100. Lewin M., *Flame retarding polymer nanocomposites: Synergism, cooperation, antagonism*. Polymer Degradation and Stability, 2011. **96**(3): p. 256-269.
101. Lewin M., *Unsolved problems and unanswered questions in flame retardance of polymers*. Polymer Degradation and Stability, 2005. **88**(1): p. 13-19.
102. Hornsby P.R. and Watson C.L., *A study of the mechanism of flame retardance and smoke suppression in polymers filled with magnesium hydroxide*. Polymer Degradation and Stability, 1990. **30**(1): p. 73-87.
103. Horn W.E., *Recent Improvements in Inorganic Flame Retardant Performance*, in *9th BCC Conference on Flame Retardancy* 1998, : Stamford, CT.
104. Miyata S., *Composite metal hydroxide and its use*. US Patent 5,571,526, Kabushiki Kaisha Kaisui Kagau Kenkyujo, 1996,
105. Shanmuganathan K., Deodhar S., Dembsey N., Fan Q., Calvert P.D., Warner S.B. and Patra P.K., *Flame retardancy and char microstructure of nylon-6/layered silicate nanocomposites*. Journal of Applied Polymer Science, 2007. **104**(3): p. 1540-1550.
106. Troitzsch J., *Overview of flame retardant*. Chemistry Today, 1998(Jan–Feb16).
107. BoraxFR. *Firebrake® zinc borates in nylon engineering plastics*. Available from: <http://www.boraxfr.com>.
108. Myers R.E., Dickens E.D., Licursi E. and Evans R.E., *Ammonium Pentaborate: an Intumescent Flame Retardant for Thermoplastic Polyurethanes*. Journal of Fire Sciences, 1985. **3**(6): p. 432-449.
109. Morgan A.B., *Polymer-Clay Nanocomposites: Design and Application of Multi-Functional Materials*, in *Material Matters 2007*, Aldrich Chemical Co.
110. Sinha Ray S. and Okamoto M., *Polymer/layered silicate nanocomposites: a review from preparation to processing*. Progress in Polymer Science, 2003. **28**(11): p. 1539-1641.
111. Ha J.U. and Xanthos M., *Functionalization of nanoclays with ionic liquids for polypropylene composites*. Polymer Composites, 2009. **30**(5): p. 534-542.
112. Beyer G., *Nanocomposites offer new way forward for flame retardants*. Plastics, Additives and Compounding, 2005. **7**(5): p. 32-35.
113. Fujiwara S. and Sakamoto K., *Flammability properties of Nylon-6/mica nanocomposites*. Japanese Patent No. JPA51-109998, Toyota, 1976, Japan.
114. Gilman J.W., Kashiwagi T. and Lichtenhan J.D., *Nanocomposites: A Revolutionary New Flame Retardant Approach*. SAMPE Journal, 1997. **33**(4): p. 40-46.
115. Hu Y., Wang S., Ling Z., Zhuang Y., Chen Z. and Fan W., *Preparation and Combustion Properties of Flame Retardant Nylon 6/Montmorillonite Nanocomposite*. Macromolecular Materials and Engineering, 2003. **288**(3): p. 272-276.
116. Zhang J., Lewin M., Pearce E., Zammarano M. and Gilman J.W., *Flame retarding polyamide 6 with melamine cyanurate and layered silicates*. Polymers for Advanced Technologies, 2008. **19**(7): p. 928-936.

References

117. Fang K., Li J., Ke C., Zhu Q., Tao K., Zhu J. and Yan Q., *Intumescent flame retardation of melamine-modified montmorillonite on polyamide 6: Enhancement of condense phase and flame retardance*. Polymer Engineering & Science, 2011. **51**(2): p. 377-385.
118. Miyata S., Hirose T. and Iizima N., *Fire-retarding thermoplastic resin composition*. US Patent 4,085,088, Kyowa Chemical Industry, 1978, Japan.
119. Manzi-Nshuti C., Zhu L., Nyambo C., Wang L., Wilkie Charles A. and Hossenlopp Jeanne M., *Use of Layered Double Hydroxides as Polymer Fire-Retardant Additives: Advantages and Challenges*, in *Fire and Polymers V 2009*, American Chemical Society. p. 35-46.
120. Zammarano M., Franceschi M., Bellayer S., Gilman J.W. and Meriani S., *Preparation and flame resistance properties of revolutionary self-extinguishing epoxy nanocomposites based on layered double hydroxides*. Polymer, 2005. **46**(22): p. 9314-9328.
121. Du L., Qu B. and Zhang M., *Thermal properties and combustion characterization of nylon 6/MgAl-LDH nanocomposites via organic modification and melt intercalation*. Polymer Degradation and Stability, 2007. **92**(3): p. 497-502.
122. Bravo-Suárez J., Páez-Mozoll E. and Oyama III T., *Models for the estimation of thermodynamic properties of layered double hydroxides: application to the study of their anion exchange characteristics*. Química Nova, 2004. **27**(4): p. 574-581.
123. Levis S.R. and Deasy P.B., *Characterisation of halloysite for use as a microtubular drug delivery system*. International journal of pharmaceutics, 2002. **243**(1-2): p. 125-134.
124. Cooper S.M., Fleischer C., Duffy M. and Wagner A., *Polymeric composite including nanoparticle filler*. US 2007/0106006, NaturalNano, Inc., 2007, United States.
125. Marney D.C.O., Russell L.J., Wu D.Y., Nguyen T., Cramm D., Rigopoulos N., Wright N. and Greaves M., *The suitability of halloysite nanotubes as a fire retardant for nylon 6*. Polymer Degradation and Stability, 2008. **93**(10): p. 1971-1978.
126. Peeterbroeck S., Laoutid F., Taulemesse J.M., Monteverde F., Lopez-Cuesta J.M., Nagy J.B., Alexandre M. and Dubois P., *Mechanical Properties and Flame-Retardant Behavior of Ethylene Vinyl Acetate/High-Density Polyethylene Coated Carbon Nanotube Nanocomposites*. Advanced Functional Materials, 2007. **17**(15): p. 2787-2791.
127. Jin Z., Pramoda K.P., Xu G. and Goh S.H., *Dynamic mechanical behavior of melt-processed multi-walled carbon nanotube/poly(methyl methacrylate) composites*. Chemical Physics Letters, 2001. **337**(1-3): p. 43-47.
128. Cooper C.A., Ravich D., Lips D., Mayer J. and Wagner H.D., *Distribution and alignment of carbon nanotubes and nanofibrils in a polymer matrix*. Composites Science and Technology, 2002. **62**(7-8): p. 1105-1112.
129. Cipiriano B.H., Kashiwagi T., Raghavan S.R., Yang Y., Grulke E.A., Yamamoto K., Shields J.R. and Douglas J.F., *Effects of aspect ratio of MWNT on the flammability properties of polymer nanocomposites*. Polymer, 2007. **48**(20): p. 6086-6096.
130. Kashiwagi T., Du F., Winey K.I., Groth K.M., Shields J.R., Bellayer S.P., Kim H. and Douglas J.F., *Flammability properties of polymer nanocomposites with single-walled carbon nanotubes: effects of nanotube dispersion and concentration*. Polymer, 2005. **46**(2): p. 471-481.
131. Bocchini S., Frache A., Camino G. and Claes M., *Polyethylene thermal oxidative stabilisation in carbon nanotubes based nanocomposites*. European Polymer Journal, 2007. **43**(8): p. 3222-3235.

References

132. Reilly R.M., *Carbon Nanotubes: Potential Benefits and Risks of Nanotechnology in Nuclear Medicine*. Journal of Nuclear Medicine, 2007. **48**(7): p. 1039-1042.
133. Kashiwagi T. and Gilman J.W., *Silicon-Based Flame Retardants*, in *Fire Retardancy of Polymeric Materials*, Grand A.F. and Wilkie C.A., Editors. 2000, Taylor & Francis.
134. Dasari A., Yu Z.-Z., Mai Y.-W., Cai G. and Song H., *Roles of graphite oxide, clay and POSS during the combustion of polyamide 6*. Polymer, 2009. **50**(6): p. 1577-1587.
135. Horrocks R., *Handbook of Technical Textile 2000*: Wood Head Publishing.
136. Zhang S. and Horrocks A.R., *A review of flame retardant polypropylene fibres*. Progress in Polymer Science, 2003. **28**(11): p. 1517-1538.
137. Botkin J.H. and Kaprinidis N. *Advances in Flame Retardant Compositions*. in *NPE 2003*. 2003. Chicago, Illinois.
138. Butylkina N.G., Ivanova A.Y. and Tyuganova M.A., *Polycaproamide fibres with reduced combustibility*. Fibre Chemistry, 1989. **20**(3): p. 170-172.
139. Tyuganova M.A., Butylkina N.G., Yavorskaya E.G. and Tarakanov V.P., *Preparation of fire-resistant polycaproamide fibres*. Fibre Chemistry, 1988. **20**(1): p. 70-72.
140. Bender K. and Schach G., *Flame-Retardant Polymer Fibres And Use Thereof And Textile Fabric Comprising These Polymer Fibres*. EMS-PATENT AG (Domat/Ems, CH), 2013, United States.
141. Bourbigot S., Devaux E. and Flambard X., *Flammability of polyamide-6/clay hybrid nanocomposite textiles*. Polymer Degradation and Stability, 2002. **75**(2): p. 397-402.
142. Shanmuganathan K., Deodhar S., Dembsey N.A., Fan Q. and Patra P.K., *Condensed-phase flame retardation in nylon 6-layered silicate nanocomposites: Films, fibers, and fabrics*. Polymer Engineering & Science, 2008. **48**(4): p. 662-675.
143. Bourbigot S., Bras M.L., Flambard X., Rochery M., Devaux E. and Lichtenhan J.D., *Micro-Sized Fire Retarding Mineral Fillers. Polyhedral Oligomeric Silsesquioxanes: Application to Flame Retardant Textiles*, in *Fire Retardancy of Polymers*, Le Bras M., Wilkie C.A. and Bourbigot S., Editors. 2005, The Royal Society of Chemistry. p. 187-200.
144. Bellayer S., Bourbigot S., Flambard X., Rochery M., Devaux E. and Gilman J.W. *Polymer/MWNTs nanocomposite yarns and fabrics: processing, characterization and flammability and thermal properties*. in *4th Autex World Textile Conference*. 2004. Roubaix.
145. Smart G., Kandola B.K., Horrocks A.R., Nazaré S. and Marney D., *Polypropylene fibers containing dispersed clays having improved fire performance. Part II: characterization of fibers and fabrics from PP-nanoclay blends*. Polymers for Advanced Technologies, 2008. **19**(6): p. 658-670.
146. Horrocks A.R., Kandola B.K., Smart G., Zhang S. and Hull T.R., *Polypropylene fibers containing dispersed clays having improved fire performance. I. Effect of nanoclays on processing parameters and fiber properties*. Journal of Applied Polymer Science, 2007. **106**(3): p. 1707-1717.
147. Kandola B.K., Smart G., Horrocks A.R., Joseph P., Zhang S., Hull T.R., Ebdon J., Hunt B. and Cook A., *Effect of different compatibilisers on nanoclay dispersion, thermal stability, and burning behavior of polypropylene-nanoclay blends*. Journal of Applied Polymer Science, 2008. **108**(2): p. 816-824.
148. International Organization for Standardization, *ISO 4589-2:1996 - Plastics -- Determination of burning behaviour by oxygen index -- Part 2: Ambient-temperature test*, 1996.

References

149. International Organization for Standardization, *ISO 13927:2001 - Plastics -- Simple heat release test using a conical radiant heater and a thermopile detector*, 2001.
150. Underwriters Laboratories Inc., *UL 94, the Standard for Safety of Flammability of Plastic Materials for Parts in Devices and Appliances testing*, 2001: Northbrook, IL.
151. Hartmann S.R. and Hahn E.L., *Nuclear Double Resonance in the Rotating Frame*. *Physical Review*, 1962. **128**(5): p. 2042-2053.
152. Huggett C., *Estimation of rate of heat release by means of oxygen consumption measurements*. *Fire and Materials*, 1980. **4**(2): p. 61-65.
153. Lyon R.E. and Walters R.N., *Pyrolysis combustion flow calorimetry*. *Journal of Analytical and Applied Pyrolysis*, 2004. **71**(1): p. 27-46.
154. Jang J. and Lee E., *Improvement of the flame retardancy of paper-sludge/polypropylene composite*. *Polymer Testing*, 2000. **20**(1): p. 7-13.
155. Wilkie C.A., Chigwada G., Gilman S.J.W. and Lyon R.E., *High-throughput techniques for the evaluation of fire retardancy*. *Journal of Materials Chemistry*, 2006. **16**(21): p. 2023-2030.
156. Yang C.Q. and He Q., *Applications of micro-scale combustion calorimetry to the studies of cotton and nylon fabrics treated with organophosphorus flame retardants*. *Journal of Analytical and Applied Pyrolysis*, 2011. **91**(1): p. 125-133.
157. Yang C.Q., He Q., Lyon R.E. and Hu Y., *Investigation of the flammability of different textile fabrics using micro-scale combustion calorimetry*. *Polymer Degradation and Stability*, 2010. **95**(2): p. 108-115.
158. Lyon R.E., Walters R.N. and Stoliarov S.I., *Thermal analysis of flammability*. *Journal of Thermal Analysis and Calorimetry*, 2007. **89**(2): p. 441-448.
159. Lin T.S., Cogen J.M. and Lyon R.E. *Correlations between microscale combustion calorimetry and conventional flammability tests for flame retardant wire and cable compounds*. in *Proceedings of the 58th International Wire & Cable Symposium*. 2007. Eatontown, NJ.
160. Scharfel B., Pawlowski K.H. and Lyon R.E., *Pyrolysis combustion flow calorimeter: A tool to assess flame retarded PC/ABS materials?* *Thermochimica Acta*, 2007. **462**(1-2): p. 1-14.
161. Jang B.N. and Wilkie C.A., *The effect of clay on the thermal degradation of polyamide 6 in polyamide 6/clay nanocomposites*. *Polymer*, 2005. **46**(10): p. 3264-3274.
162. Costache M.C., Jiang D.D. and Wilkie C.A., *Thermal degradation of ethylene-vinyl acetate copolymer nanocomposites*. *Polymer*, 2005. **46**(18): p. 6947-6958.
163. Jang B.N. and Wilkie C.A., *The thermal degradation of polystyrene nanocomposite*. *Polymer*, 2005. **46**(9): p. 2933-2942.
164. Sonnier R., Ferry L., Longuet C., Laoutid F., Friederich B., Laachachi A. and Lopez-Cuesta J.M., *Combining cone calorimeter and PCFC to determine the mode of action of flame-retardant additives*. *Polymers for Advanced Technologies*, 2011. **22**(7): p. 1091-1099.
165. Clariant. *Exolit® OP 950 - Product Data Sheet*. 2011; Available from: <http://www.additives.clariant.com/>.
166. Clariant. *Exolit® OP 1230 - Product Data Sheet*. 2010; Available from: <http://additives.clariant.com>.
167. Thor. *AFLAMMIT® PCO - Organic Phosphorus compounds*. 2011; Available from: <http://www.thor.com/>.

References

168. Lewin M., Zhang J., Pearce E. and Gilman J., *Flammability of polyamide 6 using the sulfamate system and organo-layered silicate*. *Polymers for Advanced Technologies*, 2007. **18**(9): p. 737-745.
169. Gilman J.W., Morgan A.B., Harris R., Manias E., Giannelis E.P. and Wuthenow M. *Polymer layered-silicate nanocomposites: polyamide-6, polypropylene and polystyrene*. in *New advances in flame retardant technology*, Fire Retardant Chemicals Association. 1999.
170. Thostenson E.T., Ren Z. and Chou T.-W., *Advances in the science and technology of carbon nanotubes and their composites: a review*. *Composites Science and Technology*, 2001. **61**(13): p. 1899-1912.
171. David D.J., *Polymer Nanocomposites*, in *Fire Retardancy of Polymeric Materials, Second Edition* 2009, CRC Press. p. 261-299.
172. Bellayer S., Bourbigot S., Flambard X., Rochery M., Gilman J.W. and Devaux E. *Polymer/MWNTs nanocomposite yarns and fabrics: processing, characterization and flammability and thermal properties*. in *Proceedings of the 4th AUTEX Conference* 2004. ENSAIT, Roubaix.
173. Horrocks A.R. and Kandola B.K., *Potential Applications of Nanocomposites for Flame Retardancy*, in *Flame Retardant Polymer Nanocomposites* 2006, John Wiley & Sons, Inc. p. 325-353.
174. Dahiya J.B., Rathi S., Bockhorn H., Haußmann M. and Kandola B.K., *The combined effect of organic phosphinate/ammonium polyphosphate and pentaerythritol on thermal and fire properties of polyamide 6-clay nanocomposites*. *Polymer Degradation and Stability*, 2012. **97**(8): p. 1458-1465.
175. Alix S., Follain N., Tenn N., Alexandre B., Bourbigot S., Soulestin J. and Marais S., *Effect of Highly Exfoliated and Oriented Organoclays on the Barrier Properties of Polyamide 6 Based Nanocomposites*. *The Journal of Physical Chemistry C*, 2012. **116**(8): p. 4937-4947.
176. ScharTEL B., Bartholmai M. and Knoll U., *Some comments on the main fire retardancy mechanisms in polymer nanocomposites*. *Polymers for Advanced Technologies*, 2006. **17**(9-10): p. 772-777.
177. Zheng X. and Wilkie C.A., *Nanocomposites based on poly (ϵ -caprolactone) (PCL)/clay hybrid: polystyrene, high impact polystyrene, ABS, polypropylene and polyethylene*. *Polymer Degradation and Stability*, 2003. **82**(3): p. 441-450.
178. Kashiwagi T., Harris R.H., Zhang X., Briber R.M., Cipriano B.H., Raghavan S.R., Awad W.H. and Shields J.R., *Flame retardant mechanism of polyamide 6-clay nanocomposites*. *Polymer*, 2004. **45**(3): p. 881-891.
179. Varley R.J., Groth A.M. and Leong K.H., *The role of nanodispersion on the fire performance of organoclay-polyamide nanocomposites*. *Composites Science and Technology*, 2008. **68**(14): p. 2882-2891.
180. Samyn F., Bourbigot S., Jama C. and Bellayer S., *Fire retardancy of polymer clay nanocomposites: Is there an influence of the nanomorphology?* *Polymer Degradation and Stability*, 2008. **93**(11): p. 2019-2024.
181. Bourbigot S. and Duquesne S., *Fire retardant polymers: recent developments and opportunities*. *Journal of Materials Chemistry*, 2007. **17**(22): p. 2283-2300.
182. Morgan A.B. and Wilkie C.A., *Practical Issues and Future Trends in Polymer Nanocomposite Flammability Research*, in *Flame Retardant Polymer Nanocomposites* 2006, John Wiley & Sons, Inc. p. 355-399.

References

183. Hedicke-Höchstötter K., Lim G.T. and Altstädt V., *Novel polyamide nanocomposites based on silicate nanotubes of the mineral halloysite*. Composites Science and Technology, 2009. **69**(3-4): p. 330-334.
184. VanderHart D.L., Asano A. and Gilman J.W., *Solid-State NMR Investigation of Paramagnetic Nylon-6 Clay Nanocomposites. 1. Crystallinity, Morphology, and the Direct Influence of Fe³⁺ on Nuclear Spins*. Chemistry of Materials, 2001. **13**(10): p. 3781-3795.
185. VanderHart D.L., Asano A. and Gilman J.W., *Solid-State NMR Investigation of Paramagnetic Nylon-6 Clay Nanocomposites. 2. Measurement of Clay Dispersion, Crystal Stratification, and Stability of Organic Modifiers*. Chemistry of Materials, 2001. **13**(10): p. 3796-3809.
186. Pötschke P., Dudkin S.M. and Alig I., *Dielectric spectroscopy on melt processed polycarbonate—multiwalled carbon nanotube composites*. Polymer, 2003. **44**(17): p. 5023-5030.
187. Dobrescu V.E. and Radovici C., *Temperature dependence of melt viscosity of polymers*. Polymer Bulletin, 1983. **10**(3-4): p. 134-140.
188. Sathyanarayana S. and Hübner C., *Thermoplastic Nanocomposites with Carbon Nanotubes*, in *Structural Nanocomposites*, Njuguna J., Editor 2013, Springer Berlin Heidelberg. p. 19-60.
189. Domenech T., Peuvrel-Disdier E. and Vergnes B., *Influence of Twin-Screw Processing Conditions on Structure and Properties of Polypropylene – Organoclay Nanocomposites*. International Polymer Processing, 2012. **27**(5): p. 517-526.
190. Kasaliwal G., Gödel A. and Pötschke P., *Influence of processing conditions in small-scale melt mixing and compression molding on the resistivity and morphology of polycarbonate–MWNT composites*. Journal of Applied Polymer Science, 2009. **112**(6): p. 3494-3509.
191. Kashiwagi T., *Use of Nanocomposite Materials: Flammability of Nanocomposites: Effects of the Shape of Nanoparticles*, in *Fire Retardancy of Polymers: New Applications of Mineral Fillers*, Le Bras M., Wilkie C.A. and Bourbigot S., Editors. 2005, The Royal Society of Chemistry. p. 79-99.
192. Yamaoka I., *Effects of morphology on the toughness of styrene—butadiene—styrene triblock copolymer/ methyl methacrylate—styrene copolymer blends*. Polymer, 1998. **39**(10): p. 1765-1778.
193. Özkoç G., Bayram G. and Quaedflieg M., *Effects of microcompounding process parameters on the properties of ABS/polyamide-6 blends based nanocomposites*. Journal of Applied Polymer Science, 2008. **107**(5): p. 3058-3070.
194. Wagner Jr J.R., Mount III E.M. and Giles Jr H.F., *Plastic Behavior in Twin Screw Extruders*, in *Extrusion: The Definitive Processing Guide and Handbook* 2013, Elsevier Science. p. 149-169.
195. Logakis E., Pandis C., Peoglos V., Pissis P., Stergiou C., Pionteck J., Pötschke P., Mičušík M. and Omastová M., *Structure–property relationships in polyamide 6/multi-walled carbon nanotubes nanocomposites*. Journal of Polymer Science Part B: Polymer Physics, 2009. **47**(8): p. 764-774.
196. Vijaya K.R., Mohammed Y., Shaik J., Merlyn X.P. and Valery N.K., *Alignment of carbon nanotubes and reinforcing effects in nylon-6 polymer composite fibers*. Nanotechnology, 2008. **19**(24): p. 245703.

References

197. Padbury S.A., *Possible interactions between char-promoting flame retardants and nanoclays in polyamide films*, 2004, University of Bolton: Bolton, Lancashire, England.
198. Zhu J., Uhl F.M., Morgan A.B. and Wilkie C.A., *Studies on the Mechanism by Which the Formation of Nanocomposites Enhances Thermal Stability*[†]. *Chemistry of Materials*, 2001. **13**(12): p. 4649-4654.
199. Dahiya J.B., Kandola B.K., Sitpalan A. and Horrocks A.R., *Effects of nanoparticles on the flame retardancy of the ammonium sulphamate-dipentaerythritol flame-retardant system in polyamide 6*. *Polymers for Advanced Technologies*, 2013. **24**(4): p. 398-406.
200. *Improvements in or relating to the flameproofing of fabrics* GB750262, 1956, United Kingdom.
201. Gilleo K.B., *Nylon Flammability-Effects of Thiourea, Ammonium Sulfamate, and Halogen Compounds*. *Product R&D*, 1974. **13**(2): p. 139-143.
202. Levchik S.V., Costa L. and Camino G., *Effect of the fire-retardant, ammonium polyphosphate, on the thermal decomposition of aliphatic polyamides. I. Polyamides 11 and 12*. *Polymer Degradation and Stability*, 1992. **36**(1): p. 31-41.
203. Levchik S.V., Costa L. and Camino G., *Effect of the fire-retardant, ammonium polyphosphate, on the thermal decomposition of aliphatic polyamides: Part II—polyamide 6*. *Polymer Degradation and Stability*, 1992. **36**(3): p. 229-237.
204. Braun E. and Levin B.C., *Nylons: A review of the literature on products of combustion and toxicity*. *Fire and Materials*, 1987. **11**(2): p. 71-88.
205. Braun U. and Dümichen E. *Techniques for Understanding Fire Retardant Behaviour: Molecular Degradation and Decomposition Schemas*. in *Fire Retardant Technologies 2014*. 2014. University of Central Lancashire (UCLan), Preston, UK.
206. Pramoda K.P., Liu T., Liu Z., He C. and Sue H.-J., *Thermal degradation behavior of polyamide 6/clay nanocomposites*. *Polymer Degradation and Stability*, 2003. **81**(1): p. 47-56.
207. "Infrared Spectra" by NIST Mass Spec Data Center, S.E. Stein, Director, in *NIST WebBook, Standard Database References*, Linstrom P.J. and Mallard W.G., Editors., National Institute of Standards and Technology: Gaithersburg MD, 20899.
208. Seefeldt H., Duemichen E. and Braun U., *Flame retardancy of glass fiber reinforced high temperature polyamide by use of aluminum diethylphosphinate: thermal and thermo-oxidative effects*. *Polymer International*, 2013. **62**(11): p. 1608-1616.
209. Pretsch E., Bühlmann P. and Affolter C., *Structure Determination of Organic Compounds: Tables of Spectral Data 2000*: Springer - Verlag.
210. Socrates G., *Infrared and Raman Characteristic Group Frequencies: Tables and Charts 2004*: Wiley.
211. Fuller M.P. and Griffiths P.R., *Infrared Microsampling by Diffuse Reflectance Fourier Transform Spectrometry*. *Applied Spectroscopy*, 1980. **34**(5): p. 533-539.
212. Lehrle R.S., Parsons I.W. and Rollinson M., *Thermal degradation mechanisms of nylon 6 deduced from kinetic studies by pyrolysis-g.c.* *Polymer Degradation and Stability*, 2000. **67**(1): p. 21-33.
213. Weeding T.L., Veeman W.S., Gaur H.A. and Huysmans W.G.B., *Structural investigation of polyamide-6 and polyamide-6 composites using carbon-13 cross polarization/magic angle spinning NMR*. *Macromolecules*, 1988. **21**(7): p. 2028-2032.
214. SDBS. ¹³C NMR spectrum; SDBS No. 3784CDS-10-745 Available from: <http://riodb01.ibase.aist.go.jp/sdbs/>.

References

215. Levchik S.V., Balabanovich A.I., Levchik G.F. and Costa L., *Effect of melamine and its salts on combustion and thermal decomposition of polyamide 6*. Fire and Materials, 1997. **21**(2): p. 75-83.
216. Jahromi S., Gabriëlse W. and Braam A., *Effect of melamine polyphosphate on thermal degradation of polyamides: a combined X-ray diffraction and solid-state NMR study*. Polymer, 2003. **44**(1): p. 25-37.
217. Wagner Jr J.R., Mount III E.M. and Giles Jr H.F., *Scale-up*, in *Extrusion: The Definitive Processing Guide and Handbook 2013*, Elsevier Science. p. 199-201.
218. Funt J.M. and Magill J.H., *Thermal decomposition of polystyrene: Effect of molecular weight*. Journal of Polymer Science: Polymer Physics Edition, 1974. **12**(1): p. 217-220.
219. Panicker S.S. and Ninan K.N., *Influence of molecular weight on the thermal decomposition of hydroxyl terminated polybutadiene*. Thermochimica Acta, 1997. **290**(2): p. 191-197.
220. Chrissafis K., Paraskevopoulos K.M. and Bikiaris D.N., *Effect of molecular weight on thermal degradation mechanism of the biodegradable polyester poly(ethylene succinate)*. Thermochimica Acta, 2006. **440**(2): p. 166-175.
221. Sepe P., *Differential Scanning Calorimetry*, in *Thermal Analysis of Polymers 1997*, Rapra Technology Limited. p. 3-12.
222. Handge U.A., Hedicke-Höchstötter K. and Altstädt V., *Composites of polyamide 6 and silicate nanotubes of the mineral halloysite: Influence of molecular weight on thermal, mechanical and rheological properties*. Polymer, 2010. **51**(12): p. 2690-2699.
223. Hoffendahl C., Fontaine G., Duquesne S., Taschner F., Mezger M. and Bourbigot S., *Fire retardant mechanism of ethylene vinyl acetate elastomer (EVM) containing aluminium trihydroxide and melamine phosphate*. RSC Advances, 2014.
224. Kandola B.K., Price D., Milnes G.J. and Da Silva A., *Development of a novel experimental technique for quantitative study of melt dripping of thermoplastic polymers*. Polymer Degradation and Stability, 2013. **98**(1): p. 52-63.
225. Braun U., Schartel B., Fichera M.A. and Jäger C., *Flame retardancy mechanisms of aluminium phosphinate in combination with melamine polyphosphate and zinc borate in glass-fibre reinforced polyamide 6,6*. Polymer Degradation and Stability, 2007. **92**(8): p. 1528-1545.
226. Camino G., Costa L. and Luda di Cortemiglia M.P., *Overview of fire retardant mechanisms*. Polymer Degradation and Stability, 1991. **33**(2): p. 131-154.
227. Braun U. and Schartel B., *Effect of Red Phosphorus and Melamine Polyphosphate on the Fire Behavior of HIPS*. Journal of Fire Sciences, 2005. **23**(1): p. 5-30.
228. Chen Y. and Wang Q., *Reaction of melamine phosphate with pentaerythritol and its products for flame retardation of polypropylene*. Polymers for Advanced Technologies, 2007. **18**(8): p. 587-600.
229. Bourbigot S., Bras M.L. and Delobel R., *Carbonization mechanisms resulting from intumescence association with the ammonium polyphosphate-pentaerythritol fire retardant system*. Carbon, 1993. **31**(8): p. 1219-1230.
230. Duquesne S. and Futterer T., *Intumescent Systems*, in *The Non-halogenated Flame Retardant Handbook*, Morgan A.B. and Wilkie C.A., Editors. 2014, Wiley. p. 293-346.
231. Davies P.J., Horrocks A.R. and Alderson A., *The sensitisation of thermal decomposition of ammonium polyphosphate by selected metal ions and their potential for improved cotton fabric flame retardancy*. Polymer Degradation and Stability, 2005. **88**(1): p. 114-122.

References

232. Lewin M. and Endo M., *Catalysis of intumescent flame retardancy of polypropylene by metallic compounds*. *Polymers for Advanced Technologies*, 2003. **14**(1): p. 3-11.

APPENDIX A

imageJ macro:

```
run("Set Scale...", "distance=238 known=500 pixel=1 unit=µm");
//hide scalebar
fillRect(1080, 1094, 485, 82);
//Hide lens info
fillRect(1, 1148, 296, 52);
//hide vignetting
fillRect(1424, 0, 176, 164);
fillRect(0, 0, 240, 200)
fillRect(1308, 997, 292, 203);
fillRect(0, 1028, 186, 172);
waitForUser( "Pause", "Select Brush \n Delete artifacts with the brush !");
ID = getImageID();
run("Threshold..."); // open Threshold tool
  title = "Set threshold";
  msg = "If necessary, use the \"Threshold\" tool to\nadjust the threshold, then click
  \"OK\".";
  waitForUser(title, msg);
  selectImage(ID);
  getThreshold(lower, upper);
  name = getTitle();
  path = getDirectory("image");
run("Analyze Particles...", "size=5-Infinity circularity=0.05-1.0 show=Outlines display clear
summarize");
```

APPENDIX B

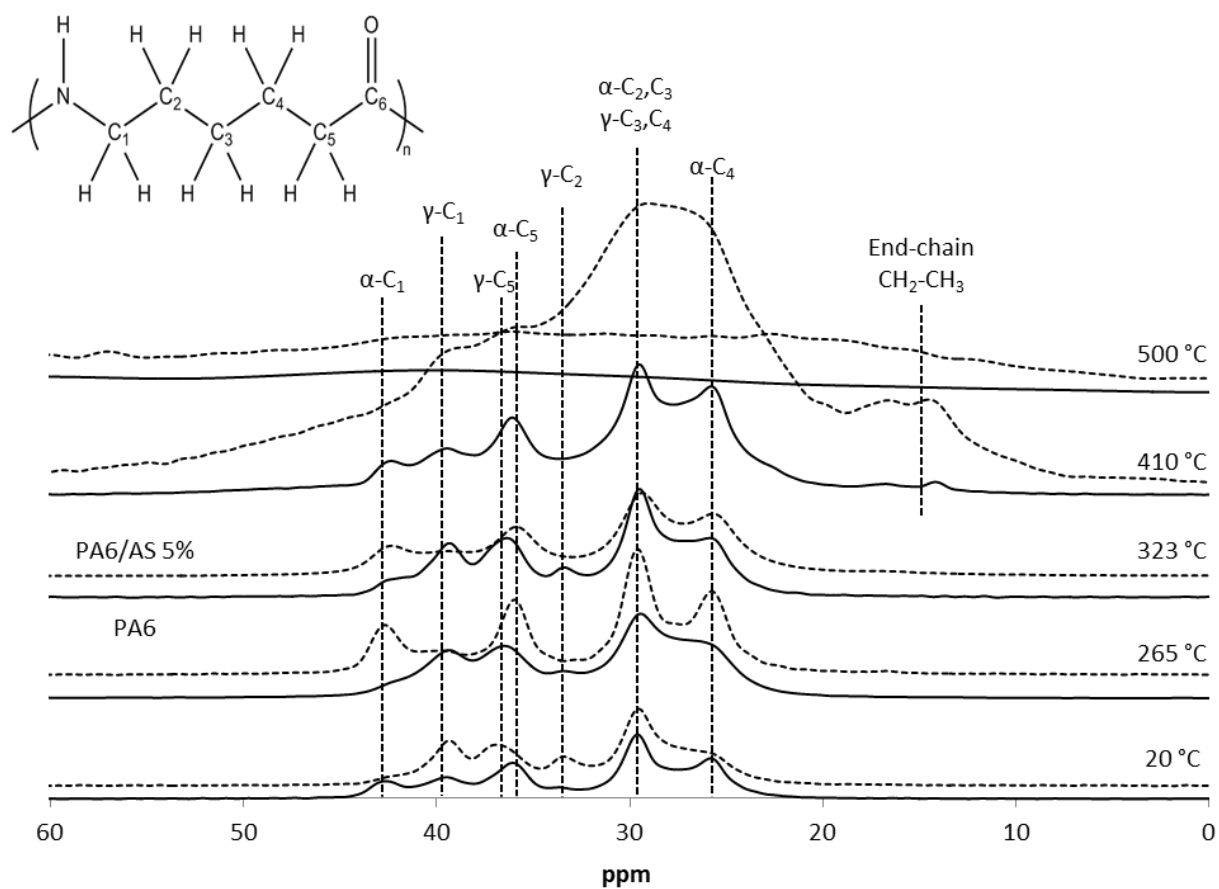


Figure 99: Enlargement of the aliphatic region of the ^{13}C CP-MAS NMR spectra of the PA6 (—) and PA6/AS residues obtained after thermal treatments at 20, 265, 323, 410 and 500 °C

APPENDIX C

Pictures of the PA6/nanoGO 1% fibers are presented in **Figure 100**. Aggregates of nanoGO can be observed on both pictures. Except the width of the fibers, both look very similar. “Big” and “small” aggregates are present and they seem pretty well dispersed in the matrix.

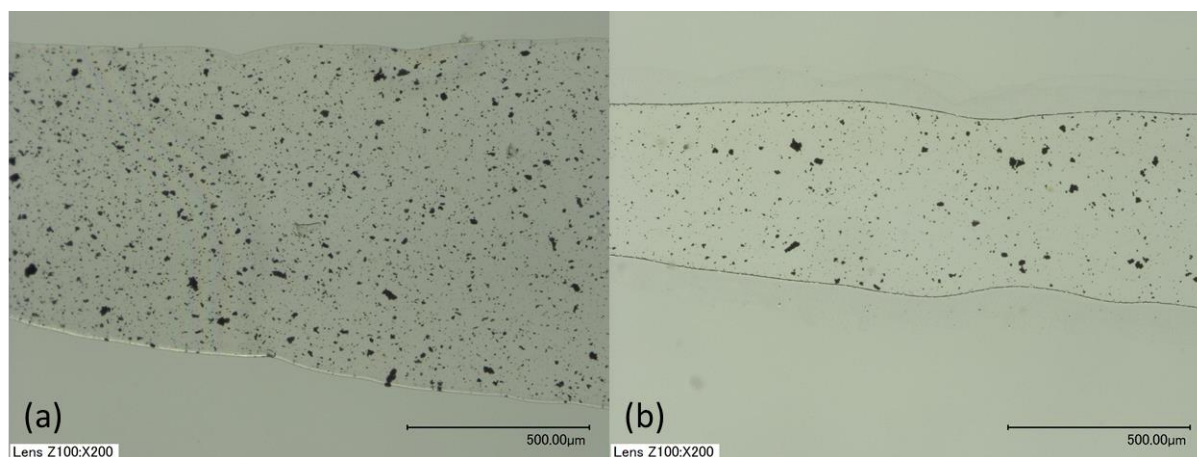


Figure 100: Digital microscope pictures of PA6/nanoGO 1% f1 (a) and f12 (b) formulations, dark dots correspond to nanoGO aggregates

The average particles count and size are reported in **Table 33**. More particles are observed in the formulation made with the parameter f1 than f12, around twice more for the f1 fiber. However, the width of the f1 fiber observed in **Figure 100(a)** is around twice longer as the f12 fiber width observed in **Figure 100(b)**. The particle density, corresponding to the number of particles on an area of 1 mm², was thus calculated for each sample. The results show that there are more particles in the f1 fibers, in terms of density (+19% compared to f12 fibers). The average size of the aggregates is 22% wider for the f1 formulation, but considering the scale the difference is not significant.

Table 33: Results of particles analysis from images of f1 and f12 PA6/nanoGO 1% formulations

Formulation parameters	Average particles count	Density (particles/mm ²)	Average size (µm ²)
f1	1290	879	43.9
f12	533	714	34.2

The normalized distribution of the particles sizes and the cumulative percentage for both fibers made with the f1 and f12 parameters are presented in Figure 101. It can be seen that most aggregates (around 85%) have a size smaller than 64 µm². The larger size ranges decrease rapidly and less than 1% of aggregates are 1024 µm² or larger.

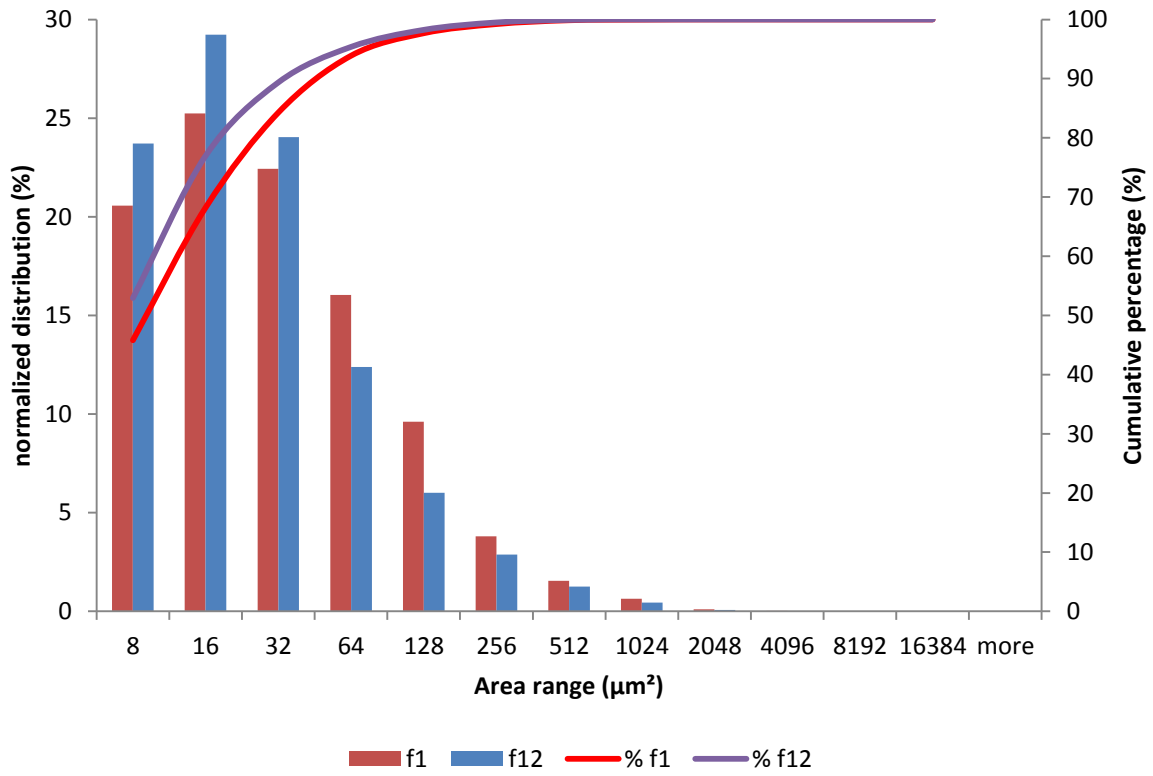


Figure 101: Particle size distribution of f1 and f12 PA6/nanoGO 1% formulations

APPENDIX D

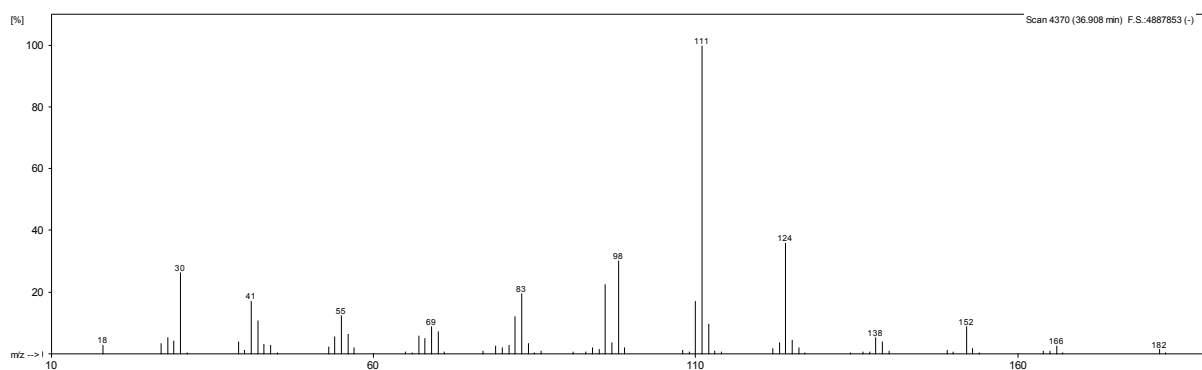


Figure 102: Mass spectrum of compound a

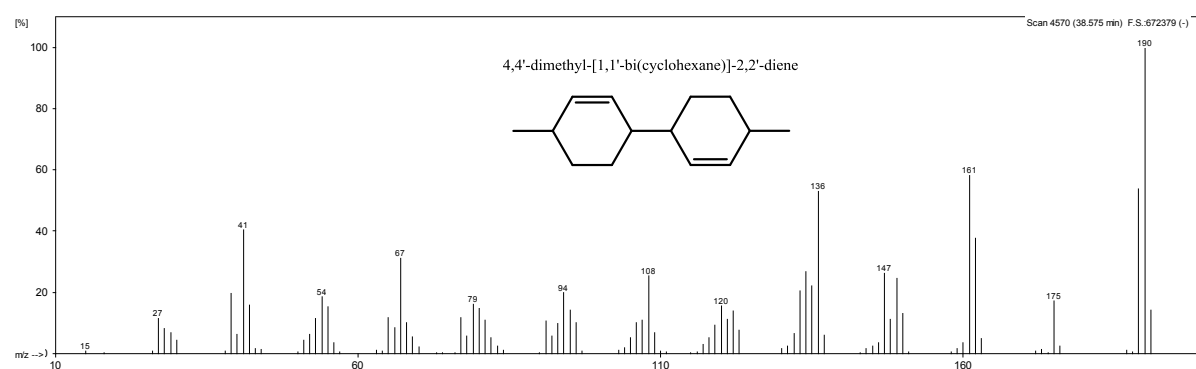


Figure 103: Mass spectrum of compound b

PROCEDE D'IGNIFUGATION DES FIBRES DE POLYAMIDE 6 – UTILISATION DES SELS DE SULFAMATE

RESUME – L'objet de cette thèse est l'ignifugation de fibres textiles de type polyamide 6 (PA6). Parmi les différentes techniques utilisées pour modifier une fibre ou un textile synthétique, l'ajout en masse de retardateurs de flamme (RF) durant le procédé d'extrusion a été choisi. Les températures de mise en œuvre du PA6 étant assez élevées (généralement supérieures à 250 °C) une sélection rigoureuse de retardateurs de flamme à base de phosphore et de soufre a été faite. Cette sélection a également pris en compte le fait que le RF doit être efficace à de faibles taux de charge (<10% en masse) pour permettre de filer la matrice. Il est ressorti de cette étude que les sels d'acide sulfamique, tels que le sulfamate d'ammonium (AS) et le sulfamate de guanidinium (GAS) sont efficaces et que les formulations sont filables. Les modes d'action en phase condensée et en phase gaz ont été étudiés et décrits. On observe respectivement une carbonisation plus importante et une modification de la composition des gaz émis lors de la dégradation thermique des matériaux. Cependant, lors du passage de l'échelle laboratoire (micro extrudeuse) à l'échelle pilote, des problèmes de dégradation de la matrice polymère sont survenus. De manière à pallier cette difficulté, l'utilisation d'un co-additif (polyphosphate de mélamine), offrant un effet de synergie avec les sels de sulfamate, a permis de réduire la quantité de GAS tout en améliorant les propriétés feu du PA6 et la formulation a pu être extrudée à échelle pilote.

MOTS CLES : ignifugation, polyamide 6, fibres, sels de sulfamate, polyphosphate de mélamine

FLAME RETARDANCY OF POLYAMIDE 6 FIBERS - THE USE OF SULFAMATE SALTS

ABSTRACT – The aim of this Ph.D. work is the fire retardancy of polyamide 6 (PA6) fibers. Among the different techniques used to modify a synthetic fiber or fabric, the incorporation of fire retardants (FR) directly in the melt during extrusion was chosen. Processing temperatures of PA6 being rather high (generally > 250 °C), a rigorous selection of phosphorus and sulfur based FR was done. Moreover, FR must be stable at the processing temperature, while being spinnable and efficient at low loadings (<10 wt.-%). Sulfamate salts such as ammonium and guanidine sulfamate (AS and GAS) were found efficient and the PA6 formulations were spinnable. The modes of action were investigated through a study of the condensed and gas phase. However, when scaling up the process from microextruder to a large-scale extruder, processing issues were observed. In order to overcome this problem, the use of a co-additive (melamine polyphosphate), offering a synergistic effect with sulfamate salts, allowed to decrease the amount of GAS in the PA6 formulation while enhancing the FR performance. Thus, large-scale extrusion of the FR PA6 was performed successfully.

KEYWORDS: flame retardancy, polyamide 6, fibers, sulfamate salts, melamine polyphosphate